

EVALUATION OF AN ADVANCED
ENGINEERING TEST REACTOR DESIGN

July 15, 1958

Prepared by:

Marvin McVey, Project Engineer


and

J. O. Bradfute	R. Quilici
K. E. Buck	I. Richardson
K. T. Chow	J. Webster
R. J. Jaffe	F. Weil

Engineering Development Branch, Division of Reactor Development
U. S. Atomic Energy Commission

Contract No. AT(04-3)-109, Directive L

Approved by:


Charles M. Rice
Reactor Engineering Department

A M E R I C A N - S T A N D A R D
Atomic Energy Division Mountain View, California

DISCLAIMER

This report was prepared as an account of work sponsored by an agency of the United States Government. Neither the United States Government nor any agency Thereof, nor any of their employees, makes any warranty, express or implied, or assumes any legal liability or responsibility for the accuracy, completeness, or usefulness of any information, apparatus, product, or process disclosed, or represents that its use would not infringe privately owned rights. Reference herein to any specific commercial product, process, or service by trade name, trademark, manufacturer, or otherwise does not necessarily constitute or imply its endorsement, recommendation, or favoring by the United States Government or any agency thereof. The views and opinions of authors expressed herein do not necessarily state or reflect those of the United States Government or any agency thereof.

DISCLAIMER

Portions of this document may be illegible in electronic image products. Images are produced from the best available original document.

ACKNOWLEDGMENT

Appreciation is expressed to Mr. D. G. Boyer, Engineering Development Branch, and Mr. T. L. Dunckel, San Francisco Operations Office of the Atomic Energy Commission for their technical assistance and guidance.

TABLE OF CONTENTS

	SUMMARY
I.	INTRODUCTION
II.	SCOPE OF THE STUDY
III.	THE INTERNUC CONCEPT
IV.	RESULTS, CONCLUSIONS, AND RECOMMENDED DESIGN
V.	RECOMMENDATIONS FOR FURTHER ANALYSIS
VI.	OPTIMIZATION OF FLUX AND POWER LEVEL
VII.	HEAT REMOVAL LIMITATIONS
VIII.	MATERIALS SELECTION AND LIMITATIONS
IX.	GAMMA HEATING AND THERMAL STRESSES
X.	DESIGN QUESTIONS
	A. Fuel Plate Orientation
	B. Type of Control System
	C. Couples vs Uncoupled Reactors
XI.	SHIELDING
XII.	PROCESS SYSTEMS
XIII.	RESEARCH AND DEVELOPMENT PROGRAM
	A. Items for the Program
	B. Estimated Cost and Time Required
XIV.	COST ESTIMATE: DESIGN, CONSTRUCTION AND OPERATION
	APPENDICES
	A. Physics Methods and Constants
	B. Thermal Performance Relationships
	C. Materials Considerations

List of Illustrations

- Figure 1. AETR Plant Layout Schematic
- Figure 2. Reactor Section
- Figure 3. Elevation, AETR Reactor
- Figure 4. Section of the AETR Fuel Element
- Figure 5. Atomic Density in Core Region vs M/W Ratio (With Wedges)
- Figure 6. Critical Mass vs M/W for Core With Wedges
- Figure 7. Reactor Power vs M/W ratio for Core With Wedges
- Figure 8. Average Power vs M/W Ratio for Core With Wedges
- Figure 9. Atomic Density for Core With No Wedges
- Figure 10. Reactor Power vs M/W Ratio for Core With No Wedges
- Figure 11. Average Power Density vs M/W Ratio for Core With No Wedges
- Figure 12. Reactor Power vs Weight Percent of Uranium in Alloy
- Figure 13. Reactor Volume vs Weight Percent of Uranium in Alloy
- Figure 14. Reactor Power vs Inner Reflector Thickness (M/W Ratio = 1.0)
- Figure 15. Average Power Density vs Reflector Thickness (M/W Ratio = 1.0)
- Figure 16. Radial Flux Distribution in a 4-in. Water Loop
- Figure 17. Radial Flux Distribution in a 3-in. Water Loop
- Figure 18. Radial Flux Distribution in a 7-in. Sodium Loop
- Figure 19. Radial Flux Distribution in a 5-in. Sodium Loop
- Figure 20. Radial Flux Distribution in a 3-in. Sodium Loop
- Figure 21. Power Density vs M/W Ratio for Various Inlet Coolant Temperatures
- Figure 22. Power Density vs M/W Ratio for Various Fuel Plate Thicknesses
- Figure 23. Power Density vs M/W Ratio for Various Coolant Velocities
- Figure 24. Radial Power Density Distribution
- Figure 25. Diagram Depicting the Annular Core Region
- Figure 26. Study of Effect of Boron in Reflector
- Figure 27. Reactivity Effect of One Reactor on Another
- Figure 28. Flux Between Coupled Reactors
- Figure 29. Gamma Dose Rate at Face of the Shield

Appendices

- Figure 30. Fermi Age of Fission Neutrons in Aluminum-Water Mixture
- Figure 31. Fermi Age of Fission Neutrons in Zirconium-Water Mixture
- Figure 32. Thermal Flux Distribution by 22 and Three Group Models
- Figure 33. Fast Diffusion Coefficients vs M/W Ratio (15% by Wt. of U With Wedges)
- Figure 34. Intermediate Diffusion Coefficients vs M/W Ratio (15% by Wt. of U With Wedges)
- Figure 35. Thermal Diffusion Coefficient vs M/W Ratio (15% by Wt. of U With Wedges)
- Figure 36. Removal Cross Section vs M/W Ratio (15% by Wt. of U With Wedges)
- Figure 37. Source (From Moderator) Cross Section vs M/W Ratio (15% by Wt. of U With Wedges)
- Figure 38. Fission Cross Section vs M/W Ratio (15% by Wt. of U With Wedges)
- Figure 39a. Fast Diffusion Coefficient vs M/W Ratio (25% by Wt. of U)
- Figure 39b. Intermediate Diffusion Coefficient vs M/W Ratio (25% by Wt. of U)
- Figure 40. Thermal Diffusion Coefficient vs M/W Ratio (25% by Wt. of U With Wedges)
- Figure 41. Removal Cross Section vs M/W Ratio (25% by Wt. of U With Wedges)
- Figure 42. Fission Cross Section vs M/W Ratio (25% by Wt. of U With Wedges)
- Figure 43. Source (From Moderator) Cross Section vs M/W Ratio (25% by Wt. of U With Wedges)
- Figure 44a. Fast Diffusion Coefficients vs M/W Ratio (35% by Wt. of U With Wedges)
- Figure 44b. Intermediate Diffusion Coefficients vs M/W Ratio (35% by Wt. of U With Wedges)
- Figure 45. Fission Cross Section vs M/W Ratio (35% by Wt. of U With Wedges)
- Figure 46. Thermal Diffusion Coefficient vs M/W Ratio (35% by Wt. of U With Wedges)
- Figure 47. Removal Cross Section vs M/W Ratio (35% by Wt. of U With Wedges)
- Figure 48. Source (From Moderator) Cross Section vs M/W Ratio (35% by Wt. of U With Wedges)

- Figure 49a. Intermediate Diffusion Cross Section vs M/W Ratio (15% by Wt. of U, No Wedges)
- Figure 49b. Fast Diffusion Cross Section vs M/W Ratio (15% by Wt. of U, No Wedges)
- Figure 50. Thermal Diffusion Coefficient vs M/W Ratio (15% by Wt. of U, No Wedges)
- Figure 51. Removal Cross Section vs M/W Ratio (15% by Wt. of U, No Wedges)
- Figure 52. Fission Cross Section vs M/W Ratio (15% by Wt. of U, No Wedges)
- Figure 53. Source (From Moderator) Cross Section vs M/W Ratio (15% by Wt. of U, No Wedges)
- Figure 54a. Fast Diffusion Coefficient vs M/W Ratio (15% by Wt. of U, No Wedges)
- Figure 54b. Intermediate Diffusion Coefficient vs M/W Ratio (25% by Wt. of U, No Wedges)
- Figure 55. Fission Cross Section vs M/W Ratio (25% by Wt. of U, No Wedges)
- Figure 56. Source (From Moderator) Cross Section vs M/W Ratio (25% by Wt. of U, No Wedges)
- Figure 57. Removal Cross Section vs Metal/Water Ratio (25% by Wt. of U, No Wedges)
- Figure 58. Thermal Diffusion Coefficient vs M/W Ratio (25% by Wt. of U, No Wedges)
- Figure 59. Thermal Diffusion Coefficient vs M/W Ratio (35% Wt. of U, No Wedges)
- Figure 60a. Fast Diffusion Coefficient vs M/W Ratio (35% by Wt. of U, No Wedges)
- Figure 60b. Intermediate Diffusion Coefficient vs M/W Ratio (35% by Wt. of U, No Wedges)
- Figure 61a. Fission Cross Section vs M/W Ratio (35% by Wt. of U, No Wedges)
- Figure 61b. Fission Cross Section vs M/W Ratio (35% by Wt. of U, No Wedges)
- Figure 62. Source (From Moderator) Cross Section vs M/W Ratio (35% by Wt. of U, No Wedges)
- Figure 63. Removal Cross Section vs M/W Ratio (35% by Wt. of U, No Wedges)

- Figure 64. Weight Density in Core Region vs M/W Ratio (15, 25 and 35% by Wt. of U, With Wedges)
- Figure 65. Weight Density in Core Region vs M/W Ratio (15, 25 and 35% by Wt. of U, No Wedges)
- Figure 66. Removal Cross Section vs Weight Percent of U--M/W=0.69 (No Wedges)
- Figure 67. Source (From Moderator) Cross Section (No Wedges)
- Figure 68. Fission Cross Section vs Weight Percent of U in Alloy (No Wedges)
- Figure 69a. Atomic Density vs Weight Percent of U in Alloy--M/W=0.69 (No Wedges)
- Figure 69b. Weight Density vs Weight Percent of U in Alloy--M/W=0.69 (No Wedges)
- Figure 70. Corrosion of (M-388) X8001 Aluminum at 250°C
- Figure 71. Corrosion of (M-388) X8001 Aluminum at 300°C
- Figure 72. Radiation Damage to Aluminum Alloy 1100 (Ref. 26)
- Figure 73. Radiation Damage to Stainless Steel ALSL Type 347 (Ref. 26)

List of Tables

Table	I	Specifications for Maximum Flux Design
Table	II	Core Power and Loop Flux
Table	III	Reactor Parameters and Composition of the Region Used for Optimization
Table	IV	Details of Inner Region for the Maximum Flux Design
Table	V	Heat Transfer Parameters
Table	VI	Hot Channel Factors
Table	VII	AETR Thermal Performance
Table	VIII	Test Reactor Comparison
Table	IX	Rate of Gamma Heat Generation
Table	X	R and D Cost Estimate
Table	XI	AETR Cost Estimate
Table	A-I	Group Structure for the 22-Group Calculation
Table	A-II	Ages in Al-H ₂ O Mixture
Table	A-III	Three Group Constants
Table	B-I	Heat Transfer Nomenclature

SUMMARY

This report presents the results of a study of certain features of the Internuclear Company concept for an Advanced Engineering Test Reactor. The scope of the study, which is given in Chapter II, was specified by Division of Reactor Development of the Atomic Energy Commission in a list of 11 items in Appendix B, Contract No. AT(04-3)-109, Mod No 4 Revision, Project L.

The Internuclear concept to achieve ultra-high thermal-flux in seven proposed testing loops called for a complex of seven, decoupled reactors located in a single, large block of concrete. Each reactor is of the flux-trap type, consisting of a cylindrical annular core of H₂O cooled Al-U elements of the general MTR class, a D₂O reflector, an annulus of H₂O just inside the core annulus, and the central loop region for materials testing.

The scope of the present study was primarily concerned with optimization of the geometrical and core-composition variables to achieve the maximum flux in the loop region per unit of power in the core without exceeding heat transfer and other engineering limitations.

Certain other design questions were to be investigated to the extent possible with the funds available

It was found that, with uniform distribution of fuel in the core annulus, it is impossible to obtain the flux in the large, sodium or air cooled loop that is desired by DRD without exceeding heat removal limitations in the core. This is partly because of the fact that the radial power distribution is very poor, creating a severe hot spot at the inside edge of the core annulus. Achievable loop fluxes and the associated core powers are determined for the seven specified loops in a design that is optimized for the large 7-in. sodium cooled loop. Achievable loop fluxes are in the range 1.16×10^{15} n/cm²/sec to the desired flux, 1.5×10^{15} n/cm²/sec, and the associated core powers are in the neighborhood of 200 MW for each reactor. This would result in a combined power for the complex of about 1400 MW; however, this can be reduced by optimizing each reactor for its loop or at least having two optimized designs, and by designing for a flatter, radial core-power distribution through the use of non-uniform radial distribution of fuel

Several design questions are discussed and recommendations given. Recommendations for further preliminary analysis are presented. A formal R & D program is laid out and the cost of this as well as the construction cost of the reactor complex is estimated.

I. INTRODUCTION

The purpose of this report is to present the results of a study of certain features of the Internuclear Company concept for an Advanced Engineering Test Reactor. The basic Internuclear concept for the AETR is described in detail in the reports AECU-3427¹ and AECU-3427² (Add.)². Subsequent work by the Internuclear people on the same items of investigation that are described here is to be published at about the same time as this report.

The assignment to American-Standard was viewed by the authors as being partially in the nature of an independent estimate of achievable fluxes and required power levels for the H₂O moderated, D₂O reflected, H₂O "flux-trap" type of research reactor. The constants of the reactor, such as macroscopic cross sections, were thus calculated without reference to the Internuc values. Where possible, refined procedures were used. Methods of reasonable brevity were, of course, appropriate and necessary in AECU-3427 because of the broad ranges of the variables in the parameter surveys. Full advantage of AECU-3427 was taken in narrowing the range of parameters to be investigated in the determination of optimum values.

The plan of the report is patterned after the scope of the study, the items of which and their order of importance being specified by the AEC. The report is thus divided into the following sections: Summary, Introduction, Scope of the Study, The Internuc Concept, Results and Conclusions, Recommendations for Further Analysis, Optimization of Flux and Power Level, Heat Removal Limitations, Materials Limitations, Gamma Heating and Thermal Stresses, Design Questions (Fuel Plate Orientation, Type of Control System, Coupled vs. Uncoupled Reactors), Shielding, Process System, Research and Development Program, and Cost Estimates. Appendices are included on the Physics Methods and Constants, Thermal Performance Relationship, and Materials Considerations. The first appendix contains numerous graphs of cross sections that were determined for three group calculations (these

¹ O. J. Elgert, C. F. Leyse, and D. G. Ott, "Preliminary Investigations for an Advanced Engineering Test Reactor," AECU-3427

² C. F. Leyse and B. H. Leonard, Jr., "Preliminary Investigations for an Advanced Engineering Test Reactor," AECU-3427 (Add.).

should be generally applicable to any Al-H₂O research reactor calculations), and analyzes the accuracy of the three group model. The appendix on Materials Considerations contains a detailed compilation of information on aluminum and other materials of interest.

II. SCOPE OF THE STUDY

The scope of the work discussed in this report was specified by the Division of Reactor Development of the AEC in a list of 11 items as set forth in Appendix B, Contract No. AT(04-3)-109, Modification No. 4, Revision, Project L. All items are in reference to the reactor design presented in AECU-3427. They are listed below in the stated order of importance to the contracting office:

1. Optimization of flux and power level in the test section to produce an average unperturbed thermal flux of 1.5×10^{15} n/cm²/sec. The test sections shall include: Two 2000 psi (550-650°F) circulating water loops, one 3-in. ID and one 4-in. ID; circular test sections, three of 7-in. ID, one of 5-in. ID and one of 3-in. ID -- all versatile loops for either gas or liquid metal capable of operating at 300 psi with temperatures in the order of 1500°F to 2000°F.
The test loops are to be 30-in. long and the axial flux variation should not exceed 50% over that length.
2. Extend the calculations on the flux distributions to determine the optimum dimensions of the fuel and moderator annuli.
3. Estimate the limit of heat-removal capacity of various fuel element arrangements in an annular system under the postulated operating conditions.
4. Study the gamma-heating problem in the "flux-trap" type reactor system with respect to the test loops using as a factor the power produced by the experiment as well as the power produced by the reactor.
5. Study the concept of completely uncoupled versus a coupled reactor (as well as varying degrees of coupling) from the standpoint of cost, flexibility, control, and independence of loop operation, assuming fuel element tests are terminated at the point of incipient failure.
6. Study a mechanical control system as opposed to a completely chemical control system.
7. Study the feasibility of using aluminum rather than zirconium or stainless steel or other materials where this appears economically desirable.
8. Study shielding requirements for access after shutdown and biological shield thickness around reactor complex.

9. Based on the results of the studies of items 1 through 8, prepare a preliminary conceptual design of a reactor facility that would incorporate, as far as practical, the most suitable arrangements that result from the studies of the major problem areas outlined above.
10. Outline and estimate the cost of the research and development program necessary to support the detailed design and construction of an advanced engineering test reactor.
11. Prepare a cost estimate for design, construction, and operation of a flux-trap AETR.

III. THE INTERNUC CONCEPT

For readers unfamiliar with the report, AECU-3427, it may be helpful at this point to present very briefly the general features of the Internuc concept for the Advanced Engineering Test Reactor.

By way of background, in December, 1956, the AEC asked several reactor design companies to study, independently, possible reactor designs that would provide an ultra-high thermal flux, greater than 10^{15} n/cm²/sec, in loop type facilities. The companies were requested to recommend a system that met certain specifications such as (1) an unperturbed flux of 10^{15} n/cm²/sec in a 3-in. and 4-in., 2000 psi, 500-600°F, circulating light-water loops, (2) an unperturbed flux of 1.5×10^{15} n/cm²/sec in three 6-in. x 6-in. versatile, gas or liquid metal loops and one 4-in. x 4-in. versatile loop, the gas loop to operate at 2200°F and 300 psi, and the liquid metal loop at 1500°F and at 300 psi, and (3) an unperturbed flux of 10^{15} n/cm²/sec in a 3-in. liquid metal loop.

Internuc decided to concentrate its effort on H₂O and D₂O cooled and moderated heterogeneous reactors on the basis that the technology of this type of research reactor is well developed and on the philosophy that "a reactor for component testing should not in itself be a developmental experiment." Internuc's recommendation was that the design consist of a complex of seven separate reactors embedded in a huge block of concrete with sufficient separation to decouple the reactors with regard to neutron interaction. The secondary cooling system would be common to all but primary cooling completely separate.

Each reactor would consist of a cylindrical annular core of aluminum-clad, H₂O-cooled elements, of the general MTR class; a D₂O reflector; an annulus of H₂O just inside the core annulus; and a central loop containing in general a fuel element to be tested or other such experiment. (These basic features were to be retained in the present study.) The inner annulus of H₂O lying between the core and loop acts to moderate neutrons into the thermal range at the same or greater rate than in the core annulus and, since the absorption is smaller in the pure H₂O than in the core annulus, the flux tends to build up and exhibit a peak in its radial distribution through the H₂O annulus, as well as in the

loop region at the center. The name flux trap has come to be associated with this design in the sense that the H_2O annulus traps the flux, that is, increases the thermal neutron concentration in this region.

For a given loop diameter, the designer is presented with an interesting problem of parameter optimization to achieve the maximum flux in the loop region per unit of power in the core without exceeding heat transfer and other engineering limitations.

IV. RESULTS, CONCLUSIONS, AND RECOMMENDED DESIGN

The following results, conclusions, and recommended design were derived from the study.

PLANT ARRANGEMENT

1. The preferred layout of the reactor complex is shown in Figure 1. The arrangement has a single control room (not shown) from which all seven reactors would be operated, so as to minimize the number of operators required. The canal arrangement is as in Internuc's "layout B". The canal system connects each reactor to an underwater storage area outside the main shield. Equipment serving each reactor is located adjacent to the shield. This equipment consists of heat exchangers, reactor coolant circulation pumps, deionizers, pressurizers, reflector poison apparatus, and other auxiliaries. The heat exchangers are located at higher elevation than the reactor core to facilitate convection cooling if coolant-pump power is lost. Experimental equipment is located in equipment rooms as shown. Instrumentation for the loops is located at the outside wall of each equipment room.

REACTOR CONFIGURATION

2. The configuration of each reactor is as shown in Figure 2, Reactor Section, and Figure 3, Reactor Elevation. The various reactor regions are as described in Chapter III, The Internuc Concept. The inner liner contains the main experimental assembly or specimen and the experiment coolant. A stainless steel expansion joint allows for the difference in thermal expansion between the large diameter stainless steel section and the aluminum lower section of the reactor vessel. Top flanges allow access for refueling the reactor and reloading the experimental facilities. The annular space between the stainless steel liner of the thimble and the wall of the aluminum thimble is normally filled with an inert gas. Outside the reactor vessel this gas-filled gap is connected to the experiment coolant through a pressure balance chamber of a gas pressurizer so that there is no pressure on the liner. The gas space will provide thermal insulation on those experiments where the test coolant temperature is higher than

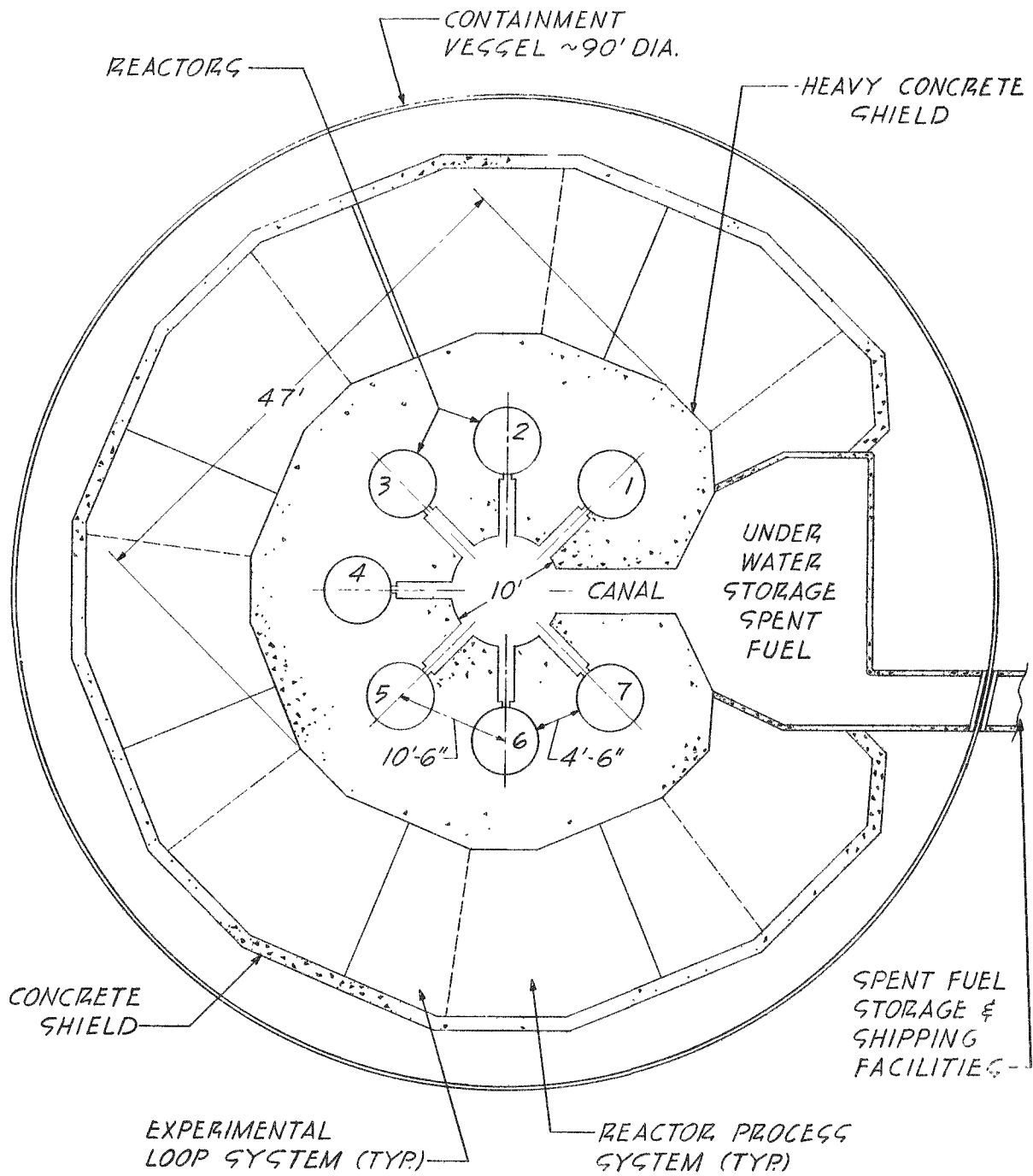
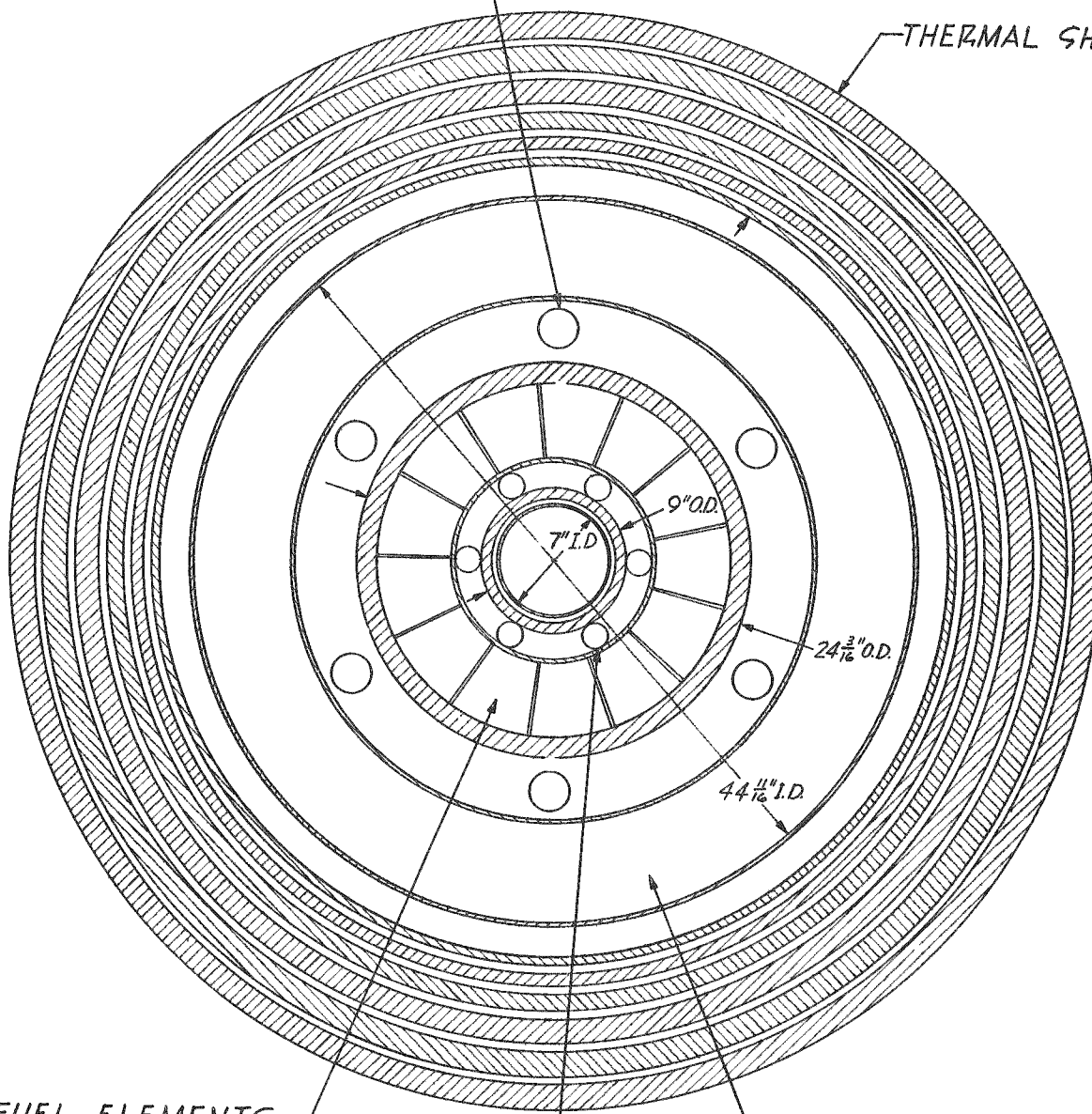


Figure 1 -- AETR Plant Layout Schematic

TUBES FOR REGULATING RODS
OR EXPERIMENTS (6)

THERMAL SHIELDS



13 FUEL ELEMENTS

REFLECTOR

INSIDE EXPERIMENT TUBES (6)

Figure 2 -- Reactor Section

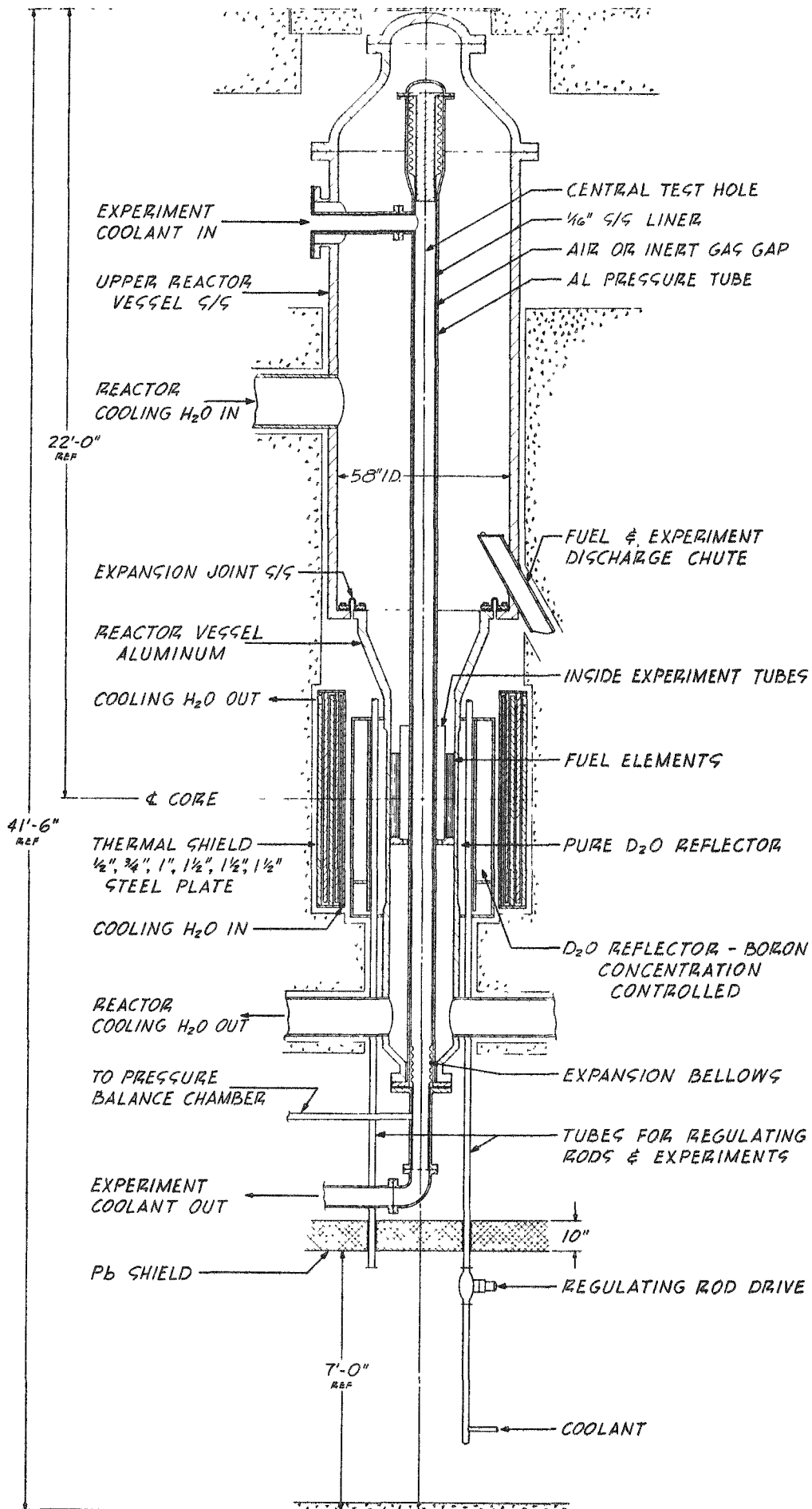


Figure 3 -- Elevation, AETR Reactor

that of the reactor coolant.

EXPERIMENTAL FACILITIES

3. The focal point of design of the facility is the central test section. Access to this is through the top cover. The experiment thimble can be replaced by cutting off the lower flange disconnecting the side flange, and removing through the reactor vessel opening. Auxiliary test space is made available where no conflict exists between efficient design and operation of the test section facility and the auxiliaries. Access to 1 1/2 in. capsule tubes in the water region between the core and the test thimble is from the top vessel opening. These capsule tubes provide space for specimens to be irradiated in a high flux and cooled with reactor water. The specimen can be transported to the canal for storage through the discharge chute. Additional irradiation space at lower available flux levels is provided in tubes that penetrate the heavy water reflector. Access to these tubes is from below in the subpile room.

OPTIMIZATION OF FLUX AND POWER

- Before listing certain itemized results and conclusions concerning optimization of flux and power, three important decisions that were made at the start of the project for budgetary reasons should be mentioned: (a) It was clear that it would be prohibitively expensive to calculate an optimum reactor design for each of the seven loops; it was determined that the really difficult design problem is to meet the specified flux magnitude in the 7-in. liquid metal cooled loop; after consultation with the contracting officer, it was decided to optimize for the 7-in. liquid metal loop and to consider tentatively, at least, that all seven reactors would be identical except for the contents of this inner 7-in. region; (b) It was decided not to design for non-uniform, radial distribution of fuel but to point out the advantages of this if it proves to be metallurgically and economically practical; (c) It was decided not to spend any money on two-dimensional flux calculations, which are very expensive, but rather to do the best possible one-dimensional computations at this stage of the design.
4. The design specifications shown in Table I gave the highest flux in the loop region for the 7-in. sodium cooled loop that is achievable under core heat transfer and other engineering limitations.

TABLE I
SPECIFICATIONS FOR THE MAXIMUM FLUX DESIGN

Inner H ₂ O Annulus		
Thickness		4 cm
Inside Radius		11.4 cm
Outside Radius		15.4 cm
Core Annulus		
Metal to Water Ratio		0.69
Volume		144 liters
Thickness		11.4 cm
Inside Radius		16.1 cm
Outside Radius		27.5 cm
Critical Mass		≈ 9 kg
Wt. percent uranium in "meat" alloy (at shutdown)		15%

5. The achievable loop fluxes and the associated required core powers for the various loops placed in this reactor (which is optimized for the 7-in. liquid metal loop) are shown in Table II. Where the flux specified by the contracting officer can be achieved under core heat transfer limitations, only this flux and the associated required power are given, that is, for the water loops a greater than called-for loop flux can be achieved at core power levels that are somewhat lower than power levels set by heat transfer limitations.
6. The loop flux and core power given in Table II for the smaller loops are for the system that is optimized for the 7-in. sodium cooled loop. If the system were optimized for the 3-in. H₂O-cooled loop, for example, the required power to achieve the desired flux for this loop would be much smaller.

TABLE II

CORE POWER AND LOOP FLUX

Test Loop	4-in. H ₂ O	3-in. H ₂ O	7-in. Na	5-in. Na	3-in. Na
Reactor Power (MW)	184	205	228	228	228
Av. Power Density (MW/liter)	1.28	1.42	1.59	1.59	1.59
Av. Unperturbed Thermal Flux in Loop (n/cm ² sec)	1.50×10^{15}	1.50×10^{15}	1.16×10^{15}	1.20×10^{15}	1.27×10^{15}
Av. Unperturbed Radial Thermal Flux in Loop Region (n/cm ² sec)	2.08×10^{15}	2.08×10^{15}	1.69×10^{15}	1.76×10^{15}	1.82×10^{15}

7. The figure of 1.59 MW/liter given in Table II for the sodium loops is the maximum allowable average power density in the core dictated by heat transfer limitations. It takes into account the poor radial power distribution that exists in this reactor type because of the fact that the flux rises sharply at the inside of the core (and then peaks in the trap region). If the radial power distribution were flat the allowable power density is 2.59 MW/liter (vertical average). A 500°F fuel plate surface temperature and a coolant velocity of 25 ft/sec were used.
8. Because of power density limitations, it is highly desirable in this reactor type to use fuel elements that completely fill the annular core region and do not require wedges such as would be required in a square box type assembly of fuel plates.
9. A slight gain in achievable loop flux without increase of core power density could probably be obtained by using a lower weight percent fuel in the plate alloy (than the 15% shown in Table I), but the required total powers would be even higher than those given in Table II.

10. The total core power necessary to achieve a given flux decreases rapidly if the weight percent fuel in the alloy is increased (and the core annular thickness is decreased to maintain criticality), but the heat transfer limitations on power density will not permit this decrease of core size and increased fuel loading (for uniform radial distribution of fuel). If the fuel is distributed non-uniformly in the radial direction to flatten radial power distribution, the average fuel content per plate could be increased, the core thickness decreased, and the total power decreased for the same loop flux.
11. It seems advisable to include in the reactor complex at least two optimized designs, one for the large loops and one for the small loops. This will result in smaller power requirements to achieve a specified flux in the small loops and will probably permit achievement of the loop flux specified by the contracting officer in the small sodium loops. This was not achieved in Table II.
12. It was found that three group, reactor physics calculations are satisfactory for this type of reactor, but an error of about 20% in loop flux is introduced compared to 22-group results. Also the reactivity is about 4% too high in three-group calculations compared to 22-group if classic values of "age", that is, $1/6$ second moment of slowing down density from a point source, are used. It is believed by the authors that this explains the fact that few group calculations of critical mass in MTR type reactors have been nearly all too low.

MATERIALS SELECTION

13. The chosen fuel element cladding material (aluminum X8001) will give satisfactory performance at the maximum safe operating conditions chosen and at a much lower cost than zirconium.
14. Aluminum is the most economical material to use for the pressure vessel and experimental loop test sections, and has satisfactory corrosion resistance when water conditions are satisfactorily controlled.

GAMMA HEATING AND STRESSES

15. None of the combined stresses imposed by gamma heating exceed the yield point of the reactor wall materials at operating temperatures. On this basis, the thermal stresses are not excessive. However, a true evaluation of the acceptability of the computed stresses requires an estimate of the number of cycles expected during the life of the reactor components.

ORIENTATION OF FUEL PLATES

16. It is believed by American-Standard Atomic Energy Division that curved tangential fuel plates as shown in Figure 4 will provide the most satisfactory arrangement in that these offer simple fabrication, good mechanical strength, and easy achievement of non-uniform radial distribution of fuel if it is decided to incorporate this design feature. (The ingenuity of the curved, radial fuel plate design with non-uniform loading that has been suggested is impressive, but it is felt that it will be difficult to fabricate.)
17. In a radial arrangement of fuel plates, the lateral heat conduction along the plates will not appreciably relieve the hot spot at the inner face of the core annulus.

CONTROL SYSTEM ANALYSIS

18. The amount of excess reactivity needed in the reactor is too large for reflector control alone. Burnable poison must be used to decrease the amount of control needed.
19. The reflector level control system has many disadvantages. The only advantage offered by the system is that it permits high neutron leakage, which may be used for external experiments. This can be achieved equally well by mechanical positioning of voids in the reflector. Mechanical control rods at the core-reflector interface decrease the flux in the reflector by only about 25% so they also permit substantial neutron leakage. Either of these two systems are better than the level control system.
20. The control system which seems preferable is to have an inner 5-cm annulus around the core filled with D_2O , the level of which can be suddenly dropped for scrams. This action will provide a maximum effect on reactivity of about 21%. The estimated delay time is 0.2 second. Outside the 5-cm

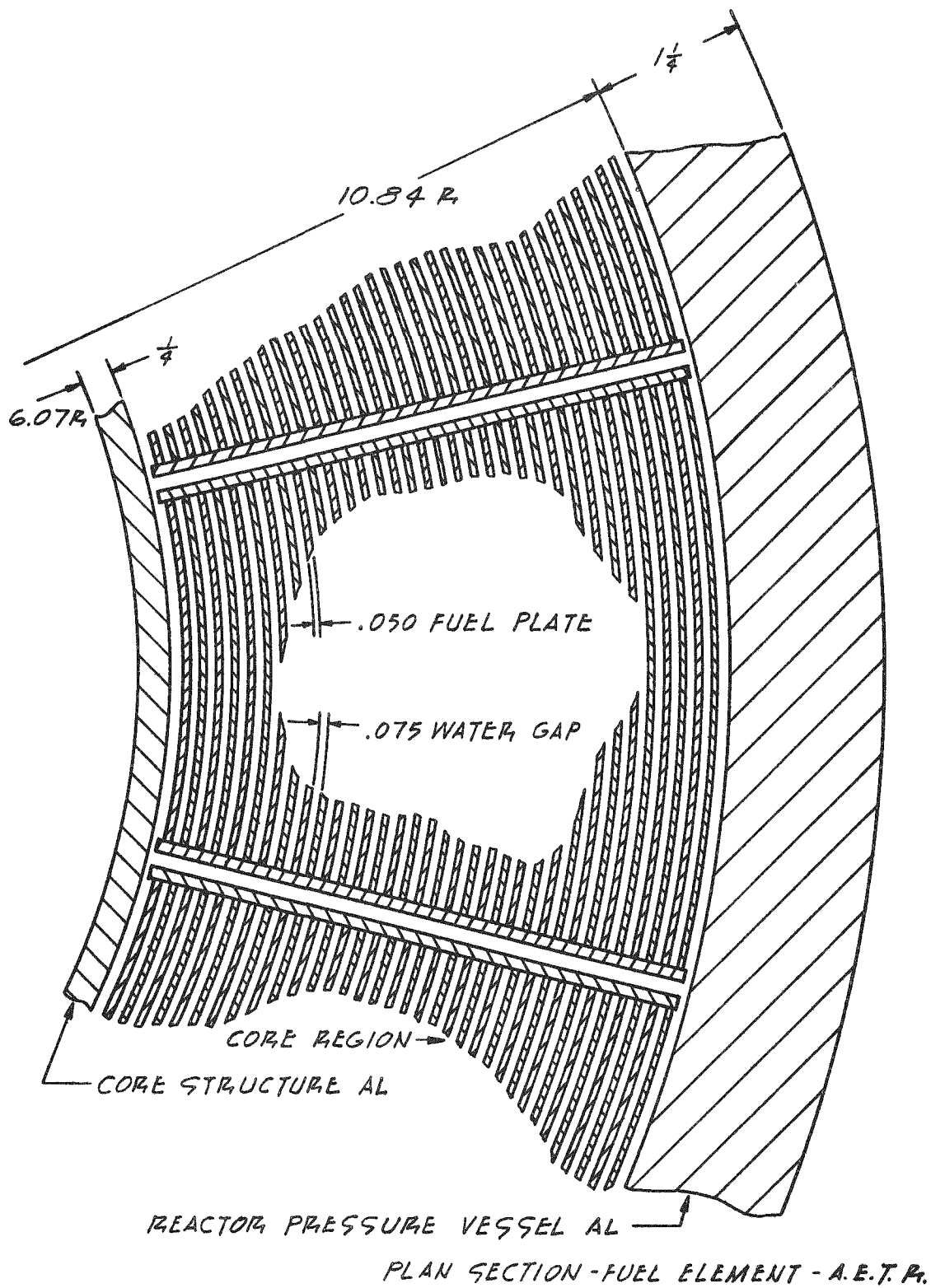


Figure 4 -- Section of the AETR Fuel Element

scram channel is a 20-cm annulus filled with borated D₂O for shimming. Change of boron concentration can change reactivity a maximum of 10%. Fine control seems best accomplished with mechanical rods in the reflector.

COUPLED VS. UNCOUPLED REACTORS

21. None of the advantages to be gained from coupling the reactors warrants sacrificing the flexibility of uncoupled reactors that permits shutdown on failure of a test element.

SHIELDING

22. Calculations indicate that about 8 feet of barytes concrete will be needed for shielding.

RESEARCH AND DEVELOPMENT PROGRAM

23. The R and D program necessary for the AETR encompasses the development of satisfactory materials, fuel elements, components, control system, and special kinds of equipment. The estimated time required by the program is 30 months. The cost is estimated to be about \$2,500,000.

COST ESTIMATING

24. It is estimated that the plant cost will be less than \$60,000,000. The exact figure is dependent of course on total cooling requirements and this depends on design decisions as to whether to have one, two, or more optimized reactor configurations, that is, whether to have all reactors identical or not, and on the practicality of non-uniform radial fuel loading. The annual operating cost is estimated at \$5,000,000, not including fuel. Fuel costs are about \$9,000,000/yr, again, of course, dependent on total power requirement, a figure of about 1500 MW having been used in these calculations.

V. RECOMMENDATIONS FOR FURTHER ANALYSIS

Before beginning the formal research and development program and detailed plant design it is recommended that the analysis be extended to include the following:

1. Determine the effect of the following design modifications or refined calculations on the power required to produce the flux level specified for the AETR design:

Determination of an optimum reactor configuration for the smaller loops and from consideration of total power savings and a forecast of experiments for the AETR, a decision as to whether there should be one, two, or more, types of reactor configurations in the seven-reactor complex.

- b. Further analysis of possible methods of alleviating the problem of the hot spot at the inner face of the core annulus, e.g., non-uniform radial distribution of fuel by varying the content per plate or by having cylindrical regions of different plate spacing (in the tangential arrangement) or non-uniform fuel distribution in each plate in the radial arrangement
 - c. Performances of a few, two-dimensional calculations to determine flux contours in more detail.
 - d. Investigation of the true energy distribution of the slow neutrons -- the deviation from Maxwellian -- and the effect of this on the thermal cross sections, reactivity and flux distributions
 - e. Experimental determination of the "age" in Al-H₂O mixtures of high Al/H₂O ratio and adjustment of the few group constants accordingly (this experiment can probably be done using an existing reactor, such as the UTR-1* and a source plate).
2. Evaluate an AETR core design with uranium-oxide fuel elements and compare the merits of this design with the U-Al alloy design, considering physics characteristics, safety, and economics.
 3. Evaluate further the use of heavy water as coolant-moderator as compared to light water

4. Make a reference design of both a chemical-mechanical and a completely mechanical control system and compare the merits of the two systems, considering operating characteristics, safety, and economics, to allow an objective selection of the best system.
5. Extend the analysis of the AETR core heat-transfer conditions with particular attention devoted to determining the possibilities of operating with nucleate boiling and to other such possible advances over MTR-ETR technology and operating philosophy.
6. Analyze the reactivity losses that will be sustained in the reactor with particular attention to non-uniform fuel burnup. Determine an appropriate form, quantity, and distribution of burnable poison for the core.
7. Determine the void and temperature coefficient and the contributing effect on these of various test loops.
8. Analyze the behavior of the reactor under transient conditions and make a preliminary safeguards analysis. This should include a study of the reactor response to sudden stoppage of flow of an absorbing material in a loop, for example, and the effect of suddenly flooding the test holes in the D_2O reflector region.
9. Pull the graphite and core tanks in the UTR-1 and mock up the AETR design to experimentally check the flux distributions which are predicted theoretically.

* UTR-1 is the first production model of American-Standard Atomic Energy Division's University Training Reactor, and is now in operation at Mountain View, California.

VI. OPTIMIZATION OF FLUX AND POWER LEVEL

The objective of the AETR physics analysis is the optimization of the fuel region and internal moderator annuli dimensions to achieve maximum flux in the central, loop region for a given total power in the fuel region. The desired average unperturbed thermal flux in the loop region is 1.5×10^{15} n/cm²/sec. Since the analysis represents an independent check and refinement of the calculations of the Internuclear Company, the validity of a three-group model for a reactor with such a thin annular core was first explored. Part of the effort was thus a preliminary verification that the methods to be used in the optimization calculations would be reasonably accurate. This is described in detail in Appendix A; in brief it consisted of a comparison of the few-group model with a 22-group calculation. The 22-group computation was used throughout all the work as a means of obtaining good constants for the few-group calculations. Experimental data on such quantities as age to thermal in Al-H₂O mixtures were utilized.

It is not difficult to design a test reactor that will provide a thermal flux of 1.5×10^{15} in an H₂O cooled loop because the loop coolant itself acts to "trap" the flux. The difficult job is to design a reactor that will provide this specified flux in a liquid metal or gas-cooled loop, especially the large 7-in. loop. Therefore the AETR optimization analysis was performed for the 7-in. liquid metal loop.

Results will be given on individual optimization computations of power density, total power, and critical mass with the variables being the annular thickness of the inner water annulus, the metal-to-water ratio in the core, and weight percent fuel in the fuel plate meat.

A nine-regional, one-dimensional and three-neutron-group model was used to obtain the optimum system. All values of reactor power required to achieve the specified flux in the test section are evaluated when the reactor is at the end of the run and with $k_{\text{eff}} = 1$. Hence all the cores contained the equilibrium value of samarium and xenon poisoning. The reactor geometry and composition used as a basis for optimizing critical mass, reactor power and power density (one at a time) as a function of metal-to-water ratio are as shown in Table III.

TABLE III

REACTOR PARAMETERS AND COMPOSITION OF REGIONS USED FOR OPTIMIZATION

<u>Region</u>	<u>Annular Thickness ($R_o - R_i$) cm</u>	<u>Composition</u>
1	8.89	Sodium (200°F)
2	.1589	Stainless Steel
3	1.112	Void
4	1.27	Aluminum
5	6.0325	Water
6	0.635	Aluminum
7	Varied	Core M/W ratio and fuel con- centration varied
8	2.222	Aluminum
9	25.4	D ₂ O

Two possible designs for the AETR core were surveyed, one case having aluminum wedges to fill the triangular spaces between rectangular fuel elements in the annulus and the other case having a continuous core without the aluminum wedges.

A. THE CORE WITH ALUMINUM WEDGES

Two values of fuel plate loading are examined, namely 25 and 35% by weight of uranium in the uranium-aluminum alloy. The respective U-235 concentrations as a function of metal-to-water ratio are plotted in Figure 5.

The critical mass was calculated with respect to the metal-to-water ratio for both types of U-235 concentrations. The results are plotted in Figure 6. This graph shows there is a definite minimum critical mass of 8.4 kg and 9.0 kg for 25 and 35% alloy respectively. The minimum critical mass occurred at the metal-to-water ratio of 0.5 ($M/W = 0.5$) for both cases.

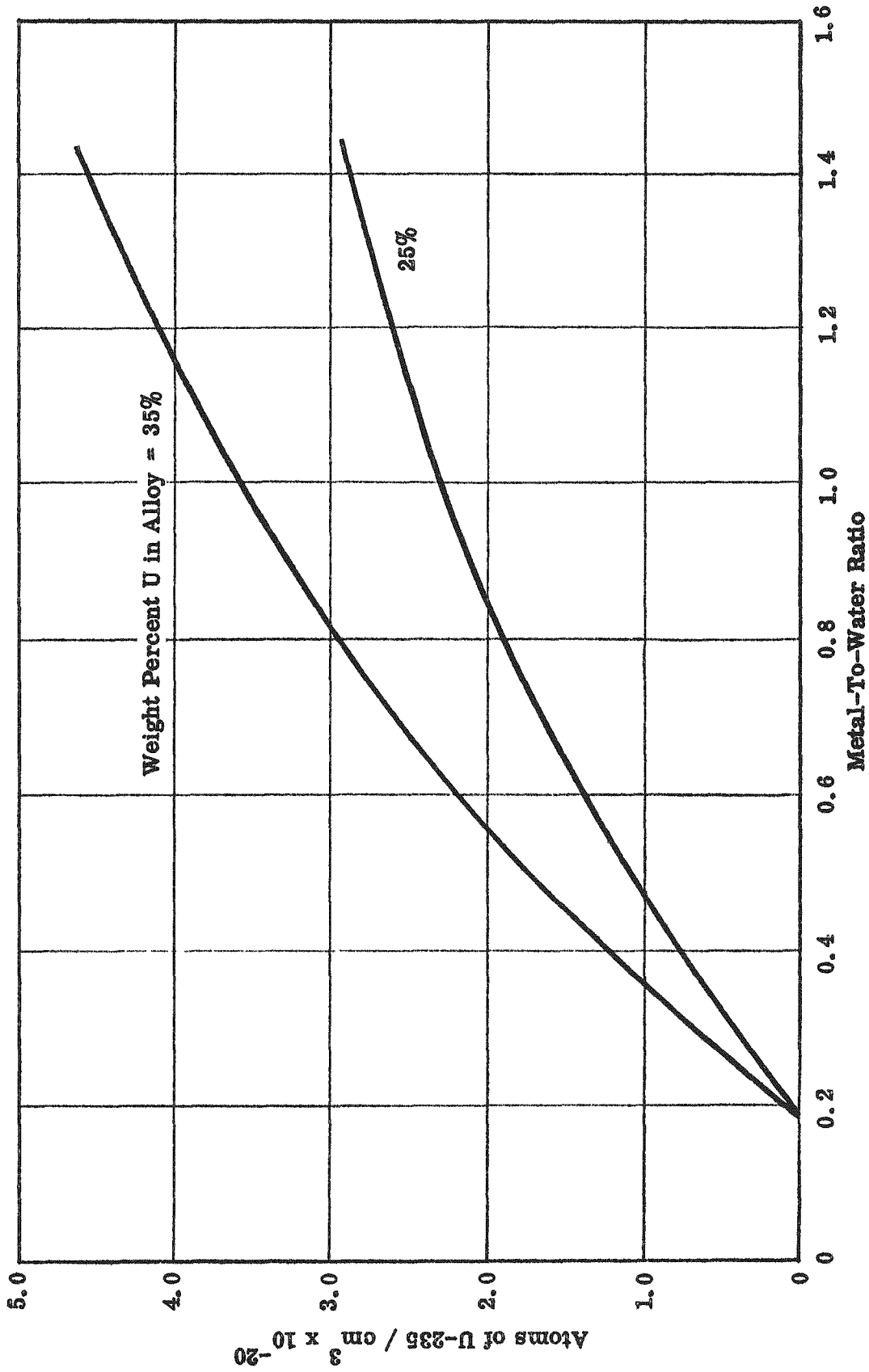


Figure 5 -- Atomic Density in Core Region vs M/W Ratio (With Wedges)

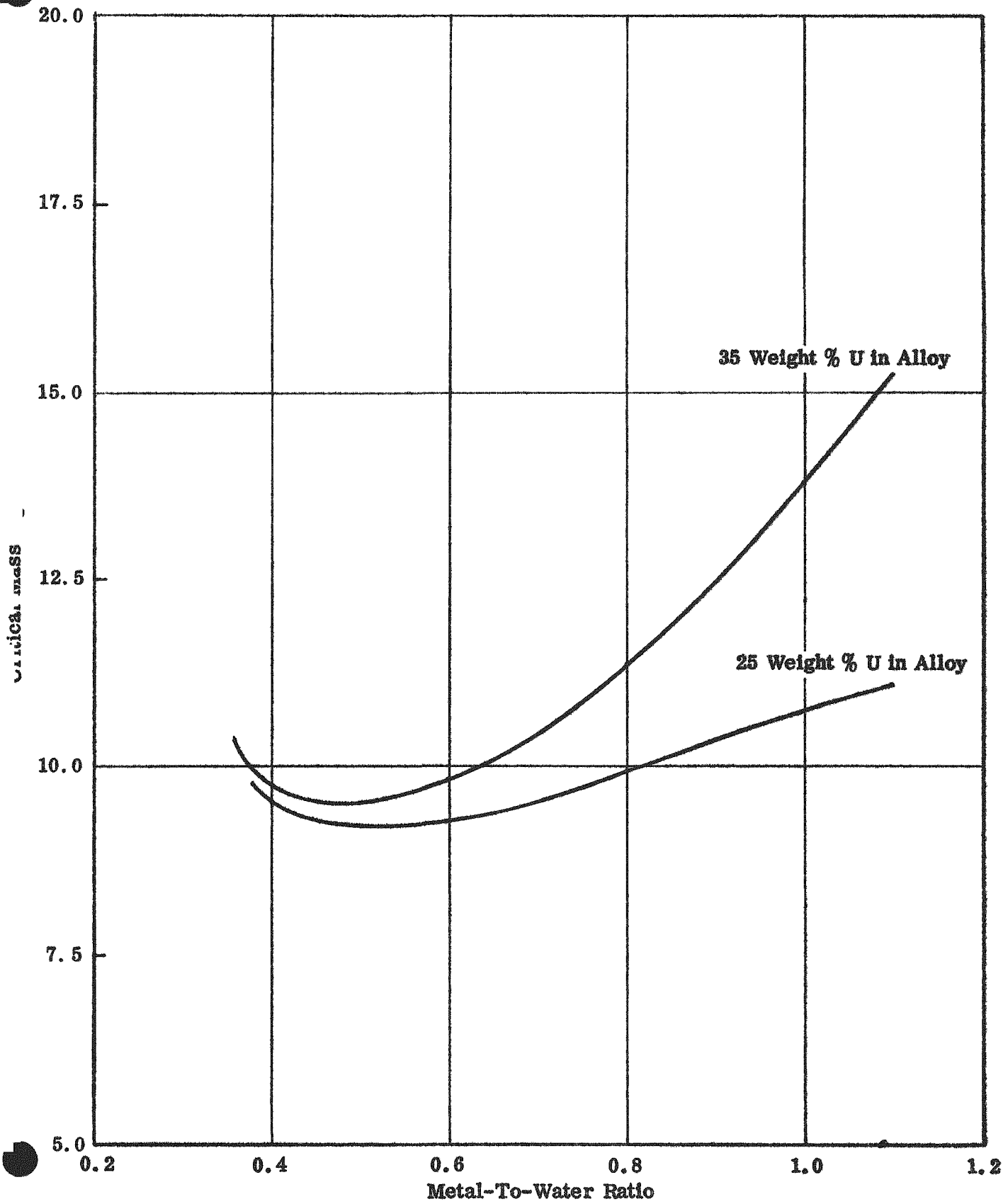


Figure 6 -- Critical Mass vs M/W for Core With Wedges

The reactor power and the power density required to achieve the specified flux in the test section as a function of metal-to-water ratio were then calculated. The results are plotted in Figures 7 and 8.

The power and power density required for the core of minimum critical mass are not optimum values. Because of heat transfer limitations it develops that power density is a more important constraint in the design of the AETR than is critical mass. The core with minimum critical mass has really little significance. Figure 7 seems to indicate that the higher the metal-to-water ratio and weight percent of uranium in the fuel plate the lower the reactor power. However, the computations for no wedges, to be discussed below, demonstrate that a minimum reactor power vs weight percent fuel would appear if further choices of weight percent fuel were examined.

The survey of average power density vs metal-to-water ratio, Figure 8, shows that the power densities required for AETR will be very high. For a given thickness of core annulus the aluminum wedge area is not available for heat removal purposes; hence by removing the aluminum wedges and replacing this volume with core matrix the required power density can be decreased. For this reason the desirability of a core design without wedges is treated in more detail.

B. THE CORE WITHOUT ALUMINUM WEDGES

Three different values of fuel plate content are used for this optimization survey, namely 15, 25 and 35% by weight of uranium in the alloy. The respective U-235 concentrations as a function of metal-to-water ratio are plotted in Figure 9.

It was pointed out earlier that the core of minimum critical mass has little significance in the AETR. Hence the optimization of critical mass was not repeated for this case.

The reactor power and the power density required to achieve the desired flux in the test section as a function of core metal-to-water ratio are determined and the results are plotted in Figures 10 and 11. It will be noted from the curves in Figure 10 that a definite minimum exists for total power

b

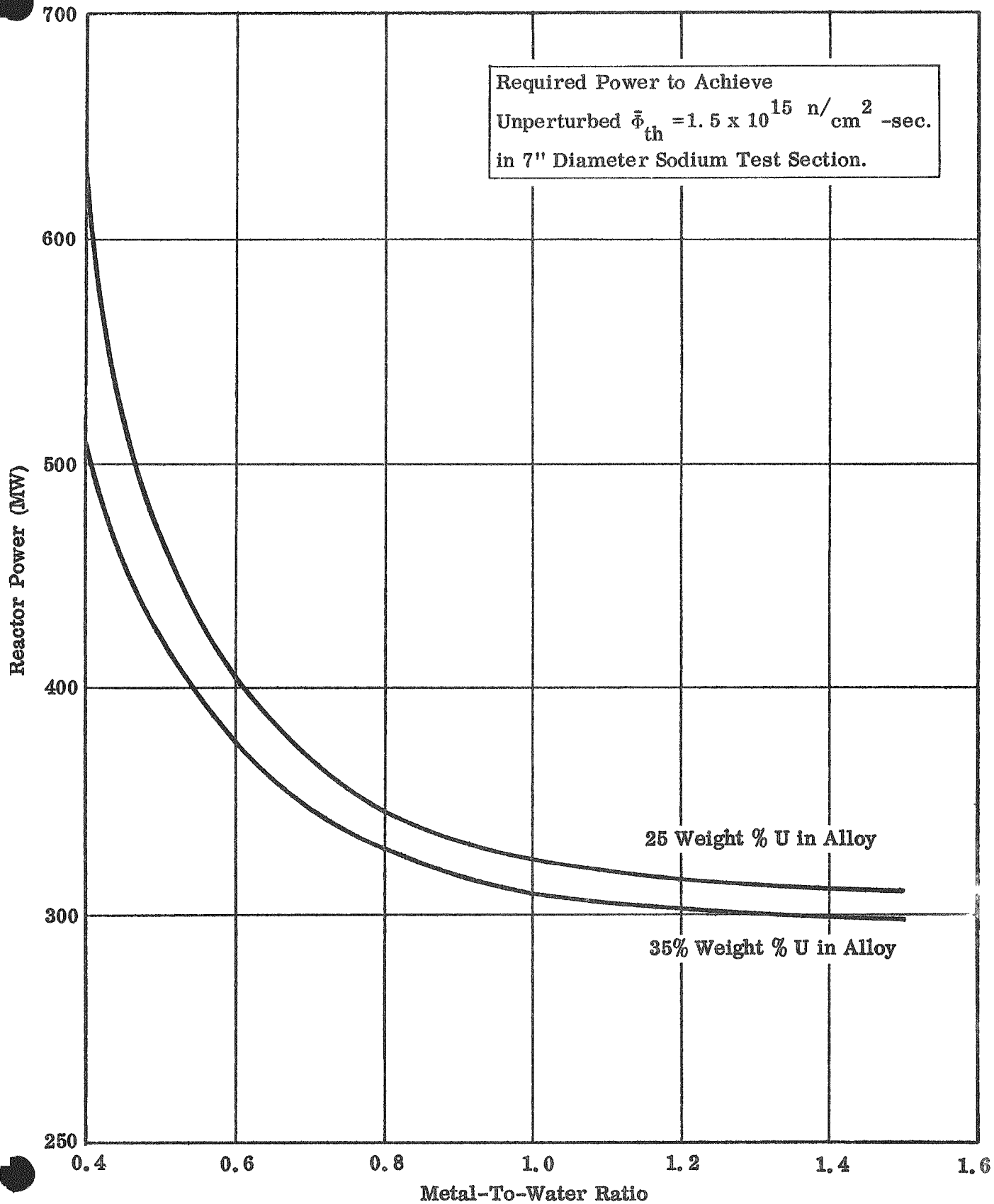


Figure 7 -- Reactor Power vs M/W ratio for Core With Wedges

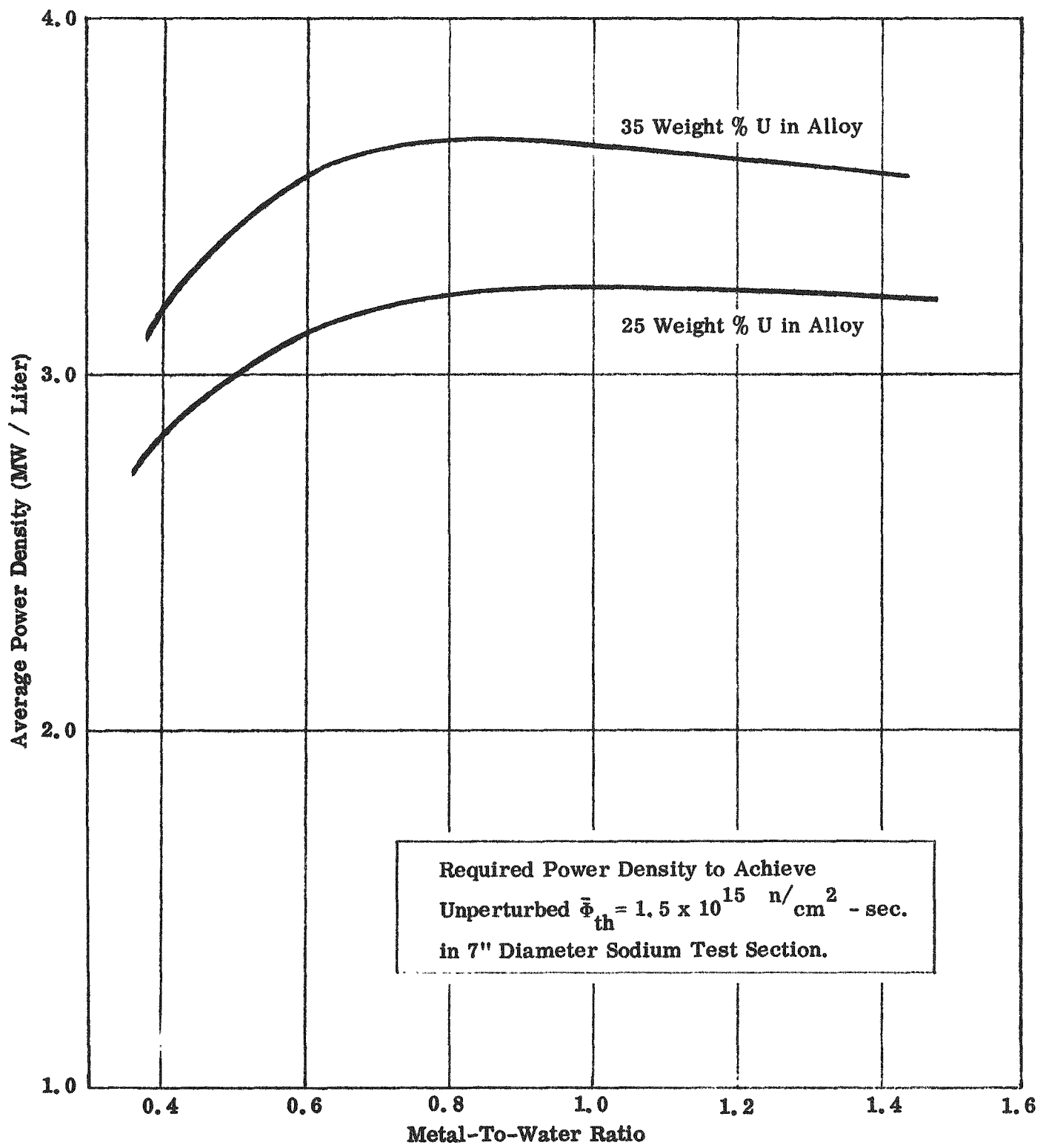


Figure 8 -- Average Power vs M/W Ratio for Core With Wedges

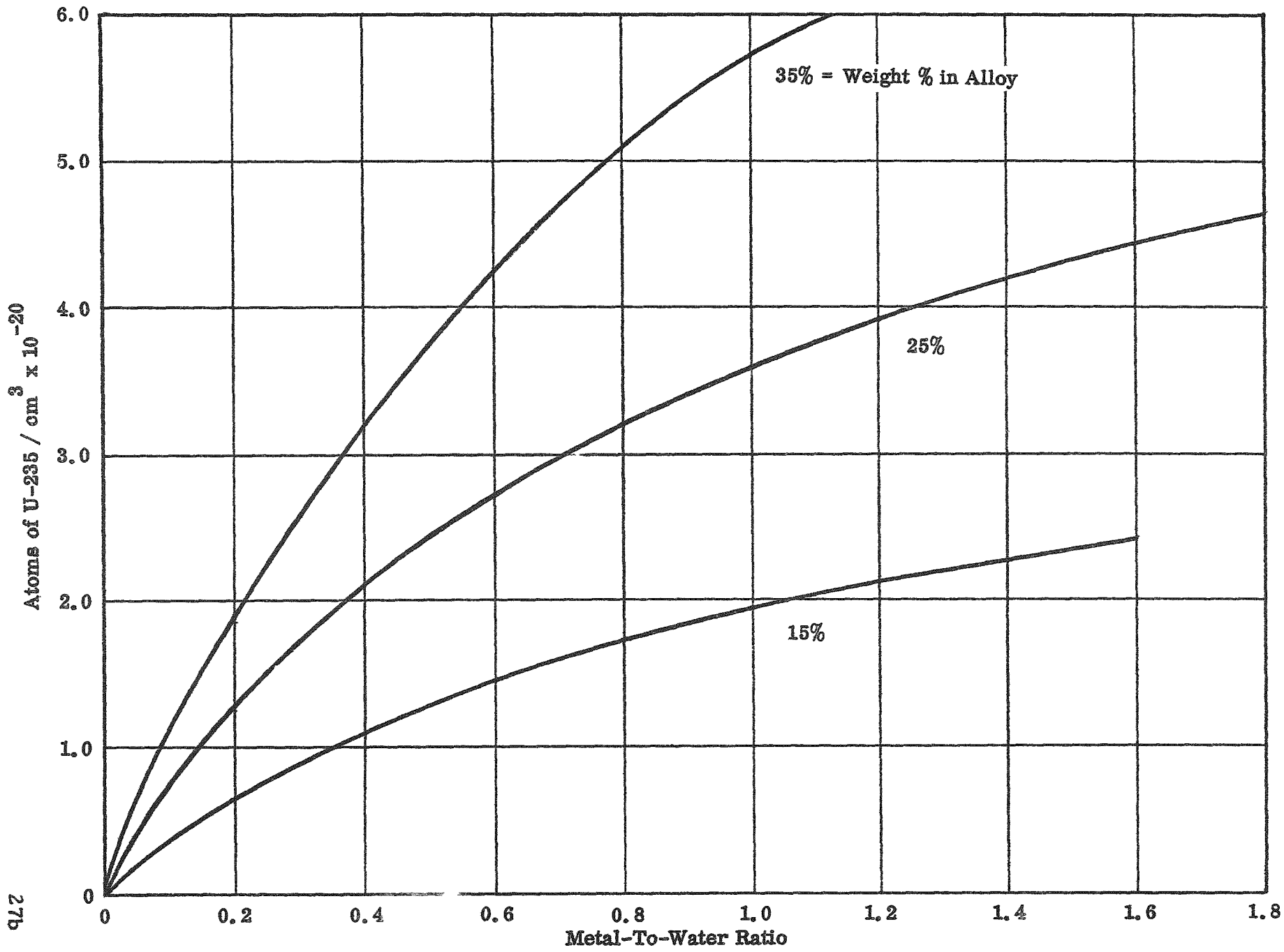


Figure 9 -- Atomic Density for Core With No Wedges

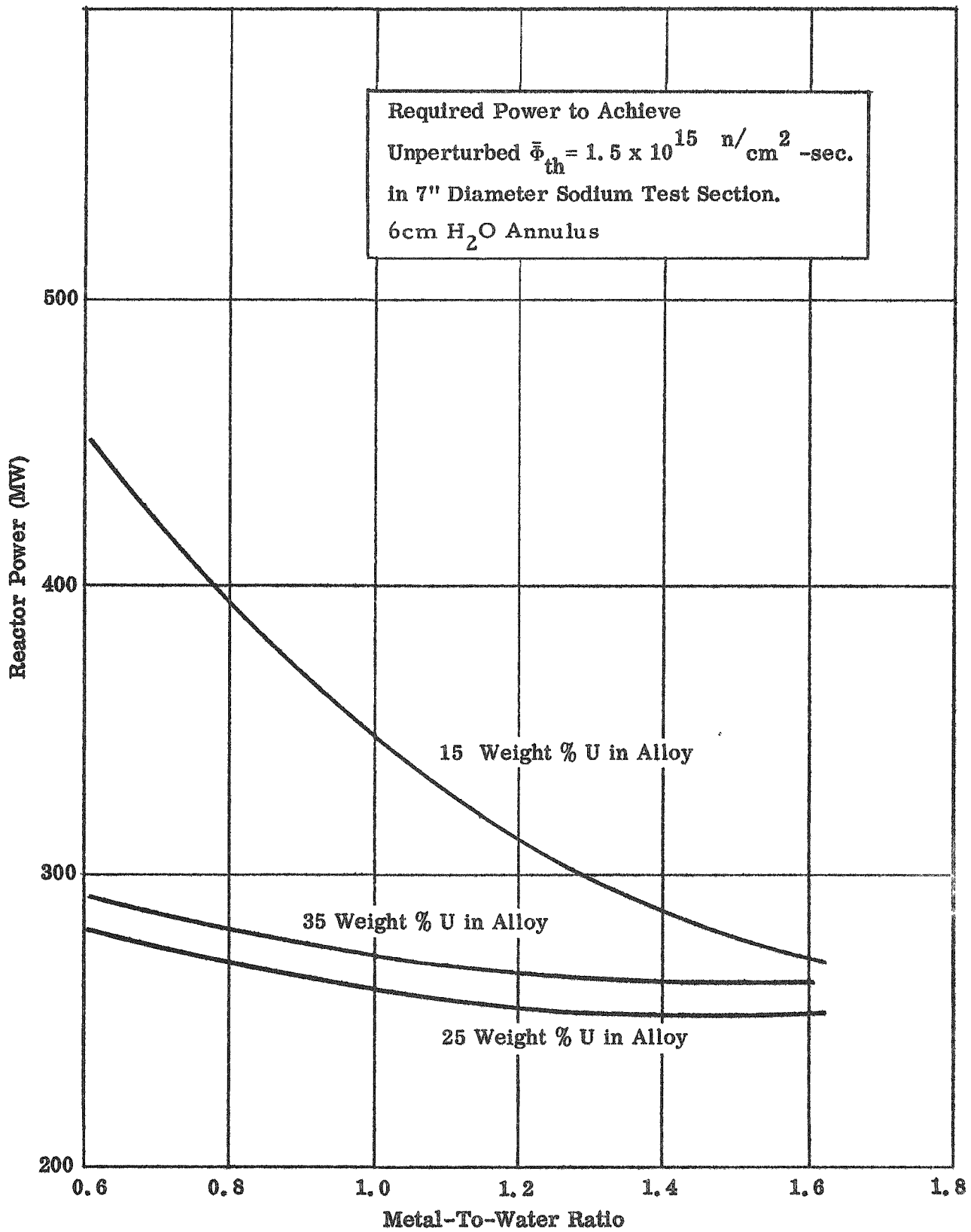


Figure 10 -- Reactor Power vs M/W Ratio for Core With No Wedges

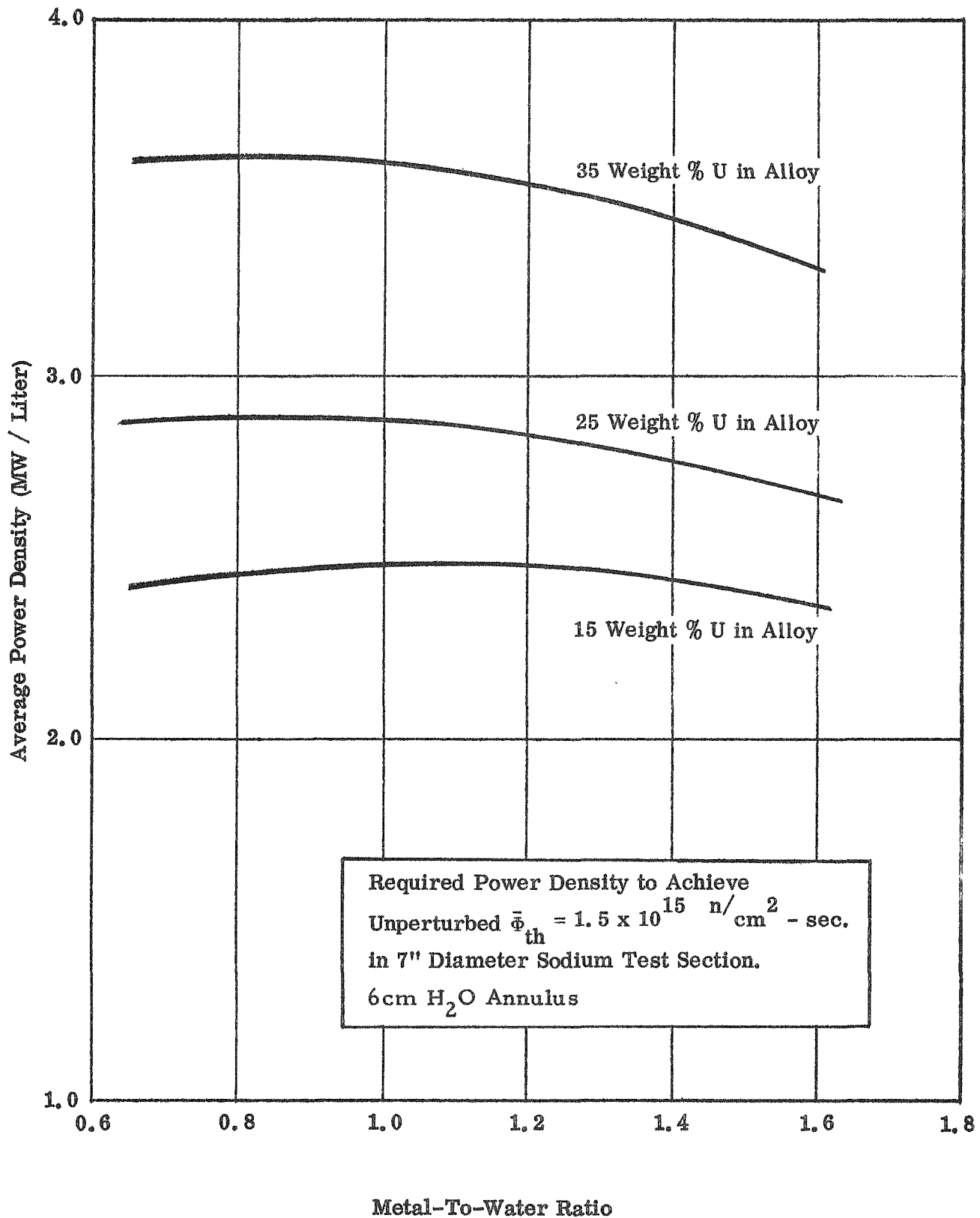


Figure 11 -- Average Power Density vs M/W Ratio for Core With No Wedges

as a function of weight percent fuel in the fuel plates. This is shown more clearly in Figures 12 and 13, which present the reactor power and volume as a function of weight percent fuel at a constant metal-to-water ratio of 0.69. The total power of a reactor is the sum of the contribution from the thermal, intermediate, and fast fissions. At low weight percent fuel the thermal fissions are the main contributors to the reactor power because the system is well moderated. As the weight percent fuel increases, the power from thermal fission decreases rapidly and eventually becomes virtually constant. The reactor power from the intermediate fissions increases for large weight percent fuel; eventually it rises to a point where it has considerable contribution to the total reactor power. The contribution of fast fissions is small. Because of the behavior of the contribution from intermediate fissions, the total power exhibits a definite minimum.

The design of the core will be dictated by the power density required to achieve the specified flux in the test section. The 15% figure for weight of uranium in the alloy is the most attractive as far as required power density is concerned. However, even the 15% case does not meet the limitations imposed by heat transfer, fluid flow, and metallurgy. The achievable average power density dictated by these limitations is about 1.6 MW/liter at 0.69 M/W ratio for the peak-to-average power ratio determined for the 15% case. It appears from Figure 11 that the flux specification cannot be achieved with this average power density. Slightly higher fluxes could probably be achieved under the limitations by going to a lower weight percent fuel, but since Figure 10 indicates that such high values of total power would be necessary, lower values of fuel percent were not investigated. It may be seen from Figure 10 that the required total power will be very high even for 15% fuel plates. This is the result of both a non-optimum weight percent fuel and non-optimum metal-to-water ratio, that is, non-optimum from the total power standpoint. It might appear at first glance at the graphs that large decreases in power requirement could be achieved for a small reduction in flux specification by using 25% plates or a higher metal-to-water ratio. However, this is not the case, because the radial peak-to-average power density ratio increases severely for higher plate loading or closer spacing, with the result that the average power density must be much lower than in

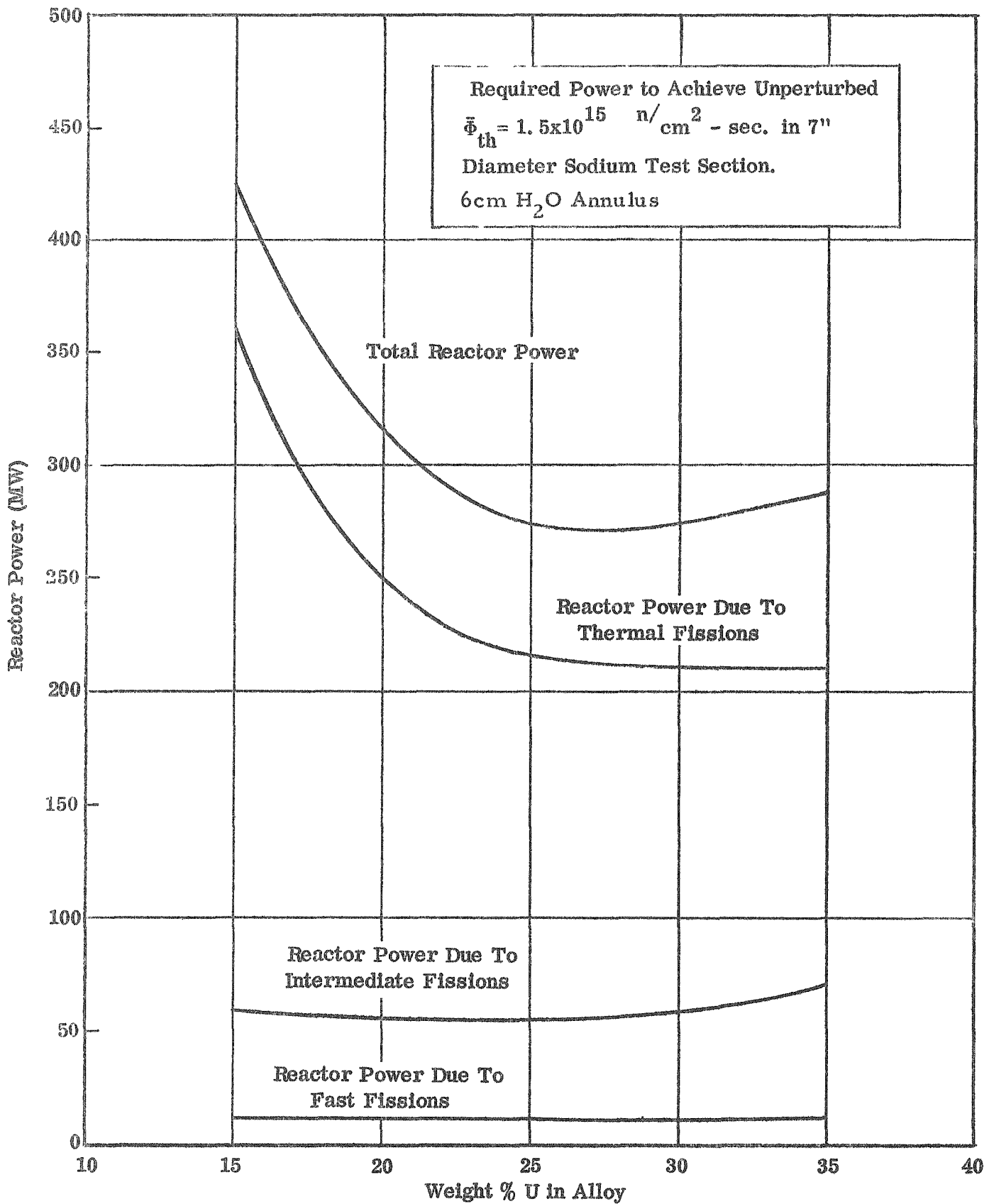


Figure 12 -- Reactor Power vs Weight Percent of Uranium in Alloy

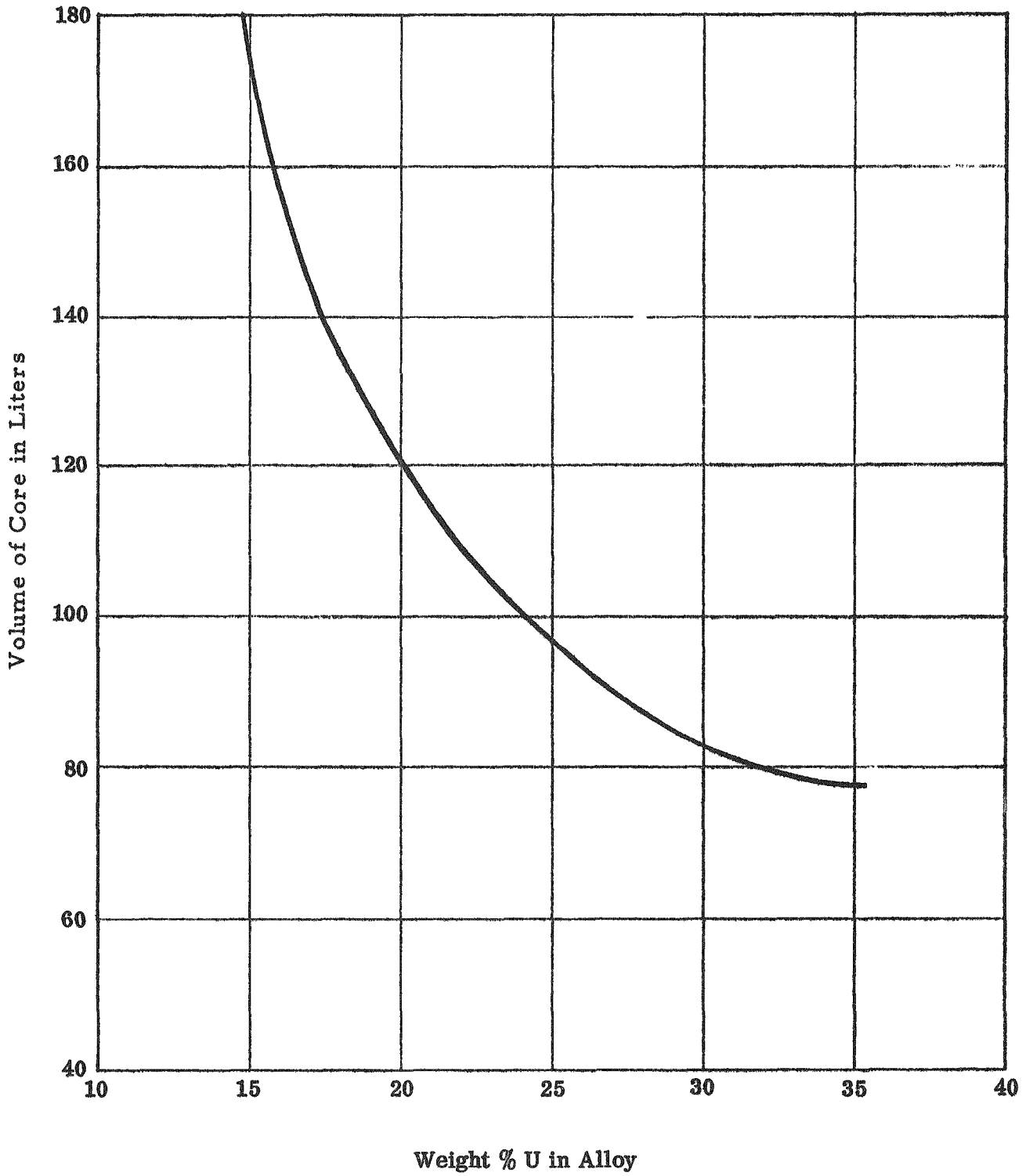


Figure 13 -- Reactor Volume vs Weight Percent of Uranium in Alloy

the 15% loaded case. The over-all result is that the achievable flux and required core power are roughly proportional, and it thus seems best to choose the design that can operate at the greatest total power, that is, the 15% plates at 0.69 M/W ratio.

The parameters used for the optimization of the inner reflector (H_2O) annulus thickness were similar to those tabulated in Table III, except that the core used to study the inner reflector thickness was cold and clean and the metal-to-water ratio was unity. The required reactor power as a function of inner reflector thickness is plotted in Figure 14. The result indicates a 4 cm thickness of H_2O annulus will require the minimum power to achieve the specified flux in the 7-in. diameter sodium-cooled test section. But the 5 cm H_2O annulus requires minimum power density. The power density vs thickness of H_2O annulus is plotted in Figure 15. Although the optimization of H_2O annulus for the recommended core was not done, it has been verified that the required power density of the recommended core with 4 cm water annulus is lower than the core with 6 cm water annulus.

As the result of the survey described above, the parameters were established for what may be called the maximum flux design. These specifications were presented in Table I, Chapter IV. It is possible that slightly higher fluxes could be achieved by using lower fuel content per plate, but the cost in total power is prohibitive. The core will accommodate the 7, 5 and 3-in. sodium-cooled test sections and 4 and 3-in. water-cooled test sections. The required power is evaluated for achieving the average unperturbed thermal flux of 1.5×10^{15} n/cm²/sec in the test section where possible. The required average power density for the three sodium-cooled-loop reactors exceeds the heat transfer limitation, which is 1.59 MW/liter. Hence the sodium-cooled-loop reactors can be operated at only 228 MW maximum, which means that the average unperturbed thermal flux in the sodium-cooled test section will be somewhat lower than the desired flux (1.5×10^{15}). Details of the inner, 7" region for the various loops are given in Table IV. The available fluxes in the test section with respect to reactor power and power density are given in Table II in Chapter IV.

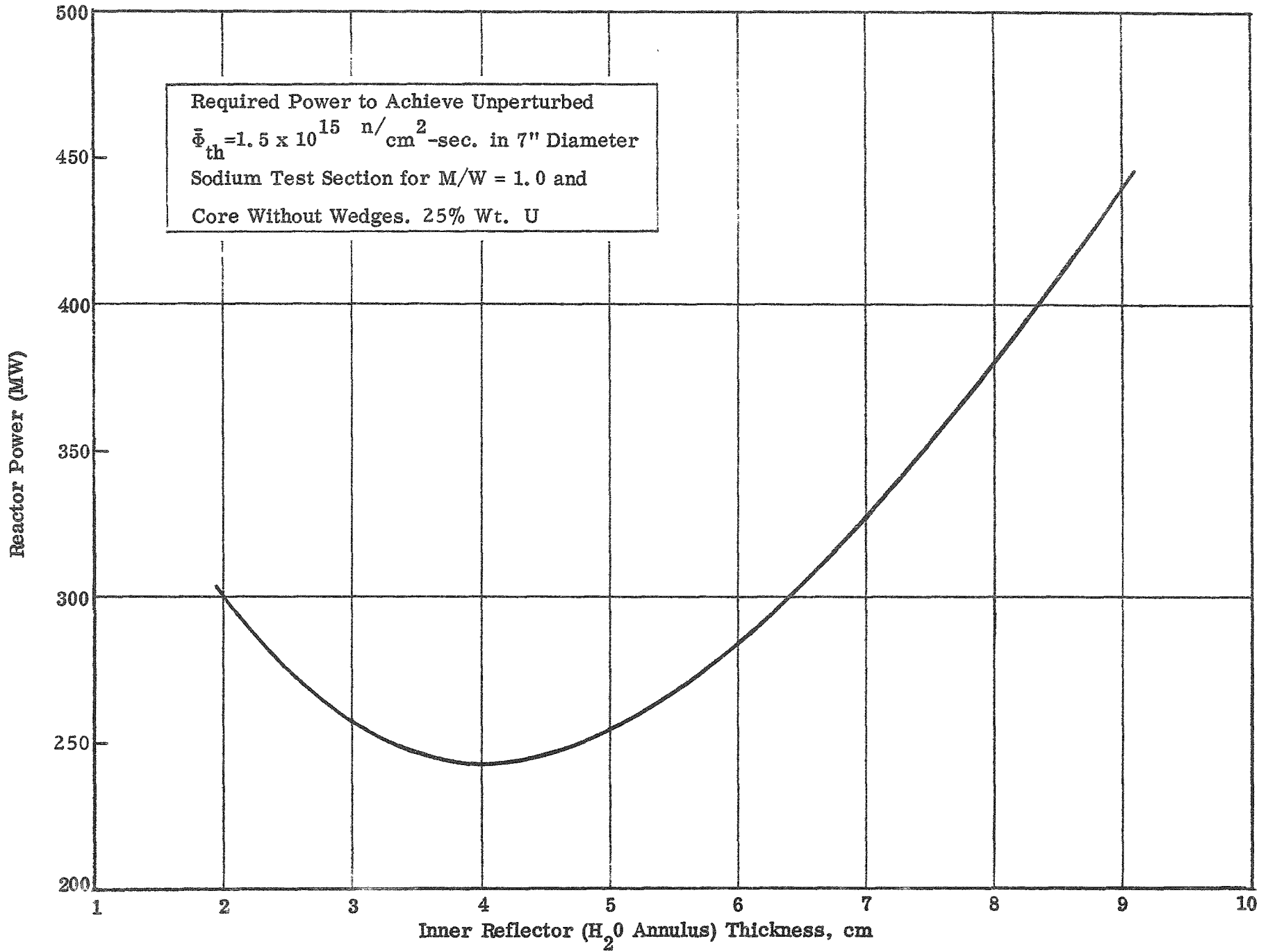


Figure 14 -- Reactor Power vs Thickness of Inner H₂O Annulus (M/W Ratio = 1.0)

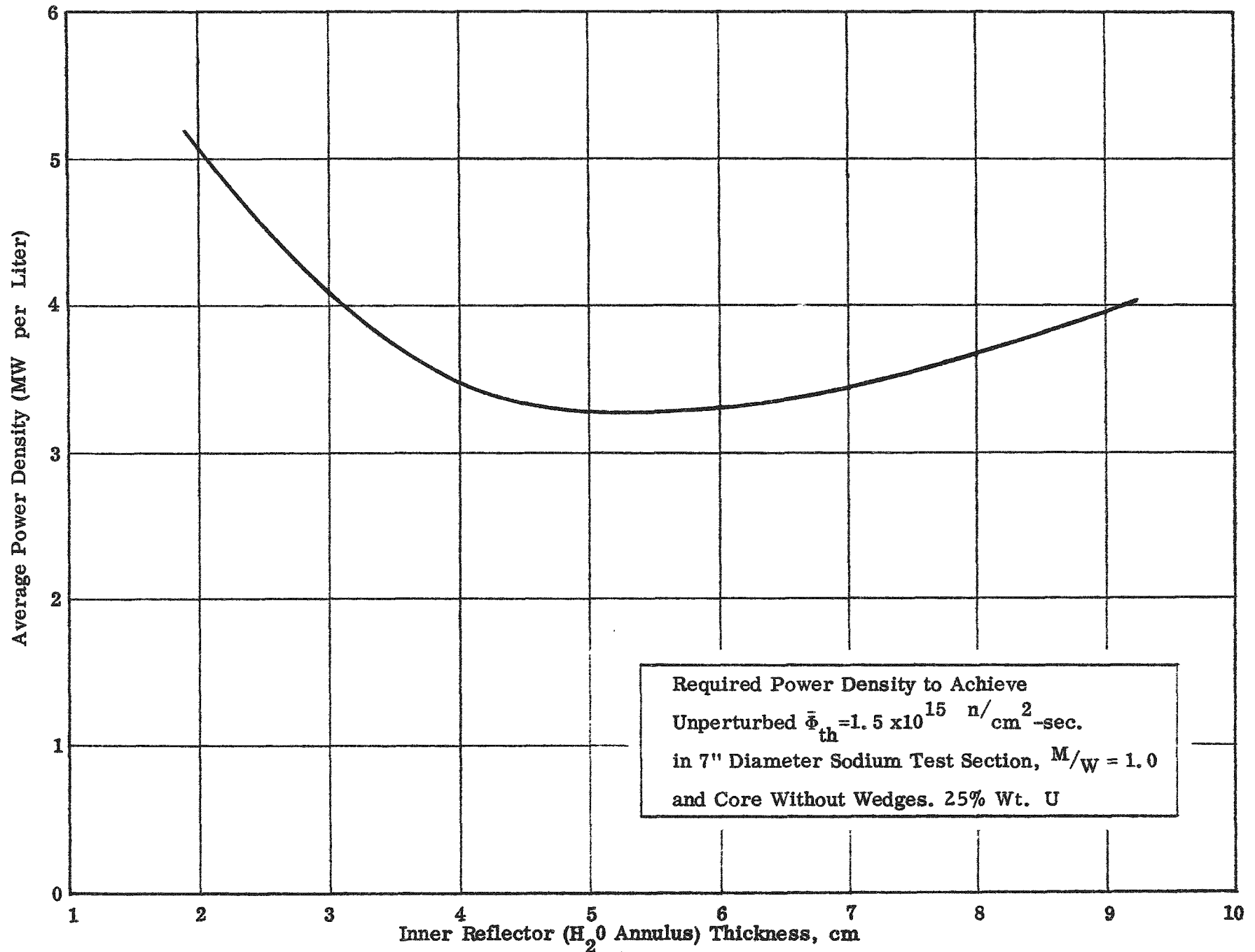


Figure 15 -- Average Power Density vs Thickness of Inner H₂O Annulus (M/W Ratio = 1.0)

The radial flux distributions at the midplane for 4 and 3-in. diameter water-cooled and 7, 5, and 3-in. sodium-cooled-loop reactors are plotted in Figures 16-20.

TABLE IV

DETAILS OF INNER REGION FOR THE MAXIMUM FLUX DESIGN*

Test Loop Region	4-in. H ₂ O Loop		3-in. H ₂ O Loop		7-in. Na Loop		5-in. Na Loop		3-in. Na Loop	
	R _O (cm)	Comp.	R _O (cm)	Comp.	R _O (cm)	Comp.	R _O (cm)	Comp.	R _O (cm)	Comp.
1	5.08	H ₂ O	3.81	H ₂ O	8.89	Na	6.35	Na	3.81	Na
2	5.239	SS	3.969	SS	9.049	SS	6.509	SS	3.969	SS
3	10.161	Void	(Region 3 through 9 same for all reactors)							
4	11.431	Al								
5	15.431	H ₂ O								
6	16.066	Al								
7	27.534	Core								
8	29.756	Al	R _O = outer radius of the region							
9	55.156	D ₂ O	Comp. = composition of the region							

* All cores are 91.44 cm high and 7 cm reflector saving added to the top and bottom of the core. Cosine distribution was assumed in longitudinal directions. The longitudinal $\frac{\phi_{\max}}{\phi_{\text{avg}}} = 1.38$.

All density and thermal absorption cross sections are corrected to 200°F values except in Region One. For the water in Region One the density and the thermal absorption cross section used are 600°F and 2000 psi values. For the sodium in Region One the density is equivalent to 1500°F and 300 psi and thermal absorption is corrected to 200°F.

Midplane Neutron Flux, $10^{15} \text{ n/cm}^2\text{-sec.}$

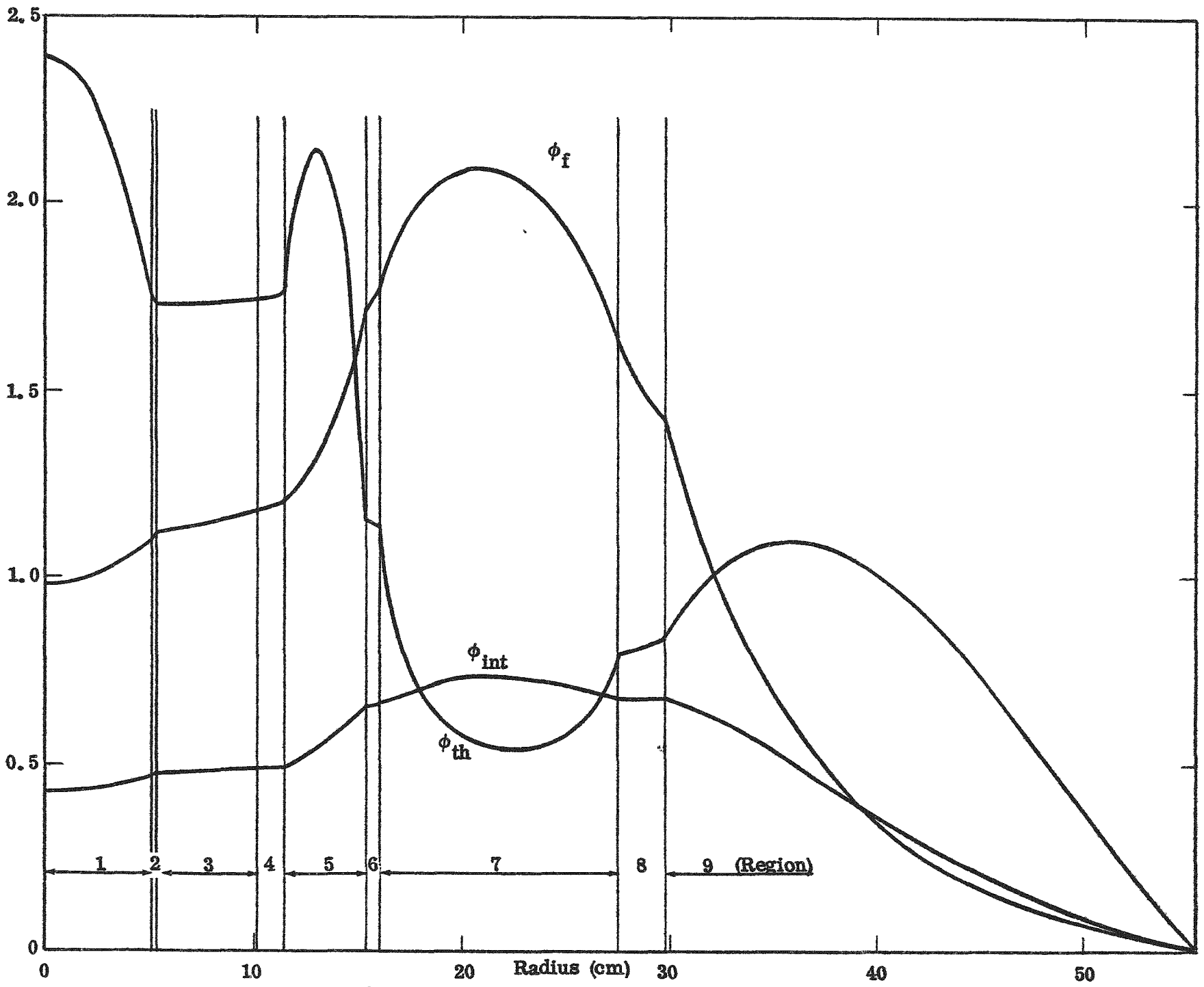


Figure 16 -- Radial Flux Distribution in a 4-in. Water Loop

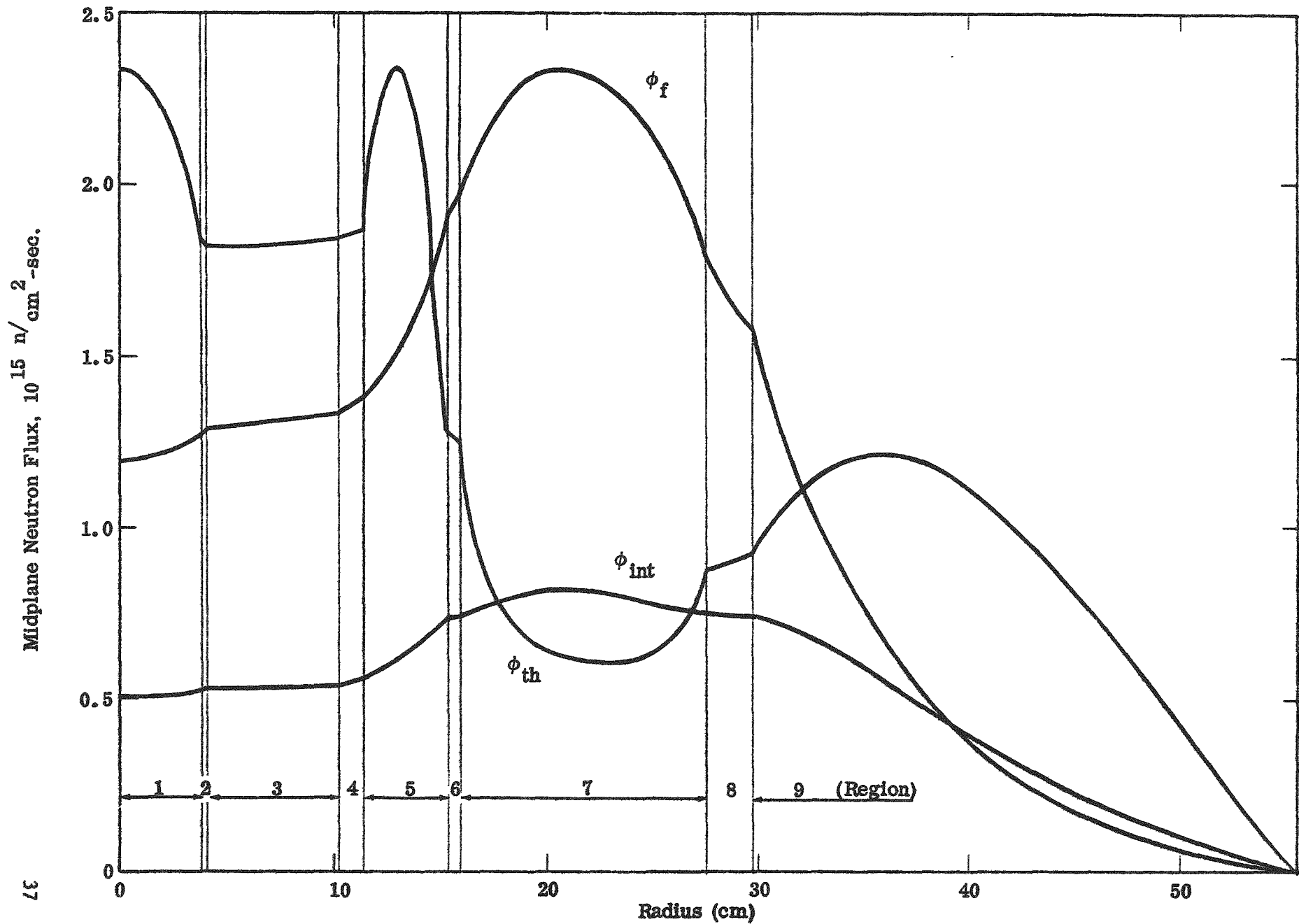


Figure 17 -- Radial Flux Distribution in a 3-in. Water Loop

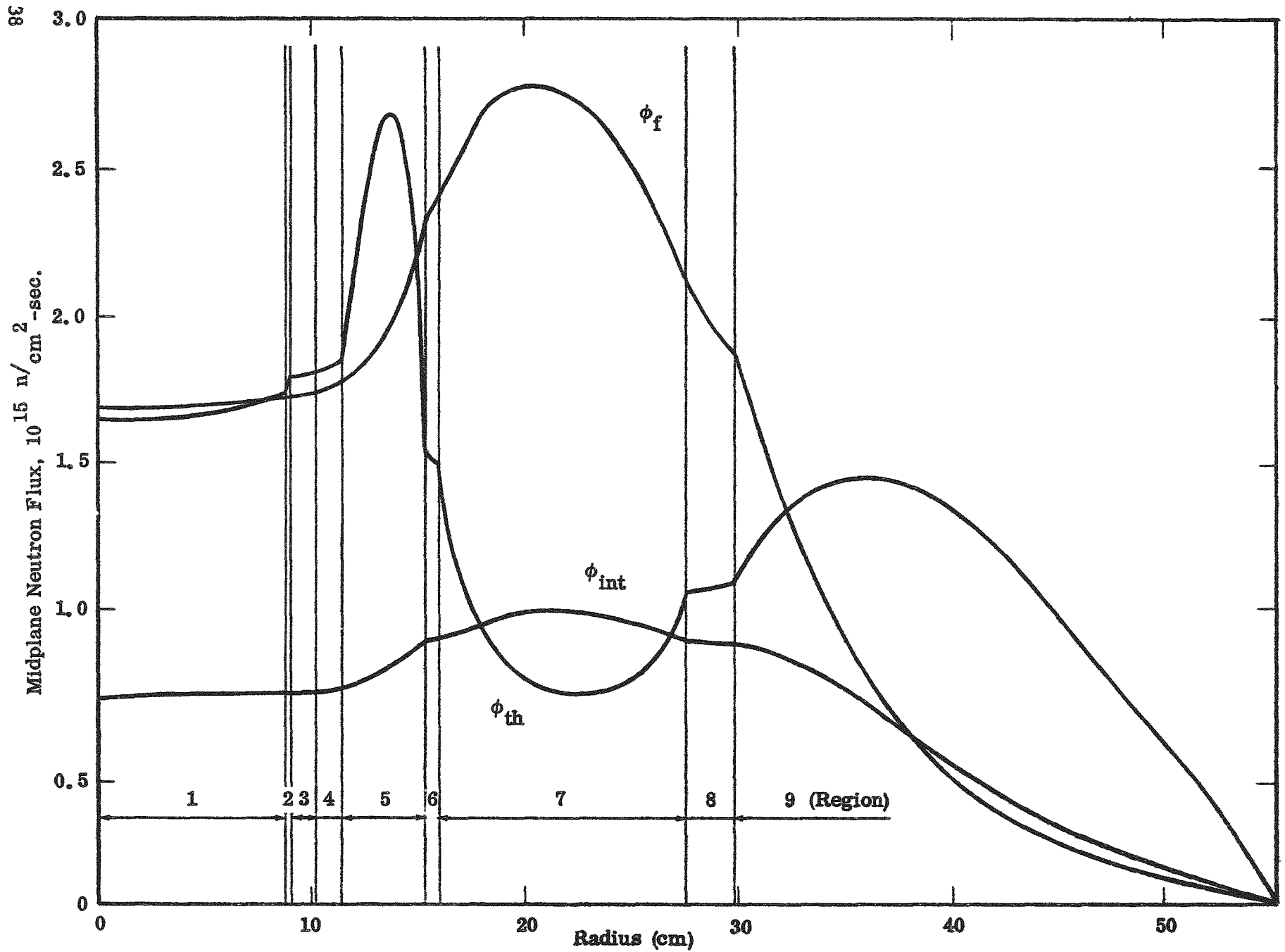


Figure 18 -- Radial Flux Distribution in a 7-in. Sodium Loop

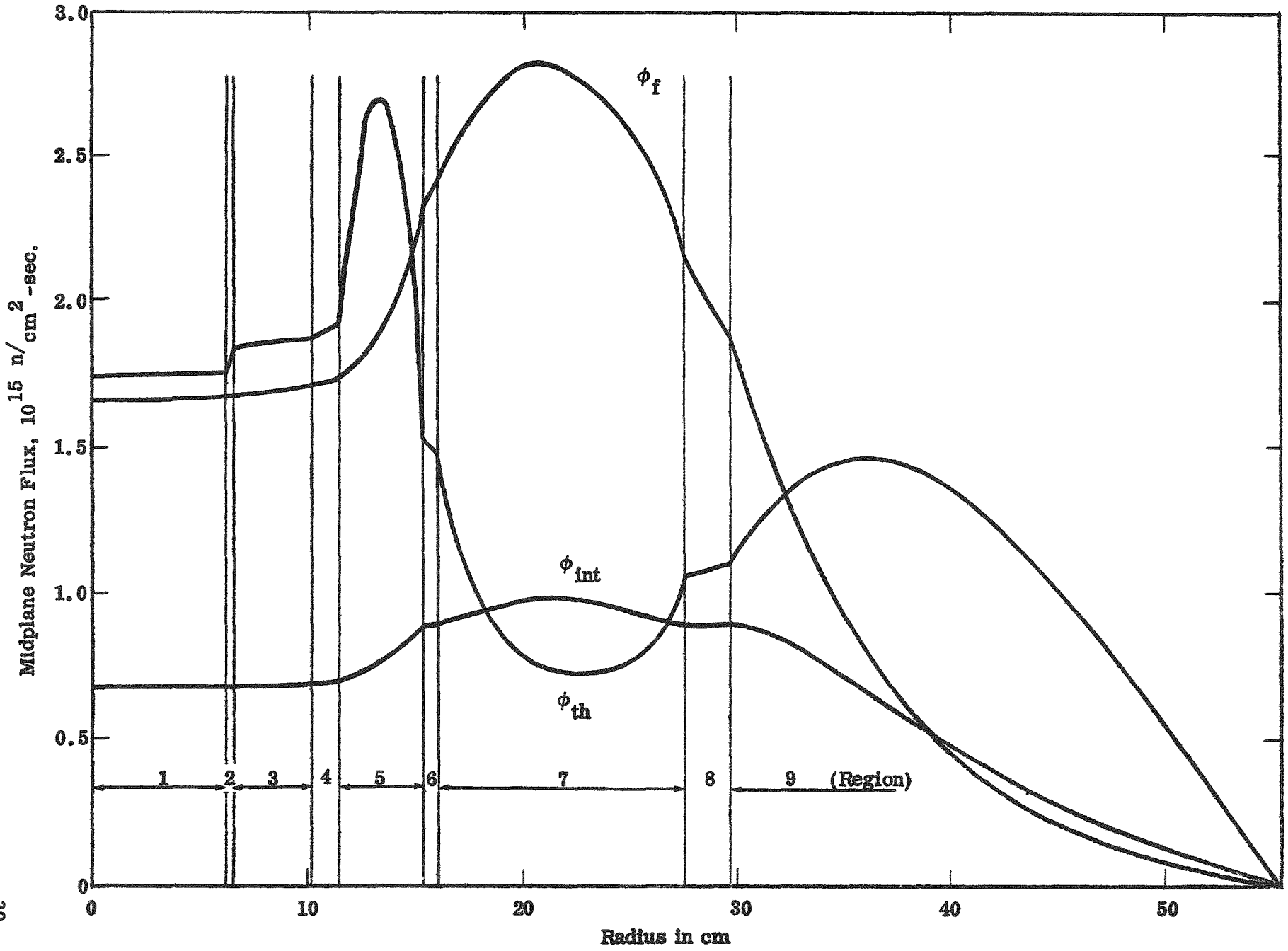


Figure 19 -- Radial Flux Distribution in a 5-in. Sodium Loop

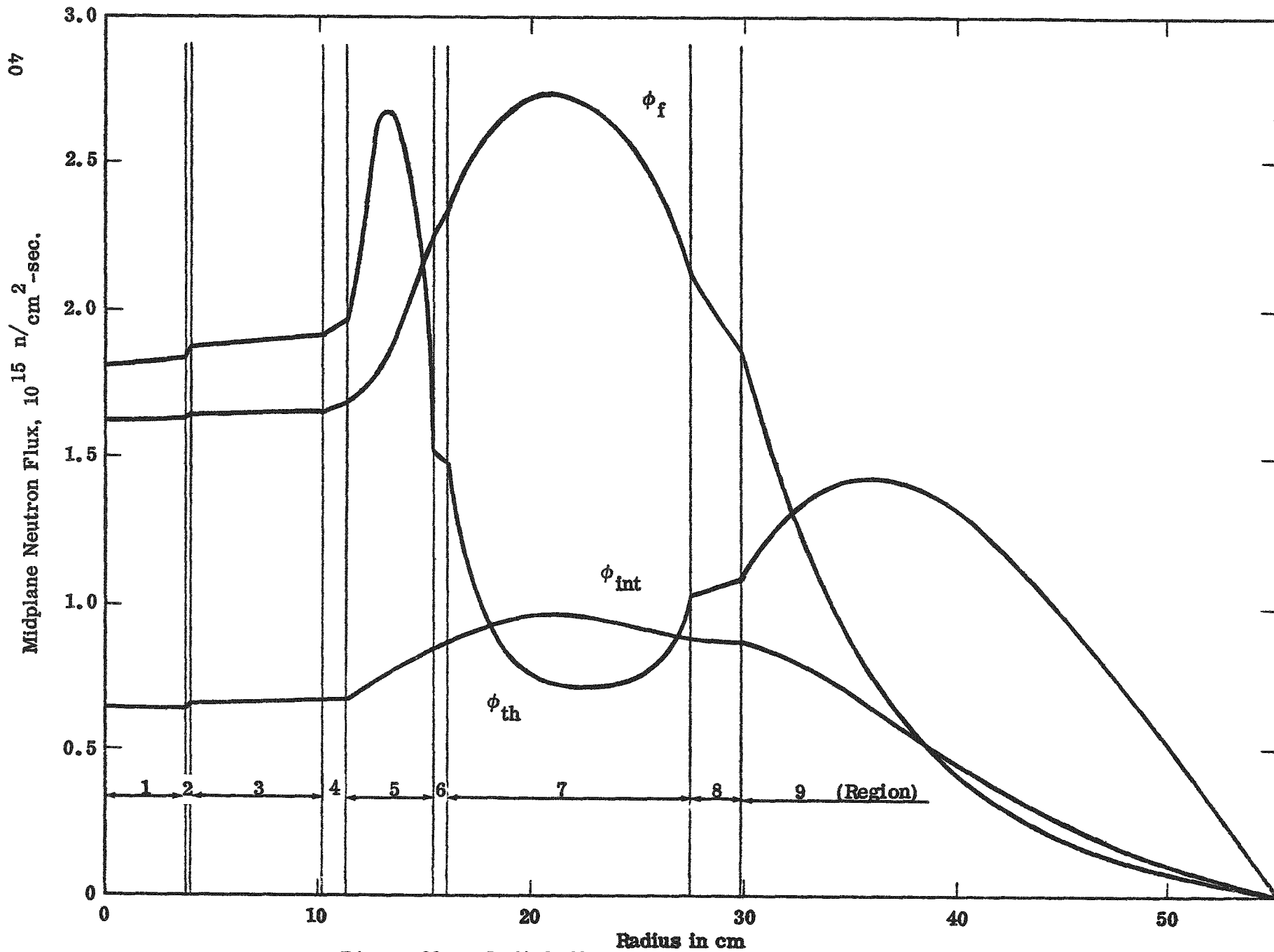


Figure 20 -- Radial Flux Distribution in a 3-in. Sodium Loop

The additional fuel loading necessary to achieve a two week run of the 7-in. diameter sodium-cooled-loop test reactor at design power of 228 MW was calculated. A two week cycle has been found at the MTR to be about the minimum acceptable cycle time (MTR returned to three weeks because of the heavy burden on the Experiment Project Engineers created by the two week cycle.) The calculation was based on 1.26 grams of U-235 disappearance per MWD, including U-235 fission and conversion to U-236. The additional fuel loading for burn-up was 4.0 kg of U-235. The corresponding effect on reactivity is 16%.

VII. HEAT REMOVAL LIMITATIONS

The objective of the thermal performance analysis is to find the combination of design parameters that will permit the maximum continuous rate of heat removal consistent with the limitations imposed by physics, mechanical, and corrosion limitations. Since maximum heat transfer rate, or power density, corresponds to the maximum neutron flux attainable in the active core, and since the neutron flux in the test section is proportional to the flux in the active core region, the combination of parameters that yields maximum power density corresponds to the maximum neutron flux in the central test region.

An equation is derived that relates the thermal performance parameters, and the use of this equation permits a systematic evaluation of each variable governing the reactor performance. Table V lists those parameters that are significant; note that several of them are not independent when considered within the framework of the assumed geometry.

The thermal analysis of the AETR core performance is based on several assumptions:

- (1) The active fuel bearing region of the reactor core is a right circular annulus containing plate type fuel elements separated by water coolant channels. The annular geometry of the active region is not significant with respect to the analysis involving power density; the annular configuration becomes significant when total reactor power is sought.
- (2) No boiling of the coolant within the core is permitted. The postulated means by which boiling is prevented is to fix the operating pressure in such manner that the saturation temperature is equal to the maximum allowable surface temperature. If the maximum temperature of the heat transfer surface is not permitted to exceed the coolant saturation temperature, no boiling can occur. This assumption is predicated on the requirement that the reactor design be within the limits of existing technology.

TABLE V

HEAT TRANSFER PARAMETERS

<u>Variable</u>	<u>Remarks</u>
Inlet coolant temperature, T_{in}	Fixed by the local conditions as low as is practical
Maximum fuel surface temperature, T_s	Dependent on and limited by erosion, corrosion, coolant velocity, and core life
Coolant velocity, v	Governs pressure drop and maximum allowable surface temperature
Power density, \bar{p}	Expresses the thermal performance; its value is proportional to the thermal neutron flux in the central test region
Fuel element geometry	
Core length, L	A specified requirement
Reflector savings, δ	Fixed by the reflector material
Annulus thickness, W	Not significant
Fuel Plate thickness, t_p	Limited by mechanical strength and feasibility and economics of fabrication
Water gap thickness, t_w	Dependent on fuel plate thickness and metal-to-water ratio
Metal-to-water volume ratio, R	An independent parameter

Since the acceptability of boiling in this high performance system is uncertain,¹ the possibility must be eliminated from this analysis so as to comply with the "existing technology" requirements.

- (3) The axial power distribution is the central, symmetrical segment of the cosine function; that is to say a "chopped" cosine. The chopped portions represent reflector savings.
- (4) The modified Colburn equation describes the film heat transfer coefficient or surface conductance. This equation is recommended by the Phillips Reactor Safeguard Committee, which has closely examined the five most used correlations.² The modified Colburn equation gives results that are very close to that of the McAdams-Colburn equation, the accuracy of which has been determined to be within ± 9 percent. The modified Colburn equation predicts slightly more conservative values, particularly in the regions where confirmatory experimental data are sparse. A functional relationship among the parameters presented in Table V is required so as to examine objectively the effect of each variable on the core's performance and to determine that combination of heat transfer parameter values that will represent the highest performance possible for any given core. The results of the heat transfer analysis will be interpreted in the light of the physics analysis and of the economics and practicability of fuel element fabrication. The limitations imposed by corrosion will be included quantitatively in this analysis.

¹R. S. Marsden, G. H. Nanso, R. J. Howerton, and D. R. deBoisblanc, Review of Internuclear Company Report Number 9, "Preliminary Investigations for an Advance Test Reactor".

²R. J. Nertney, Ed, Calculated Surface Temperatures for Nuclear Systems and Analysis of their Uncertainties, IDO 16343, (1957).

The equation

$$\bar{p} = \frac{8va(T_s - T_{in}) \sin \frac{\pi L}{4a}}{\pi L t_p \left(\frac{1}{R} + 1\right) \left[\frac{F_{film eq} D^4 V^4 \pi \rho C_p t_p}{b \sqrt{(4aRb)^2 + (\pi \rho C_p t_p D^2 V^2)^2}} + \frac{F_{bulk} 16a^2 R^2 b^2}{\pi \rho C_p t_p \sqrt{(4aRb)^2 + (\pi \rho C_p t_p D^2 V^2)^2}} + \frac{F_{bulk} 4aR \sin \frac{\pi L}{4a}}{\pi \rho C_p t_p} \right]} \quad (1)$$

relates the variables that govern or influence thermal performance. The derivation and nomenclature are given in Appendix B. Since the form of the flux distribution is independent of power level, the thermal flux in the fuel annulus is proportional to the thermal flux in the test section. Since the thermal flux at a point is proportional to the fissioning rate per unit volume at that point, the fissioning rate or power density in the fuel region is proportional to the thermal neutron flux in the test region. That is to say, the maximum power density in the active portion of the core is directly proportional to the maximum unperturbed thermal neutron flux in the test region.

An evaluation, then, of the conditions under which power density is maximum is tantamount to finding the conditions under which neutron flux in the test region is maximum. The relationship between power density and several of the design parameters is graphically shown in Figures 21, 22, and 23. In all cases power density in megawatts per liter is plotted versus the metal-to-water volume ratio in the active portion of the core. Note that all the curves show the same general characteristics. That is, they show a positive slope for low metal-to-water ratios and a negative slope for large metal-to-water ratios. The relationship implies that the system is capable of removing the heat generated at the power density values shown. Since high flux, consequently high power density, is sought, the reactor design point will lie near the peak of the appropriate curve. An examination of the effect of each of the other design parameters will permit their selection in such manner that

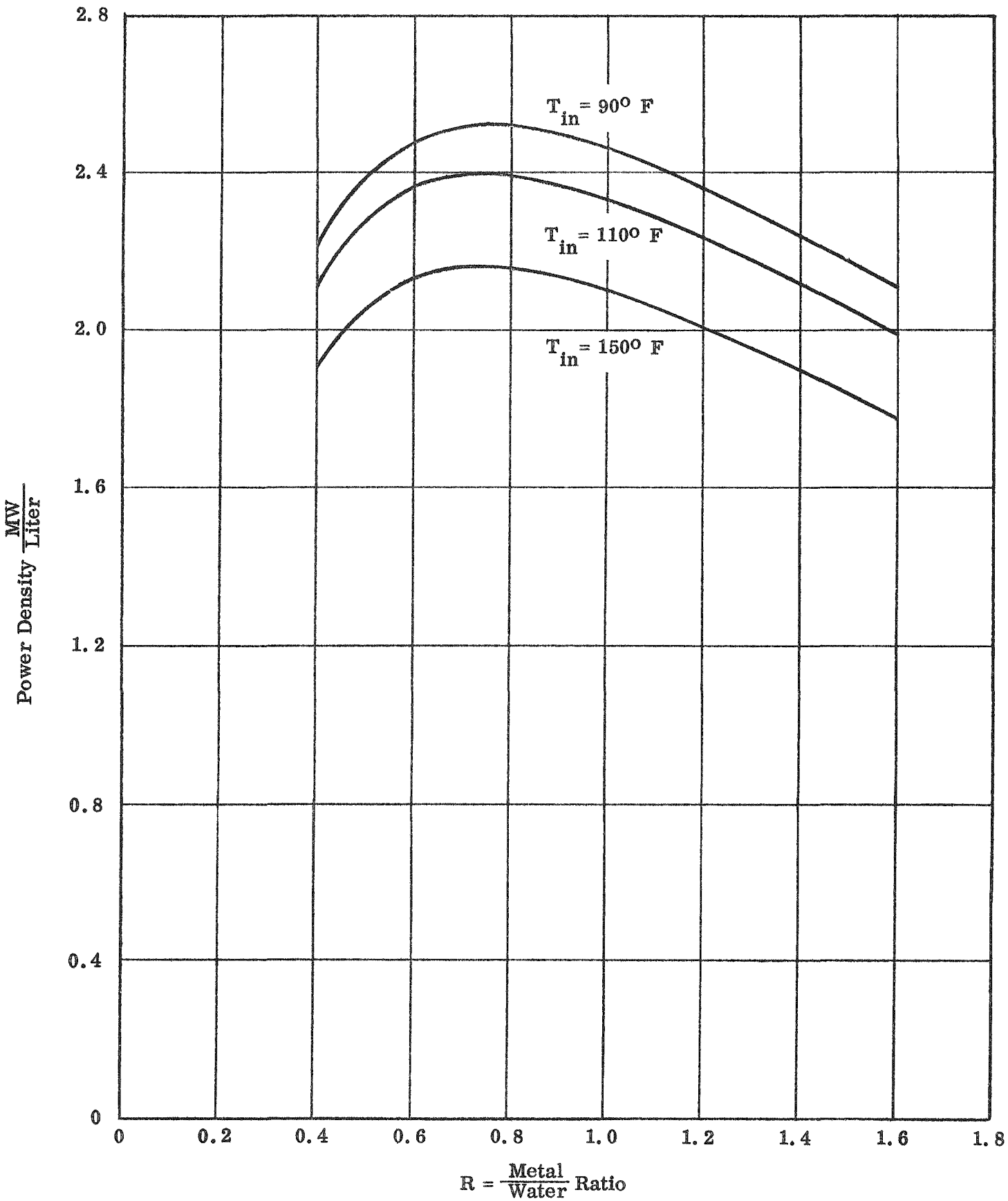


Figure 21 -- Power Density vs M/W Ratio for Various Inlet Coolant Temperatures

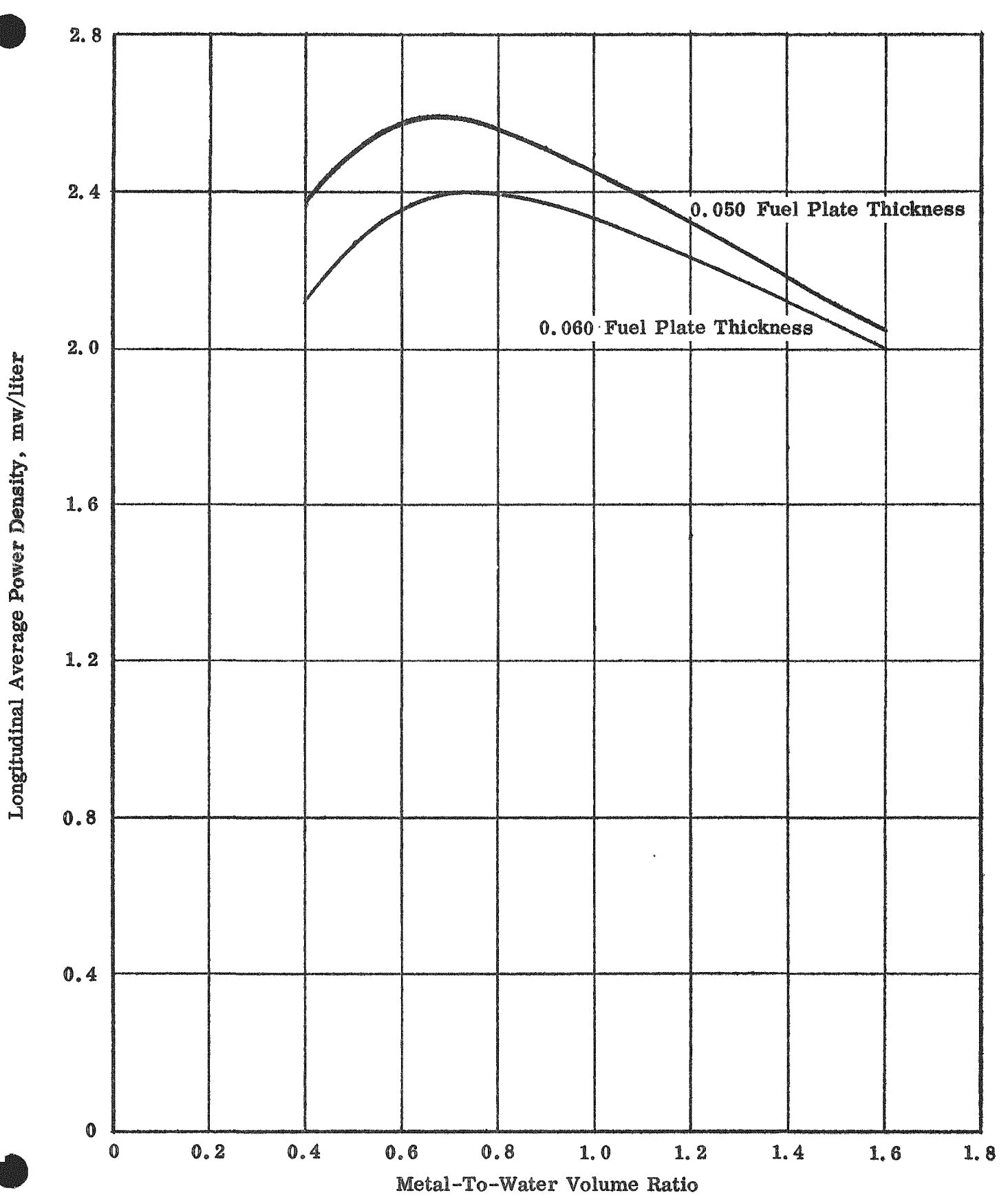


Figure 22 -- Power Density vs M/W Ratio for Various Fuel Plate Thicknesses .47

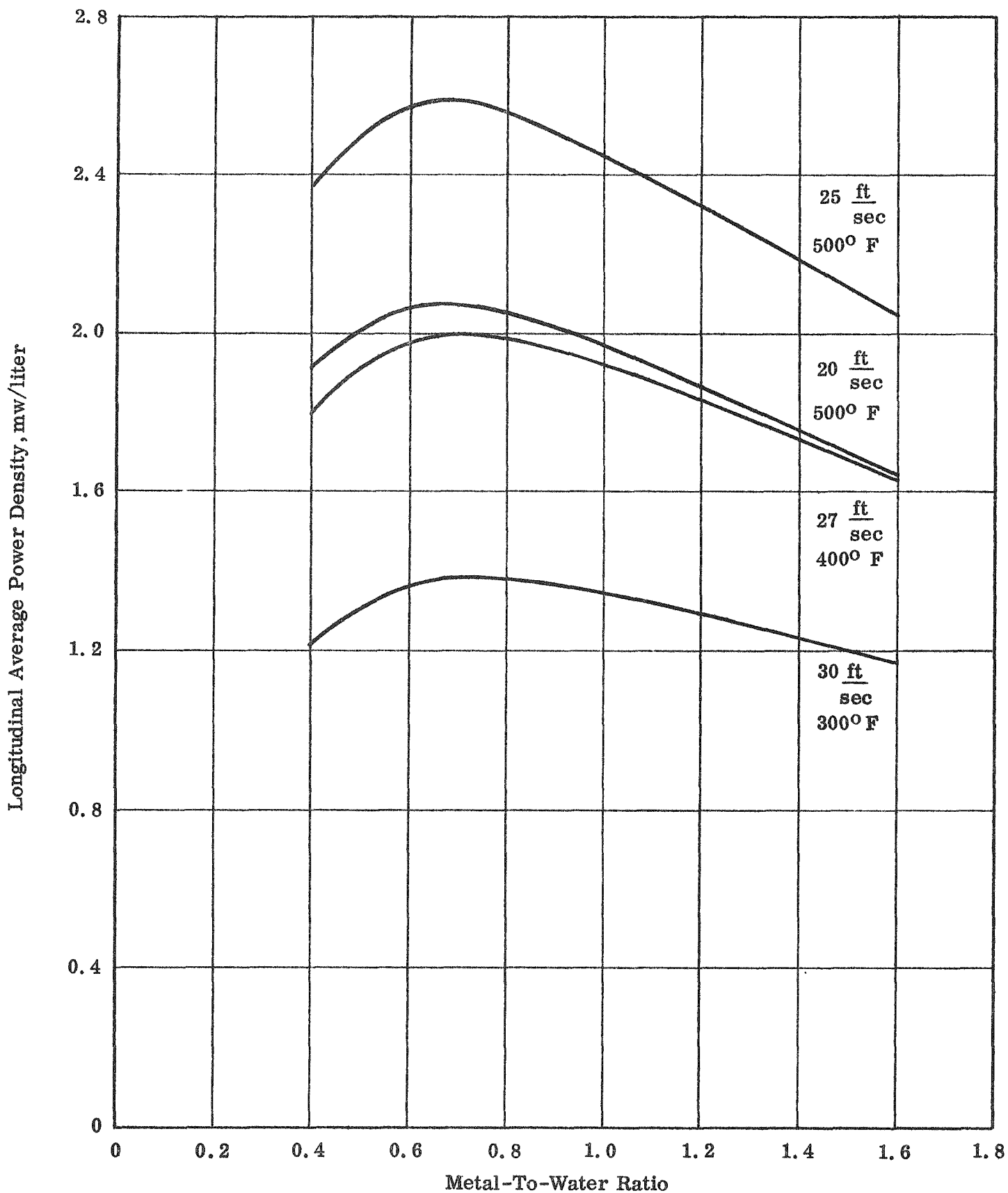


Figure 23 -- Power Density vs M/W Ratio for Various Coolant Velocities

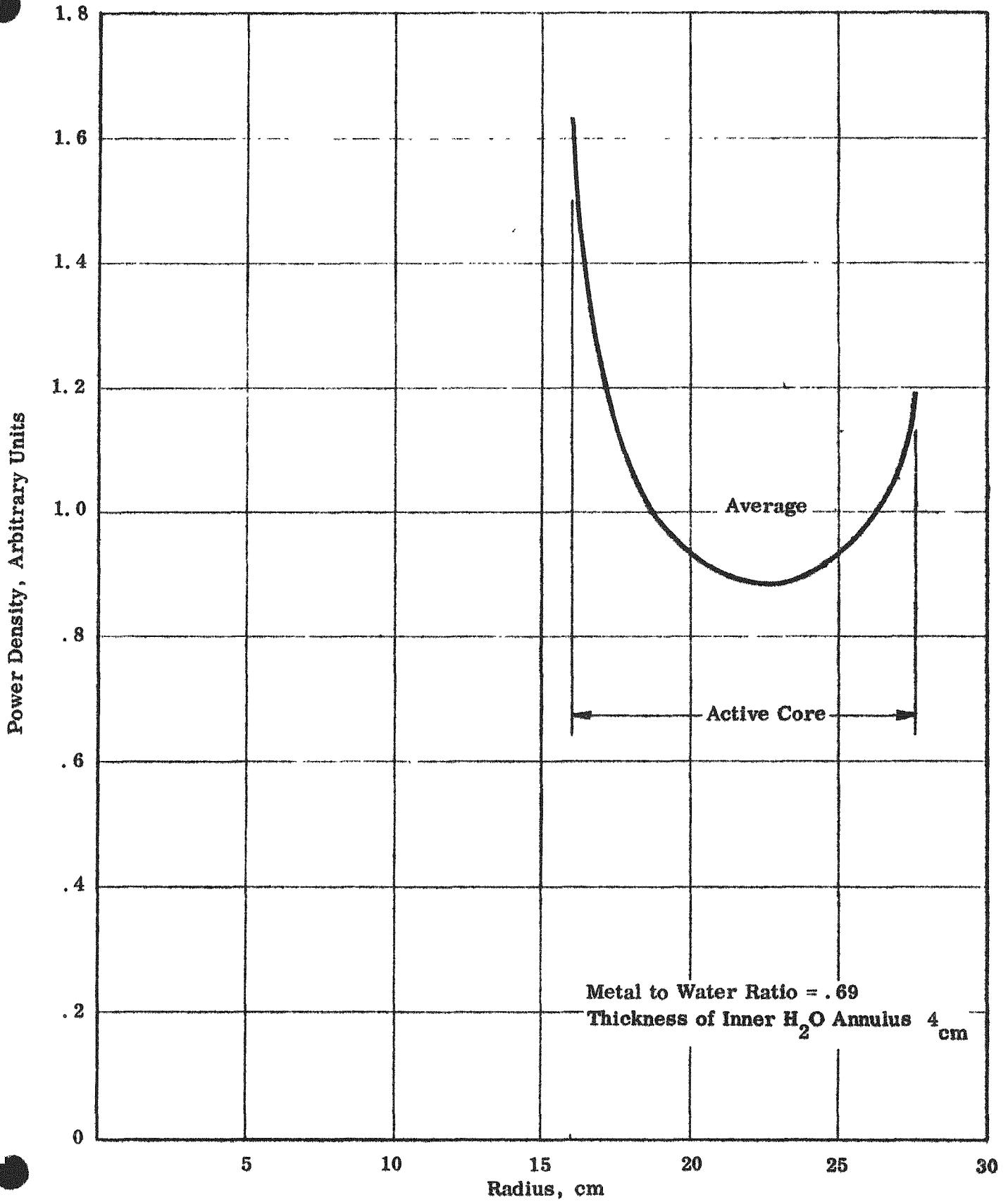


Figure 24 -- Radial Power Density Distribution

the maximum neutron flux consistent with heat removal is achieved.

Figure 21 shows the effect of inlet coolant temperature. Fuel plate thickness, inlet velocity and maximum surface temperature are fixed arbitrarily at the values shown. As may be observed from an examination of Equation (1), the lower the inlet coolant temperature the higher will be the corresponding power density. The value of 110°F was used in the design of the ETR, and the quantity will be fixed at this value in the remainder of this analysis so as to compare the effects of other parameters. An amplification of the basis for the selection of 110°F was given in Chapter XII, Process Systems.

Figure 22 shows the effect of varying fuel plate thickness. The two thicknesses chosen, 50 and 60 mils, probably represent the extremes of the range in which a realistic design would fall. There is a marked advantage in the use of the thin plates; however, mechanical strength becomes a limitation at approximately 50 mils and further reduction is not consistent with a feasible design under the conditions of existing technology.

The four curves in Figure 23 show the considerable effect of variable coolant velocity. Note that the maximum power density is associated with a coolant velocity of 25 ft/sec. The power density is less for velocities of less than 25 and for velocities greater than 25 ft/sec. The latter effect simply reflects the material limitation rather than a fundamental characteristic. A maximum surface temperature of 500°F is allowable for velocities up to 25 ft/sec. If the coolant velocity is increased above this value, the allowable surface temperatures are reduced accordingly. At 27 ft/sec the maximum allowable temperature is presumed to be 400°F and at 30 ft/sec the allowable temperature is reduced another 100°F . The basis for this limiting temperature-velocity relationship is presented in Chapter VIII, Materials Selection and Limitations. The curves in Figures 21, 22, and 23 reflect the effect of hot channel factors as applied both to the bulk temperature rise and the film temperature difference. These hot channel factors are summarized in Table VI. The individual values in the table are obtained directly from Table A4.3 of

the Internuclear Company Report AECU 3427.³ Note that in Table VI factors are multiplied to give the totals, whereas the portion of the factors greater than one were added to give the portion of the total factor greater than one in Table A4.3 of Internuc - 9. A discussion of the individual factors may be found in the reference.

TABLE VI
HOT CHANNEL FACTORS

	F_{bulk}	F_{film}
1. Power distribution calculations	1.10	1.10
2. Power measurement	1.05	1.05
3. Heat transfer coefficient calculations	1.00	1.10
4. Fuel concentration tolerance	1.01	1.01
5. Fuel core dimensions tolerance	1.02	1.05
6. Channel width tolerance	<u>1.10</u>	<u>1.04</u>
Products	1.31	1.40

It will be noted that the three figures (21, 22, and 23) show the longitudinal average power density assuming a cosine distribution. In addition a radial power generation distribution exists, the effect of which is not included in these figures. Figure 24 is a plot showing the radial power distribution for the particular conditions noted, which are a metal-to-water ratio of 0.69 and an inside reflector thickness of 4 cm. The maximum to average ratio is observed to be 1.63. This ratio must be applied to the power densities presented in the three performance figures to obtain the over-all average power density as shown later in Table VII.

³O. J. Elgert, C. F. Leyse, D. G. Ott, Preliminary Investigations for an Advanced Engineering Test Reactor, Internuc - 9, AECU 3427, February 1957.

It would be more appropriate to obtain the over-all average power density by dividing the longitudinal average by the radial maximum to average fuel plate temperature, since the maximum surface temperature actually limits performance. An examination of the equation that describes the radial temperature distribution assuming the fuel plates are set radially reveals that the conduction term is small and the temperature ratio will be only slightly less than the power density ratio. For this reason the power density ratio is used.

The equation, assuming conduction within the plate in only the r direction is,

$$k \frac{d^2 T(r)}{dr^2} + q'''(r) - \frac{2q''(r)}{t_p} = 0 \quad (2)$$

$q'''(r)$ is the function shown in Figure 28

$q''(r)$ is the surface heat flux and is given by

$$q''(r) = h \left[T_s(r) - T_m(r) \right] \quad (3)$$

Substituting and dividing by k

$$\frac{d^2 T_s(r)}{dr^2} + \frac{q'''(r)}{k} - \frac{2h}{kt_p} \left[T_s(r) - T_m(r) \right] = 0 \quad (4)$$

If $\frac{2h}{kt_p} \left[T_s(r) - T_m(r) \right]$ is large compared to the second derivative term, the

latter may be neglected. With a water gap thickness of .075 in. and a coolant velocity of 25 ft/sec, h may be evaluated by using the modified Colburn

Equation (Ref. 2), and is found to be $10,340 \frac{\text{Btu}}{\text{hr ft}^2 \text{ } ^\circ\text{F}}$; k for aluminum is approximately $145 \frac{\text{Btu}}{\text{hr ft } ^\circ\text{F}}$, $t_p = .050$ inches and

$$\frac{2h}{kt_p} = 34,260 \frac{1}{\text{ft}^2}$$

$T_s(r) - T_m(r)$ at the point where $T_s(r)$ is maximum is roughly

$$T_s(r) - T_m(r) = 500 - 140 = 360^\circ\text{F}$$

and the numeral value for the third term in (4) is about

$$\frac{2h}{kt_p} \left[T_s(r) - T_m(r) \right] = 12,300,000 \frac{^{\circ}\text{F}}{\text{ft}^2}$$

Neglecting the diffusion term temporarily and solving for $T_s(r)$

$$T_s(r) = T_m(r) + \frac{t_p}{2h} q'''(r)$$

Differentiating

$$\frac{d^2 T_s(r)}{dr^2} = \frac{t_p}{2h} \frac{d^2 q'''(r)}{dr^2} \quad (5)$$

$q'''(r)$ may be approximately represented by the function

$$q'''(r) = \bar{q}''' (1.63 - 12.72x + 84.93x^2 - 262.5x^3 + 315.2x^4) \frac{\text{Btu}}{\text{hr ft}^3}$$

where x is in feet

so

$$\frac{d^2 q'''(r)}{dr^2} = (169.9 - 1575r + 3782r^2) \bar{q}'''$$

Solving for the numerical value of $\frac{d^2 T_s(r)}{dr^2}$ at $r = 0$

$$\frac{d^2 T_s(r)}{dr^2} = \frac{.050}{(2)(10,340)(12)} \cdot 169.9 (8.187 \times 10^8) = 28,026$$

Numerical values of the two terms differ by a factor of 440; consequently, it is concluded that diffusion will have a negligible effect on the radial temperature distribution in the fuel plate.

The optimum combination of design parameters is presented in Table VII. AETR Thermal Performance. Also shown are the values of several dependent variables attendant to the optimum performance characteristics. Note that these values are obtained from the maximum point of the curve in Figure 23, although the inclusion of the radial maximum to average heat flux ratio which

is a function of metal-to-water ratio will adjust the position of the maximum somewhat. This combination of design parameters approximates the conditions of maximum heat transfer performance for the AETR core with flat parallel plate type fuel elements regardless of their orientation. Departure of any values from these optimum values implies either a reduced performance or a marginally-feasible component. That is to say, these conditions will closely approximate the maximum power density (consequently the highest neutron flux) at which continuous operation is possible. If power level were increased above that which is implied, the system would not be capable of removing the additional heat; boiling and possible fuel element damage would result.

By way of comparison with other high-performance reactors, the power density of the ETR is 0.494 MW/l. The maximum surface heat flux is quoted as 1.15×10^6 Btu/hr ft². For the AETR, the maximum flux is about 1.8×10^6 Btu/hr ft².

TABLE VII

AETR THERMAL PERFORMANCE

Fuel plate thickness	0.050 in.
Water gap width	0.075 in.
Average coolant velocity	25 ft/sec
Inlet coolant temperature	110°F
Outlet coolant temperature	185°F
Maximum surface temperature	500°F
Optimum metal-to-water ratio	0.666
Pressure drop through core	28 psi
Maximum heat flux	1.8×10^6 Btu/hr ft ²
Longitudinal average power density	2.59 MW/liter
Radial maximum to average power density ratio	1.63 (See Fig. 24)
Over-all average power density (allowable)	1.60 MW/liter
Needed to meet specifications:	
4-in. Water Loop	1.28 MW/liter
3-in. Water Loop	1.42 MW/liter
7-in. Na or Gas Loop	2.05 MW/liter
5-in. Na or Gas Loop	1.89 MW/liter
3-in. Na or Gas Loop	1.88 MW/liter

VIII. MATERIALS SELECTION AND LIMITATIONS

High power densities are inherent in the AETR core design. Moreover, the nuclear requirements for meeting the high flux levels of this reactor severely restrict the choice of materials. Therefore, the technological status of applicable materials must be completely reviewed to assign realistic design limitations. Three main areas of materials application in the core that require study are fuel plates, pressure vessels, and experimental thimbles. The criteria of selection vary somewhat among the three areas. The most economical materials have been chosen for application to this reactor. Technical evaluation of materials was based on operating experience where available, and on the published results of reliable laboratory investigations. Conservative operational limitations were chosen so as to ensure a high degree of dependability of reactor components. It is possible that with more operating experience and more complete testing of the new alloys, some of the operating limitations employed in this study can be relaxed.

A. FUEL ELEMENTS

Corrosion resistance, cross section, and adequate strength at operating temperature are the main problems connected with fuel element cladding.

The severe cross section limitations imposed by this reactor design eliminate from consideration all common materials except aluminum and zirconium as fuel cladding materials. Zirconium would cost about five times as much as aluminum for the elements, and fuel reprocessing costs would also be higher. Cost is not a major consideration in this study; however, because of the large number of fuel elements in the reactor and the high frequency of change, use of zirconium as a cladding material would be prohibitively expensive. Zirconium-clad elements would cost approximately \$8,500,000 per year as compared with \$1,700,000 per year for aluminum-clad elements. In addition, there are several important limitations on the use of zirconium such as low thermal conductivity and the limit of about 15% uranium content of the meat. However, operating conditions could be 750^oF maximum at about 30 ft/sec flow

velocity if zirconium were employed.

Conventional aluminum alloys are limited to a maximum temperature of about 400°F, above which catastrophic intergranular corrosion occurs. In the last few years new aluminum alloys have been developed that resist this intergranular attack to at least 650°F, although the uniform corrosion rate is fairly high at that temperature. The most developed of these alloys is X8001, formerly known as M-388. This alloy was chosen for use in the AETR fuel elements on the basis of the available corrosion data. The data supporting this decision and the selection of operating conditions are given in Appendix C. The assumptions used in arriving at maximum temperature and flow rates for this system are:

1. Maximum fuel element life will be one month
2. Water conductivity will be 2 micromhos or better
3. pH will be 5.5 to 6
4. Fuel elements will be sufficiently rigid to be free of vibration and deformation
5. There will be no boiling or cavitation at the plate surface.

Using these assumptions, maximum safe operating conditions were chosen to be 25 ft/sec water velocity at 500°F. The AETR conditions (35 ft/sec at 300°F) were chosen as maximum at lower temperature. Strength at elevated temperature, as well as corrosion resistance, entered into the choice of operating conditions. It is possible that future development will permit operating at higher flow rates and temperatures.

B. PRESSURE VESSELS

The main limitations of materials for pressure vessels are strength and absorption cross section. Strength is necessary for minimum required wall thickness which, in turn, results in lower absorption as well as lower thermal stress levels resulting from gamma heating.

At the pressure vessel outlet temperature of 210°F there should be no appreciable corrosion problem with the use of aluminum if the water purity and pH are properly controlled. Alloy 6061 was chosen because of high strength, good weldability, and acceptable corrosion resistance.

Stainless steels with adequate high temperature strength have objectionable parasitic absorption and very poor thermal conductivity for the flow of gamma heat. The following example illustrates the problem. Based on the values of thermal and pressure stress for a planned ETR test (3) it appears doubtful that a design using stainless steel would be feasible. Conditions are shown below:

IN-PILE TEST ETR-C66 M-13 (3)

Geometry	Tube 5.5 in. OD x 4.628 in. ID
Material	347 SS
Heat Removal	Both walls held at equal temperature
Maximum Gamma Heat	24 watts per gram
Maximum Calculated Stress	14,000 psi pressure, 97,500 psi thermal

C. EXPERIMENT THIMBLES

Some limitations in the central test thimble design are the same as those discussed in the preceding section. Further limitations on the design and material of the experimental test thimble appear to be in the flux depression and flux distortion resulting from parasitic neutron absorption.

These limitations, with that of the thermal stress problem, eliminate the consideration of stainless steel and allows use of an aluminum alloy tube having only about 5/8 in. thick wall in the high flux region. Such a size and material limitation causes a problem in the water-cooled experiments because of the 2000 psi pressure.

Hence, a high strength aluminum, alloy 2014 or ASTM designation CS41A, was selected for the test thimble material in the water-cooled experiments. This alloy is somewhat less corrosion resistant and less weldable than the aluminum alloy 6061 but its high strength is necessary to the design. It may be desirable to clad the 2014 alloy with a more corrosion resistant aluminum. Added details are given in Appendix C Materials Considerations. If a detailed metallurgical investigation proves the 2014 aluminum alloy to be

unacceptable as a construction material, the design of the test thimble or the experimental operating requirements must be modified. Since the water loop reactors do not need as high a power level for the specified flux it may be desirable to use a thicker walled tube of the better-quality but lower-strength aluminum alloy 6061 for the test thimble. Stainless steel is unacceptable in the present design because of its high cross section. Zirconium also is rejected because of high gamma absorption and low conductivity, which result in high thermal stresses. This would necessitate the use of large thicknesses adversely affecting the void and water annuli dimensions in the reactor.

D. EXPERIMENT THIMBLE LINERS

The annular space between the liner of the loop and the wall of the aluminum thimble will normally be filled with an inert gas. Outside the reactor vessel this gas-filled gap is connected to the experiment coolant through a pressure balance chamber or a gas pressurizer so that there is no pressure on the liner. The gas space will provide thermal insulation on those experiments where the test coolant temperature is higher than that of the reactor coolant.

Corrosion resistance is important in the choice of materials for thimble liners. Strength is not important since the liners are pressurized on both sides, but the thickness must be minimized. The corrosion conditions and temperatures are set by the type of test being run in the reactor. It will be difficult to find materials adequate to meet the conditions of some of the tests planned for this reactor. Stainless steel was chosen as the best material for general use as the experimental loop liners. The liner is provided with an expansion bellows to allow for the difference in thermal expansion between stainless steel and aluminum. The liners are quite thin, 1/16 in., since they do not contain pressure. Thus, their cross section is not a significant factor. For sodium loops up to about 1500^oF, and for some of the gas-cooled loops, type 316 stainless steel is used. For higher temperatures and more corrosive gases and liquid metals, special materials are used. In such extreme cases, select-

ion of materials must be made on the basis of specific test conditions. Materials such as niobium, high temperature alloys, and the like would be required.

Recent experience at the MTR (3, 4) points out the benefits of providing drainage for test facilities and of the use of inert gas, rather than air, atmospheres. The experience referred to is the unexpected failure, resulting from a corrosion rate of about 0.1 inch per month, of a test loop. It is hypothesized that nitrogen in the air gap surrounding the tube was converted to nitrogen oxides, which dissolved in condensed water at the bottom of the re-entrant thimble.

This experience, in addition to its application to test loop design, points out the need for caution in selecting materials for the AETR. Where only a small gain is possible in the use of an unproved material it should not be selected. If a large advantage can accrue then its use should be considered, provided extensive testing can be performed.

-
3. D. C. King, High Pressure Water Loop Experiments in the MTR, IDO 16426 (1957)
 4. M. S. Robinson, Failure of WAPD-30 High Pressure Loop, IDO 16338 (1957)

IX. GAMMA HEATING AND THERMAL STRESSES

GAMMA HEATING

Before deriving the equations needed for calculating the rate of gamma heat generation in the various regions of the reactor core, the geometry of the problem was examined. Figure 25 is a simplified system diagram that depicts the annular core region and the coordinate system used in the following solution. The heating is calculated at the plane perpendicular to the core axis at the point $H/2$; that is, the midplane, because this gives the points of maximum gamma heat generation.

The gamma energy flux is calculated by summing all the contributions to the flux at the observation point P from the differential source volume dV . Gamma rays emanating from dV are attenuated by absorption along the path R and are also diminished by the inverse square law. Therefore, the gamma energy flux at the midpoint of the axis is expressed by

$$\phi = S_v \int_{\text{vol}} \frac{e^{-\mu R}}{4\pi R^2} dV$$

where

$\mu \equiv$ total linear absorption coefficient

$S_v \equiv$ the gamma energy source density in the fuel region

$\text{vol} \equiv$ the volume of the fuel region

and

$$dV = R^2 \sin\theta \, d\theta \, d\phi \, dR$$

Although the geometry being considered is cylindrical, the solution is most easily accomplished in spherical coordinates. The limits of integration which define the source volume are,

R: the portion of the radius in the source region varies from

$$R_1 = \frac{c}{\sin\theta} \text{ to } R_2 = \frac{b}{\sin\theta} ,$$

ϕ : the angle of revolution varies from 0 to 2π , and

θ : θ goes from approximately $\tan^{-1} \frac{c}{(H/2)}$ to $\pi/2$.

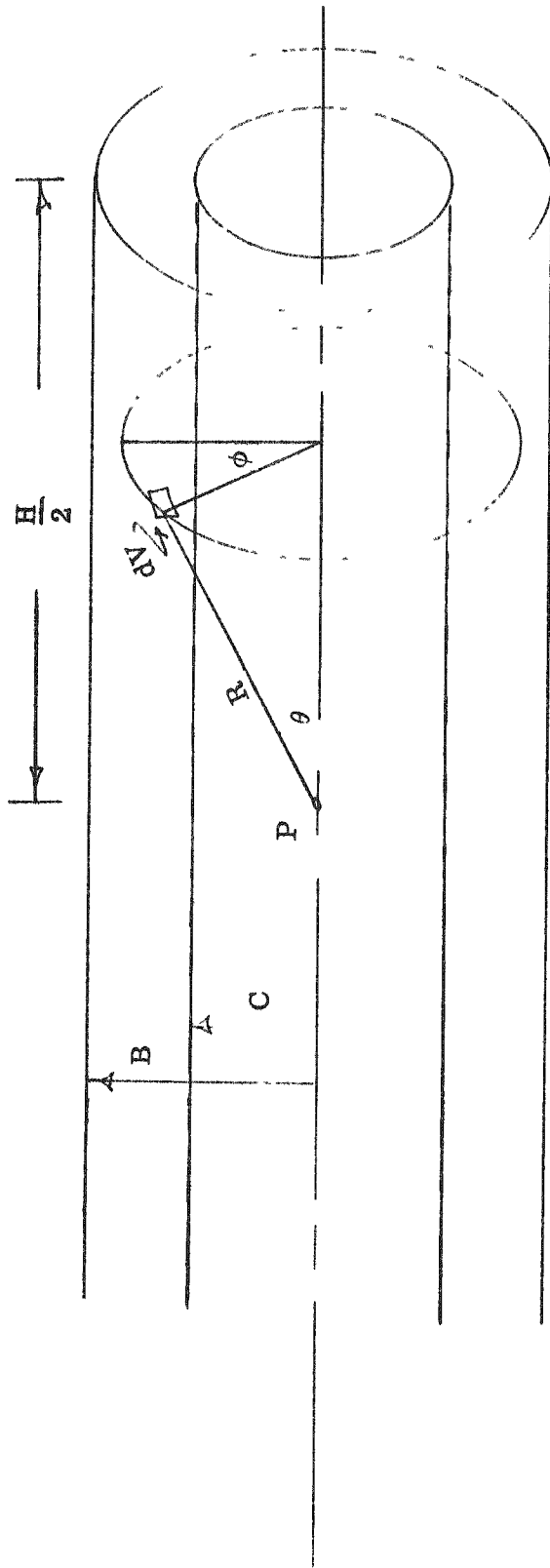


Figure 25 -- Diagram Depicting the Annular Core Region



The lower limit of θ can be found by considering the geometry and volume of the source region. The integrated volume of this region, which is

$$\text{vol} = 2 \int_{\theta_1}^{\pi/2} \int_0^{2\pi} \int_{R_1}^{R_2} R^2 \sin\theta \, dR \, d\phi \, d\theta$$

has to equal $\pi(R_0^2 - R_1^2) H$. Integrating the above expression gives

$$\text{vol} = \frac{4\pi}{3} (R_2^3 - R_1^3) \text{ctn}\theta_1$$

making it possible to evaluate θ_1 . This process is necessary since at the outer edge of the cylinder, the spherical coordinates cannot define the flat top surface of the annulus. The correction makes a difference of only 1.5% in the flux as compared to using $\theta_1 = \tan^{-1} \frac{c}{(H/2)}$.

Using these limits, the expression for the flux becomes

$$\phi = 2S_v \int_{\theta_1}^{\pi/2} \int_0^{2\pi} \int_{c/\sin\theta}^{b/\sin\theta} \frac{e^{-\mu R}}{4\pi R^2} R^2 \sin\theta \, dR \, d\phi \, d\theta$$

where the integral is doubled because of the symmetry about the midplane. The final form of this equation,

$$\phi = \frac{S_v}{\mu} \int_{\theta_1}^{\pi/2} \left(e^{-\mu \frac{c}{\sin\theta}} - e^{-\mu \frac{b}{\sin\theta}} \right) \sin\theta \, d\theta$$

is integrated numerically by Simpson's rule. Besides the geometric dimensions, several physical quantities are needed for the solution of the above equation. The calculation of the linear absorption coefficient μ involves two simplifying generalizations. The first is that the mass coefficient is equal to $0.04 \text{ cm}^2/\text{gm}$ for all the materials encountered by the gamma rays; the second is that

$$\mu = 0.04 \frac{\sum_i P_i T_i}{\sum_i T_i}$$

where T_1 is the thickness of any annular region such as the water reflector. The gamma energy source density was calculated using a power density of 2×10^3 watts/cm³. The prompt gamma activity is 7.8 Mev per fission¹ and the fission products during operation emit a total of 2.28×10^{11} Mev/watt-sec². Therefore, the energy density from fission captures is

$$2 \times 10^3 \text{ watts/cm}^3 \times 2.28 \times 10^{11} \text{ Mev/watt-sec}$$

plus

$$2 \times 10^3 \text{ watts/cm}^3 \times 3.15 \times 10^{10} \text{ fissions/watt}$$

In finding the contribution to the gamma ray energy source density from captures in the water, the following MTR datum is used: capture in water results in one 2 Mev gamma³. If 2.5 neutrons are produced per fission and only one is needed in a fission capture to continue the chain reaction, then 1.5 neutrons are left to be absorbed or to be lost by leakage. As a conservative estimate, it is assumed that there is no leakage and that the 1.5 neutrons are absorbed in water, producing 3 Mev's of gamma energy per fission. Therefore, the total energy source density is

$$S_v = 1.14 \times 10^{15} \text{ Mev/cm}^3\text{-sec}$$

The gamma energy flux at the center of the core region is

$$\phi = 3.78 \times 10^{15} \text{ Mev/cm}^2\text{-sec}$$

Beside having the centerline flux, it is necessary to know the spatial distribution of the flux. A reasonable assumption, considering the short distance from the axis to the inner wall of the source region, is that the flux falls off

¹Rockwell, page 34, Table 3.2, The Reactor Shielding Manual
²Rockwell, page 39, Table 3.5, The Reactor Shielding Manual
³ORNL-963 (Classified) page 203

as $e^{-\mu r}$. For this distance the attenuation is about a factor of 0.46. The cylindrical geometry lends itself easily to a P-3 solution for the gamma energy flux; such a calculation was performed using gamma absorption coefficients and Compton scattering cross sections. The attenuation given by this calculation was 0.45. This is in excellent agreement with the previous estimate. In spite of this agreement, the P-3 centerline flux is slightly high; to correct for this, the P-3 fluxes are normalized to give an axial flux of 3.78×10^{15} Mev/cm²-sec as calculated previously. Once the gamma energy fluxes are determined the rate of heat generation is calculated via

$$\rho = \phi \mu_e$$

where μ_e is the gamma energy absorption coefficient of the material. The heat generations in all the inner core regions are given in Table IX.

TABLE IX
RATE OF GAMMA HEAT GENERATION

Material	ρ (watts/cm ³)
Na (test loop coolant)	14.0
SS (thimble)	155
Al (inner reflector wall)	58.8
H ₂ O (reflector)	31.5
Al (outer reflector wall)	96.2

The gamma heating in the aluminum vessel separating the core from the D₂O reflector is calculated assuming the core to be an infinite slab. The simple formula utilized is

$$\phi = \frac{1}{2} S_a e^{-\mu t}$$

where t is the penetration into the aluminum and

$$S_a = \frac{S_y}{\mu}$$

This results in an average rate of heat generation of $= 103 \text{ watts/cm}^3$. This results in an answer that agrees fairly well with the heat generation in the aluminum wall separating the core and the inner water reflector (96.2 watts/cm^3).

The gamma heat generation in the thimble caused by photons originating in the core region are supplemented by gamma rays emanating from an experiment in the test section. The experiment considered in the following calculations is assumed to have a power density of 50 kw per linear foot and be 2 ft. long. Since the geometry of the tests varies considerably, this power is uniformly distributed in the test region. This results in a gamma energy density of $3.13 \times 10^{12} \text{ Mev/cm}^3 \text{ sec}$ in the 8.89 cm radius test section.

The gamma flux in the steel thimble is calculated by the following formula¹

$$\phi = \frac{S_v}{4\mu_s} [G(\mu_s h_1, b_5) + G(\mu_s h_2, b_5) + G(\mu_s h_1, b_6) + G(\mu_s h_2, b_6)]$$

where the notation and a table of G functions is given in the reference. The resulting flux of $1.35 \times 10^{13} \text{ Mev/cm}^2 \text{ sec}$ is a factor of 100 smaller than the flux due to gamma rays from the core region and capture in the water. Therefore, this heating need not be considered.

¹Rockwell, page 365, The Reactor Shielding Manual

THERMAL STRESSES RESULTING FROM GAMMA HEATING

Thermal stresses in the cylindrical stainless steel and aluminum shells are calculated with the idealizations that the shells are long, thin-walled cylinders and that the temperature is a function of radius only. Under these conditions the axial stress at axial locations remote from the cylinder ends is given by the equation

$$\sigma_z(r) = \frac{E \alpha}{1 - \nu} [t_m - t(r)]$$

in which t_m is the mean temperature of the wall. At the wall surfaces the axial and circumferential stresses are equal and the radial stress is zero. The maximum thermal stress obtains at the surface for which $[t_m - t(r)]$ has its maximum value.

For the 0.0625 in. wall thimble the outer surface can be considered to be thermally insulated and the inner surface temperature can be equated to the sodium temperature. For uniform gamma heating of 155 watts/cc and a thermal conductivity of 10 Btu/hr ft² °F/ft, the temperature difference between the two surfaces of the stainless steel wall is

$$\Delta T = \frac{W \Delta^2}{2k} = \frac{155 \times 96,500}{10 \times 2} \left(\frac{0.0625}{12} \right)^2 = 20.2^\circ\text{F}$$

The temperature distribution is parabolic with the apex at the insulated wall surface. For this distribution $(t_m - t)_{\text{max}}$ is two thirds of the temperature drop across the wall.

The value of $E\alpha/1-\nu$ for stainless steel at room temperature is 364 psi/°F. The maximum thermal stress on the wall is thus

$$\sigma = \frac{2}{3} \times 364 \times 20.2 = 4920 \text{ psi (tension)}$$

and occurs at the inside surface of the wall. This stress is low enough that it does not represent a design limitation. At operating temperature levels the factor $E\alpha/1-\nu$ is lower than at room temperature and the above stress is consequently conservatively high.

The inner surface of the 5/8-in. thick reflector wall can be considered to be thermally insulated. For this condition, a thermal conductivity of 90 Btu/hr ft² °F/ft, and a gamma source of 58.8 watts/cc, the maximum temperature difference, $t_m - t$, is 57°F. The value of $E\alpha/1-\nu$ for aluminum is 200 psi/°F, which gives a tensile thermal stress of 11,400 psi at the outer surface of the wall. The thermal stress at the inside surface of the wall is compressive and has a magnitude one half that of the outer surface, 5700 psi.

The fluid pressures on the inside and outside of the reflector wall are 300 and 700 psi, respectively. The circumferential stress caused by the difference between these pressures is 2700 psi compression. The thermally and mechanically induced stresses are additive, with the result that the net circumferential stress at the inside surface is 8400 psi compression and, at the outside surface, 8700 psi tension. These stresses are well below the allowable stress at the operating temperature.

The temperature distribution in the 1/4-in. thick aluminum core wall is symmetrical about the wall centerplane. For this condition the maximum value of $(t_m - t)$ is

$$(t_m - t) = \frac{2}{3} \frac{W\Delta^2}{8K}$$

which gives, for a gamma source strength of 96 watts/cc, a value of 3.9°F. The corresponding thermal stress is 770 psi, which is negligible.

Thermal stresses in the 1 1/4-in. aluminum wall separating the core and D₂O reflector are determined on the basis that the wall temperature is symmetrical about the wall centerplane. For a gamma heat generation rate of 103 watts/cc, the thermal stress at both wall surfaces is 20,000 psi tension and the thermal stress at the wall centerplane is 10,000 psi compression. The 700 psi pressure acting on the inside surface of the wall produces a uniform tension stress of 6,050 psi in the wall. The total tensile stress at both wall surfaces is thus 26,050 psi, which is well below the yield stress of 35,000 psi for the selected aluminum alloy.

None of the computed stresses exceed the yield point of the wall materials at the operating temperature levels. On this basis the thermal stresses are

not excessive. For ductile materials allowable thermal stress levels are determined in terms of the fatigue behavior of the wall following repeated cycles of operation. Evaluation of the acceptability of the computed stresses will thus require an estimate of the number of cycles expected during the life of the reactor components.

X. DESIGN QUESTIONS

A. FUEL PLATE ORIENTATION

Although the investigations and evaluations have been limited to fuel assemblies consisting of parallel plates of UAl_4 -Al alloy sandwiched between two sheets of aluminum cladding, the orientation of these plates in the annular fuel region was not specified for either the physics or the heat transfer analyses. The mechanical design of the fuel element requires that the orientation be fixed, and several of the factors that will control the selection may be examined.

Generally, two orientations are possible: The plates may be set in the annulus radially, or they may be set tangentially. Curved plates that represent an intermediate orientation might be fabricated, but it is believed that fabrication would be difficult especially if it is decided to use a non-uniform, radial distribution of fuel. Flat e.c. radial plates create a problem in that an assembly of such plates, if truly parallel, will not completely fill the annular region. Wedges of aluminum between each element would be needed to fill the coolant passage, and this results in an inefficient use of these spaces. Such pie-shaped regions could be filled with additional fuel plates that are successively narrower; however, again this would be an expensive problem in fabrication. Heat conduction through the plate or into the end support structure is not sufficient to relieve the radial maximum to average temperature ratio appreciably. This is because the heat transfer surface conductance is so large compared to the thermal conductivity of the aluminum plate that nearly all of the heat is transferred to the water while a distance of about one plate thickness from the point at which it is generated. (See Appendix B, Thermal Performance Relationships.)

Tangential plates as shown in Figure 4, Chapter IV, appear to offer a slight advantage in fabrication, although a more thorough investigation is warranted before this conclusion can be considered firm. Some coolant channeling will exist unless each plate is rolled to a different radius of curvature, in which case the slight fabrication advantage is elimi-

nated. It is not clear that the channeling effect is sufficiently severe to warrant the modifications required to eliminate it.

The tangential plate fuel element arrangement lends itself to distributing the metal-to-water ratio and/or the uranium-235 concentration radially so as to flatten the radial power distribution. This can permit operation at power densities approaching 2.59 MW/liter, which represents the maximum value attainable under the imposed requirements. To meet the requirement of 1.5×10^{15} n/cm²/sec thermal neutron flux; 2.09 MW/liter is needed consequently, the increased fuel fabrication cost may be warranted. A quantitative examination of the relative advantages and disadvantages has not been performed.

It appears probable that the curved tangential plates have an additional advantage with respect to their mechanical strength and vibrational stability in a fast moving stream of water. Table VIII provides a comparison of the fuel elements of two existing reactors with those of the proposed AETR arrangement.

TABLE VIII TEST REACTOR COMPARISON

	MTR	ETR	Proposed AETR
Plate type	curved	flat	curved
Plate thickness, mills	50	50	50
Water gap, mills	115	108	75
Active length, in.	24	36	36
Flow velocity, ft/sec	30	35	25
Pressure drop thru core, psi	9.3	26.2	22
Stability	Acceptable	Unacceptable	Unknown

It is unlikely that the vibrational stability of the element will be known until an experimental model is tested, but, if it is presumed that the significant criteria are plate type and flow velocity, the probability

that the proposed AETR element will possess acceptable mechanical and stability characteristics appears reasonably high. Observe that the MTR plates are curved and the proposed coolant velocity is less than that used in the MTR and much less than that required by the ETR.

Other possible configurations exist; one that involves coolant flow in the radial, rather than the axial direction is an interesting possibility. If used with a non-uniform water gap, the arrangement would be well suited for the AETR, since heat transfer coefficients would be highest at the inner edge of the core and this is also the point of maximum heat generation. Such an arrangement would require plenum chambers both at the inner and outer core boundaries, and seems better suited to a reactor cooled and reflected by a single fluid. Equalizing the coolant flow distribution within the restricted flow length available might be a problem.

On the basis of the consideration herein presented the fuel element configuration that appears most promising is one similar to that used in the MTR. The element consists of curved parallel plates, 50 mills thick, 36 inches long, and supported tangentially in a roughly trapezoidal support box. The elements are so sized that 13 of them completely fill the reactor's annular fuel region. Coolant flows vertically between plenums above and below the elements; these water-filled plenums also serve as the end reflectors.

It should be emphasized that the recommendation of this fuel element configuration is tentative. A detailed design and economic evaluation is required before a firm recommendation is appropriate.

B. TYPE OF CONTROL SYSTEM

The report by Internuclear Company* proposes two systems for controlling the AETR, both using reflector control. In the first system the reflector is separated into two regions, the inner and smaller region containing pure D_2O , which can be removed to scram the reactor, and the

* Op. cit.

outer region containing D_2O with a variable boron concentration to be used for shim control. The feasibility of operating the control mechanism was investigated both as proposed and also with mechanical control.

The second control system proposed by the Internuclear Company involves separating the reflector into three sections radially. The inner section would normally be completely full of D_2O . It would be emptied for a scram as in the previous system. The other two sections would be raised just high enough to make the reactor critical, the second reflector annulus being completely filled before raising the outer annulus.

Because of the distortions of flux and power distributions that result, it has been assumed that control devices cannot be installed in the core. Any mechanical control system would, therefore, have to operate in the reflector.

There are two basic requirements for any reactor control system. The first is that the system must be able to neutralize the maximum amount of excess reactivity that will ever be present in the reactor. The second is that it must be possible to change reactivity quickly enough to control the reactor. Stability may become a problem in liquid control systems. An additional requirement for a liquid control system is, therefore, that it must be capable of maintaining a given amount of control over long periods of time.

The above requirements formed the basis of the evaluation of the control system, the results of which are as follows:

1. Maximum change in reactivity resulting from the boron in the reflector is about 10%
2. Maximum rate of reactivity change resulting from the borated reflector is approximately $2 \times 10^{-3}\%$ /sec
3. Maximum change in reactivity resulting from the pure D_2O scram annulus is about 21
4. Time delay (between actuation and appreciable reactivity decrease) of scram mechanism is approximately 0.2 sec
5. Boiling cannot be permitted in partially filled control channels of

the level control system. The D_2O will have to be cooled some other way

6. The use of a vacuum system to control the D_2O level in the reflector annulus is not feasible. Positive displacement, using the D_2O as a working fluid is feasible
7. The axial flux perturbation caused by a level control system would be quite large. The ratio of the maximum to minimum flux along the test section would be greater than two to one.
8. Auxiliary equipment required to make the level control system safe would be quite complex.

The conclusions drawn from the investigations of control systems were presented in Chapter IV.

The maximum amount of reactivity that can be controlled by poison in the reflector was calculated using the PROD II code on an IBM 650. A 10-region one-dimensional model was used with three energy groups. A total reflector thickness of 25 cm was used. The inner 5 cm was assumed to be the pure D_2O scram channel and the outer 20 cm was assumed to be borated D_2O . The results of these calculations are given in Figure 26.

The maximum amount of excess reactivity that can be controlled by boric acid in the reflector is 14.4%. This is considerably less than the 26% needed for burnup and fission product poisoning. It would be possible to increase the effect of the boron by decreasing the thickness of the pure D_2O annulus. This, however, would decrease the effect of the channel as a scram mechanism.

The reactivity controlled by the borated reflector could be increased slightly also by increasing the thickness of the reflector. Unfortunately, this would tend to increase the reactor power required to achieve a given flux in the test section. Neither decreasing the scram channel thickness nor increasing the over-all reflector thickness is recommended as a method of increasing the amount of excess reactivity controlled by the reflector. Most of the excess reactivity in the AETR is needed for fuel burnup. This makes the use of burnable poison desirable. The amount of

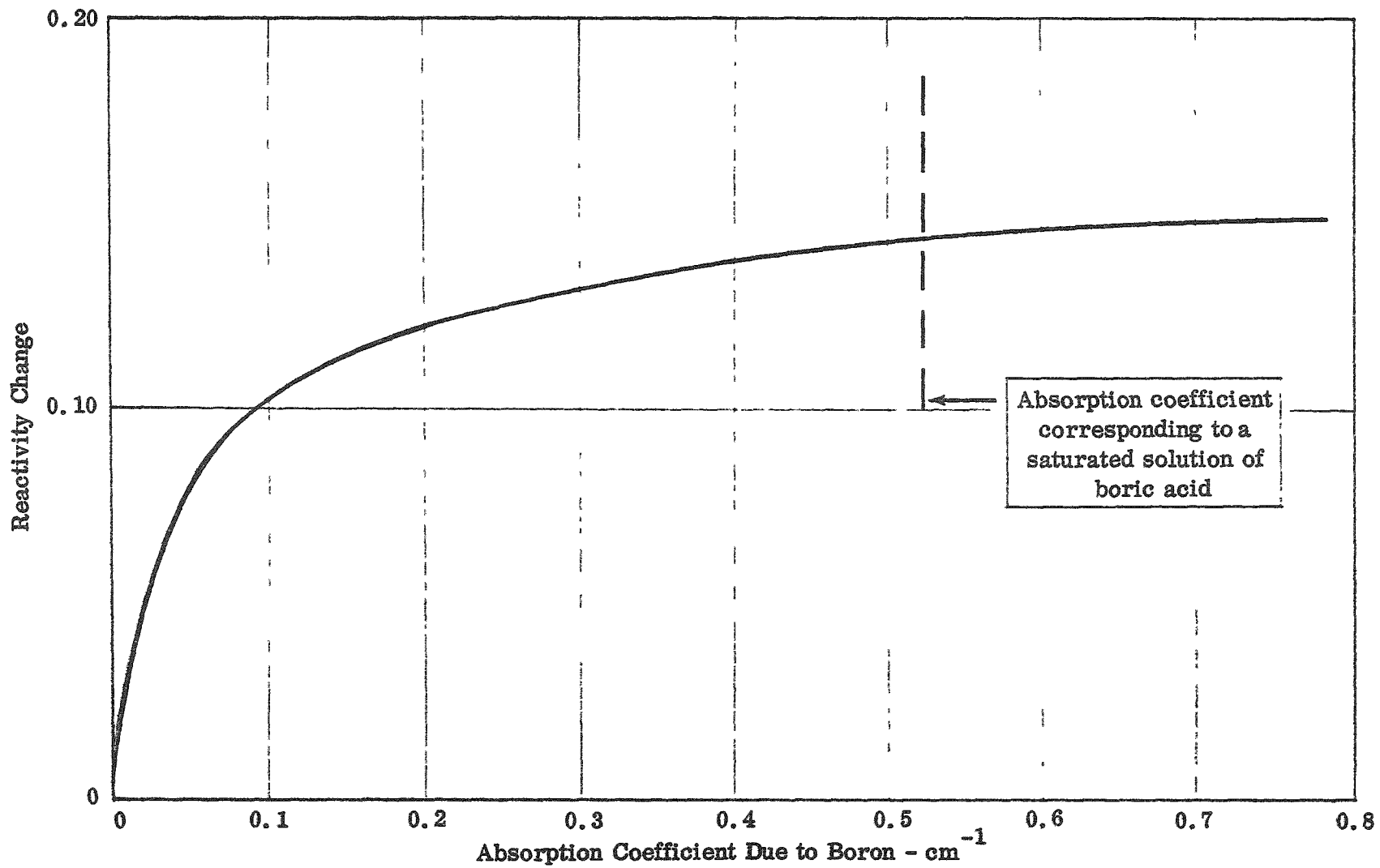


Figure 26 -- Study of Effect of Boron in Reflector (5 cm Pure D_2O Inside of 20 cm Borated D_2O)

time available to investigate control mechanisms for the AETR was not sufficient to determine quantitatively the effect of burnable poison. It is believed that it could be used to reduce the reflector control requirements to 10%.

The rate of boron (B^{10}) burnup in the reflector is a function of the boron concentration. It is estimated that the maximum rate of burnup will be less than 1% per day. The device used to control the boron concentration would have to be capable of replacing boron at a much faster rate.

An estimate of the change in reactivity resulting from a void in the inner D_2O reflector annulus was made using the machine code described above. The effect of this inner reflector annulus is a function of the boron concentration in the outer annulus. The change in reactivity is greatest when the outer annulus is not borated and least when it is heavily borated. For the worst case likely to be encountered (Σa for boron = 0.10 cm^{-1}) the change in reactivity from a completely full to a completely empty annulus is $\delta K = 0.21$.

The time response of the scram mechanism was estimated for two situations. The first estimate was made for the mechanism as described by Internuclear Company. The second estimate was made assuming that a dry pipe could be run from the scram valve to the top of the annulus to eliminate the time necessary to drain a D_2O filled pipe. In the first case the reaction time was found to be 0.6 sec and in the other 0.2 sec.

The reflector poison represents such a large amount of reactivity that the device used to control the concentration must be limited to prevent operating the reactor in a dangerous manner. One criterion for determining the maximum rate at which reactivity can be safely added to the reactor is to set a maximum allowable startup accident. It was assumed that the reactor could stand a 100% overload in power momentarily, and that the scram mechanism would trip at design power.

With a scram delay time of 0.6 sec the maximum allowable period is 0.87 sec. An approximate value of the maximum rate at which reactivity can be added to stay within this limit is

$$R = 2.5 \times 10^{-4} \text{ \%/sec}$$

This is an unreasonably slow rate even for a shim mechanism. For a scram delay of 0.2 second the allowable rate of reactivity addition is

$$R = 2 \times 10^{-3} \text{ \%/sec}$$

This may be fast enough for a shim control, but it is still too slow for a control mechanism.

Even though the rate of response of the borated reflector is slow, a system of this type offers many advantages. It can compensate for relatively large amounts of excess reactivity, the boron (B^{10}) that is consumed can be replaced easily, heat generated in the control mechanism can be removed easily, and there is no axial or angular flux perturbation.

Partial mechanical control could be used to overcome the slowness of response time without seriously affecting these advantages. Lightly loaded control rods could be inserted in tubes in the pure D_2O reflector section. These rods could have a combined worth of less than 0.7% reactivity. The time response of these rods could be made quite high since the reactor could not be made prompt critical on them alone. If enough of these rods are used and they are spaced evenly around the core, angular flux perturbation would be small. The rods could be designed with non-uniform axial loading so that axial flux perturbation could be kept small, and it might even be possible to flatten the flux somewhat.

The machine calculations used to evaluate the moderator level control system were similar to those described above. These calculations showed that the change in reactivity resulting from the outer 3 in. annulus is 4.5%. If the importance of the annulus height varies with the square of the flux and the flux is a sine function, the maximum reactivity response to reflector level is 0.21%/in. This means that the change in annulus level between critical and prompt critical is less than 4 in.

The D_2O in the partially filled annulus is not circulated, and so the heat generated by gamma radiation will boil the fluid. The heat deposition in the outer annulus was estimated to be 90 kw for reactor power of 100 MW.

The corresponding rate of steam generation would be $5.37 \text{ ft}^3/\text{sec}$. This would make the water-steam interface so unstable that the system would not be a suitable control mechanism.

The system could be modified in several ways to eliminate boiling in the reflector. If the number of regions were increased to five, alternate regions could be kept full and the D_2O in them could be easily cooled. The heat generated in the partially filled regions would be transferred across the thin aluminum walls to the cool D_2O in the completely filled region and no boiling would occur. D_2O filled cooling coils in the partially filled annulus would accomplish the same thing.

Rapid and precise level control of the reflector could not be achieved with the use of a compressible gas or vapor to transmit pressure. It is preferable to use the D_2O itself as a working fluid. This could be done by running a pipe from the bottom of the reflector annulus to a cylinder immediately outside the reactor shield. By fitting the cylinder with a piston the level in the annulus could be rapidly controlled.

To ensure safe operation it would be necessary to use a considerable amount of auxiliary equipment and instrumentation. The system would not be simple.

The unique feature of the level control system is that it permits high neutron leakage. If this is indeed an advantage, there are other control systems that permit almost as much leakage. Flux perturbation was calculated for mechanical control rods located in the reflector near the core. For a reactivity worth of 11% three group calculations showed that the thermal flux in the outer region was reduced by 25%. Fast flux would be affected even less.

C. COUPLED VS. UNCOUPLED REACTORS

In considering the operation of seven reactors within a common shield, it is evident that certain advantages or disadvantages may result from locating the reactors very near one another and separated only by a material such as D_2O . In such an arrangement the reactors would operate coupled or so that the reactivity of one reactor would materially effect

the reactivity of those adjoining it.

The question of whether or not the separate AETR reactors should be coupled was approached as follows. Several systems with varying degrees of coupling were postulated. The relative advantages and disadvantages of each system were then determined in comparison to completely uncoupled reactors.

The properties considered included the total power required, shielding requirements, control requirements, critical mass, D₂O inventory, space available for out-of-pile equipment, additional irradiation facilities provided, and convenience of operation.

The following two systems will be discussed because they represent the extreme of the possible methods of coupling.

1. Reactors coupled in pairs. Reactivity effect of one reactor on the other $1-3\% \frac{\delta k}{k}$
2. All seven reactors coupled together. Reactivity effect of six reactors on the seventh greater than $20\% \frac{\delta k}{k}$

In all cases it was assumed that the reactor would be coupled by building them close together and filling the space between them with D₂O.

The first step in the investigation was to try to determine how a coupled reactor system would behave. For the sake of simplicity, most of the work was done on a two reactor system. The degree of coupling between reactors was estimated as follows. The thermal flux around an infinitely reflected reactor was calculated using a simplified four region model. Three group calculations were made using the PROD II code on an IBM 650. It was assumed that the flux between reactors was additive. An absorption correction was made to determine the thermal flux in the core region of one reactor resulting from the other reactor. This perturbation was added to the unperturbed flux to give the perturbed flux in the core. The unperturbed adjoint flux was calculated using the same machine code described above. The reactivity effect of one reactor on the other was

then calculated using perturbation theory. The results of these calculations are shown in Figure 27.

The paired-reactor system provides additional space for neutron irradiation between the reactors. If the reactors are spaced at 130 cm center to center, an area of fairly flat flux, 40 by 50 cm, will be available as shown in Figure 28. The flux in this area will be about a factor of two lower than the flux in the central test section. The flux will have roughly a cosine distribution in the longitudinal direction. Flux perturbation in the central test section caused by coupling will be about four percent in the transverse direction. The use of borated D_2O for reactor control would not be feasible and some other system would have to be used.

The major disadvantage of this system is that operating flexibility would be decreased. When one reactor is operating, it would be possible to hold the other at very low power, but it would not be possible to reload the second reactor or make any change in the in-pile experimental apparatus.

It would be possible to overcome this disadvantage by inserting a slab of highly absorbent material between the reactors.

A second disadvantage of the paired-reactor system is that the control of two coupled reactors is more complex than that of two uncoupled reactors.

If all seven reactors are coupled closely together, the total critical mass will be reduced considerably. The total power required to achieve a given flux would also be reduced. The amount of concrete shielding needed would be decreased, but the D_2O inventory would increase. The amount of space available for out-of-pile auxiliaries would be reduced considerably.

Small areas between the reactors would be available for neutron irradiation. The flux at these locations would be nearly as high as in the central test holes, although this would depend on the control mechanism used.

The restrictions on operating flexibility of this type of reactor system would be extreme. The system would operate essentially as a single reactor.

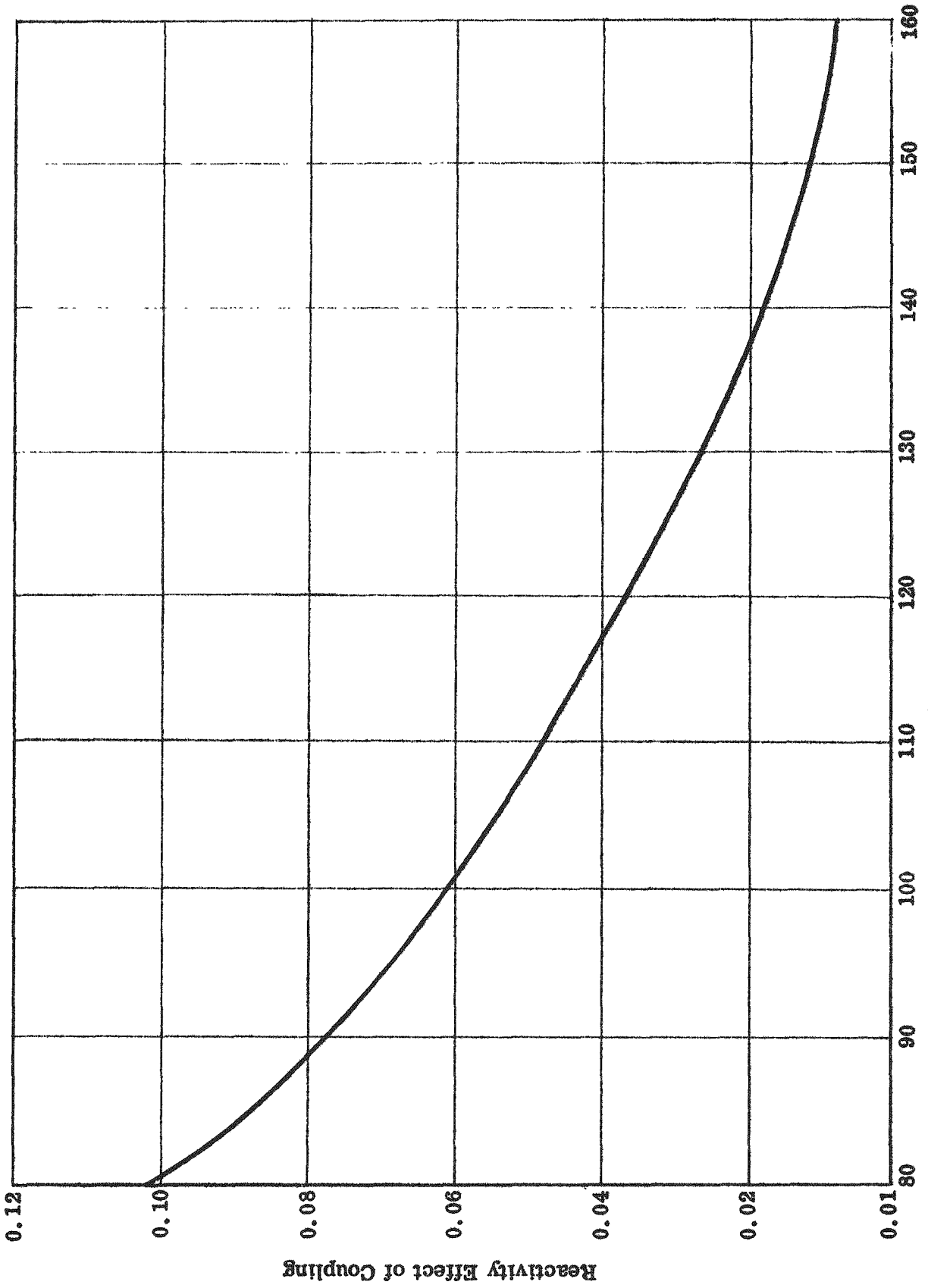


Figure 27 -- Reactivity Effect of One Reactor on Another

130 cm CENTER TO CENTER SPACING; NUMBERS INDICATE ARBITRARY UNITS OF FLUX

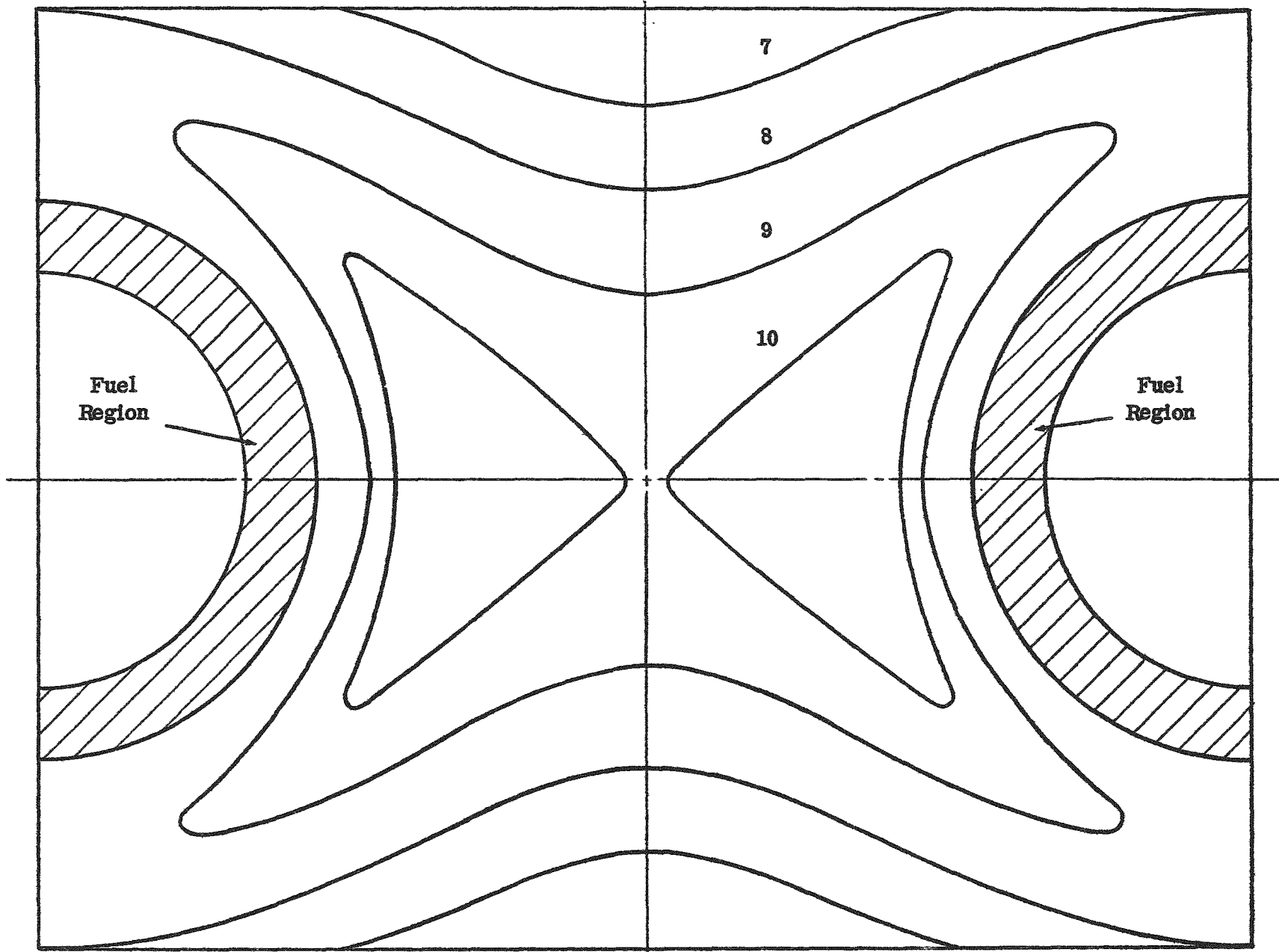


Figure 28 -- Flux Between Coupled Reactors

One of the important functions of the AETR is to test fuel elements to failure. At the completion of a test the fuel element will be moved to a hot cell, sectioned, and inspected for the cause of failure. It would be extremely undesirable to leave one of these test elements in the reactor for any length of time after failure, even at low power. The cooling system would become contaminated, and the information that could be gained from inspection of the element would be decreased. None of the advantages to be gained from coupling the reactors warrants sacrificing the flexibility of uncoupled reactors, which would permit shutdown on failure of a test element.

XI. BIOLOGICAL SHIELDING

The concrete biological shield must be designed so as to reduce to a safe level the three major sources of radiation -- fission and fission product gamma rays, secondary gammas, and fast neutrons. A dose of 1/10 of tolerance or less at the shield face will be the design criterion. Also, because of the cursory nature of this shielding study, all the assumptions and generalizations that must be made will always be conservative and often very severe. This results in shields that will definitely be adequate and will provide an upper limit to construction costs.

The maximum dose at the shield face is on the plane perpendicular to the reactor's axis and through the midpoint of the core. In finding the different source densities, the maximum power density of 1.59×10^6 watts per liter was used; a core volume of $1.436 \times 10^5 \text{ cm}^3$ gives a total power of 228 MW for the reactor considered in all shielding calculations.

Secondary gammas are generally found to be the chief offenders in this type of reactor, and therefore this gamma ray source will be considered first. Taking the total power times 3.15×10^{10} fissions, one watt-sec gives 7.18×10^8 fissions/sec in the core. Of the 2.5 neutrons released per fission, one is required to sustain the chain reaction, and the remaining are lost either by leakage or by capture. Making the severe assumption that none are lost by leakage and that the remaining 1.5 neutrons are captured uniformly in the iron thermal shield gives a gamma energy source density of

$$S_v = 3.88 \times 10^{13} \text{ Mev/cm}^3\text{-sec}$$

considering 8 Mev of gamma energy per capture.

The dose rate as a function of shield thickness was calculated for this annular source by taking the difference of cylindrical sources. The shielding material considered was barytes concrete with a density of 3.5 gm/cm^3 . Calculations were made using the following formula from The Reactor Shielding Manual (page 360) with a linear build-up factor (again a conservative approach):

$$\phi = \frac{BS_v R_o^2}{2(a+z)} F(\theta, b_2)$$

The result of these calculations is shown in Figure 29. In general, eight feet of heavy concrete will attenuate the gamma rays to 1/10 of tolerance. Because of the super-position of solutions, the dose at a point between reactors is just the sum of the doses from each.

The fast neutron volume source density is given by

$$\begin{aligned}
 S_v &= (1.59 \times 10^3 \text{ watts/cm}^3)(3.15 \times 10^{10} \text{ fissions/watt sec}) \\
 &\quad (2.5 \text{ fast neutrons/fission}) \\
 &= 1.25 \times 10^{14} \text{ fast neutrons/cm}^3 \text{ sec}
 \end{aligned}$$

and this is converted to a surface source density by multiplying by the fast neutron relaxation length in the aluminum-water core -- about 10 cm. These neutrons traverse radially through 25 cm of D₂O and 6.75 in. of iron thermal shield before entering the concrete shield. Consideration of a graph of the attenuation of fission neutrons through iron slabs and water, page 61 of The Reactor Shielding Manual, shows that the eight feet of barytes concrete needed for secondary gamma shielding will reduce the fast neutron dose to an imperceptible level. The use of data referring to water instead of concrete is valid and conservative since their respective fast relaxation lengths are 10 and 8 centimeters.

In the gamma heating analysis, a figure of $S_v = 9.47 \times 10^{14} \text{ Mev/cm}^3 \text{ sec}$ for the gamma energy source density as a result of fission and fission product gammas was calculated. Although this is about 30 times the activity found in the thermal shield, its dose contribution at the shield face will be roughly 10^{-3} less because it has to traverse the 6.75-in. iron thermal shield. Therefore, the dominant radiation source is from secondary gammas, and any shield capable of reducing them to tolerance will certainly attenuate radiation from the other two sources to negligible proportions.

Another area of the reactor that should be examined for high radiation levels is the sub-pile room. Again the flux from secondary gammas in the iron thermal shield was determined by a formula from The Reactor Shielding Manual:

$$\phi = \frac{BS_v R_o^2}{4(a+z)} [F(\theta_2, b_2) - F(\theta_1, b_2)]$$

b

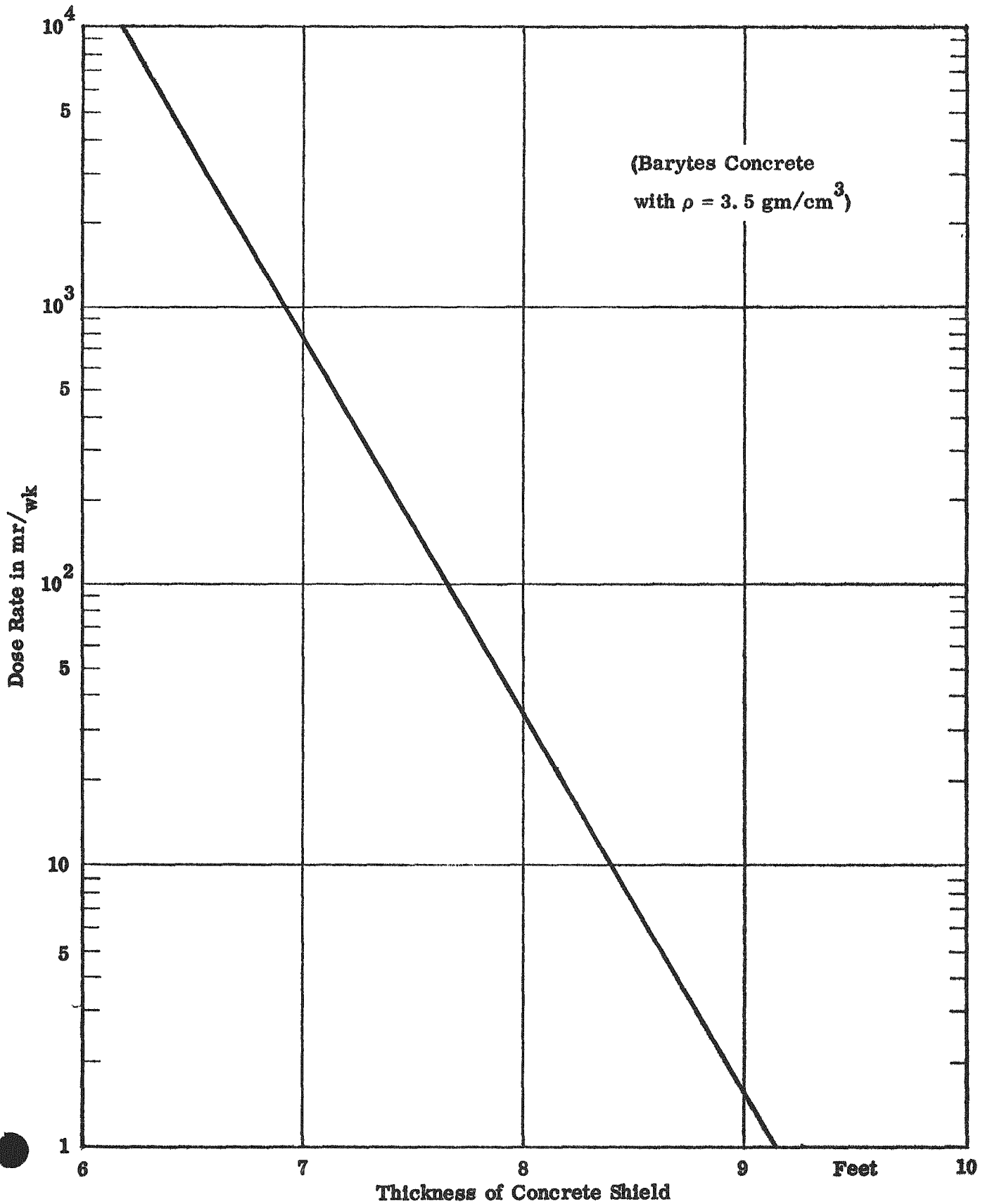


Figure 29 -- Gamma Dose Rate at Face of the Shield

At a point six feet above the floor in the room under a shutdown reactor, the dose from the two adjacent reactors was less than 1/10 of tolerance.

Because of the high power level of this reactor and also because of its "high leakage" geometry, a considerable thickness of heavy density concrete is required to attenuate the radiation to safe levels. In fact, this thickness may be as great as eight feet at the core midplane. However, after considering the methods and generalizations used in calculating this shielding, it seems likely that a more refined study would result in substantial reductions.

The secondary gammas in the steel thermal shield were found to be the chief source of radiation at the shield face. Rather than to assume that 1.5 of the 2.5 fission neutrons are absorbed uniformly in this steel, the neutron fluxes could be determined in that region and the actual activation distribution found. Also, a savings could be effected by shaping the shield carefully and by incorporating standard concrete in many regions. This could be accomplished by a large scale isodose mapping of the reactor shield.

XII. PROCESS SYSTEMS

A. COOLING SYSTEMS

The total thermal power developed by the seven reactors is as follows:

Water Loops	
4 in. Test Section	184 MW
3 in. Test Section	205
Gas or Liquid Metal Loops	
3-7 in. Test Sections	684
5 in. Test Section	228
3 in. Test Section	<u>228</u>
Total	1529 MW

The dissipation of this large amount of waste heat constitutes a considerable undertaking. Indeed the amount of waste heat will have a significant influence on choice of the geographical location of the plant, and the consequent availability and quality of cooling water will influence selection of the type of waste heat dump system to be used: Cooling towers, spray pond, circulated river water, or air-cooled exchangers. Forced draft, cooling towers were selected as being probably the most suitable for average locations. This selection prevents the waste heat problem from having the undue influence on plant location that the use of circulated river water might. Once the plant location is selected an economic study can determine which type of heat dump system should be employed.

Even with atmospheric evaporative cooling towers there exists a significant need for make-up water. For design purposes the heat removal system load rating was assumed to be 110% of the above power for the seven reactors. The make-up water to compensate for the evaporative cooling loss, entrainment loss, and blowdown of concentrated solids for this heat load was estimated to be of the order of 20,000,000 gallons per day. This make-up water can be supplied either by a river, a lake, or suitable wells.

Forced-draft cooling towers if close-packed would occupy an area of less than four acres. Optimum placement to take advantage of wind direction

and prevent water-saturated effluent air from being drawn into adjacent towers would require considerably more area. The secondary cooling system requires circulating pump stations and make-up water treatment facilities as well as the make-up water supply system.

The primary cooling system consists of circulating pumps, heat exchangers, and piping. Materials for this system will be austenitic stainless steels or aluminum to ensure system integrity and to minimize purification problems. The main reactor coolant heat exchangers will have stainless steel tubes and channels and carbon steel shells. The higher power reactors will require approximately 35,000 square feet of heat transfer surface per reactor. This probably will require two or more exchanger units per reactor. Primary coolant flow will be about 16,000 gallons per minute for each of the liquid metal and gas experimental loops and amounts for the water experimental loops will be correspondingly smaller.

Relatively small heat removal systems must be provided for each of the two heavy-water reflectors. The thermal shield cooling can employ secondary cooling water.

B. PURIFICATION SYSTEMS

The water treatment plant is equipped with the necessary supply pumps, screens, storage tanks, softening equipment, acid and caustic tanks for pH control, mixed bed demineralizers and make-up pumps. A chlorination system is included for treatment of domestic water. The system design must necessarily depend upon the water available at the selected site.

The reactor primary coolant purification system includes filters, demineralizers, heat exchangers, flow and temperature controls, and instrumentation.

The reactor control system includes equipment for both injecting and removing boron from the D_2O used in the reflector. The boron is removed by means of a demineralizer.

C. WASTE DISPOSAL

Radioactive waste water is demineralized and discharged into a cooling water discharge system or reused in plant systems when determined to

b

be within safe limits. Concentrated wastes including filter material and demineralizing chemicals are stored in underground tanks until radiation has decayed or until waste can be removed from the site for ultimate disposal.

Facilities are provided for disposing of radioactive sodium and other materials that may be used in the various test loops.

D. AUXILIARY SYSTEMS

The process systems also include a pressurizing and surge system for the primary loop, a water charging system, a pressure relief system, and an emergency shutdown cooling system. Other systems are a noncondensable gas removal system, a building emergency ventilation system, and compressed air systems for instruments and general plant use.

XIII. RESEARCH AND DEVELOPMENT PROGRAM

A. ITEMS FOR THE PROGRAM

The research and development program shall include analyses and experimentation necessary to establish the materials, components, and systems characteristics for the detailed reactor design.

Specific examples of the research and development related to the AETR are the following:

1. Fuel Elements

a. Fabrication

Plate-type fuel elements have been widely used in research and test reactors. However, several unique features of the AETR element will require developmental effort. In particular, the closer spacing of fuel plates and the varying width of plates in the same element constitute departures from currently employed designs. Also, the necessity for fuel element structural stability at elevated temperatures (500°F max) and high coolant velocity (25 ft/sec max) represents a considerably more severe requirement than has been employed in past reactors using aluminum plate-type fuel elements. The purpose of this phase of the program is to develop a dependable fuel element using economical fabrication and inspection procedures.

Choice of materials for the AETR core is severely restricted by nuclear requirements. Aluminum alloys have been specified for fuel elements and pressure vessels chiefly on this basis. However, the use of aluminum alloys imposes limitations upon the engineering design of the AETR. Materials limitations employed in this study are based largely upon previous experience in MTR and ETR design and operation, as well as upon the best available experimental data. An important aim of the research and development program is to verify and possibly modify the materials limitations currently imposed upon the AETR design. Considerable work is already in

progress in many important areas of aluminum technology. The amount of effort required on this aspect of the AETR research and development program will depend to a large extent upon the rate at which applicable information is forthcoming from these other investigations.

Current technology should be applicable to AETR fuel element fabrication with the possibility that the following items will require special consideration:

- (1) The development of fuel element assembly techniques by brazing, welding, or mechanical means to meet the AETR service conditions. In the past, no brazed fuel assemblies have been employed under as severe operating conditions. Developmental work may be necessary to produce a corrosion resistant and structurally satisfactory brazing alloy. Alternatives, such as spotwelding or mechanically joining (for example, roll swaging) will require investigation
- (2) Fabrication to close tolerances. This is especially important in the narrow channels between fuel plates
- (3) Inspection methods must be reviewed and methods chosen that are highly dependable for checking dimensional tolerances, cladding flaw detection, and examination of joint soundness. An extension of current inspection methods may be necessary on a production basis to ensure maximum quality of the large quantity of fuel elements to be produced for the AETR.

b. Corrosion of Cladding Material

Investigation of the effect of water purity on the corrosion of aluminum alloy X8001 at the operating conditions will be required. In particular, the effect of hydrogen and aluminum ion content of the water is not completely known. It is possible that corrosion rate can be reduced by not degassing the water or by not

removing all of the aluminum ions or by both. The aluminum ion and hydrogen buildups can be calculated and corrosion tests carried out at different values so that optimum water purity conditions can be selected. Allowance must be made for the hydrogen formed by radiolytic decomposition of the water. The pH will be maintained in the 5.5 to 6 range, as low as is practical with stainless steel in the system. Tests will be carried out in a dynamic loop.

It should be noted that fairly short term tests (about one month) will suffice for fuel element design. There is no interest in long term properties of cladding material for AETR application.

c. Performance and Operational Limitations

In order to demonstrate the adequacy of the fuel element design, full-size elements will be tested in an out-of-pile loop under AETR operating conditions of flow, temperature, pH and water purity. Tests will be run on elements that are at the limit of allowable dimensional tolerance to produce the severest possible conditions. Besides the mechanical design information obtained from this test, the corrosion resistance of the element under dynamic conditions also will be studied. In particular, the effect of water velocities above the current design limit will be investigated. From a corrosion standpoint, a test under radiation should not be necessary. However, several full-size prototype elements will be placed in the ETR for final verification of the out-of-pile experiments.

2. Pressure Vessel and Loop Materials

a. Radiation Damage

There are very few data on the long term radiation stability of materials. The flux in the AETR is appreciably greater than that of any reactor yet constructed. After a relatively short period of reactor operation, exposure levels of the structural materials will reach values beyond those encountered in current reactors or in most radiation damage investigations.

Some long term tests have been run in the MTR and, more

recently, materials for ETR loops have been tested. These irradiations are still in progress, and much of the information developed will be of interest to the AETR design. However, some effort will be required to evaluate the importance of radiation damage to structural material under AETR conditions. Long term tests on 6061 aluminum and 2014 aluminum will probably be required. Tensile and impact specimens would be inserted in the ETR for a period of over a year to determine the effect of high exposure levels on strength and ductility. No evidence exists which would indicate that aluminum should suffer a large degree of damage, even after an extended period of time under irradiation. However, verification of this conclusion is required.

Test specimens would be included in the AETR in positions of maximum flux. These would be removed and tested periodically. Besides indicating the condition of the reactor vessel, valuable radiation damage information would be obtained from such tests.

b. Fabrication

Some difficulty is visualized in connection with producing acceptable weldments and welded joints in the thick sections required. Welding procedures incorporating filler rods of adequate corrosion resistance must be developed.

From a corrosion standpoint, use of type 2014 aluminum in contact with process water in the pressurized water loops is somewhat questionable. As an alternative, the fabrication of aluminum-clad 2014 tubes will be investigated. If thickness requirements for these tubes can be relaxed, type 6061 can be substituted with fewer problems. If it is necessary to use 2014, extensive corrosion tests under operating conditions must be carried out.

Special liner materials will be necessary for high temperature gas and liquid metal loops, giving rise to many fabrication problems. Since exact experimental requirements are not known at this time, no estimate is made of possible research and development effort.

Such activity would be more appropriately carried out in connection with the design of the particular in-pile experiment.

3. Heat Transfer and Fluid Flow Systems

The objectives of the heat transfer and fluid flow research and development program are:

To verify the analytic prediction of the thermal and hydrodynamic performance of an AETR fuel assembly, and,

To observe fuel element structural stability.

To carry out this part of the program experimental fuel elements will be constructed with thermocouples attached at various places on and within the cladding so as to evaluate thermal conductivity. The specimens will be subjected to in-pile testing and will later be examined for irradiation damage.

Out-of-pile tests will be conducted using a pressurized loop and simulated fuel elements, the latter to be of a geometrical configuration and size similar to the elements. The loop will have a recirculating pump and piping, a control valve, pressurizing heating coils, and a flanged removable test section. Instrumentation will consist of thermocouples, recorders, pressure indicators and flow indicator-recorders.

Structural stability of various fuel element configuration will be observed and the mechanical design of the elements modified as found necessary.

The adequacy of the fuel element design will be demonstrated by these in-pile and out-of-pile tests.

4. Reactor System Kinetics

The AETR concept differs significantly from conventional heterogeneous reactor designs in that control is accomplished by changing the reflector characteristics and by regulating type control rods. For this reason it is important to determine the response of the reactor system to changes in temperature, pressure, and flow rate.

In this part of the research and development program, the reactor control system stability and scram response time of the reactor system

will be demonstrated. Over-all reactor control and self-regulating characteristics will be investigated on a reactor simulator. Quantitative comparisons of the influence on stability of important design variations will be made, and the minimum dynamic performance required of various system components will be specified. The time required to drop the reflector level for scram, and the rate at which boron concentration in the outer reflector region can be changed, will be demonstrated by a mock-up of the reflector control systems. The mock-ups will consist of the necessary control annuli, control valves, piping, instrumentation, pumps, and demineralizer system.

Critical components of the control systems must be developed and tested for operating integrity and reliability. These components will include pumps, regulating rods and drive mechanism, valves and concentration controls.

It is also necessary to demonstrate the stability of the borated D_2O solution under intense radiation. This requires irradiation of samples in a high flux test reactor. Other conditions that may affect the borated D_2O solution stability, such as temperature, pH, and corrosion products must be investigated.

5. Instrumentation and Special Components

The principal objective of this part of the research and development program is to investigate and experimentally demonstrate satisfactory performance characteristics of those portions of the AETR system that cannot be reliably subjected to analysis. Some of the areas of investigation would be instrumentation, thermal stresses in the pressure vessel, core structure, and test sections. The feasibility of keeping the test loop thimble liner at essentially zero pressure differential will be demonstrated. A mock-up of the pressure balance chamber or gas pressurizer will be necessary.

Because of the high burnup rate of the fuel elements in the AETR, it is mandatory that fuel be replaceable in the most expeditious manner. A development effort will be made for fuel handling and shipping

equipment. This equipment will include special tools for manual lifting of spent fuel elements from the core region and for insertion of new ones. Storage racks will be developed for safe handling and storage of fuel within the canal. In the event of fuel element warpage or rupture, special tools will be needed to correct and repair the damage from a safe distance.

Also included in the program will be the development of handling and storage procedures.

6. Test Loops and Associated Equipment

Very little is known of the nature of the actual tests to be performed by the AETR. Therefore, no attempt has been made to describe a research and development program for the test loops other than that described above for the test loop thimble liner. The operating temperatures and conditions specified for these loops do indicate that a research and development program will be necessary for the test loops and other testing equipment and instrumentation. In the case of high-temperature circulation of liquid metals, an extensive development program would be required. No known installation, experimental or otherwise, has performed such circulation at the higher temperature specified.

B. ESTIMATED COST AND TIME REQUIRED

The total estimated cost of the research and development program outlined above is \$2,376,000 (See Table X). This figure does not include any post-critical research or development work, nor does it reflect any expenses for a critical assembly or an experimental core.

The estimated cost appears to be very modest, but it might well be so for several reasons. Although the AETR fuel elements are unique in design, they still represent flat plate fuel elements on which considerable manufacturing and operating experience has been accumulated. Other features of the plant also are pushing the limits of known technology, but by and large have been proved.

The temperature, pressure, and velocity conditions of the auxiliary

systems are all within the range of "off the shelf" equipment and should require virtually no research or development.

It should be again pointed out that this program and cost estimate does not allow any expenses for development of the reactor test loops and associated equipment nor for development of special equipment for handling test specimens.

When the exact nature of the tests have been determined, it is recommended that a detailed Research and Development program be outlined. Only after a detailed program including consideration of the tests to be performed, the site selected, and the element of time has been outlined, can an accurate estimate of the cost be made.

It is estimated that the time for completion of the Research and Development program would be in the neighborhood of 30 months. This, of course, would depend largely upon the urgency of the plant construction schedule. A considerable proportion of the program could be done concurrently with the design and construction of the plant.

TABLE X

R & D COST ESTIMATE

A. FUEL ELEMENT DEVELOPMENT

1. Fabrication

Tooling, Jigs and Fixtures	\$ 20,000
Materials (including U metal conversion cost)	10,000
Engineering - 30 MM	60,000
Technician - 60 MM	<u>90,000</u>
Subtotal	\$180,000

2. Corrosion Experiments

Engineering - 24 MM	\$48,000
Dynamic Autoclave and Accessories	30,000

Technician - 30 MM	\$ <u>45,000</u>
Subtotal	\$123,000
3. Metallurgical Performance and Operational Limitations	
Materials and Supplies - out-of-pile tests	\$ 5,000
Loop design and construction	200,000
Prototype fuel elements irradiation (incl. facility charges)	35,000
Engineering - 20 MM	40,000
Technician - 24 MM	<u>36,000</u>
Subtotal	\$316,000
B. PRESSURE VESSEL AND LOOP MATERIALS DEVELOPMENT	
1. Radiation Damage - Static In-pile Capsule Tests	
Engineering - 20 MM	\$ 40,000
Technician - 20 MM	30,000
Irradiation and Hot Cell Charges	<u>100,000</u>
Subtotal	\$170,000
2. Fabrication	
Materials and supplies	\$ 10,000
Engineering - 12 MM	24,000
Technician - 12 MM	<u>18,000</u>
Subtotal	\$52,000
Total	\$841,000
C. HEAT TRANSFER AND FLUID FLOW	
1. Temperature Distribution	
Materials and supplies	\$20,000

Engineering 12 MM	\$ 24,000
Technician 24 MM	<u>36,000</u>
Subtotal	\$ 80,000
2. Determine Hydrodynamic Characteristics	
Materials, supplies, loop operation	\$ 50,000
Engineering 10 MM	20,000
Technician 10 MM	<u>15,000</u>
Subtotal	\$ 85,000
3. Verify Thermal Performance	
Materials and supplies	\$ 35,000
Engineering 20 MM	40,000
Technician 20 MM	<u>30,000</u>
Subtotal	\$105,000
4. Observe Fuel Element Stability	
Fabrication of dummy elements	\$ 10,000
Materials and supplies, loop operation	60,000
Engineering 24 MM	48,000
Technician 24 MM	<u>36,000</u>
Subtotal	\$154,000
D. REACTOR SYSTEM KINETICS	
1. Reactor Control	
Control mock-up design and construction incl. experimental mechanical rod drive	\$135,000
Engineering 12 MM	24,000

Technician 20 MM	<u>\$ 30,000</u>
Subtotal	\$189,000
2. Performance and Operational Limitations	
Materials and supplies	\$ 20,000
Engineering 24 MM	48,000
Technician 20 MM	<u>30,000</u>
Subtotal	\$ 98,000
3. General Reflector Systems Development	
Equipment and Facilities	\$ 100,000
Engineering 24 MM	48,000
Technician 24 MM	<u>30,000</u>
Subtotal	\$178,000
4. Determine Stability of Borated D ₂ O Under Irradiation and Other Operating Conditions	
Irradiation Facility charge	\$ 35,000
Materials and supplies	20,000
Engineering 12 MM	48,000
Technician 10 MM	<u>30,000</u>
Subtotal	\$133,000
E. INSTRUMENTATION AND SPECIAL COMPONENTS	
1. Instrumentation	
Materials and supplies	\$ 50,000
Engineering 12 MM	24,000
Technician 24 MM	<u>36,000</u>
Subtotal	\$110,000

2. Thermal Stress Analysis

Material and supplies	\$ 25,000
Engineering 10 MM	20,000
Technician 20 MM	<u>30,000</u>
Subtotal	\$ 75,000

3. Fuel Handling Equipment

Materials and supplies	100,000
Engineering 12 MM	48,000
Technician 10 MM	<u>15,000</u>
Subtotal	\$163,000

F. HEAVY CONCRETE SHIELDING

Materials and supplies	\$ 10,000
Engineering 6 MM	12,000
Technician 6 MM	<u>8,000</u>
Subtotal	\$ 30,000

G. FACILITY EXPENSE

1. Rent 30 months @ \$3500	\$105,000
Utilities 30 months @ \$1000	<u>30,000</u>
Subtotal	\$135,000

GRAND TOTAL \$2,376,000

XIV. AETR COST ESTIMATE

A cost estimate covering design, construction and annual operating expenses is presented in Table XI. The estimate is based on the preliminary conceptual design of the reactor facility described in this report.

The design cost includes design effort for the complete facility. Design effort on the experimental specimen and the auxiliary, experimental process equipment is not included because the exact nature of the experiments are not known. Also, field engineering, liaison effort, and inspection during fabrication and construction are not included.

The cost estimate for construction is broken down into 16 items covering equipment, systems or services. Comments are made on several of the listed items. Items not listed and not estimated are discussed.

The reactor vessels include the installed cost of the seven vessels with the associated tubes for experimental specimen. Primary heat removal systems contain stainless steel piping, circulating pumps, and heat exchangers with stainless steel tubes. Main coolant heat exchangers will be large as some 35,000 square feet of heat transfer surface is required per reactor. Heat removal for two reflector systems per reactor is provided.

Instrumentation includes reactor building area monitors as well as reactor instrumentation. Experimental loop instrumentation is not included. Control systems cover regulating rods and drive mechanisms, pure reflector level controls, and poisoned reflector concentration control. Reactor auxiliary equipment includes purification, gas handling, pressure balance chamber equipment, tanks and other miscellaneous reactor equipment.

The secondary water system will contain the ultimate heat dump for all of the reactor facility. As the seven reactors have an accumulated thermal power rating of 1530 MW, the waste heat dump system is necessarily large. This necessity undoubtedly will be a significant factor on the geographical location of such a reactor facility. For cost estimating purposes the design heat removal load is taken at 110% of the above power rating of the reactors. After briefly considering how the heat load affects the plant location and how the location affects the selection of the type of heat removal system, the necessity of using

atmospheric evaporative type cooling towers is assumed. Makeup water can be supplied either by a river, a lake, or from wells. Although dependent on factors other than heat load, the makeup flow to the cooling towers is estimated to be in the order of 20,000,000 gallons per day; hence, the source must be a good one. Forced draft cooling towers themselves can be placed in an area of less than four acres. A suitable arrangement would probably require more room. Installed cooling towers, pump stations, piping, makeup water supply, and makeup water treatment system are included in the cost estimate.

Shielding cost for the facility appears low, especially for seven fairly high-power reactors. However, the reactors utilize mutual shielding to a considerable degree. The reactor design with a heavy water reflector and a thick steel thermal-neutron shield surrounding the reflector provides an inexpensive type shield for the high-flux central experiment. Philosophy adopted for the design allows access to reactor process and experimental equipment after the reactor is shut down but with adjacent reactors operating. Heavy concrete is used for the biological shield near the reactor. An ordinary concrete shield is used below and above the heavy concrete as well as for equipment shielding.

With such factors as location, nature and details of experimental requirements, and experiment coolant unknown, the proper evaluation of the need for containment is difficult. The purpose of the facility is for high performance testing, in fact, testing some specimens to failure. The unknown coolants, especially liquid metals or liquid fuels, probably contain more radioactivity than reactor cooling water. Further, the liquid metals probably have exothermic chemical reactions with water. Hence a containment vessel is assumed necessary. The design of the vessel is influenced more by plant layout and other requirements than by the volume of released fluids. The large volume of reactor cooling water is below atmospheric boiling temperature; hence, released energy of significant amounts must come from failure of the high pressure experimental loops or from exothermic chemical reactions. It is interesting to note that a containment vessel replaces a reactor building and may not be much more expensive than a so-called gas-tight building. Certain problems are common to each, such as the need for foundations, ventilation, insulation, personnel locks, and fuel transfer locks.

Experimental facilities are intended to include laboratories, hot cells, manipulators, and other laboratory equipment needed to carry on the huge experimental program. The estimate covers only the support facility external to the reactor building. It is conceivable that the actual cost for this item is considerably more than the figure listed. Experimental loop equipment and instrumentation are not included in the item.

Waste and sewage disposal covers gaseous, liquid and solid disposal. The gas disposal system includes retention tanks, blowers, and a stack. Liquid disposal includes retention tanks and basins, and processing equipment. Solid disposal will involve volume reduction and burial or storage. Electrical services provide a substation, in-plant distribution, and a small amount of emergency power. No transmission lines are included. The latter is a significant location-sensitive cost as the design power requirement is in the order of 40,000 to 50,000 kilowatts. Only a small amount of power is assumed for the experimental loops; bulk of the power goes to the primary and secondary reactor cooling systems.

Spent fuel storage and handling provides in-plant storage and transfer facilities including shielding. No shipping facilities, such as shipping coffins and a railway spur, are provided for in the estimate.

The requirements for buildings for reactor control areas, offices, shops and miscellaneous purposes are not well defined. Likewise ventilation or air conditioning requirements, primarily for the containment vessel, and the location-dependent site preparation effort are not defined. It is felt that the cost figures for these three items are good representative figures.

The contingencies for the construction cost of the facility were taken as 25% of the estimate. This high figure is appropriate for the preliminary status of the conceptual design, the large number of unknowns, and uninvestigated areas.

It should be noted that the construction costs do not include items for the experimental loop equipment and instrumentation nor for the cost of supplying fabricated fuel elements. Experimental loop equipment may vary considerably. For example, the cost difference between a closed-cycle recirculated gas loop and an open-cycle, once-through gas loop may be rather large. At high pressures

b

the open-cycle loop would require a costly compressor and heating installation. The closed-cycle loop would require a gas circulator. Experimental loop instrumentation would be largely dependent on the nature and objectives of the experiment.

The reactor installation annual operating costs have been estimated in part. Costs are included for the operating crew's salaries, the cost of power, and an item covering supplies, maintenance, and other indirect costs. The cost of power covers mostly the power for the primary and secondary cooling systems. The power is assumed to cost one cent per kilowatt hour. The operating factor or load factor is taken to be 80%.

No costs are estimated for fabrication of fuel elements, uranium inventory charges, value of uranium burnup, or chemical reprocessing of spent fuel. A very rough figure for fuel burnup only at a rated total power of 1530 MW and 80% operating factor was calculated to be more than \$9,000,000 per year. This indicates the total cost of fuel is a significant factor in the total operating costs. No costs for heavy water inventory charges or heavy water loss charges are included.

TABLE XI
AETR COST ESTIMATE

A.	Design	\$ 4,800,000
B.	Construction	
1.	Reactor Vessels (fuel excl.)	4,600,000
2.	Primary heat removal systems	7,700,000
3.	Instrumentation	1,900,000
4.	Control systems	1,400,000
5.	Reactor Auxiliary equip.	3,500,000
6.	Secondary water system	8,300,000
7.	Shielding	1,100,000
8.	Containment vessel, crane, foundation	2,600,000
9.	Experimental facilities (external to reactor)	4,000,000
10.	Primary water treatment and emergency cooling	2,500,000
11.	Waste and Sewage Disposal (gas and liquid)	2,500,000
12.	Electrical services (incl. substation, emergency power)	2,500,000
13.	Spent fuel storage and handling facilities	1,100,000
14.	Buildings (control, offices, shops, miscellaneous)	3,000,000
15.	Ventilation and air conditioning	1,000,000
16.	Site preparation	<u>1,000,000</u>
	Subtotal	\$ 51,100,000
	<u>Contingencies</u>	<u>8,500,000</u>
	Total, Construction	\$ 59,600,000

C. Operation (excl. fuel, D₂O costs)

1. Salaries	\$ 1,500,000	
2. Power	2,500,000	
3. Supplies, maint. etc.	<u>1,000,000</u>	
Total Cost per year		\$ 5,000,000

APPENDIX A

PHYSICS METHOD AND CONSTANTS

A. INTRODUCTION

The purpose of this appendix is to present in detail the method used in the calculations of criticality and flux. Many of the results obtained for the constants will be useful in research reactor applications other than AETR, and so they are presented here with that more general purpose in mind.

This appendix consists of the following parts: Description of Method, Comparison with Experiment (Method), Comparison With Experiment (Results), Choice of Number of Groups, The Few Group Constants.

B. DESCRIPTION OF METHOD

The procedure of calculation used was essentially that developed in this Division's report "Reactor Physics of H₂O-Moderated Power Reactors".¹ It was desired to use a many-group model for two reasons: (1) The core of the AETR is so thin that neutrons that are born within it will migrate in and out of the core many times before reaching thermal; thus, most of the neutrons that are absorbed in the core as thermal neutrons will have a life history that is not characteristic either of the core or of the reflectors; it might be expected that in this situation a multigroup approach would be needed for high accuracy; (2) Single region multigroup calculations give rise to results from which few-group constants can be conveniently and accurately determined, these few-group constants then being used in multiregion, few-group calculations.

The 22 group calculation incorporates the three methods of neutron slowing down: Inelastic scattering, Selengut-Goertzel for moderation by hydrogen, and Fermi aging for non-hydrogen elastic degradation. The neutron conservation equation that is solved is thus:

¹I. W. Richardson, J. W. Webster, et al, "Reactor Physics of H₂O-Moderated Power Reactors", ASAE-S-7 (February 1, 1958).

$$\begin{aligned}
& - D(u, \vec{r}) \nabla^2 \phi(u, \vec{r}) + \phi(u, \vec{r}) \Sigma_a(u, \vec{r}) + \phi(u, \vec{r}) \Sigma_n(u, \vec{r}) \\
& = f(u) \left[\int_0^{u_{th}} \nu \Sigma_f(u', \vec{r}) \phi(u', \vec{r}) du' + \nu \Sigma_{f_{th}}(\vec{r}) \phi_{th}(\vec{r}) \right] \\
& + \int_0^{u_{th}} g(u' \rightarrow u) \Sigma_n(u', \vec{r}) \phi(u', \vec{r}) du' - \frac{\partial \eta(u, \vec{r})}{\partial u} - \frac{\partial q(u, \vec{r})}{\partial u}
\end{aligned} \tag{1}$$

where at $u = u_{th}$, this has the special form:

$$-D_{th}(\vec{r}) \nabla^2 \phi_{th}(\vec{r}) + \phi_{th}(\vec{r}) \Sigma_{a_{th}}(\vec{r}) = \eta_{th}(\vec{r}) + q_{th}(\vec{r}) \tag{2}$$

where η is related to ϕ by the equation

$$\frac{\partial \eta(u, \vec{r})}{\partial u} + \eta(u, \vec{r}) = \phi(u, \vec{r}) \Sigma_{S_H}(u, \vec{r}) \tag{3}$$

and q is related to ϕ by:

$$q(u, \vec{r}) = \xi \Sigma_S(u, \vec{r}) \phi(u, \vec{r}) + b \frac{\partial \left\{ \phi(u, \vec{r}) \Sigma_S(u, \vec{r}) \right\}}{\partial u} \tag{4}$$

or, more approximately, just

$$q(u, \vec{r}) = \xi \Sigma_S(u, \vec{r}) \phi(u, \vec{r}) \tag{5}$$

where

$$b = \frac{\alpha - 1 - \alpha \ln \alpha + \frac{\alpha}{2} (\ln \alpha)^2}{1 - \alpha}$$

where

- $D(u, \vec{r})$ = diffusion coefficient at lethargy u and point \vec{r}
- $\phi(u, \vec{r})$ = flux per unit lethargy at point \vec{r}
- $\Sigma_a(u, \vec{r})$ = macroscopic absorption cross section at lethargy u and point \vec{r}
- $\Sigma_n(u, \vec{r})$ = inelastic scattering macroscopic cross section
- $f(u)$ = fission spectrum
- $\Sigma_f(u, \vec{r})$ = macroscopic fission cross section
- $g(u' \rightarrow u)$ = inelastic scattering spectrum
- $\eta(u, \vec{r})$ = slowing down density due to hydrogen
- $q(u, \vec{r})$ = slowing down density due to elements other than hydrogen
- Σ_{S_H} = macroscopic hydrogen scattering cross section
- Σ_S = macroscopic scattering cross section of elements other than hydrogen

$$\xi = \text{av log of energy loss per collision}$$

$$\alpha = \frac{A-1}{A+1}$$

The lethargy scale is divided into 22 intervals, including thermal, in the numerical solution of this set of equations. The group structure is shown in Table A-I. This group structure was chosen in the work of ASAE-S-7, and the same structure was used here so as to utilize some of the cross section averaging results already at hand.

The few-group model can be expressed in the form:

$$\begin{aligned}
 -D_1 \nabla^2 \phi_1 + \Sigma_{d_1} \phi_1 - \nu \sum_{i=1}^n \Sigma_{f_i} \phi_i &= 0 \\
 -D_2 \nabla^2 \phi_2 + \Sigma_{d_2} \phi_2 - p_1 \Sigma_{d_1} \phi_1 &= 0 \\
 -D_n \nabla^2 \phi_n + \Sigma_{a_n} \phi_n - p_{n-1} \Sigma_{d_{n-1}} \phi_{n-1} &= 0
 \end{aligned} \tag{7}$$

where

- ϕ_i = total flux in group i
- D_i = average diffusion coefficient for neutrons in the i th group
- Σ_{d_i} = the probability per cm of neutron travel that a neutron will be either absorbed or will drop in energy to the next lowest group i.e. group $i + 1$ (the subscript 'd' is intended to suggest the word 'disappearance').
- p_i = probability of escaping absorption in group i

The last or n th group is the thermal neutrons. The constants, Σ_{d_i} , of the few group equations for the core of the reactor can be evaluated from a knowledge of the $\phi(u)$ as obtained in the many group model for the equivalent bare reactor as follows:

$$\Sigma_{d_i} \int_{u_{i-1}}^{u_i} \phi(u) du = \int_{u_{i-1}}^{u_i} \Sigma_a(u) \phi(u) du + \int_{u_i}^{\infty} \left\{ \Sigma_a(u) + B^2 D(u) \right\} \phi(u) du \tag{8}$$

where u_{i-1} and u_i are the lethargy limits of group i . The B^2 in this equation is the buckling of the equivalent bare reactor. Equation (8) says, of course,

TABLE A-I

GROUP STRUCTURE FOR THE 22-GROUP CALCULATION

<u>Group</u>	<u>Energy Range</u>	<u>Lethargy Range</u>	<u>Lethargy Width</u>	<u>Comments</u>
1	5-10 Mev	0-.693	.69	
2	3-5	.693-1.203	.51	
3	2-3	1.203-1.609	.41	Fast Fission Range
4	1-2	1.609-2.302	.69	
5	.8-1	2.302-2.526	.23	
6	.6-.8	2.526-2.815	.29	
7	.3-.6	2.815-3.506	.69	
8	.3-.09	3.506-4.701	1.19	
9	.01-.09	4.701-6.908	2.21	
10	6 kev -.01 Mev	6.908-7.415	.51	
11	3-6 kev	7.415-8.111	.69	
12	.418-3	8.111-10.0088	1.97	
13	5 ev -.418 kev	10.0088-14.509	4.42	U-238 Resolved Resonance Region
14	2-5 ev	14.509-15.425	.92	
15	1-2	15.425-16.119	.69	
16	.4-1	16.119-17.034	.92	
17	.2-.4	17.034-17.728	.70	
18	.08-.2	17.728-18.643	.91	
19	.06-.08	18.643-18.933	.29	
20	.04-.06	18.933-19.336	.41	
21	.03-.04	19.336-19.624	.28	
22	(Maxwell-Boltzmann around kT)	(Maxwell-Boltzmann around $\ln 10^7/kT$)	1.0 (for computational purposes)	Thermal Group

that the flux in a group multiplied by the disappearance cross section must equal the total absorption rate in that group plus absorption in lower groups plus the leakage in lower groups.

The p_i can then be evaluated from

$$p_i \Sigma_{d_i} \int_{u_{i-1}}^{u_i} \phi(u) du = \int_{u_i}^{\infty} \left\{ \Sigma_a(u) + B^2 D(u) \right\} \phi(u) du \quad (9)$$

The Σ_{f_i} and D_i are evaluated from

$$\Sigma_{f_i} = \frac{\int_{u_{i-1}}^{u_i} \phi(u) \Sigma_{f_i}(u) du}{\int_{u_{i-1}}^{u_i} \phi(u) du} \quad (10)$$

$$D_i = \frac{\int_{u_{i-1}}^{u_i} \phi(u) D_i(u) du}{\int_{u_{i-1}}^{u_i} \phi(u) du} \quad (11)$$

In any region of the reactor other than the core, the $\phi(u)$ is computed for use in this formula assuming the region to be infinite in extent and taking B^2 as zero in Equation (8).

The constants in the thermal group are evaluated similarly from knowledge or assumptions regarding the spectrum of thermal neutrons.

By comparing the k_{eff} and thermal flux distribution obtained from calculation with the corresponding results of a three group calculation, the three group constants being obtained from the 22 group as described above, it was shown that a three group procedure would be adequate for the parameter optimization studies. This comparison will be described in detail in a later section of this appendix.

C. COMPARISON WITH EXPERIMENT (METHOD)

If the set of equations, (7), are only two in number and the constants are evaluated as above, then a useful check of the slowing down cross sections against experimental data can be made. The procedure concerns the age, τ , and is as follows: The Equations (7) are written:

$$-D_f \nabla^2 \phi_f + \Sigma_{d_f} \phi_f - (\Sigma_{t_s} \phi_s + \Sigma_{r_f} \phi_f) = 0 \quad (12)$$

$$-D_s \nabla^2 \phi_s + \Sigma_{a_s} \phi_s - p \Sigma_{d_f} \phi_f = 0 \quad (13)$$

Suppose the reactor is unimodal and has buckling B^2 . Then $\nabla^2 \phi_f = -B^2 \phi_f$ and it can be seen in Equation (12) that the total loss of fast neutrons is given by

$$D_f B^2 \phi_f + \Sigma_{d_f} \phi_f \quad (14)$$

On the other hand the rate of neutron becoming thermal is the last term in (13) or

$$p \Sigma_{d_f} \phi_f \quad (15)$$

From (14) and (15), the probability of any neutron becoming a thermal neutron, rather than leaking or being absorbed as a fast neutron is

$$\frac{p \Sigma_{d_f}}{D_f B^2 + \Sigma_{d_f}} \quad (16)$$

or

$$\frac{p}{\frac{D_f}{\Sigma_{d_f}} B^2 + 1} \quad (17)$$

In age theory, the corresponding expression is given by $p e^{-\tau B^2}$ (18) where τ is evaluated by the formula

$$\tau = \tau(0, u_{th}) - \int_0^{u_{th}} \tau(0, u) f(u) du$$

where $\tau(0, u) = \int_0^u \frac{D_f(u)}{\xi \Sigma_s(u)} du$ and $f(u)$ is the fission spectrum. In

Selengut-Goertzel theory for hydrogen moderation the corresponding expression can be forced into the form, (18), if τ is calculated with the inclusion of a very important first-flight term. The formula is

$$\tau = \int_0^{u_{th}} \frac{D(u)}{\Sigma_{sH}(u)} du - \int_0^{u_{th}} f(u') \int_0^{u'} \frac{D(u'')}{\Sigma_{sH}(u'')} du'' du' + \int_0^{u_{th}} f(u') \frac{D(u')}{\Sigma_{sH}(u')} du'$$

In either case these formulas for τ together with the form, (18), are correct only in the limit as $B^2 \rightarrow 0$ and for the case of no above-thermal absorption. Now, for small B^2 , the form, (18), can be written as

$$\frac{P}{1 + \tau B^2} \quad (19)$$

Furthermore, in age theory it can be shown that τ is 1/6 of the second moment of the slowing down density from a point source.

Thus, it has been shown, by a comparison of (17) and (19) that if B^2 is small and if the above thermal absorption is small then

$$\tau = \frac{D_f}{\Sigma_{d_f}} \quad (20)$$

where τ is the classic 1/6 of second moment. If these conditions, i.e., B^2 small and above-thermal absorption small, do not hold, then one can still write

$$\tau = \frac{D_f}{\Sigma_{d_f}} \quad (21)$$

but τ is now a fictitious age not equal to the classic quantity. It is obtained by using the 22 group results, Equations (8), (11), and (21).

Experimental data are available for 1/6 the second moment in various media of interest for the AETR, e.g., D_2O , $Al-H_2O$, and $Zr-H_2O$. These media satisfy the condition of small above-thermal absorption. By applying the 22 group model and Equations (8), (11), and (20) to an infinite region, when the second condition is satisfied, the age so obtained should equal the experimental value. Judicious adjustments in above-thermal cross sections associated with neutron slowing down can be made until the equality is obtained. These adjusted cross sections are then to be used in the design calculations.

D. COMPARISON WITH EXPERIMENT (RESULTS)

As was mentioned in Section B, in determining the Σ_{d_f} and D_f from Equations (8) and (11), and hence implicitly the τ , it is more accurate to use the $\phi(u)$ determined for the equivalent bare reactor based on the material buckling than to consider the core region to be infinite in extent. (This applies also to

the three group model.) However, for each change that is made to the composition of the core in the parameter survey, the material buckling is changed and therefore the above-thermal constants must be redetermined. It is more economical to use the infinite region constants if possible. It is therefore of interest to investigate, in addition to the agreement of infinite region ages with experimental values, the divergence of finite core ages from infinite core ages. The results of these two investigations will be given in this Section.

The age in D_2O (0.16% H_2O) was calculated by the method described to be $\tau(D_2O) = 124$.

The experimental value quoted in the Reactor Physics Handbook is $\tau(D_2O) = 125$.

The agreement was therefore considered excellent and the slowing down cross sections for D_2O were considered excellent.

Ages for Al- H_2O mixtures were then calculated for various metal to H_2O volume ratios. The medium was taken to be infinite and no fuel was present in the aluminum. The results are shown in Figure 30. The results shown there were arrived at with inelastic scattering for oxygen included but not for aluminum. (When inelastic scattering for aluminum was included, the calculated ages seemed unreasonably low at high Al/ H_2O ratios in the light of previous results in the literature and so it was arbitrarily omitted.) The agreement with the experiment done in 1949 at Al/ H_2O = 0.5 was excellent. Agreement is not very good with the point at Al/ H_2O = 1 from Mon P-219 quoted in the Reactor Physics Handbook. It lies somewhat above our calculated value. However, the Handbook lists this point as being dependent on theory and since it was done at such an early date, 1946, it didn't seem reasonable to take this point too seriously. Considering the excellent agreement at Al/ H_2O = 0.5, our curve shown in Figure 30 should be sufficiently accurate at all Al/ H_2O ratios for the present purposes. A good experimental measurement at Al/ H_2O = 1 would be a useful part of a continued AETR development program.

An investigation was then made of the effect on age of having 25% U-235 by weight in the meat of the fuel plates. Ages were evaluated using the multi-group, Equations (8), (11), and (21) for both infinite and finite core. Table A-II presents these results and compares them with the ages for infinite medium with no fuel present. It should be mentioned again that the ages for absorbing and/or finite systems are fictitious, effective ages.

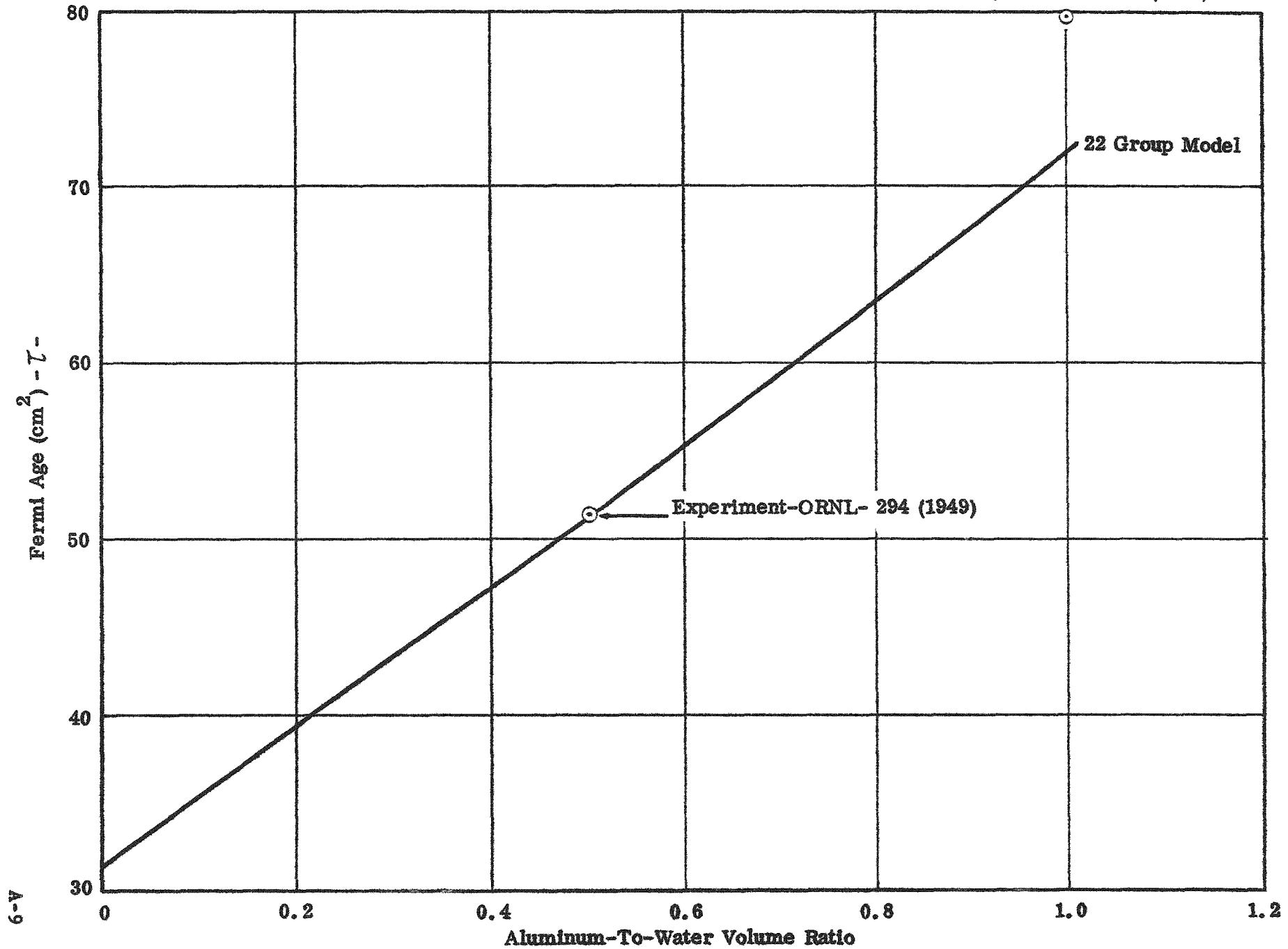


Figure 30 -- Fermi Age of Fission Neutrons in Aluminum-Water Mixture

TABLE A-II
AGES IN Al-H₂O MIXTURES

M/W Ratio	Infinite System Without Fuel	Infinite System With 25% U-235 In Fuel Plate Meat	Finite Reactor Corresponding To Material Buckling of 25% Fuel Case
0.5	51.3	49.2	--
1.0	71.8	63.8	78.6

If Equation (8) is examined it will be seen that the fictitious ages in the second column of the Table are lower than the corresponding entries of the first column because the integrated fast flux is lower per neutron born when above-thermal absorption is present (as well as because uranium provides some inelastic degradation). This makes Σ_{df} higher and τ lower. The entry in the last column is higher because the neutrons which leak as above-thermal neutrons are now absent from the right side of Equation (8) and this makes Σ_{df} lower and τ higher.

It is seen that the finite-medium age is significantly different from the infinite-medium age and really should be used to obtain accurate results for AETR. To save time and expense in the parameter studies, however, the infinite medium ages were used.

The ages in Zr-H₂O mixtures were then calculated. Figure 31 shows these results. The calculated results agree very well with the experimental point at Zr-H₂O = 0.25. They do not agree very well with the point at Zr-H₂O = 1.0 given on p. 74 of Vol. V, Geneva documents, which is stated to be based on "reactor analysis". As in the Al-H₂O mixtures there seems to be a need for a good set of experimental measurements of age for high Zr-H₂O ratios.

E. CHOICE OF NUMBER OF GROUPS

With the 22 group procedure which has just been described available to determine good constants for a few-group model and the accuracy of the cross sections known from the correlation of experiment with certain of the two group constants as discussed, then the next step is to decide how many groups are necessary for reasonable accuracy in this reactor type. It is desirable to keep the number of groups in the few-group model as small as possible, since this model is used in the parameter survey -- an extensive set of calculations.

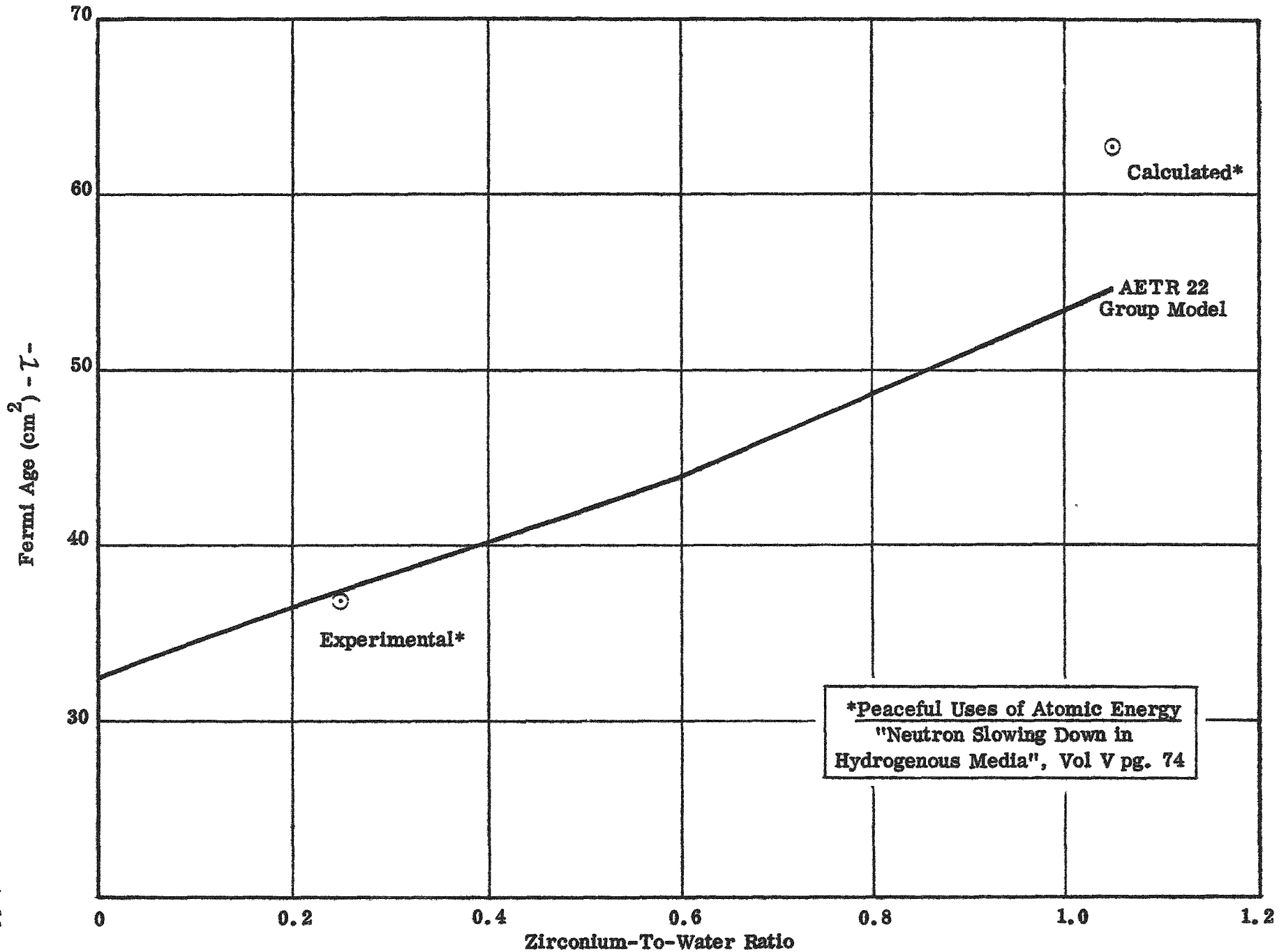


Figure 31 -- Fermi Age of Fission Neutrons in Zirconium-Water Mixture

It was decided to try three groups, with the top group extending from $u = 0$ to $u = 10.08$, which embraces the first 12 groups of the multigroup. A somewhat idealized AETR was calculated by 22 group and then by three group. The reactor had a central H_2O region, 16.83 cm in radius, an annular core of $M/W = 1.0$ with 25% weight percent uranium in the fuel plate meat extending from 16.83 cm radius to 21.27 cm, and a D_2O reflector outside the core extending to 43.81 cm. Figure 32 shows the comparison of thermal flux distribution, 22 group vs three group, this being the property of greatest interest in this reactor. It is seen that the three group flux in the test section lies slightly (20%) above the 22 group flux but sufficiently close to justify use of only three groups in the parameter studies. In a final analysis of the AETR, more groups should probably be used.

The k_{eff} for the three group calculation was about 4% higher than the 22 group result. This is believed to be directly a result of using the infinite region age in the core instead of an age based on the material buckling as was explained earlier. (This, incidentally, is believed by us to be part of the reason that MTR critical mass predictions were too low.) For this reason also it is recommended that more groups be used in a final analysis of an AETR design.

F. THE THREE GROUP CONSTANTS

With the three group model chosen and evaluated, it remained only to generate the three group constants for the parameter survey. These are plotted as curves of a particular constant vs metal-to-water ratio for the metal-water mixtures and are presented in table form for the single material regions.

Table A-III shows these results for the single materials and Figures 33 through 69b for the mixtures. These results should be useful for reactor calculations other than AETR.

TABLE A-III

THREE GROUP CONSTANTS

Material	Fe	Na	Al	D ₂ O	H ₂ O
D ^F (cm)	1.15	4.00	3.55	1.38	1.87
D ^{INT} (cm)	0.352	4.25	3.69	1.22	0.559
D TH (cm)	0.304	3.30	3.52	0.8	0.16
Σ _r ^F (cm ⁻¹)	0.00190	0.00126	0.00103	0.0213	0.0647
Σ _r ^{INT} (cm ⁻¹)	0.00987	0.000927	0.000757	0.0207	0.165
Σ _r TH (cm ⁻¹)	0.165	0.0128	0.0138	0.000027	0.0196
Σ _s ^{INT} (cm ⁻¹)	0.00190	0.00126	0.00103	0.0215	0.0640
Σ _s TH (cm ⁻¹)	0.000095	0.000238	0.000457	0.0207	0.163

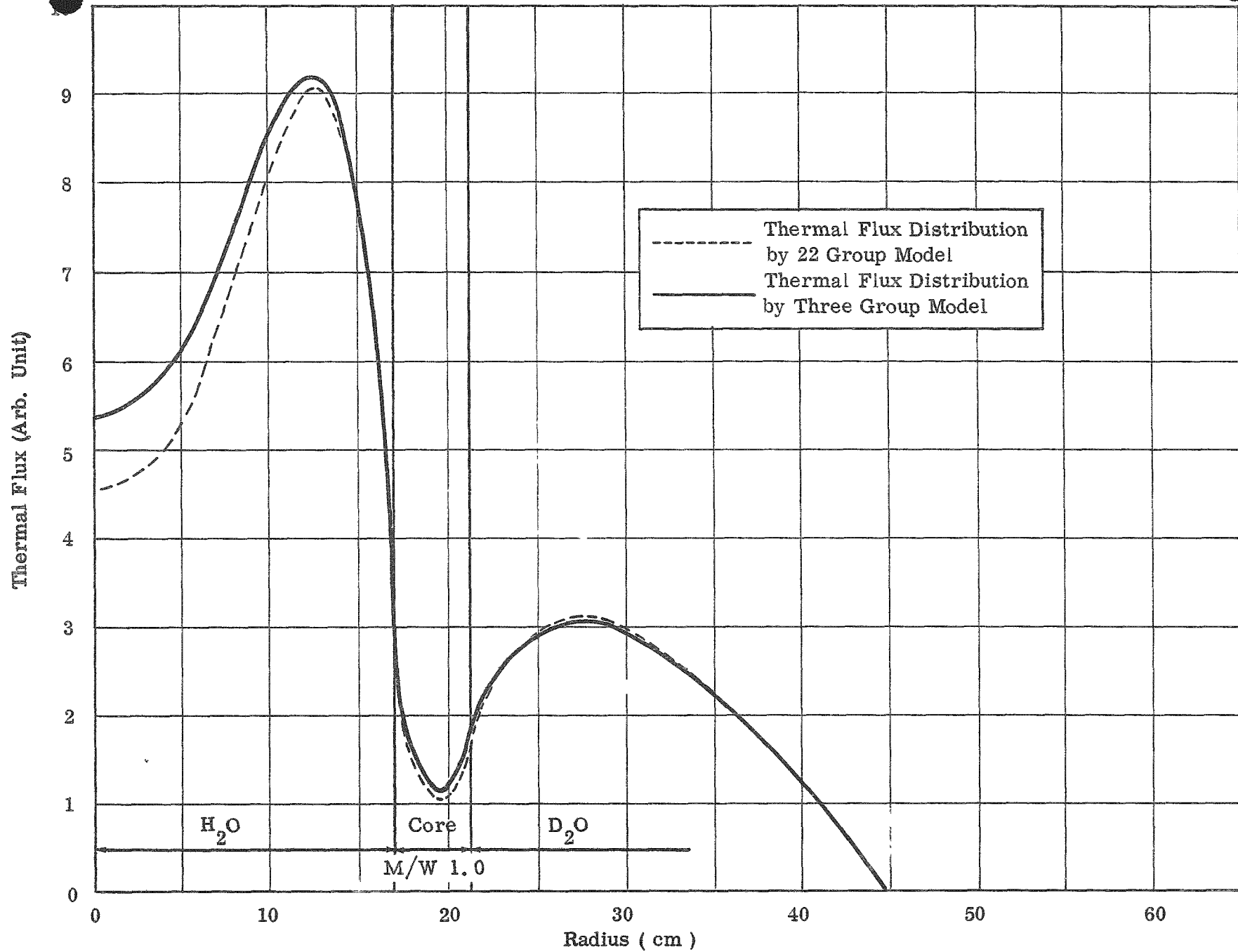


Figure 32 -- Thermal Flux Distribution by 22 and Three Group Models

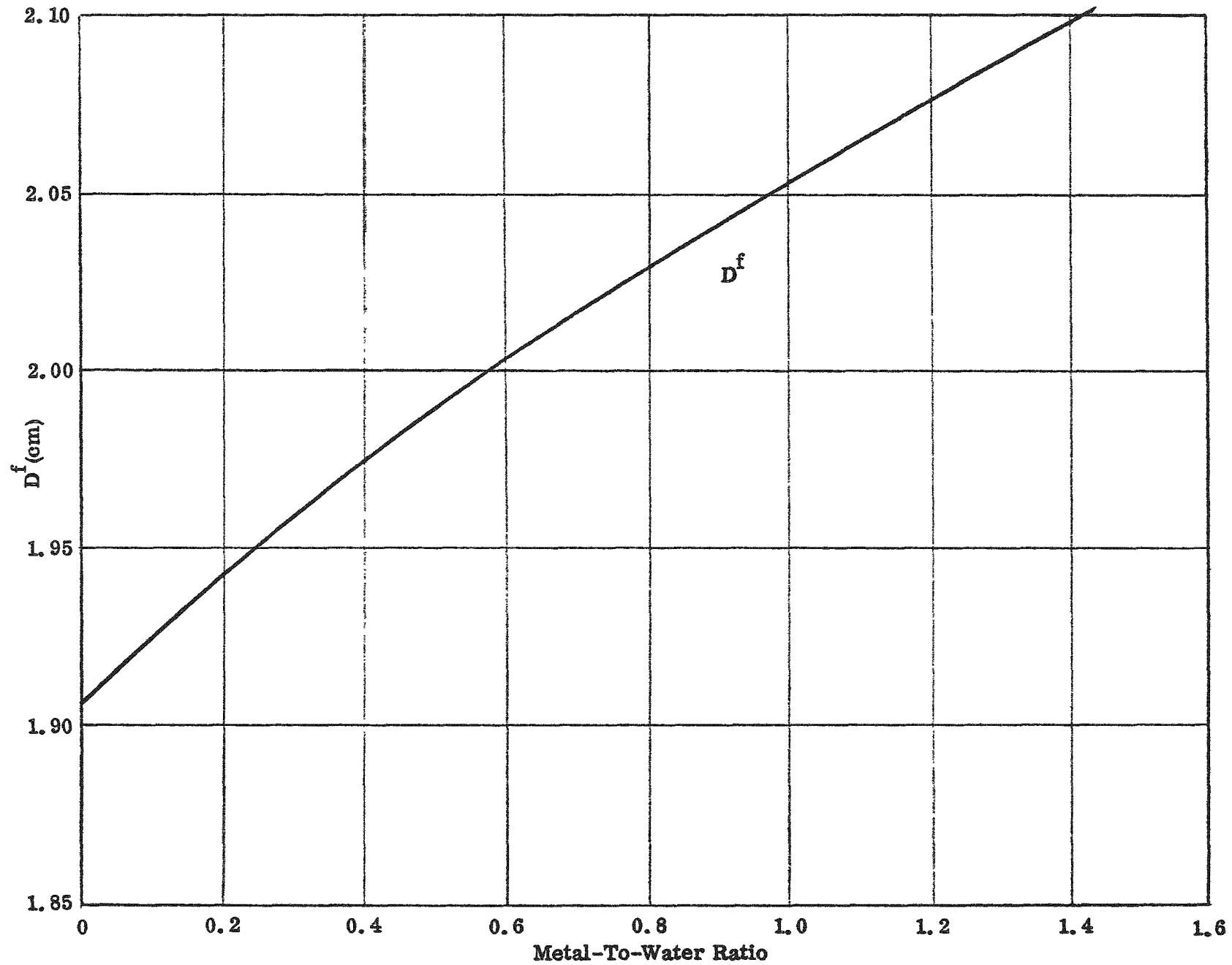


Figure 33 -- Fast Diffusion Coefficients vs M/W Ratio (15% by Wt. of U With Wedges)

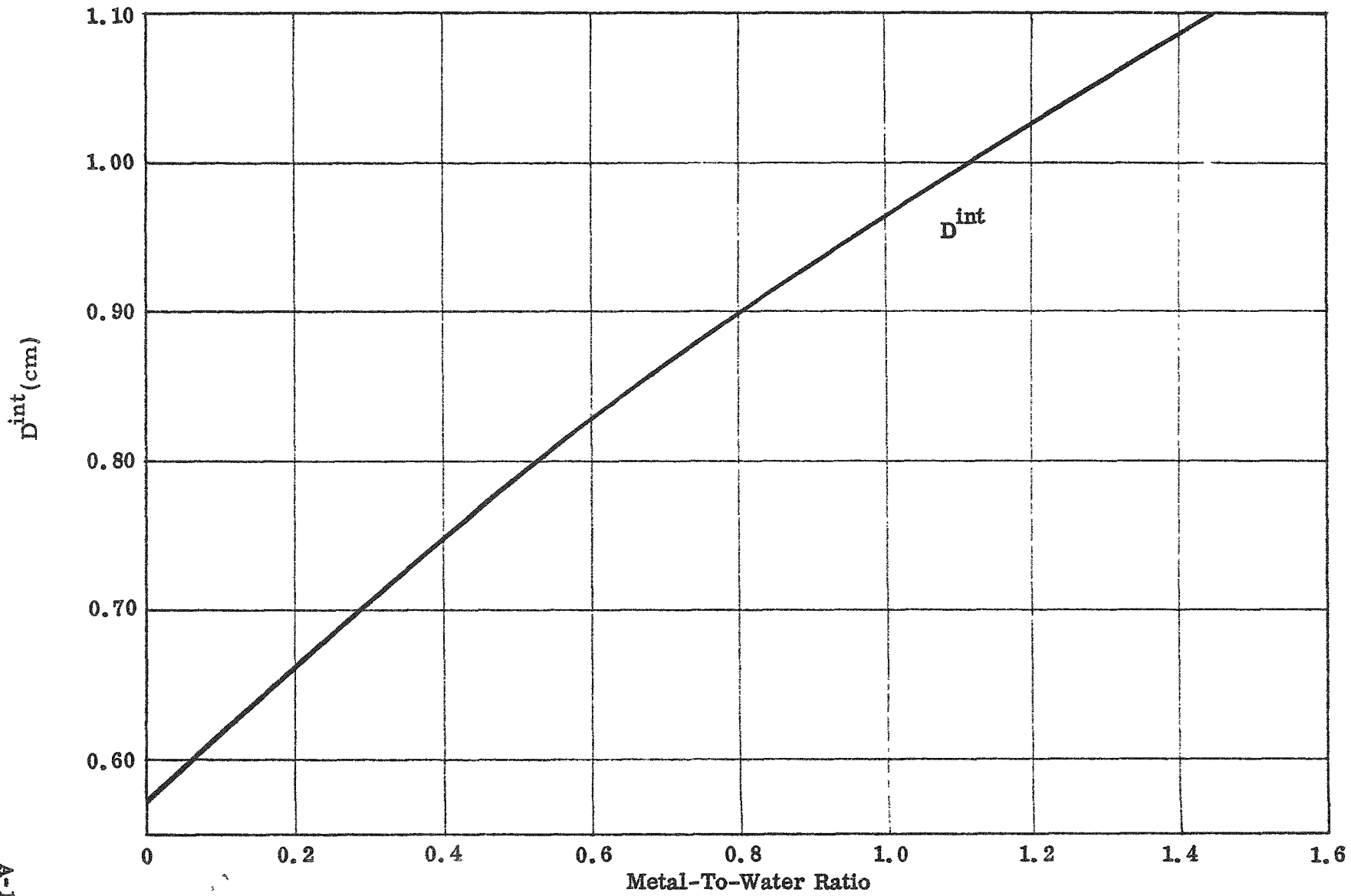


Figure 34 -- Intermediate Diffusion Coefficients vs M/W Ratio (15% by Wt. of U With Wedges)

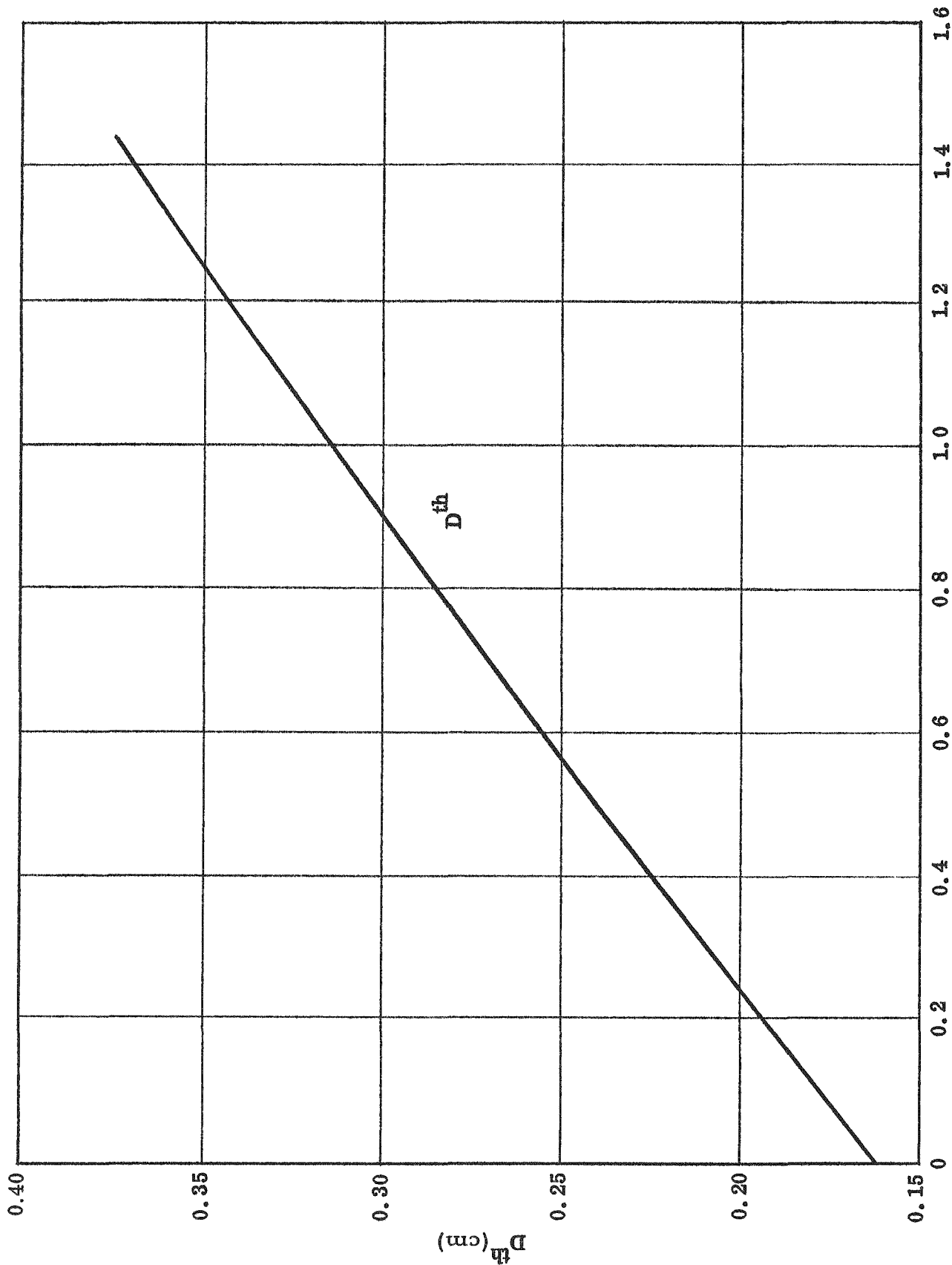


Figure 35 -- Thermal Diffusion Coefficient vs M/W Ratio (15% by Wt. of U With Wedges)

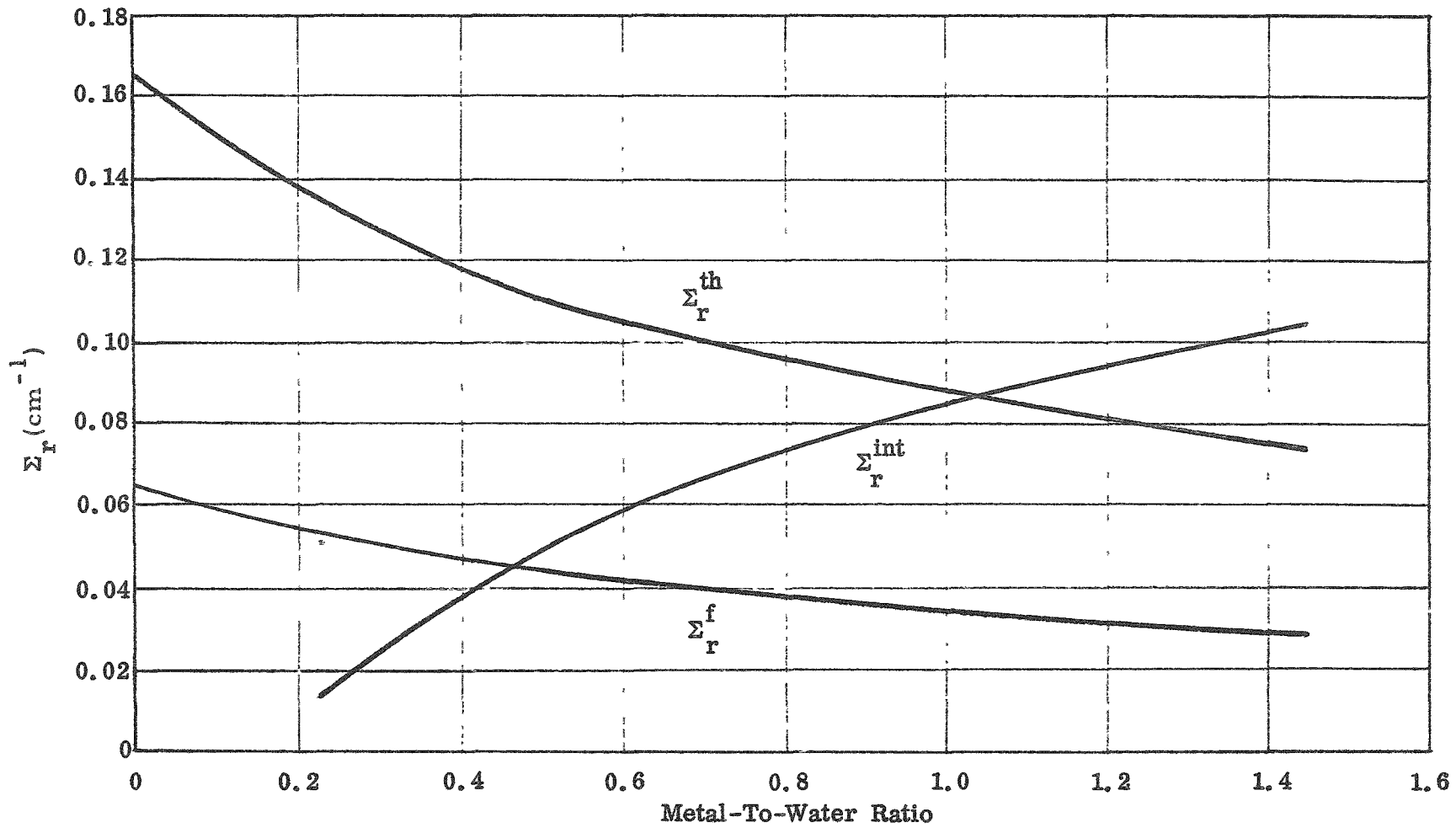


Figure 36 -- Removal Cross Section vs M/W Ratio (15% by Wt. of U With Wedges)

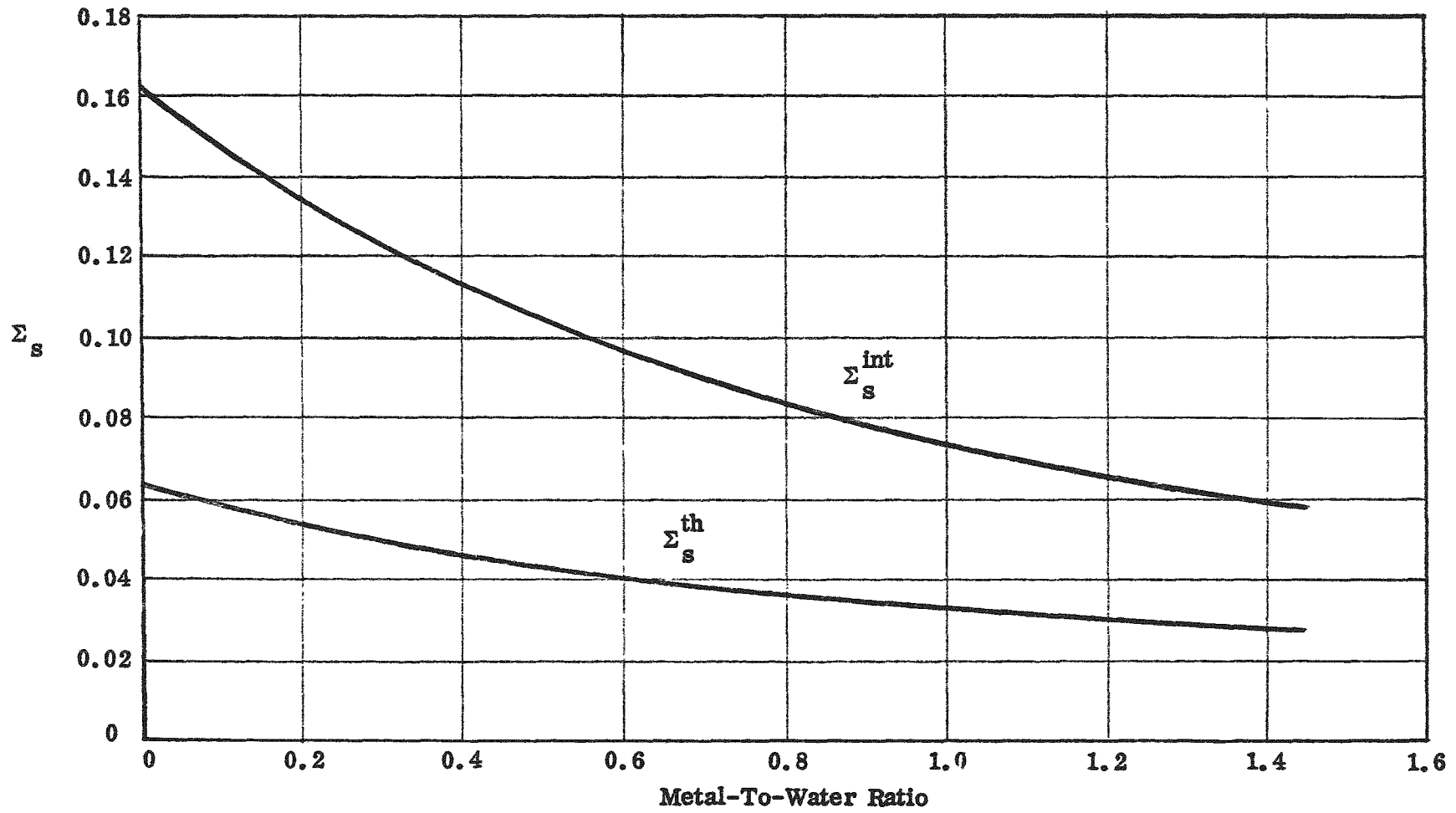


Figure 37 -- Source (From Moderator) Cross Section vs M/W Ratio (15% by Wt. of U With Wedges)

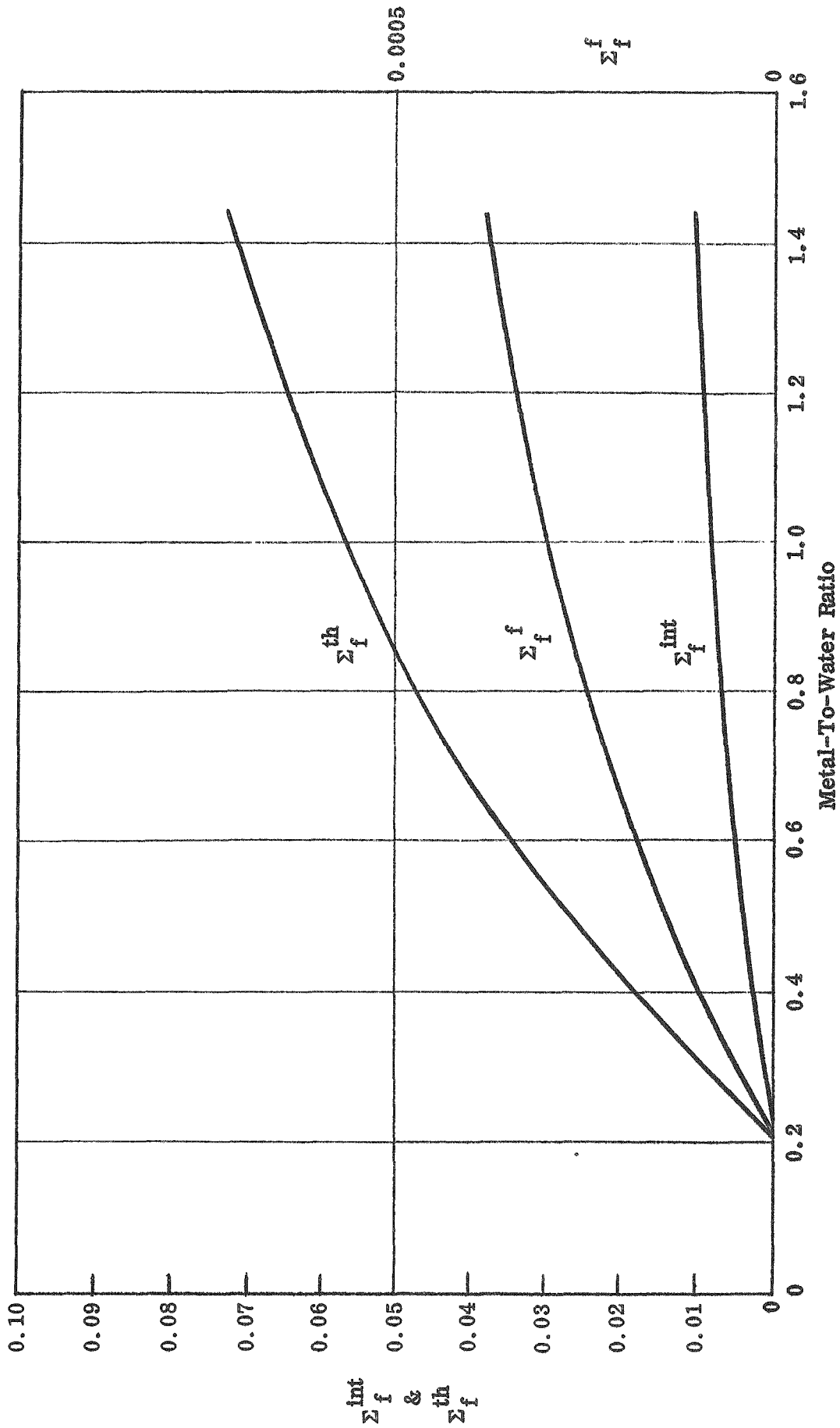


Figure 38 -- Fission Cross Section vs M/W Ratio (15% by Wt. of U With Wedges)

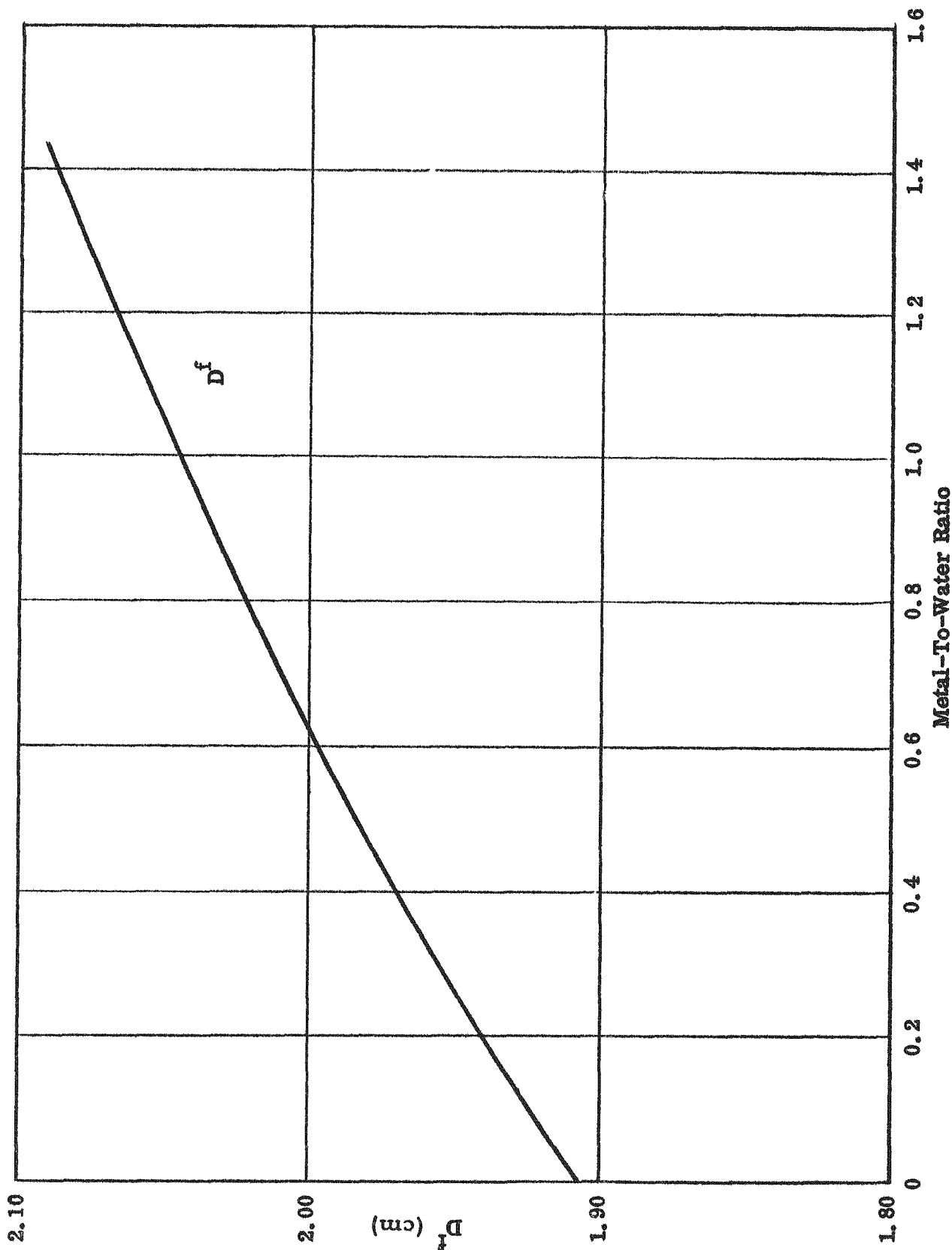


Figure 39a -- Fast Diffusion Coefficient vs M/W Ratio (25% by Wt. of U)

A-21

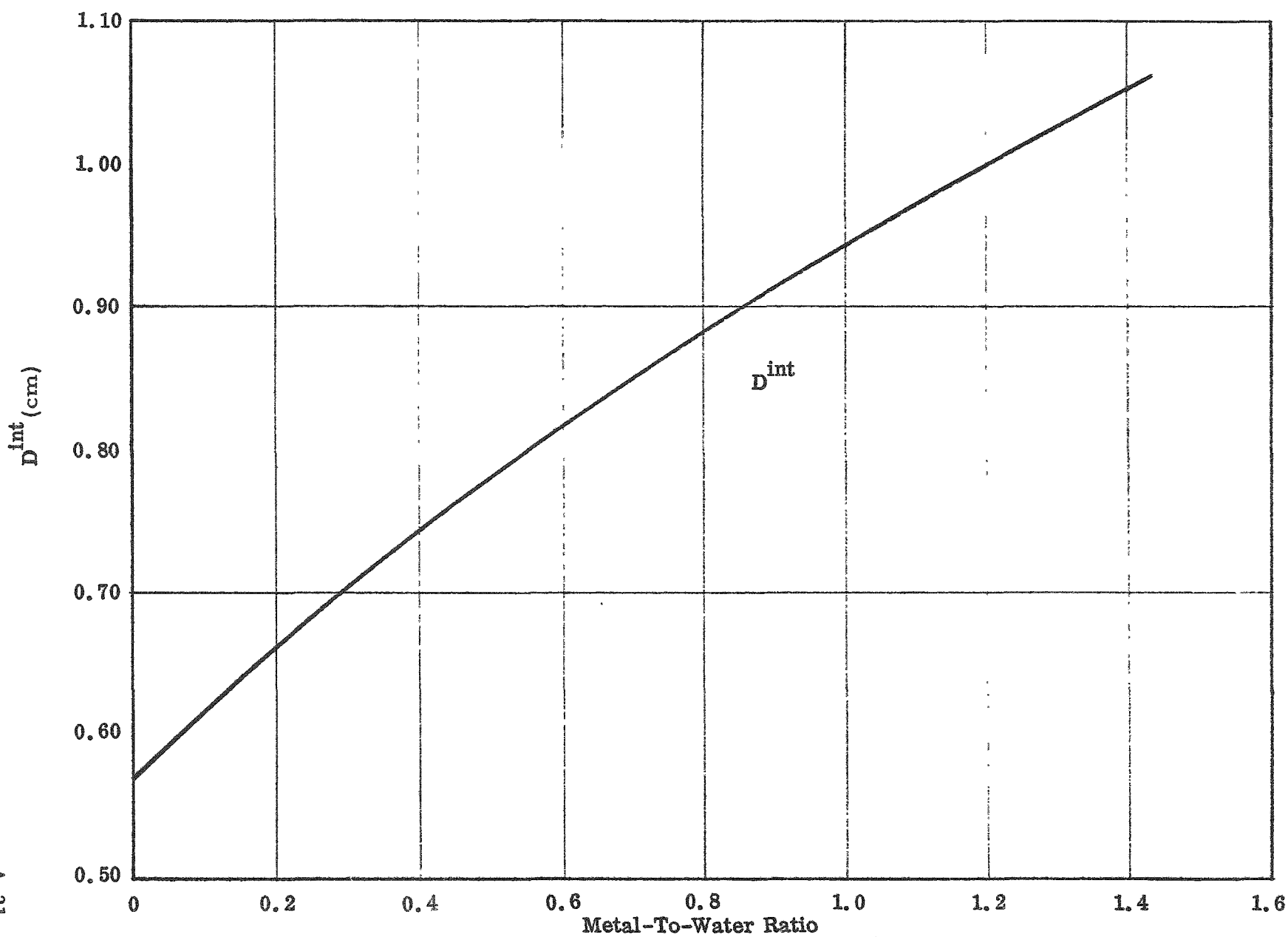


Figure 39b -- Intermediate Diffusion Coefficient vs M/W Ratio (25% by Wt. of U)

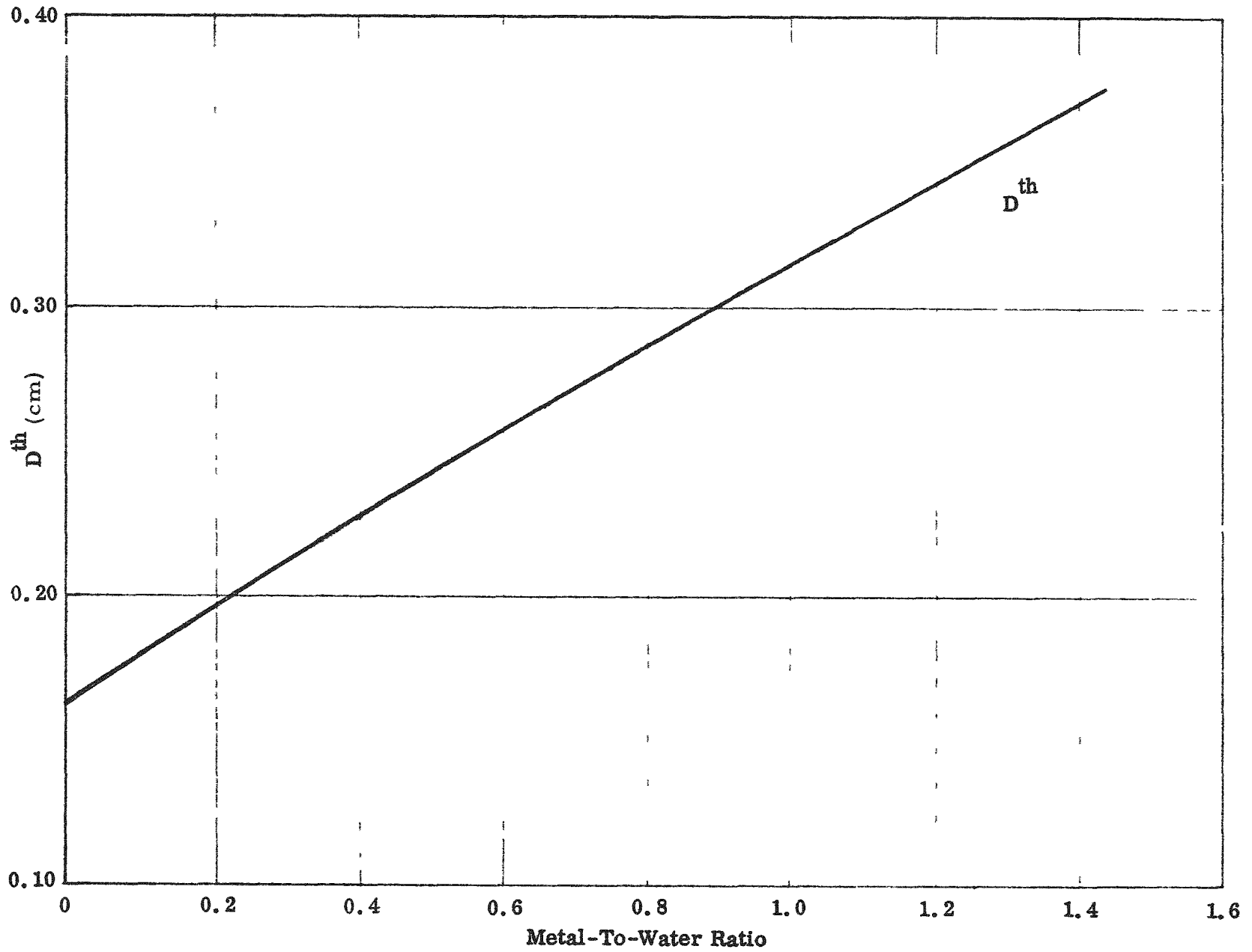


Figure 40 -- Thermal Diffusion Coefficient vs M/W Ratio (25% by Wt. of U With Wedges)

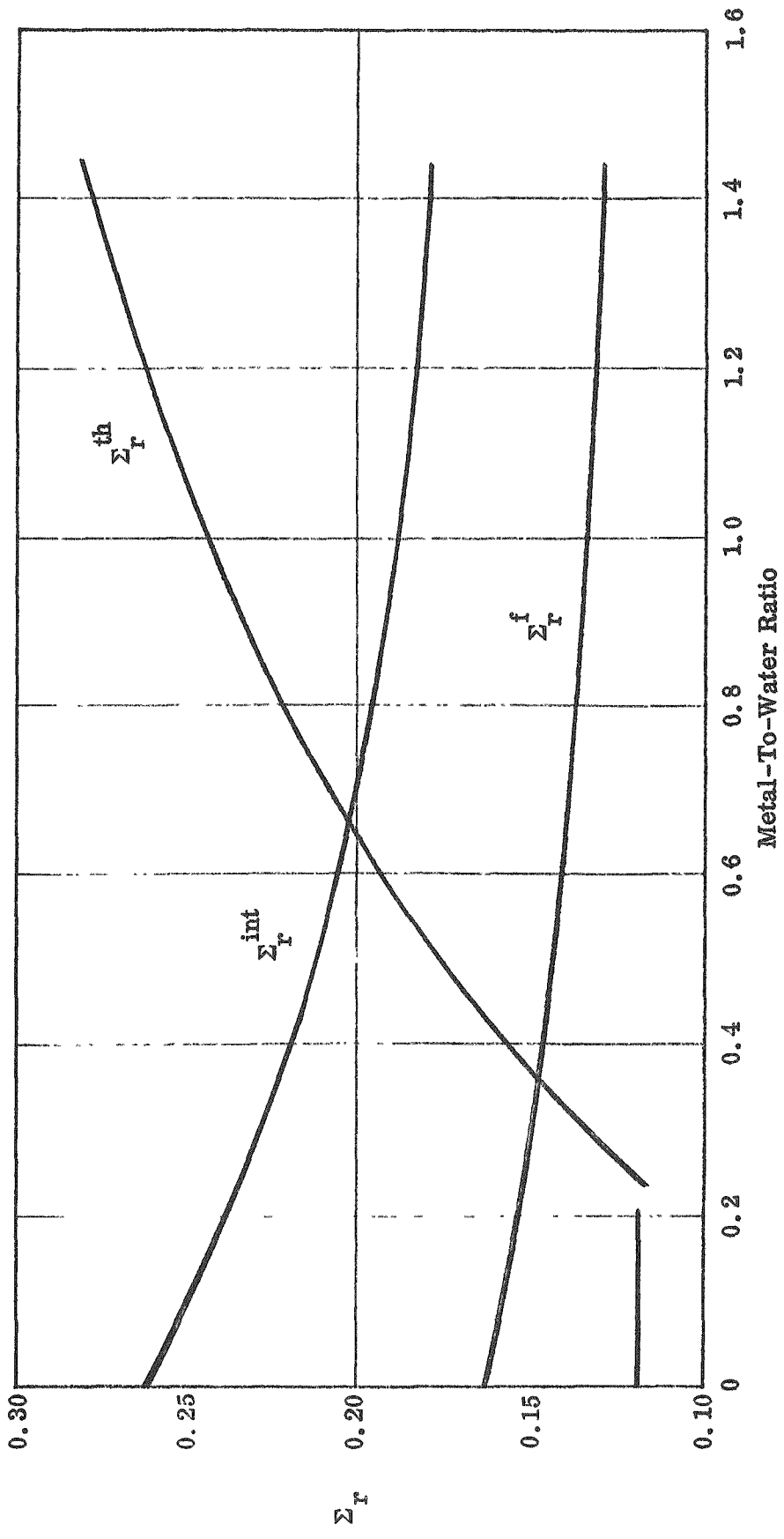


Figure 41 -- Removal Cross Section vs M/W Ratio (25% by Wt. of U With Wedges)

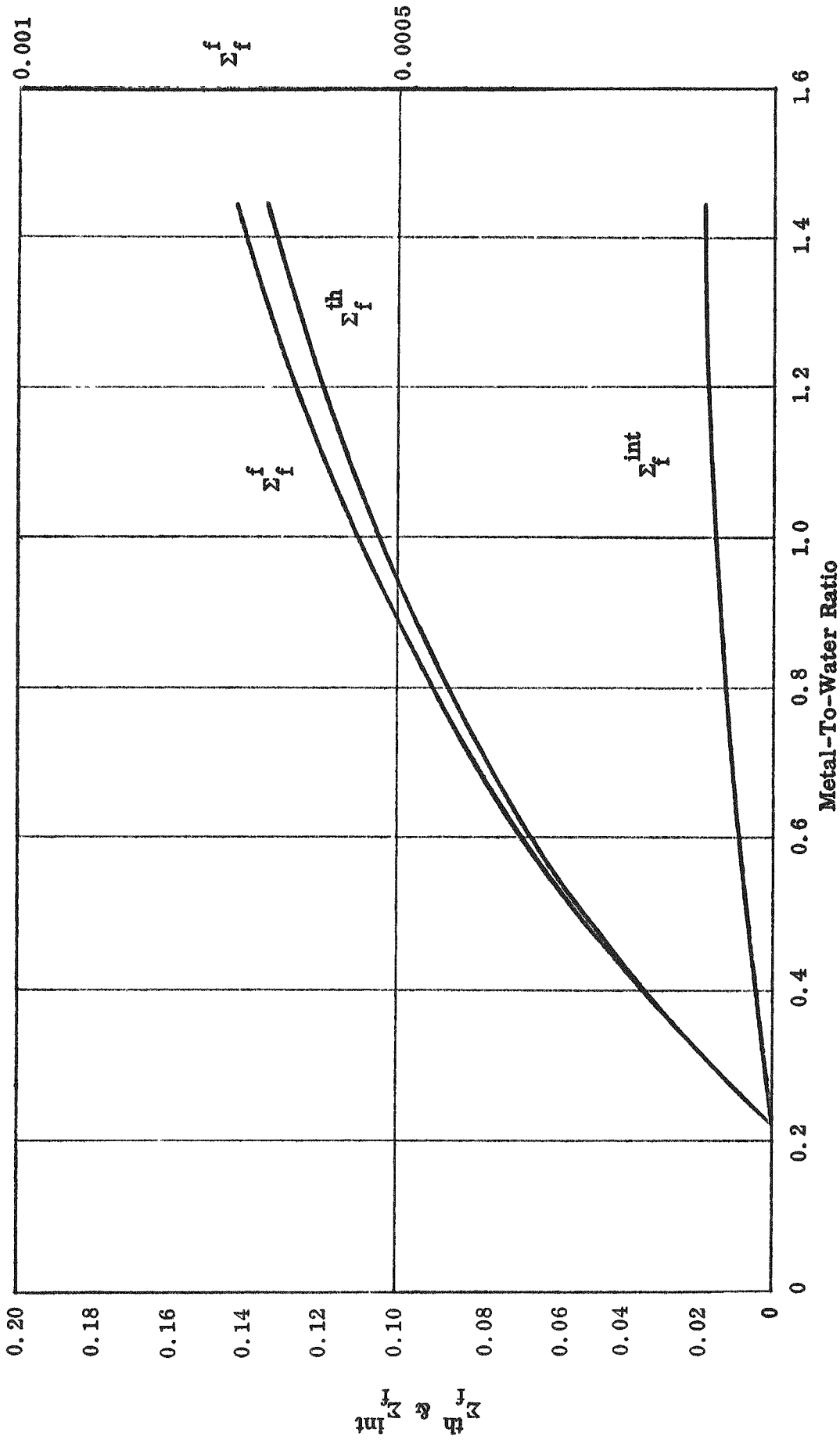


Figure 42 -- Fission Cross Section vs M/W Ratio (25% by Wt. of U With Wedges)

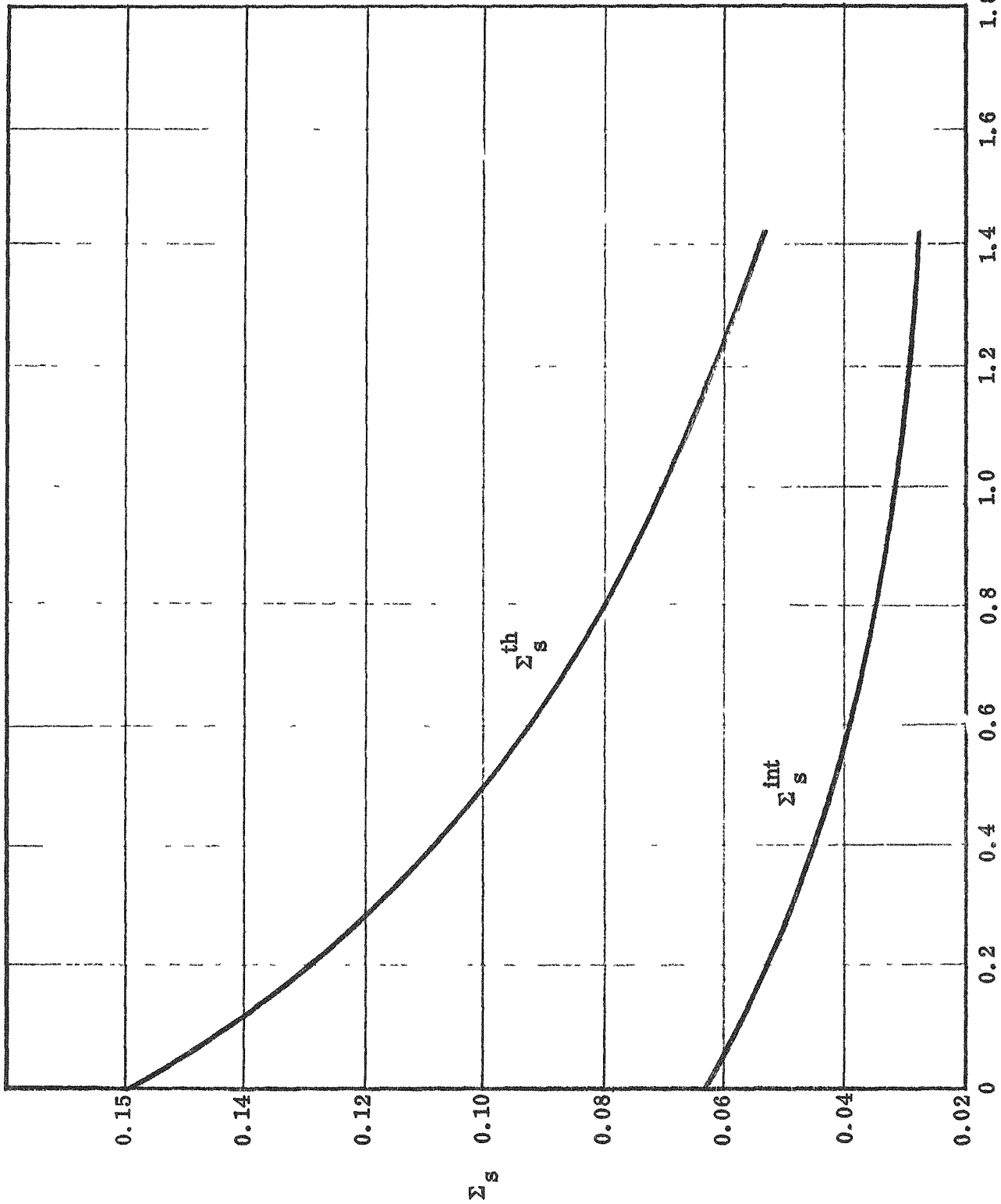


Figure 43 -- Source (From Moderator) Cross Section vs M/W Ratio (25% by Wt. of U With Wedges)

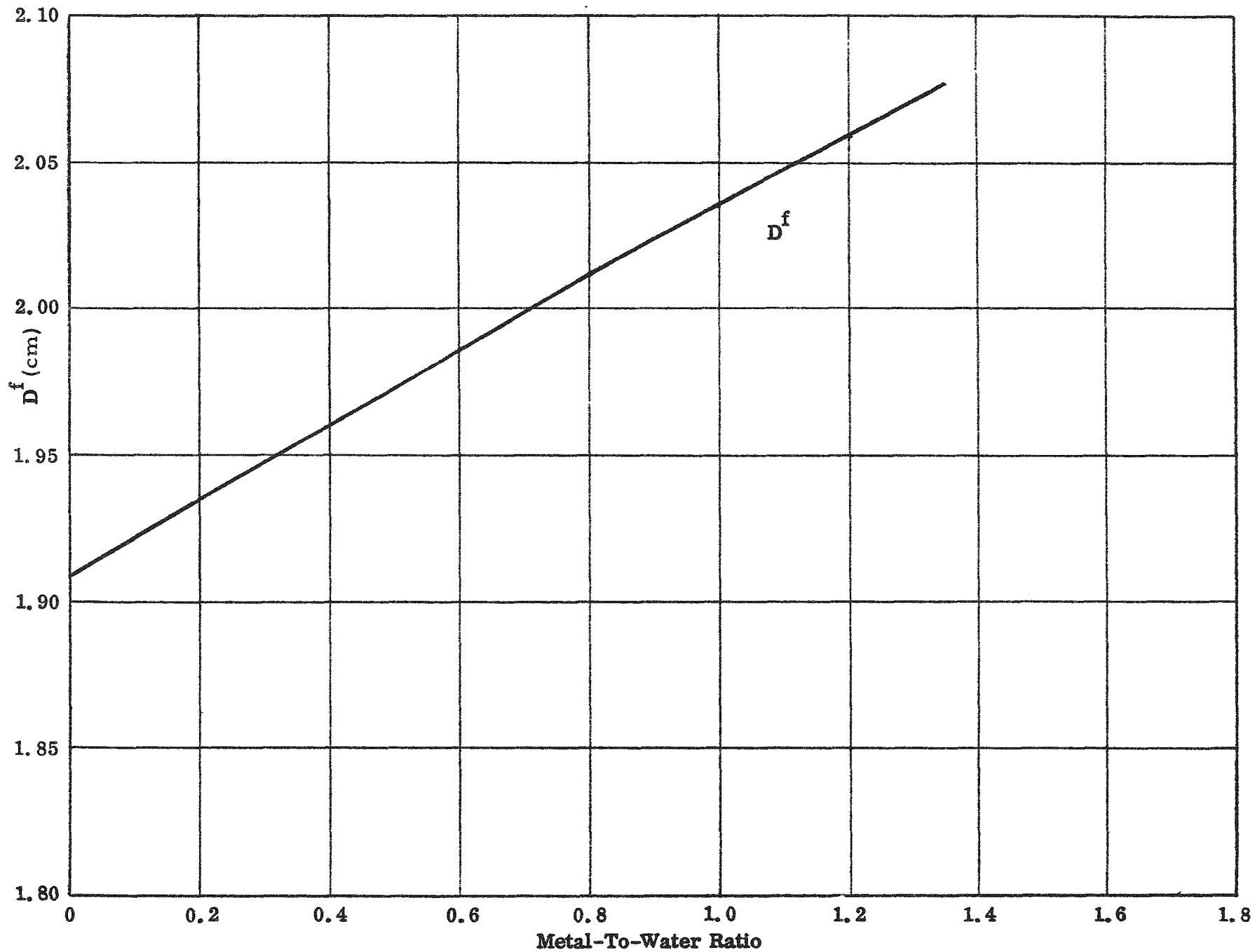


Figure 44a -- Fast Diffusion Coefficients vs M/W Ratio (35% by Wt. of U With Wedges)

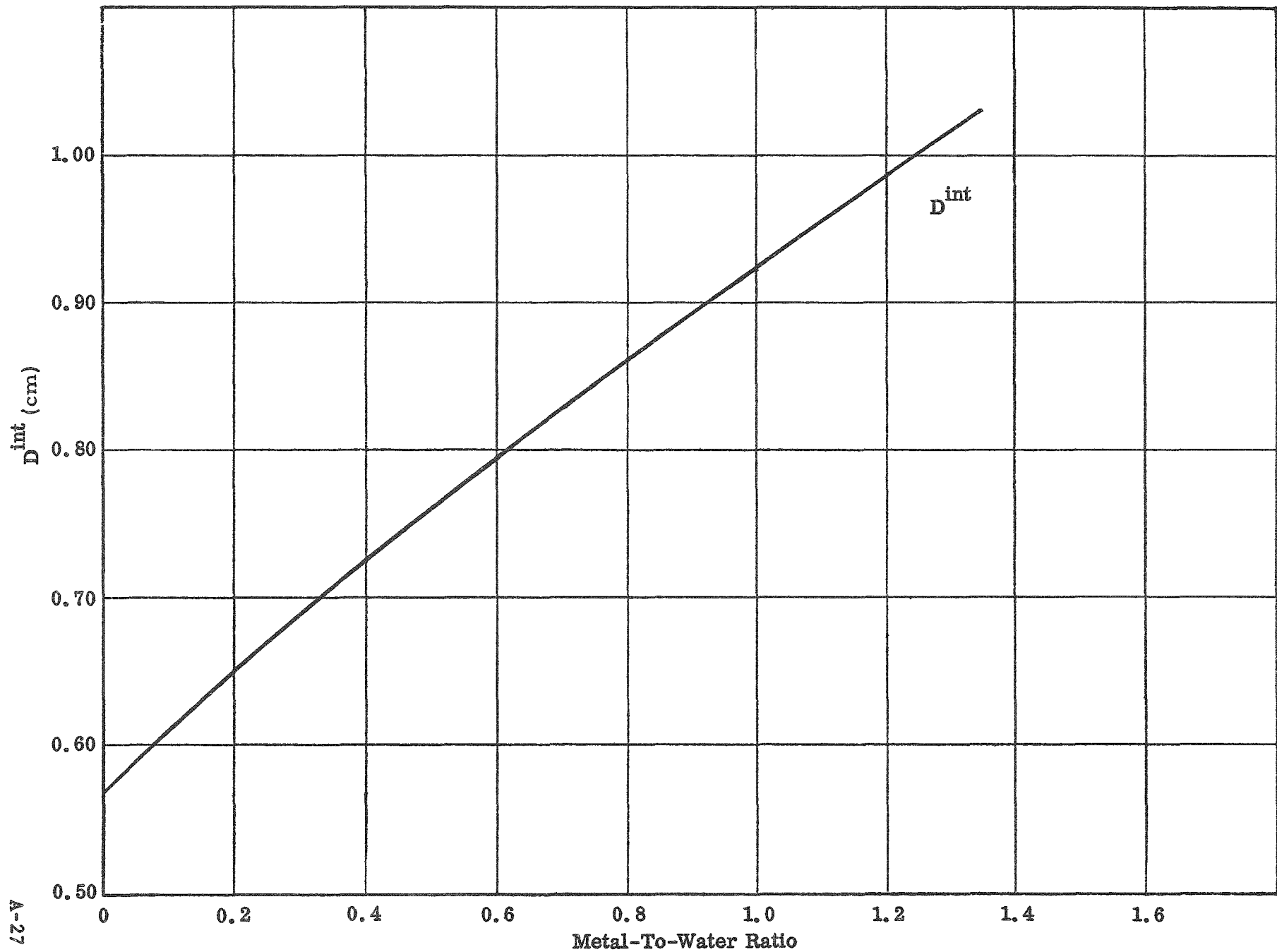


Figure 44b -- Intermediate Diffusion Coefficients vs M/W Ratio (35% by Wt. of U With Wedges)

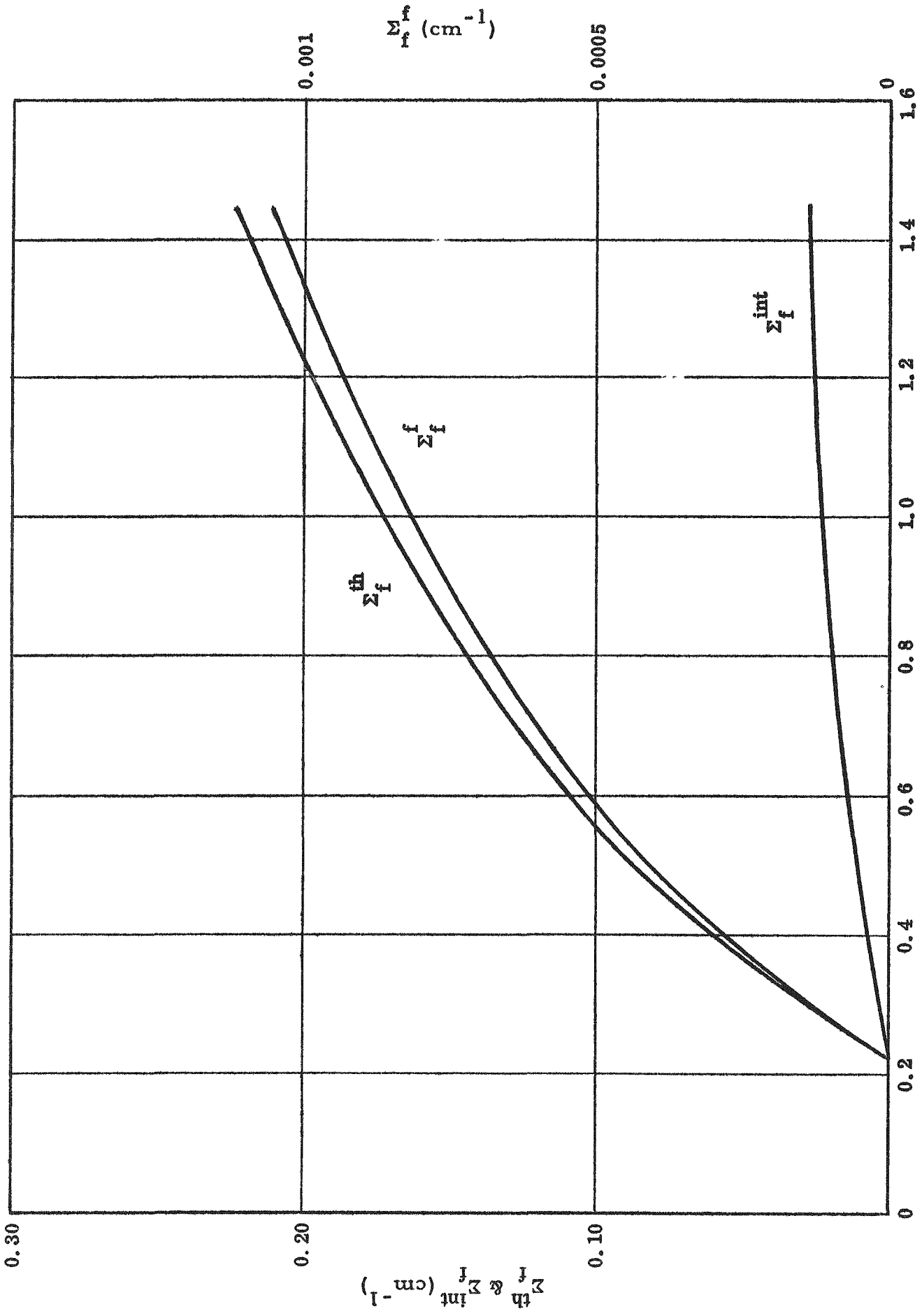


Figure 45 -- Fission Cross Section vs M/W Ratio (35% by Wt. of U With Wedges)

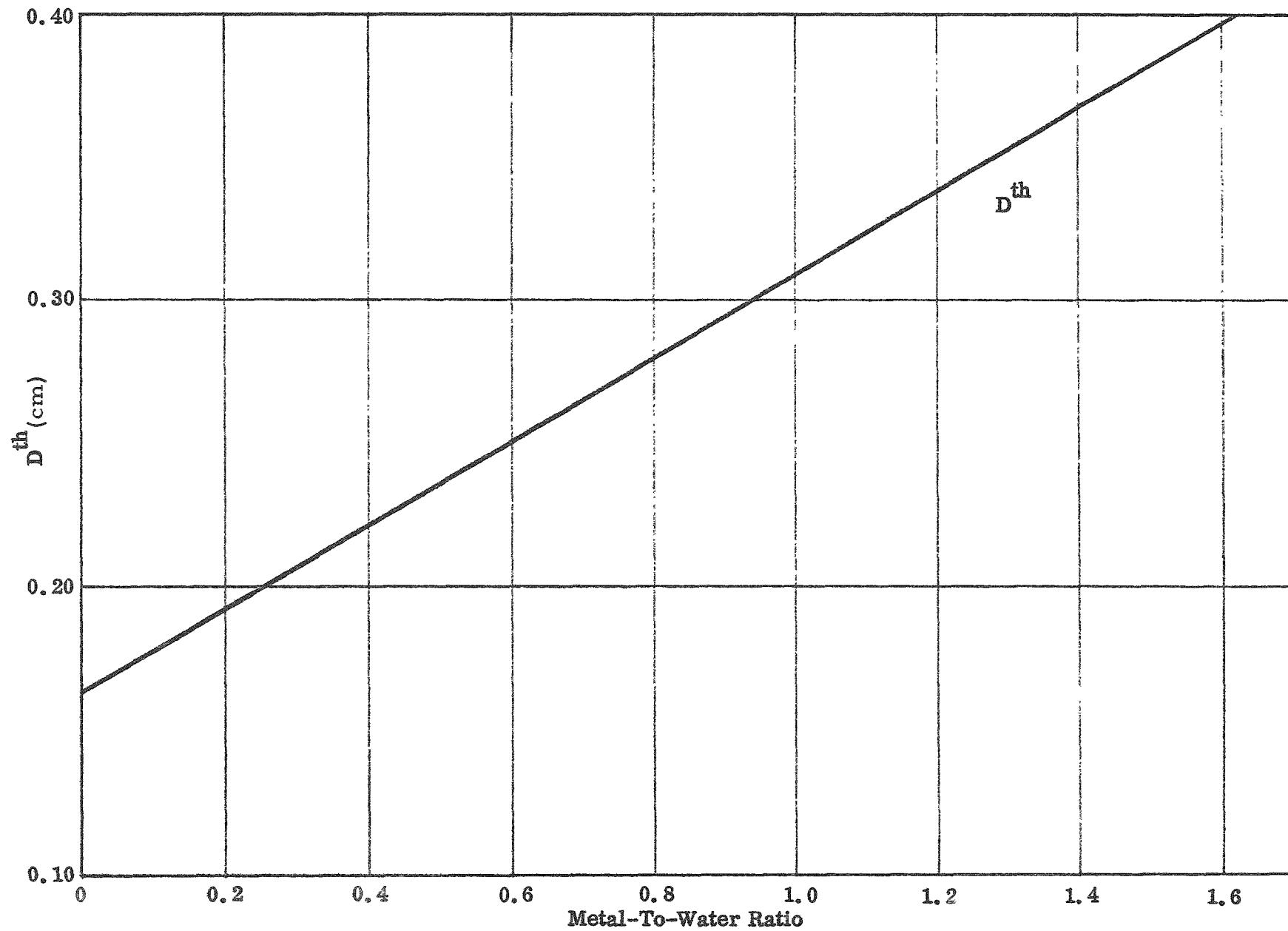


Figure 46 -- Thermal Diffusion Coefficient vs M/W Ratio (35% by Wt. of U With Wedges)

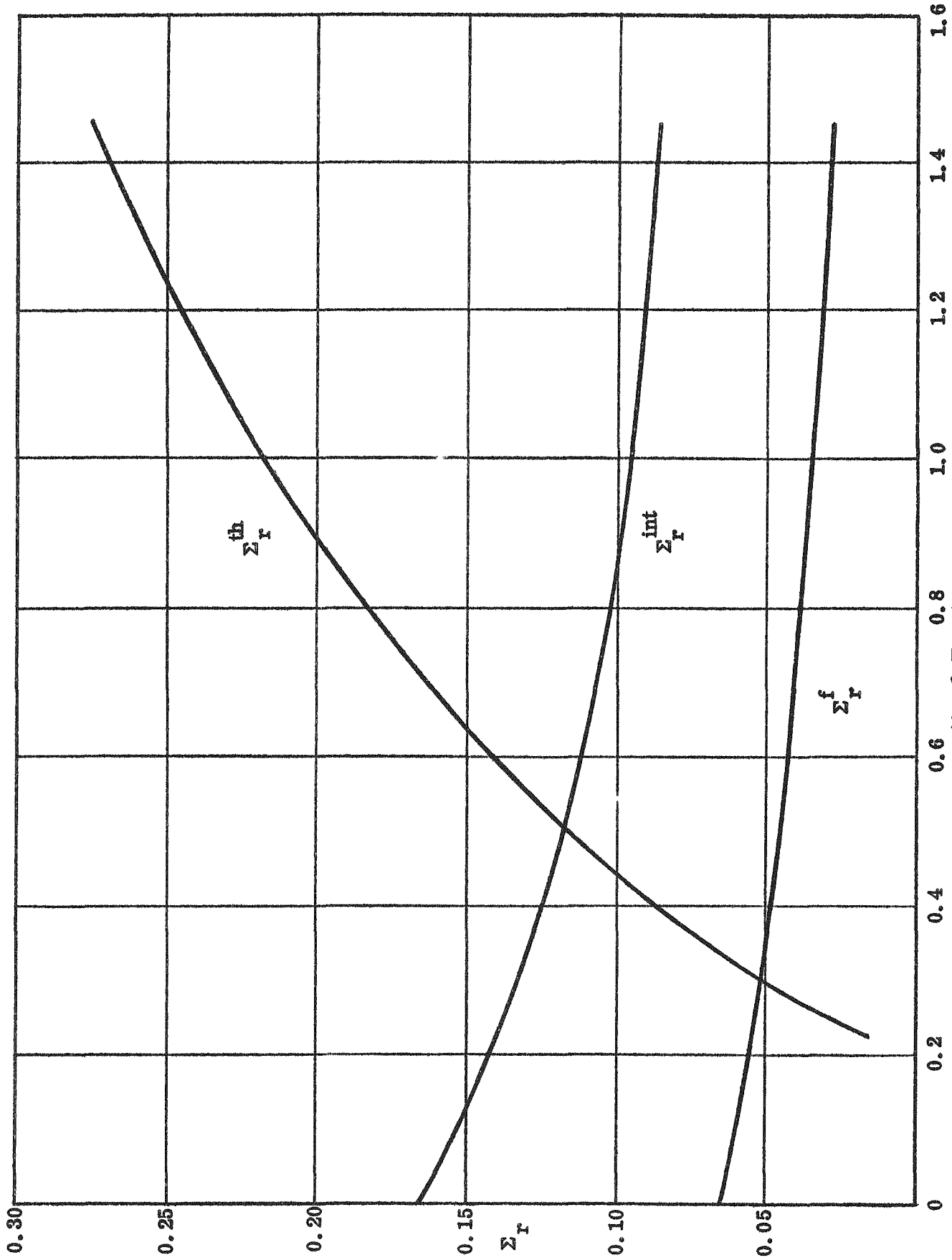


Figure 47 -- Removal Cross Section vs M/W Ratio (35% by Wt. of U With Wedges)

b

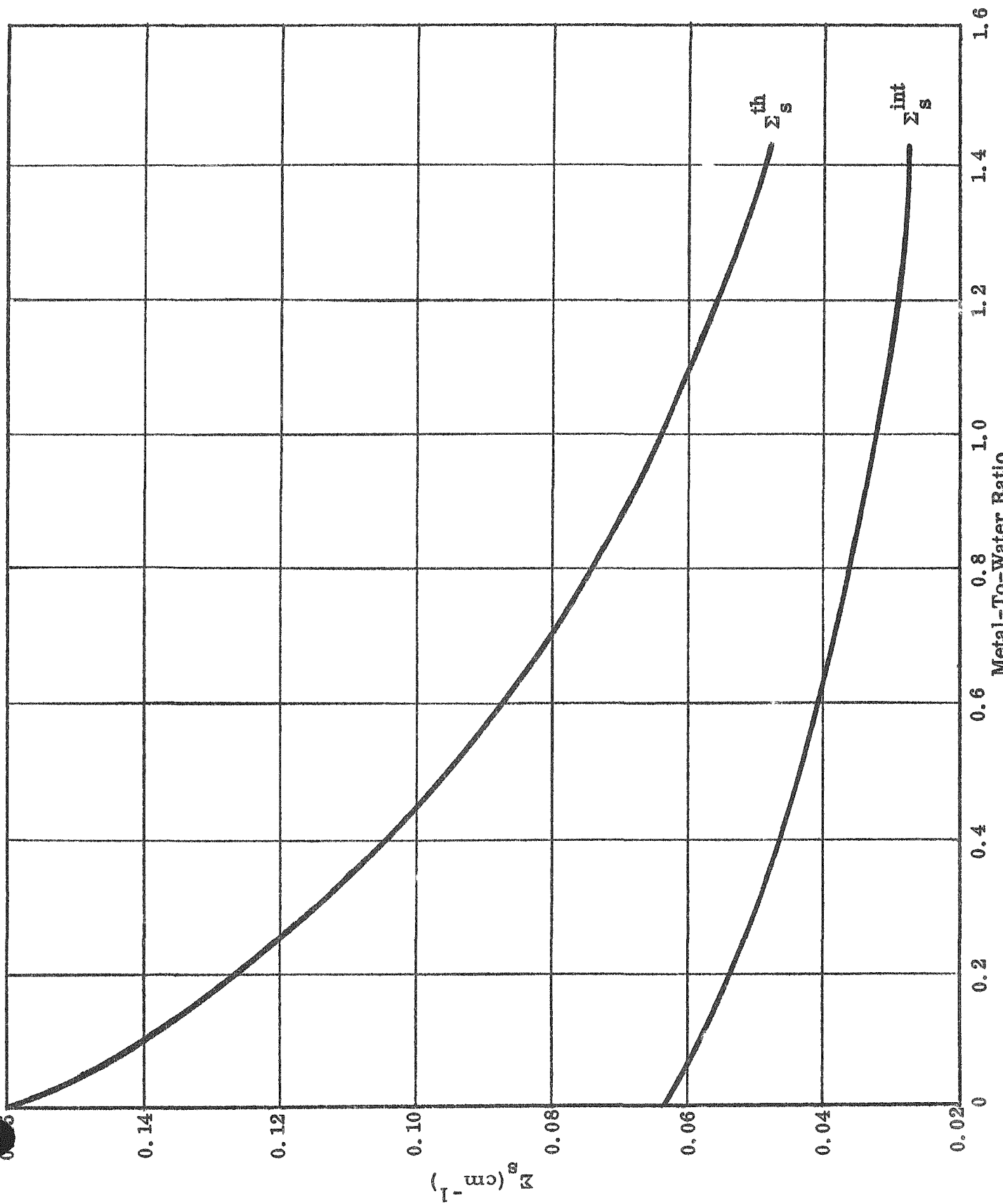


Figure 48 --- Source (From Moderator) Cross Section vs M/W Ratio (35% by Wt. of U Witt Wedges)

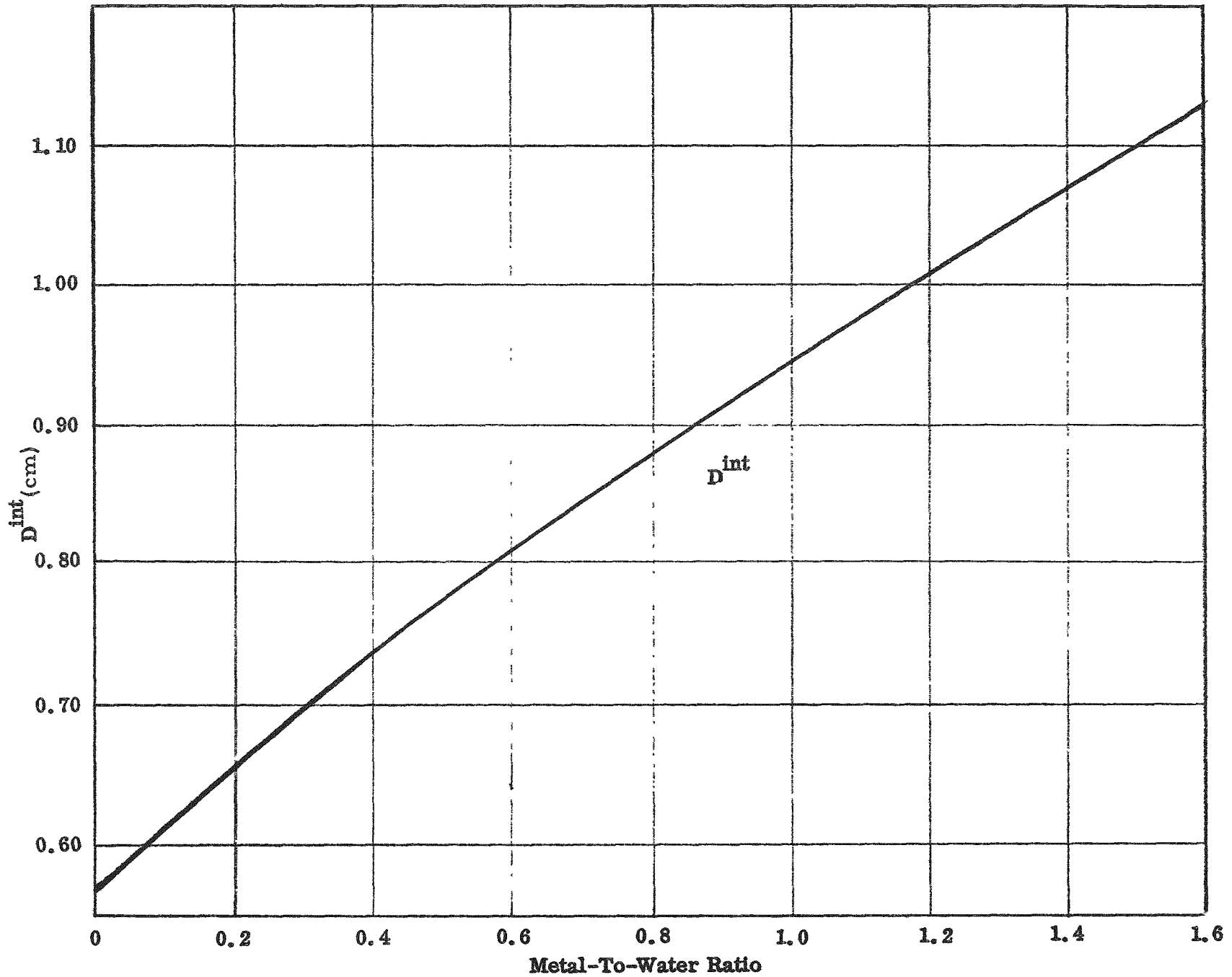


Figure 49a -- Intermediate Diffusion Cross Section vs M/W Ratio (15% by Wt. of U, No Wedges)

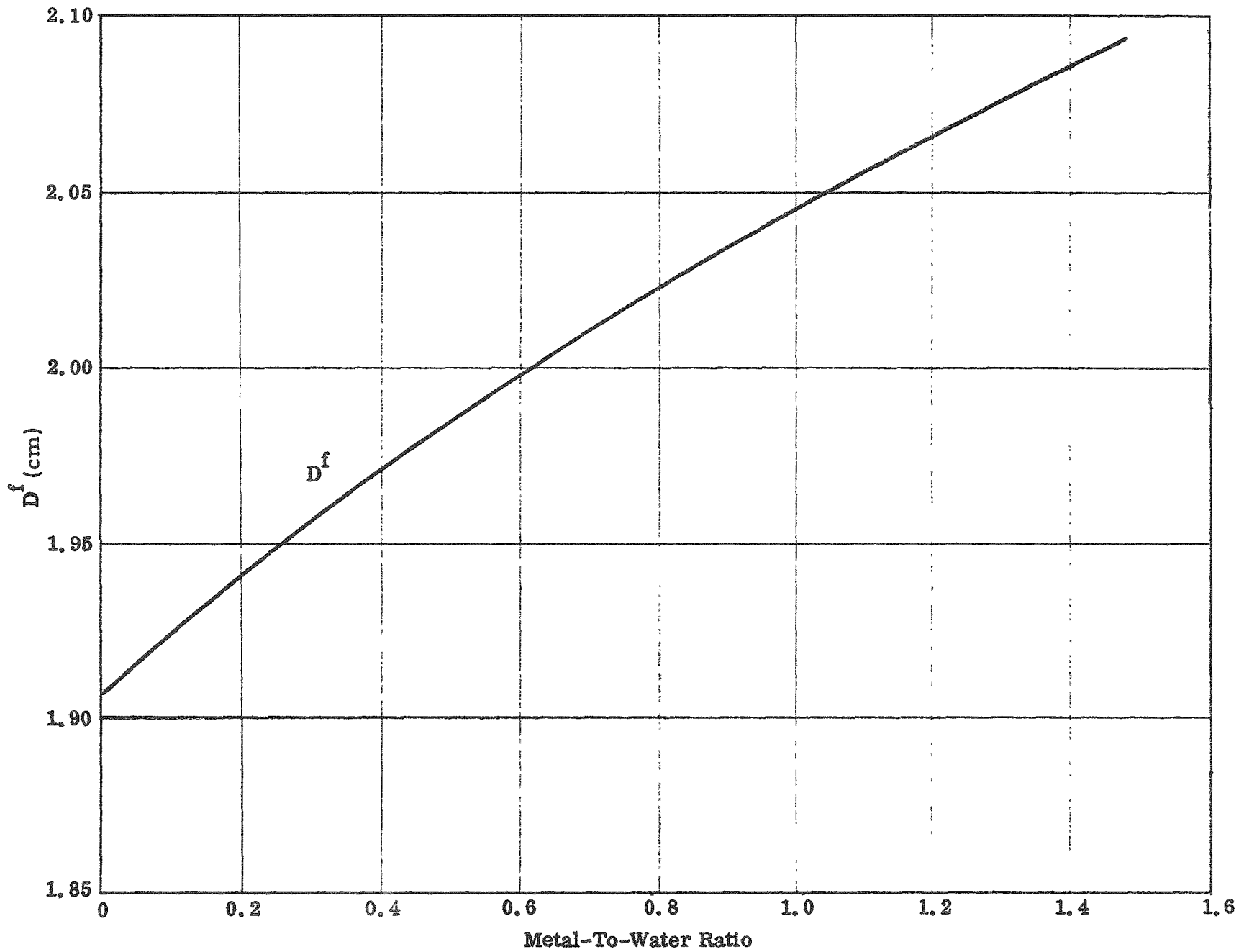


Figure 49b -- Fast Diffusion Cross Section vs M/W Ratio (15% by Wt. of U, No Wedges)

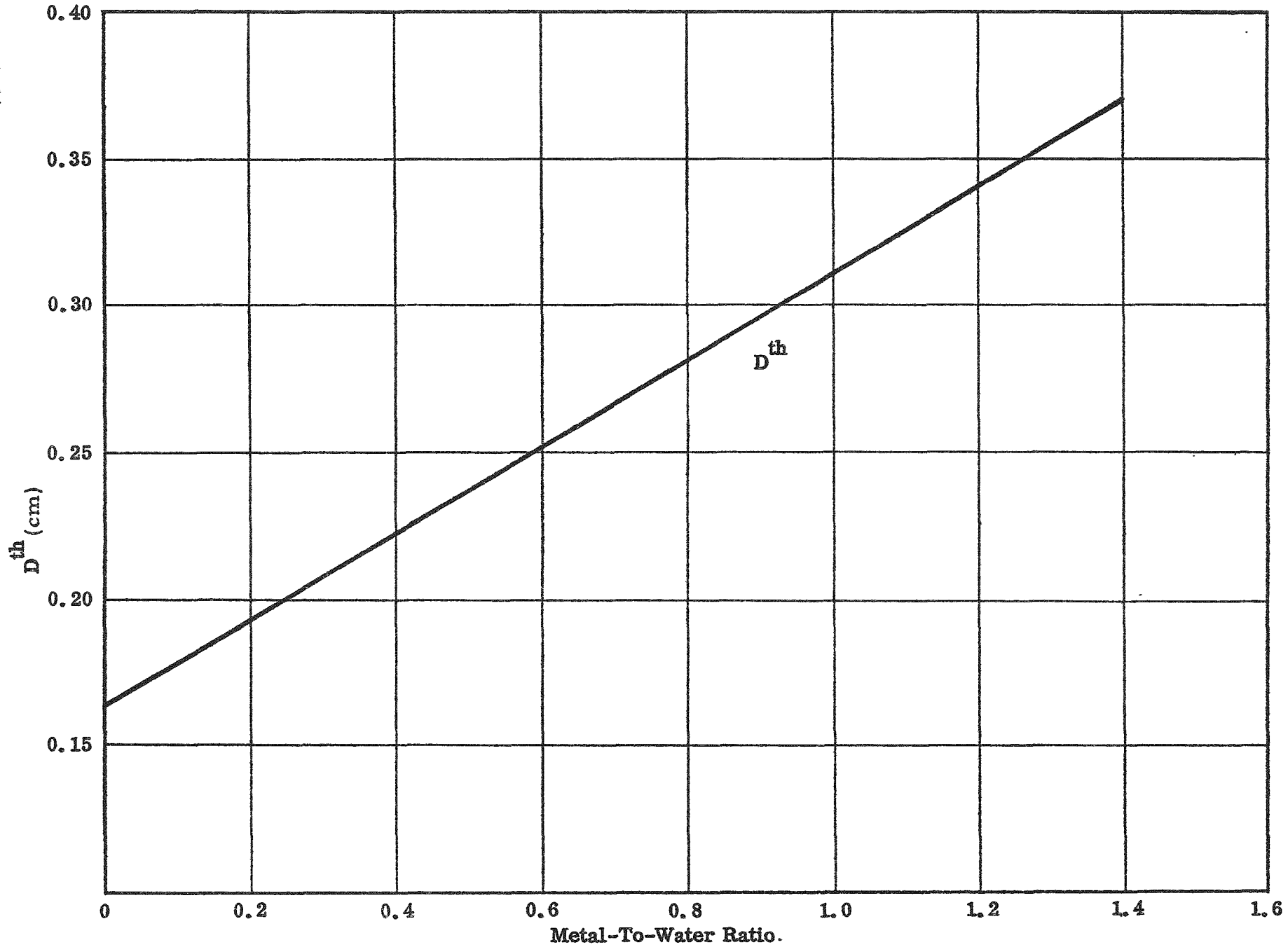


Figure 50 -- Thermal Diffusion Coefficient vs M/W Ratio (15% by Wt. of U, No Wedges)



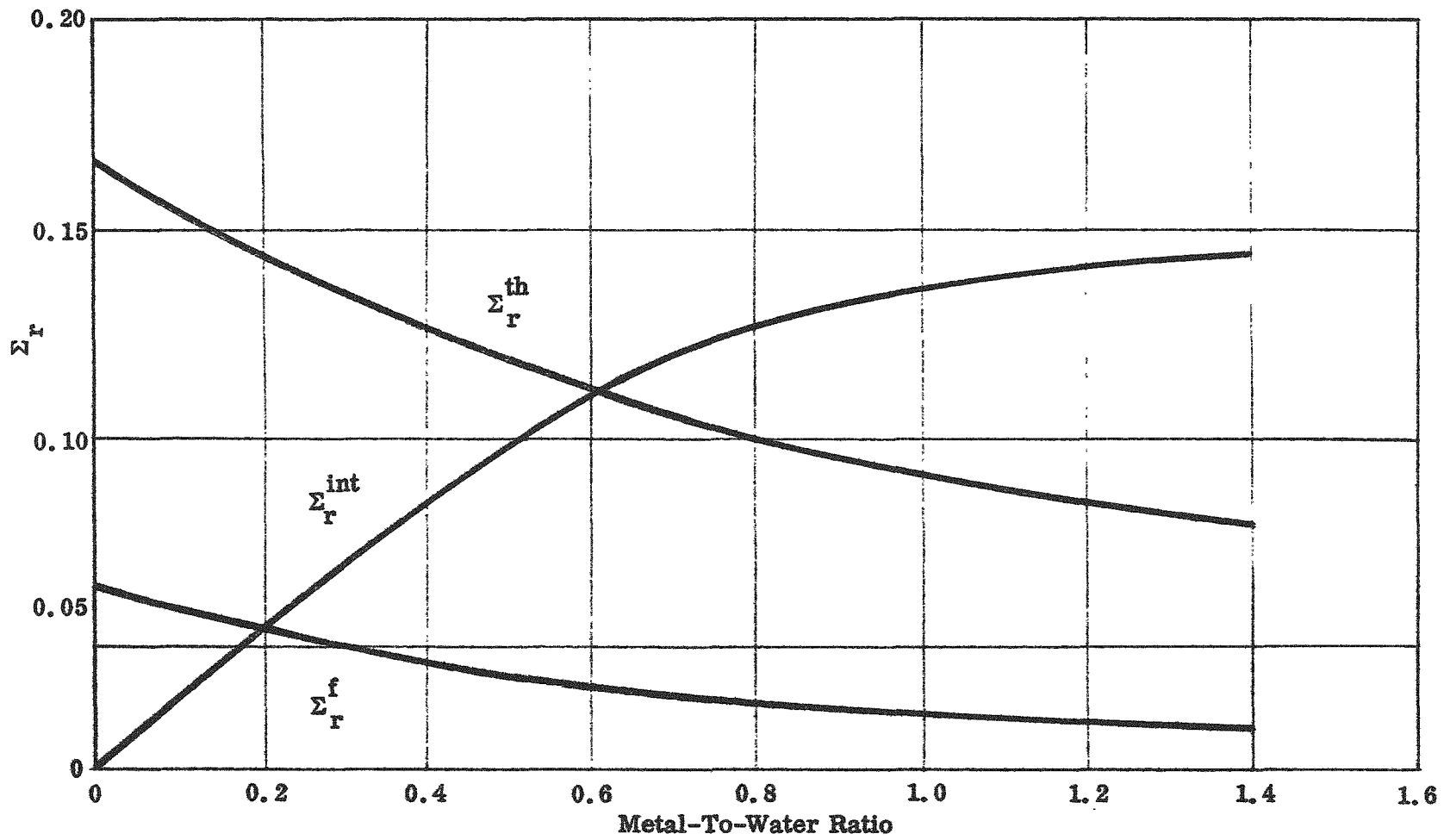


Figure 51 -- Removal Cross Section vs M/W Ratio (15% by Wt. of U, No Wedges)

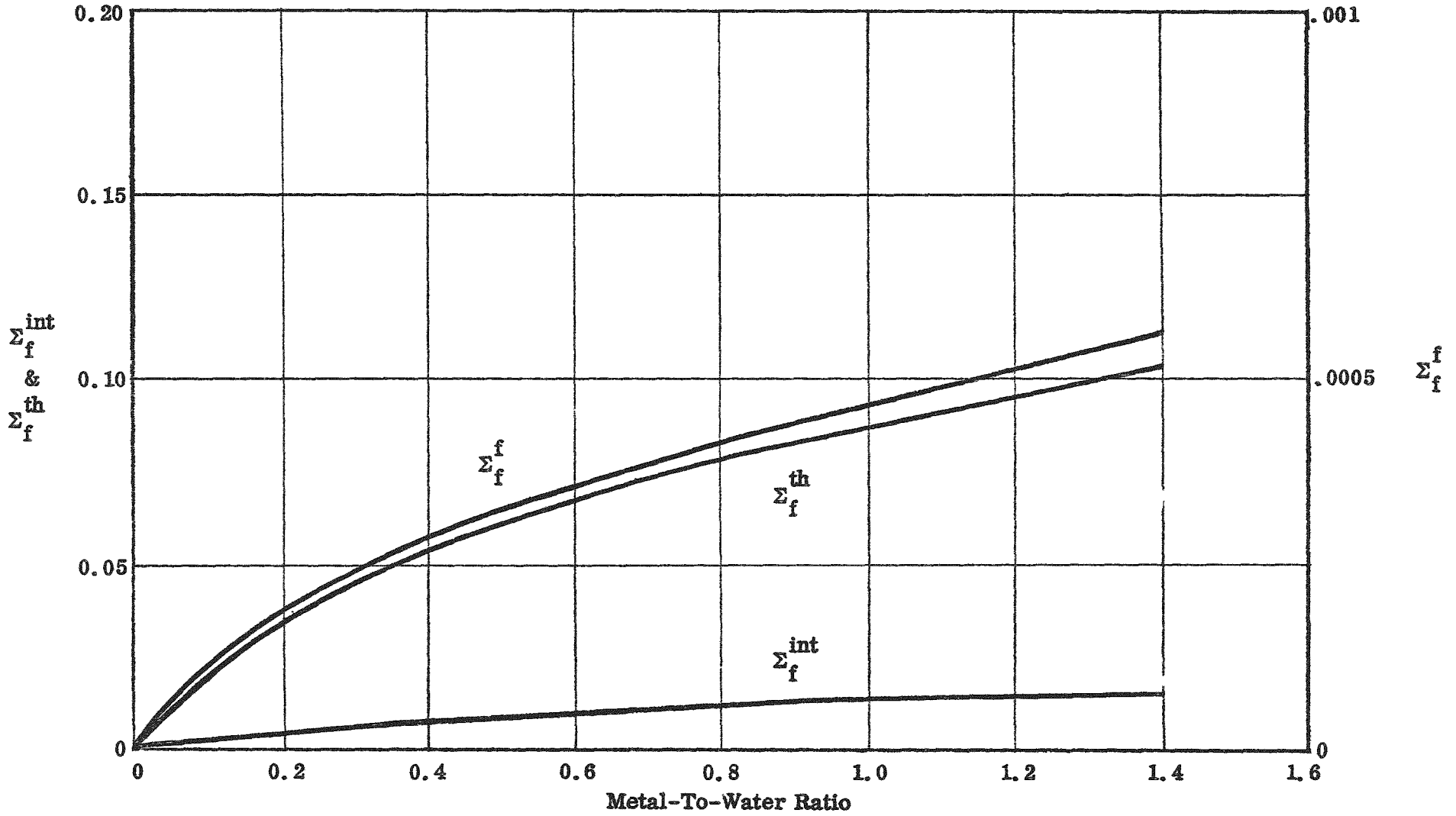


Figure 52 -- Fission Cross Section vs M/W Ratio (15% by Wt. of U, No Wedges)

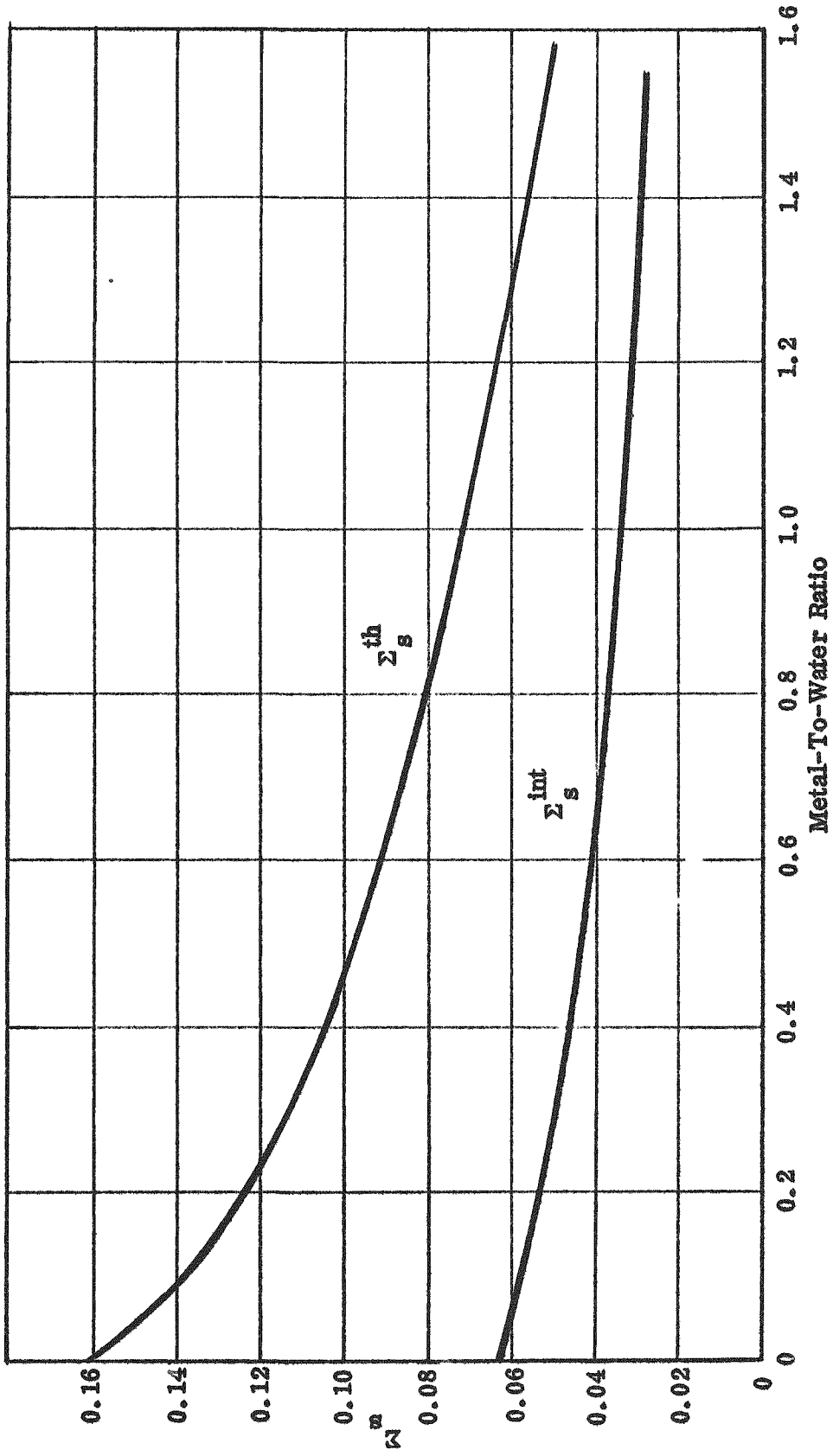


Figure 53 -- Source (From Moderator) Cross Section vs M/W Ratio (15% by Wt. of U, No Wedges)

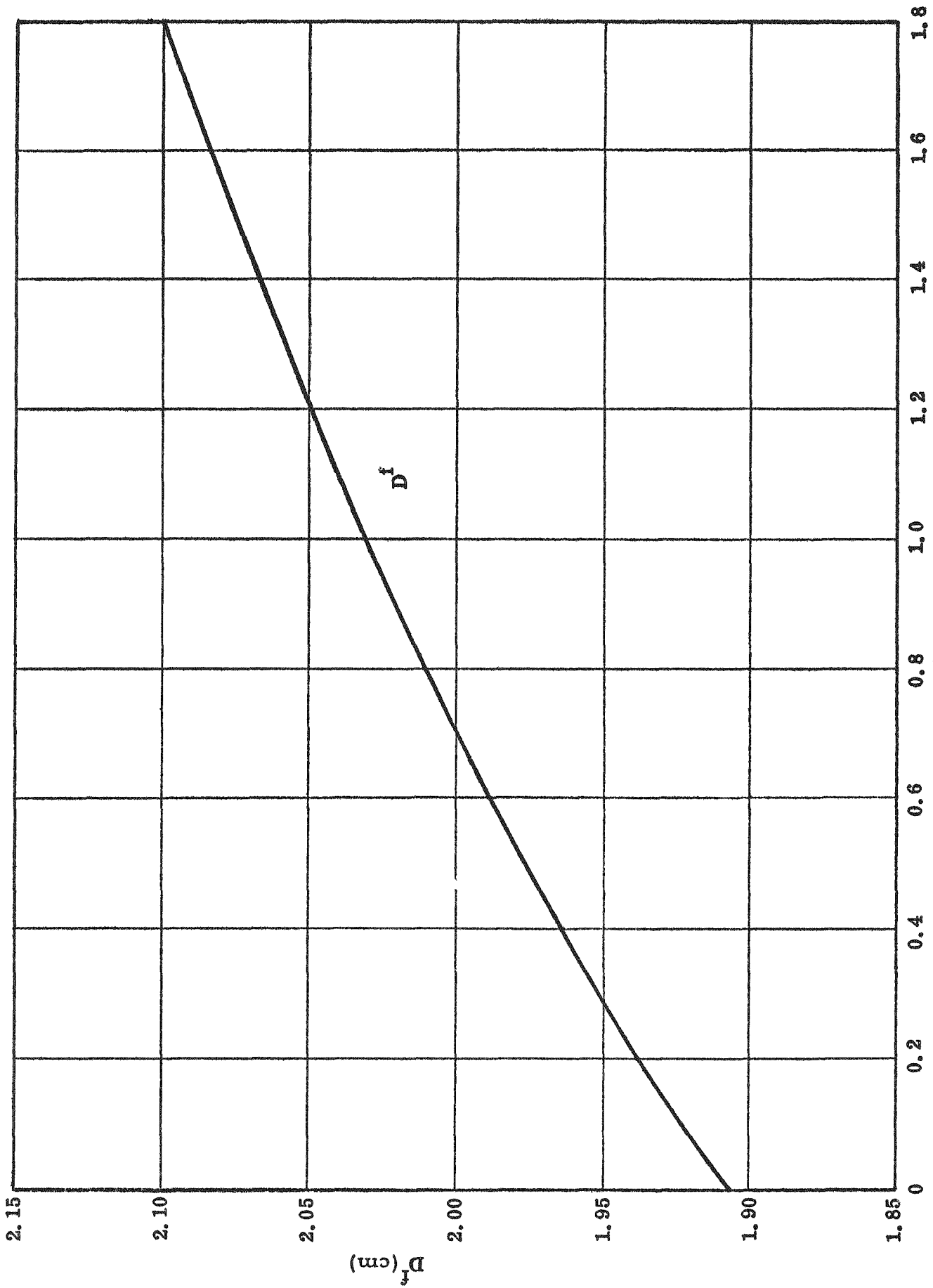


Figure 54a -- Fast Diffusion Coefficient vs M/W Ratio (15% by Wt. of U, No Wedges)

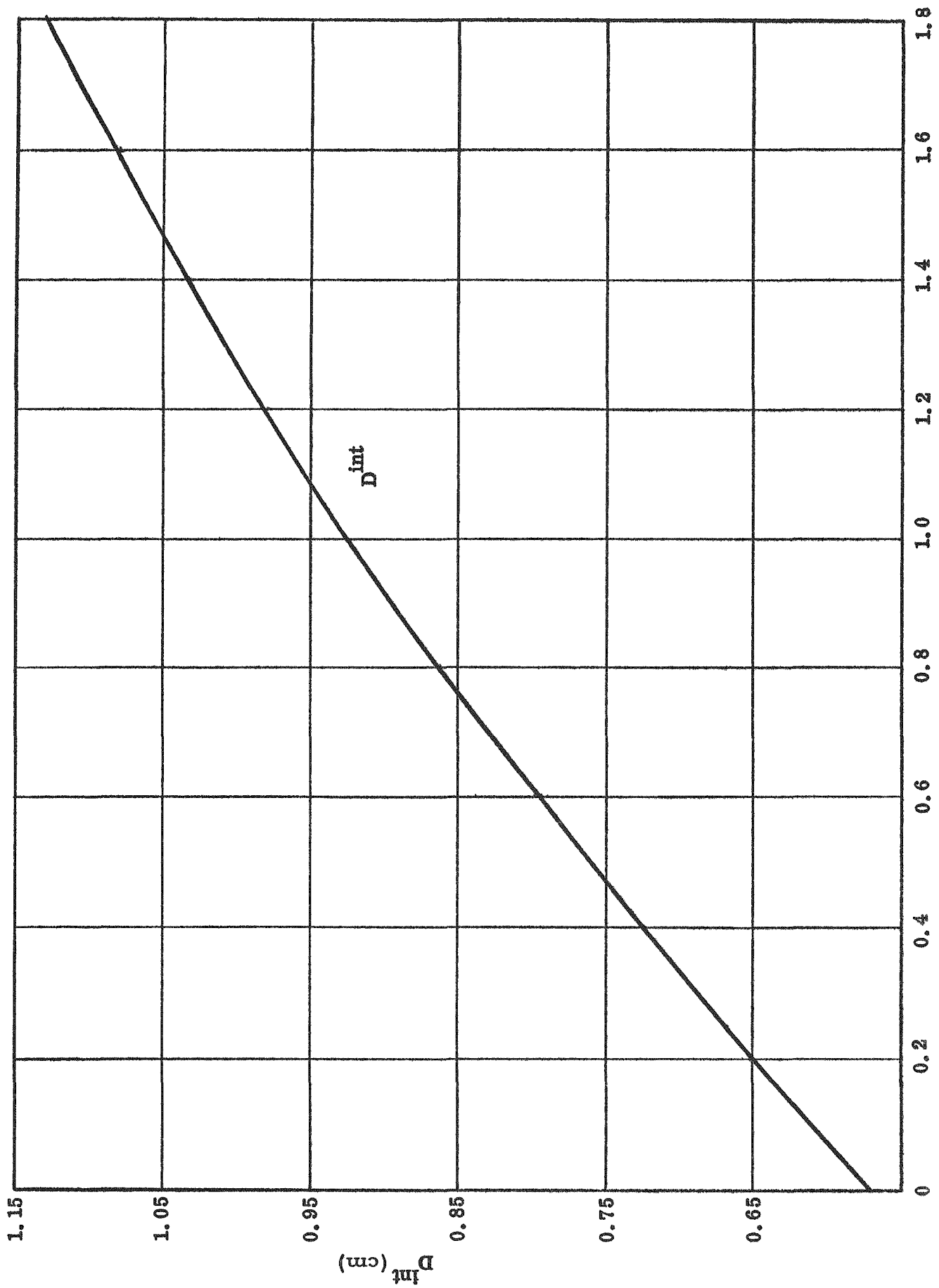


Figure 54b -- Intermediate Diffusion Coefficient vs M/W Ratio (25% by Wt. of U, No Wedges)

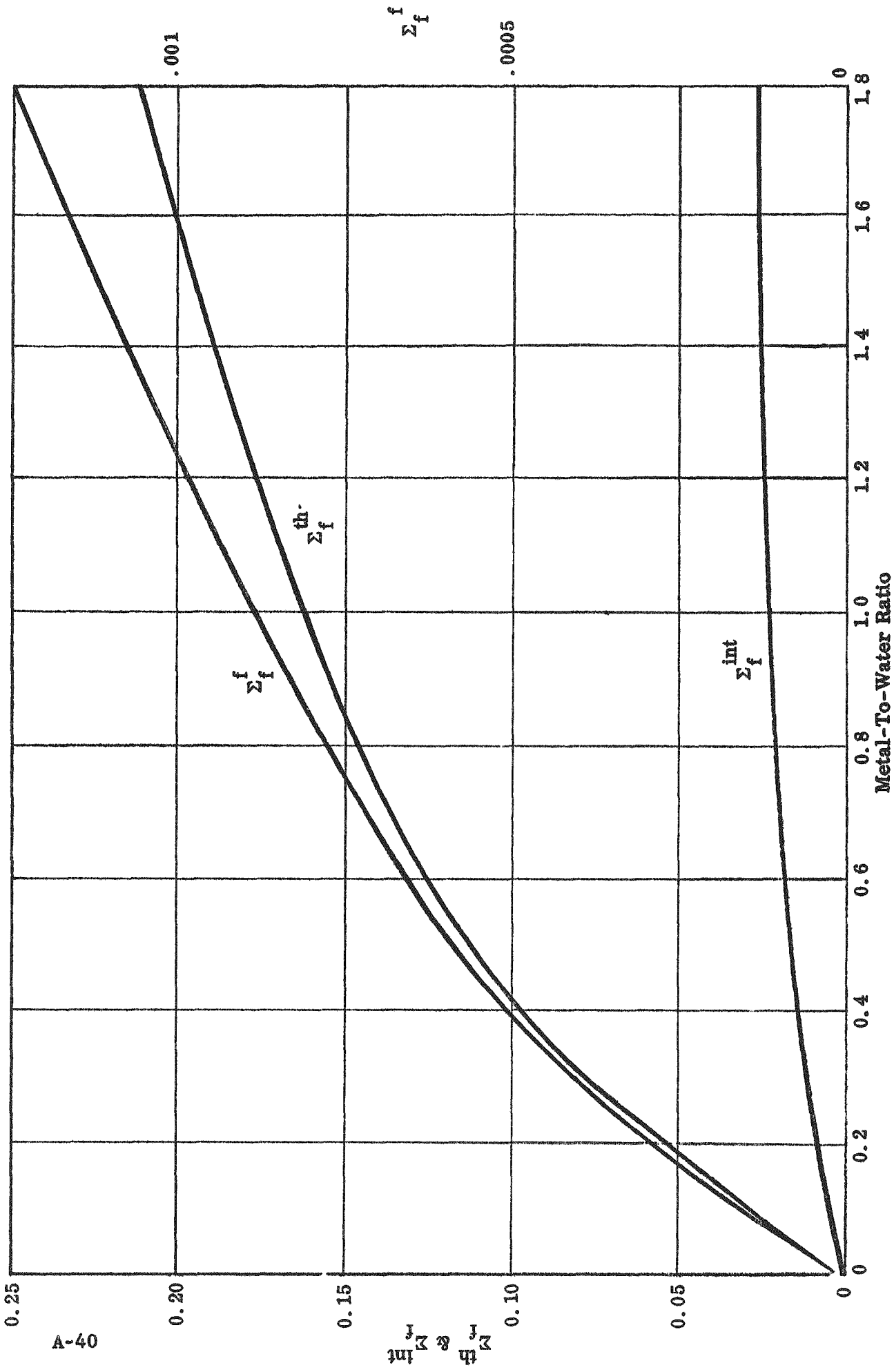
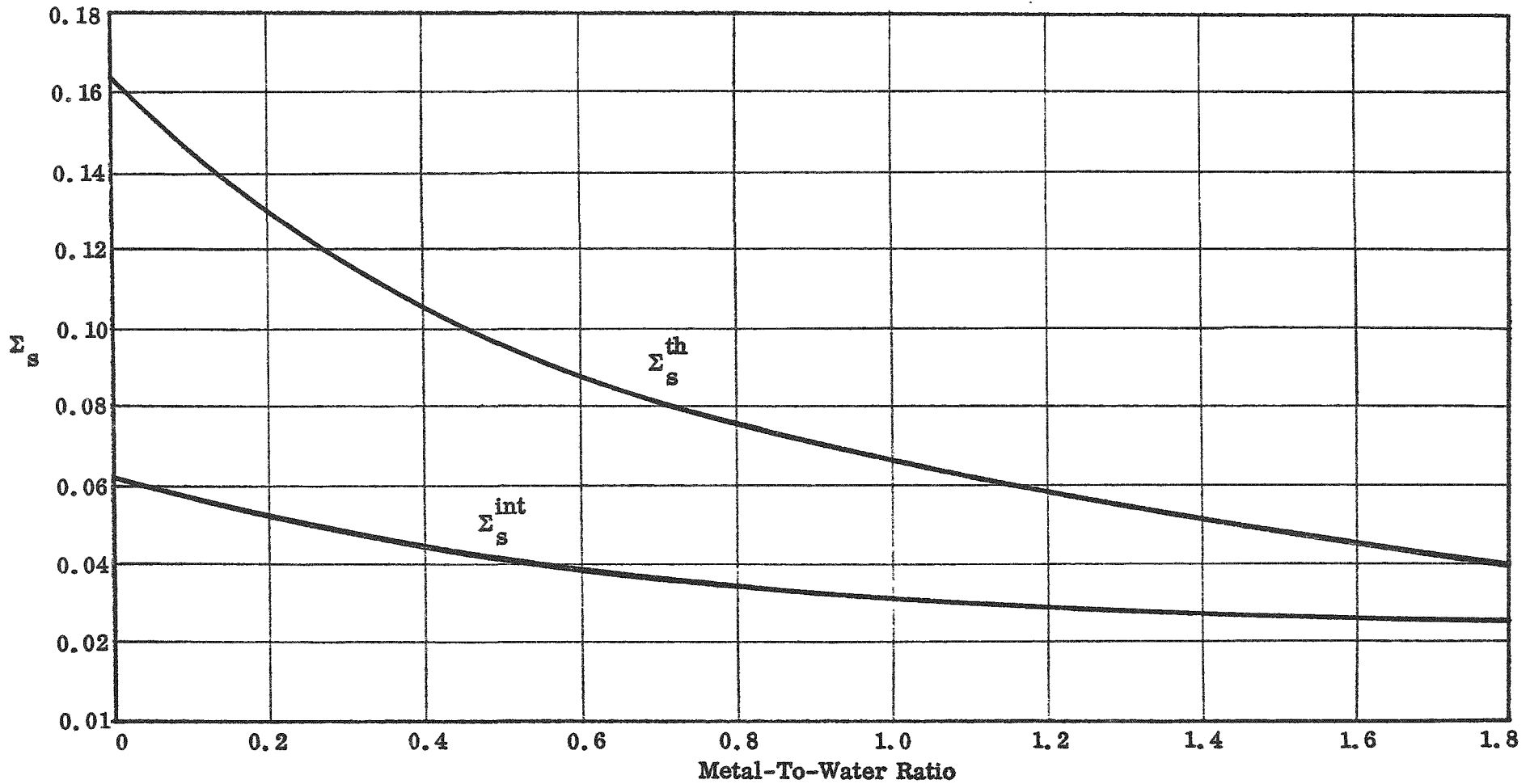


Figure 55 -- Fission Cross Section vs M/W Ratio (25% by Wt. of U, No Wedges)



A-41

Figure 56 -- Source (From Moderator) Cross Section vs M/W Ratio (25% by Wt. of U, No Wedges)

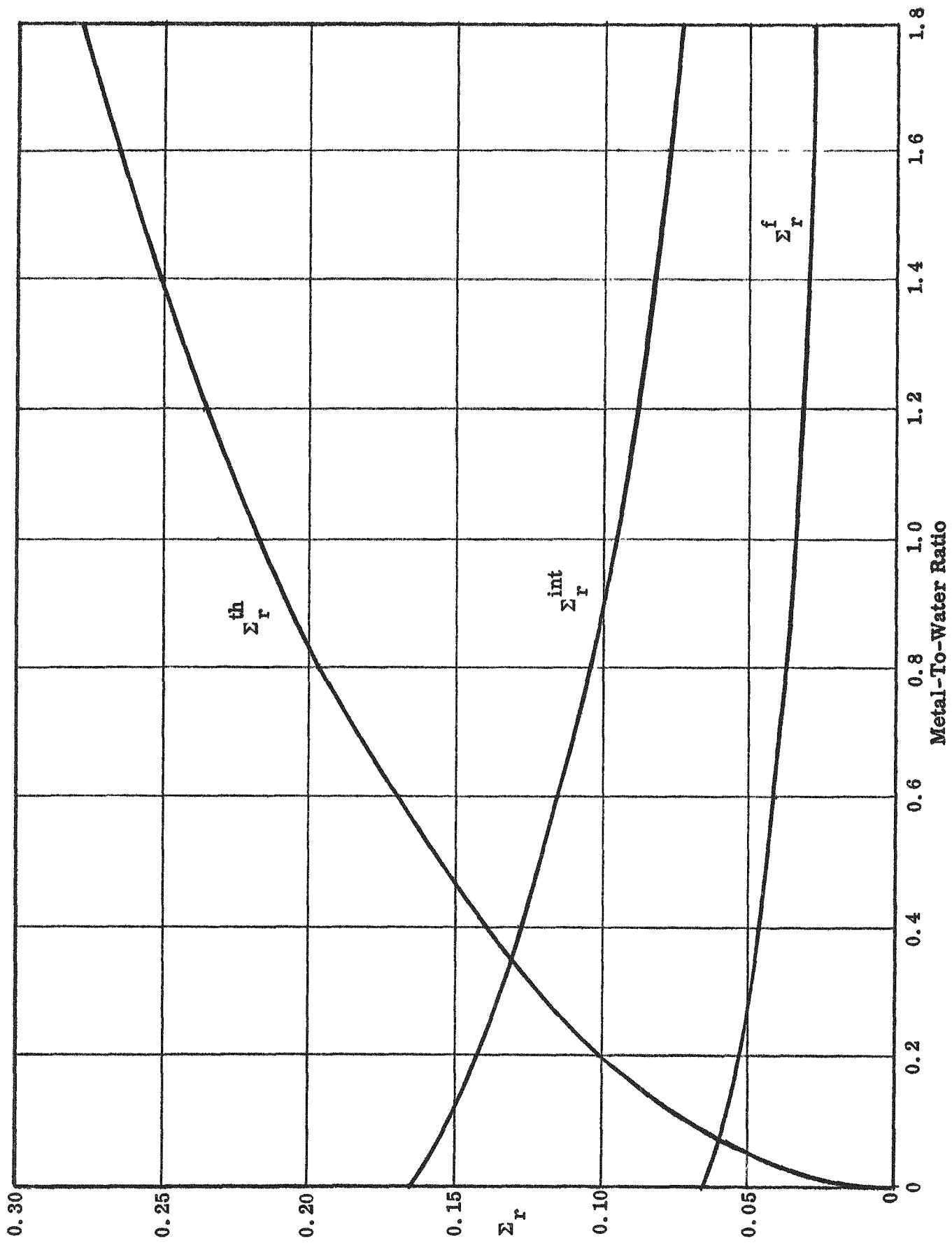


Figure 57 -- Removal Cross Section vs Metal/Water Ratio (25% by Wt. of U, No Wedges)

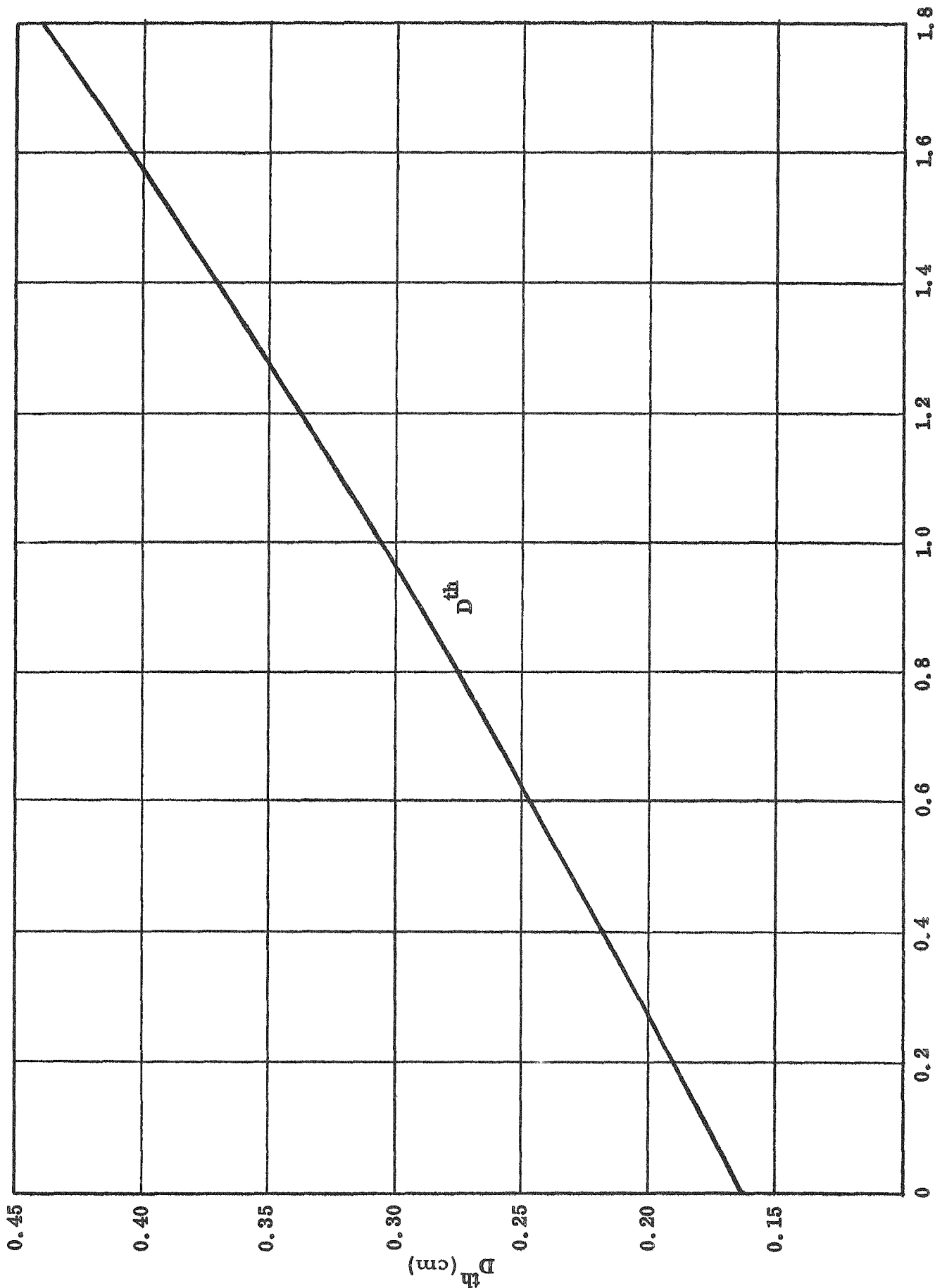


Figure 58 -- Thermal Diffusion Coefficient vs M/W Ratio (25% by Wt. of U, No Wedges)

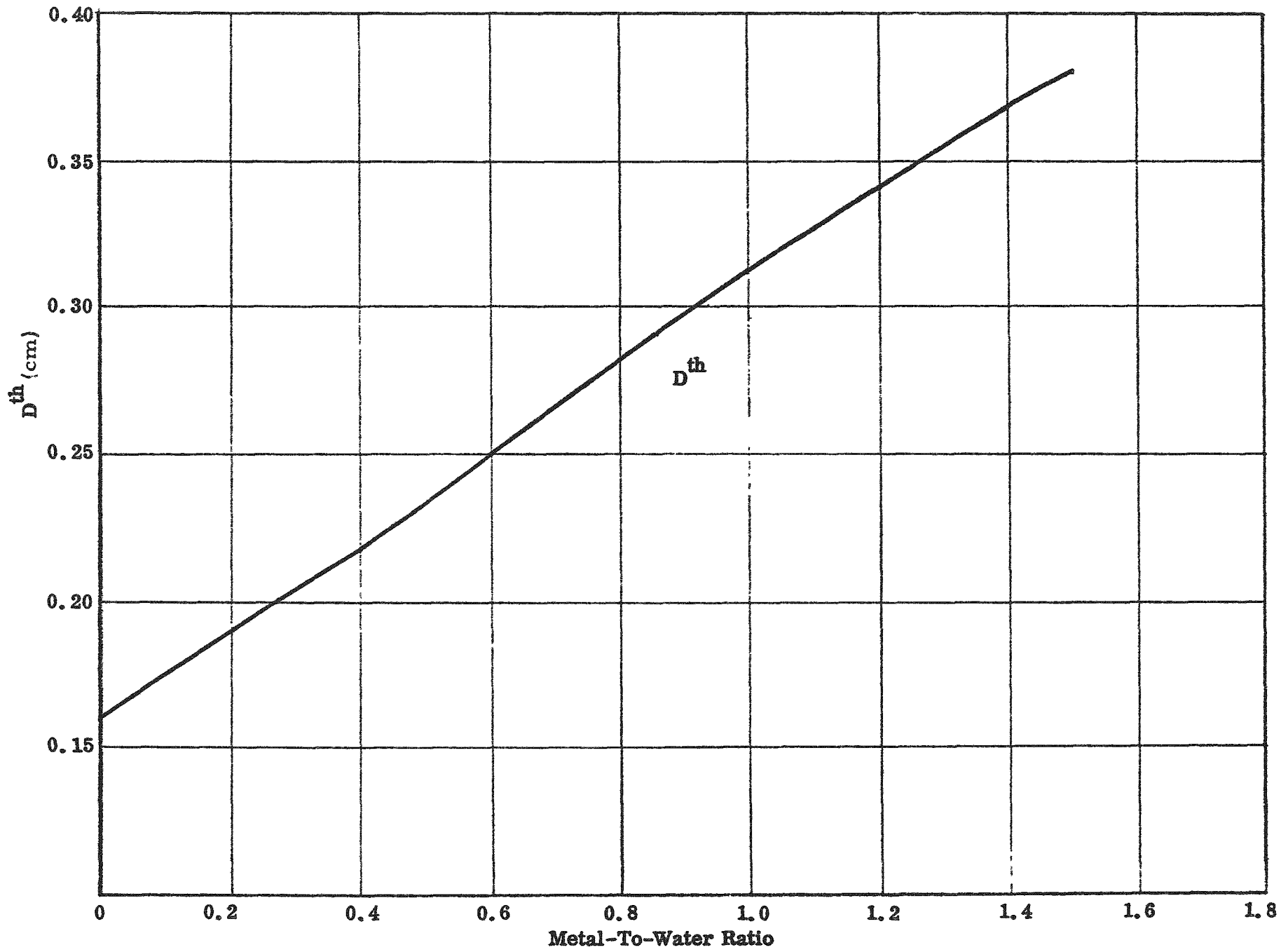


Figure 59 -- Thermal Diffusion Coefficient vs M/W Ratio (35% Wt. of U, No Wedges)

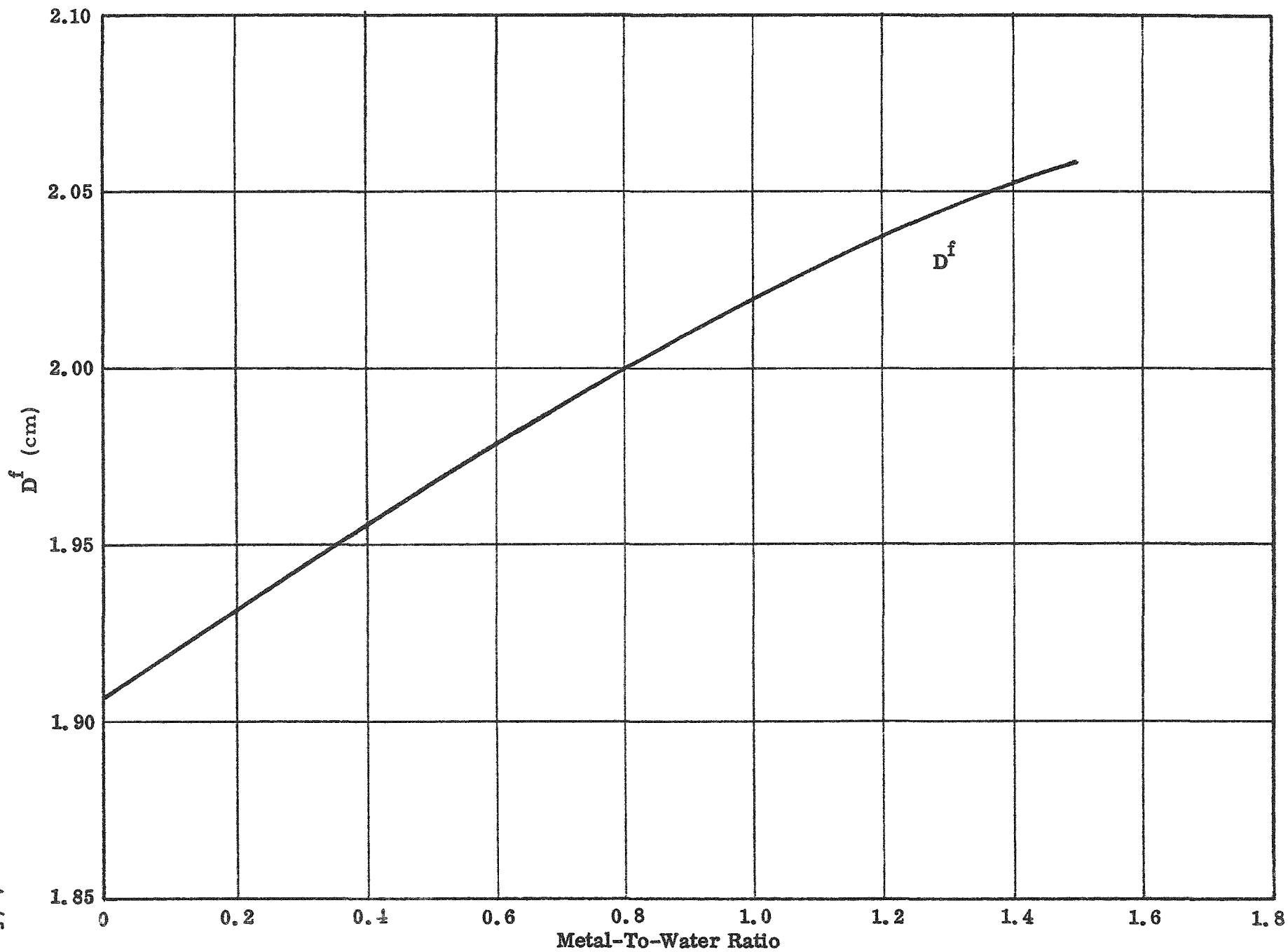


Figure 60a -- Fast Diffusion Coefficient vs M/W Ratio (35% by Wt. of U, No Wedges)

A-46

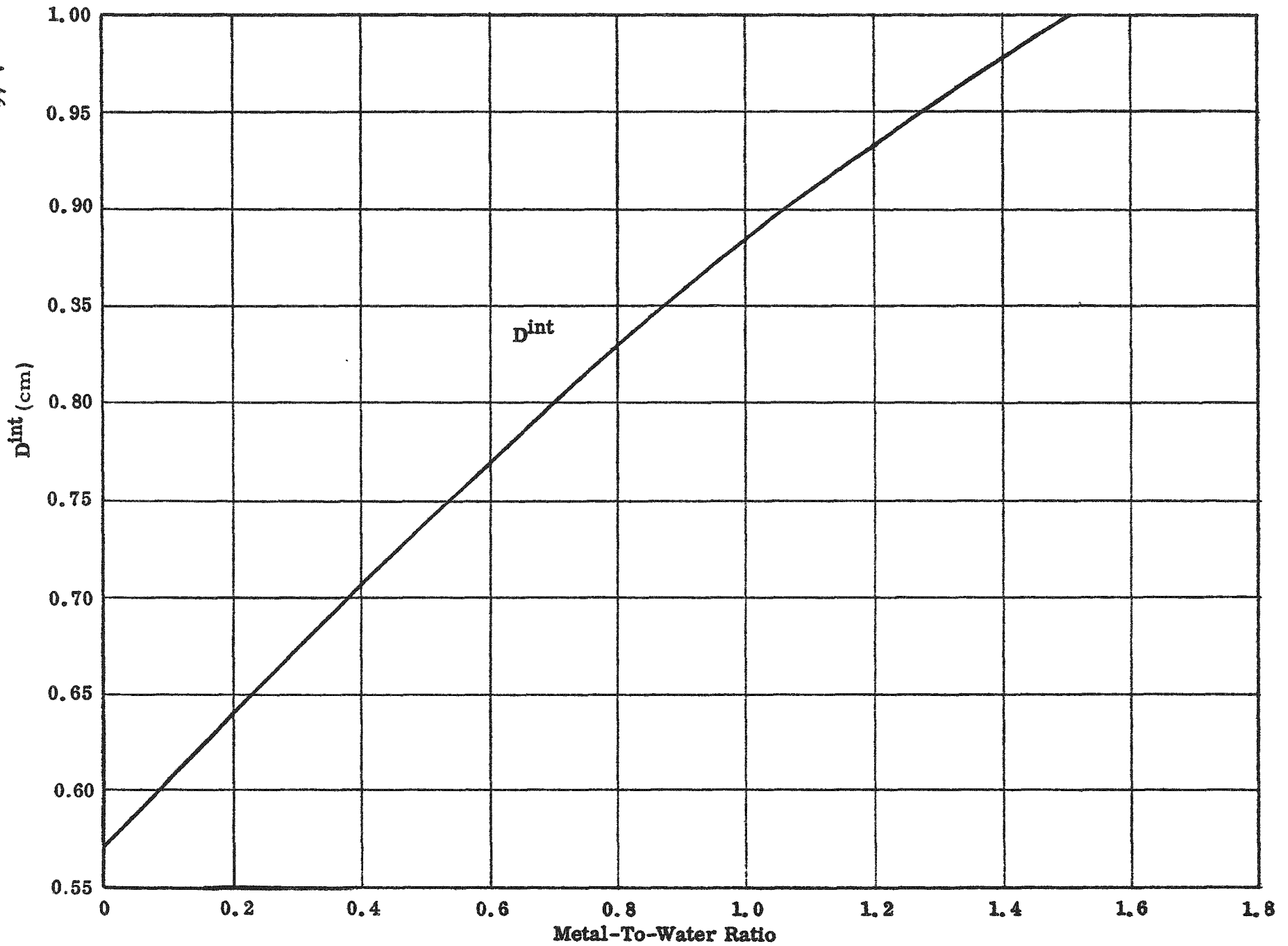


Figure 60b -- Intermediate Diffusion Coefficient vs M/W Ratio (35% by Wt. of U, No Wedges)

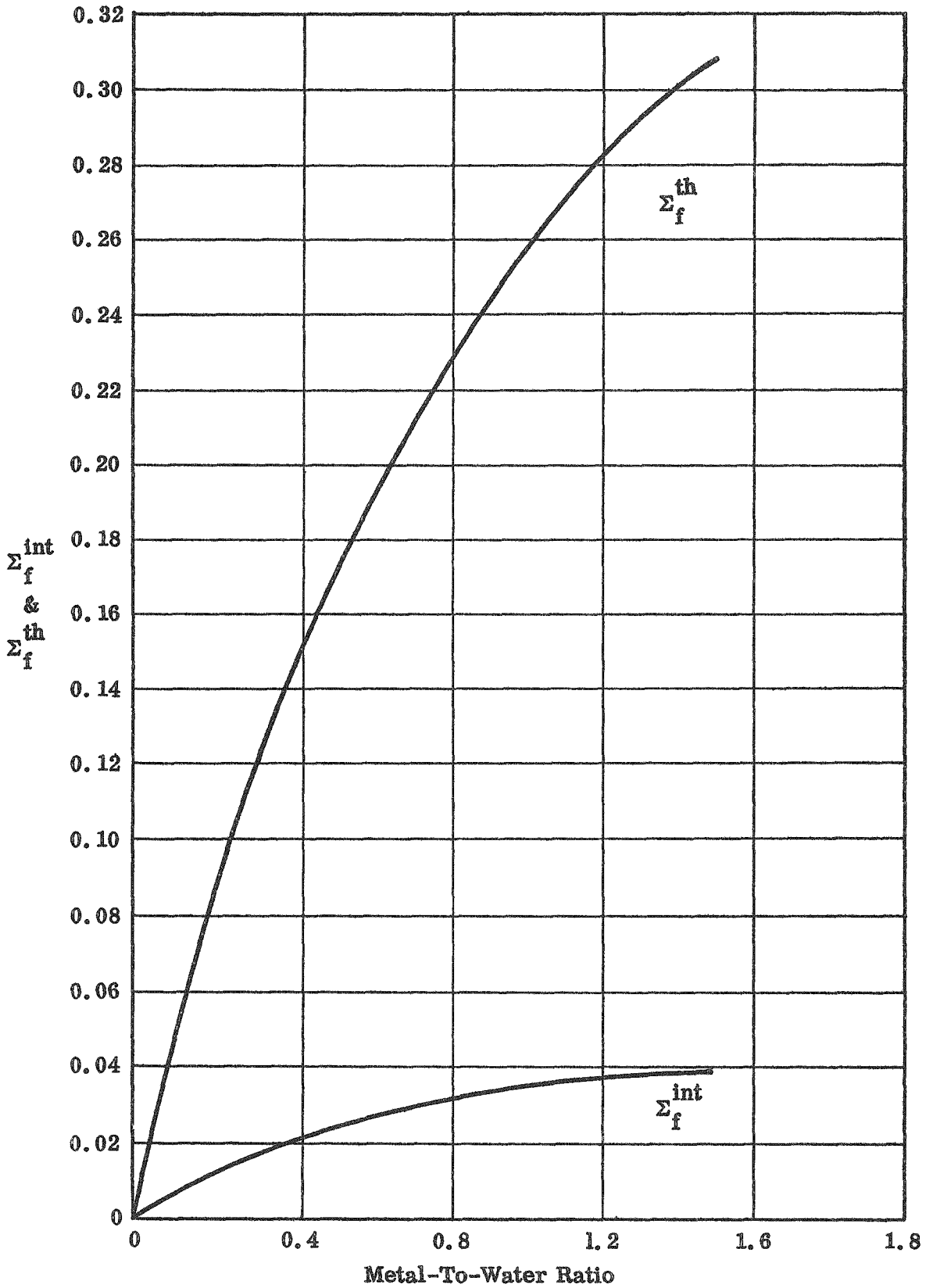


Figure 61a Fission Cross Section vs M/W Ratio (35% by Wt. of U, No Wedges)

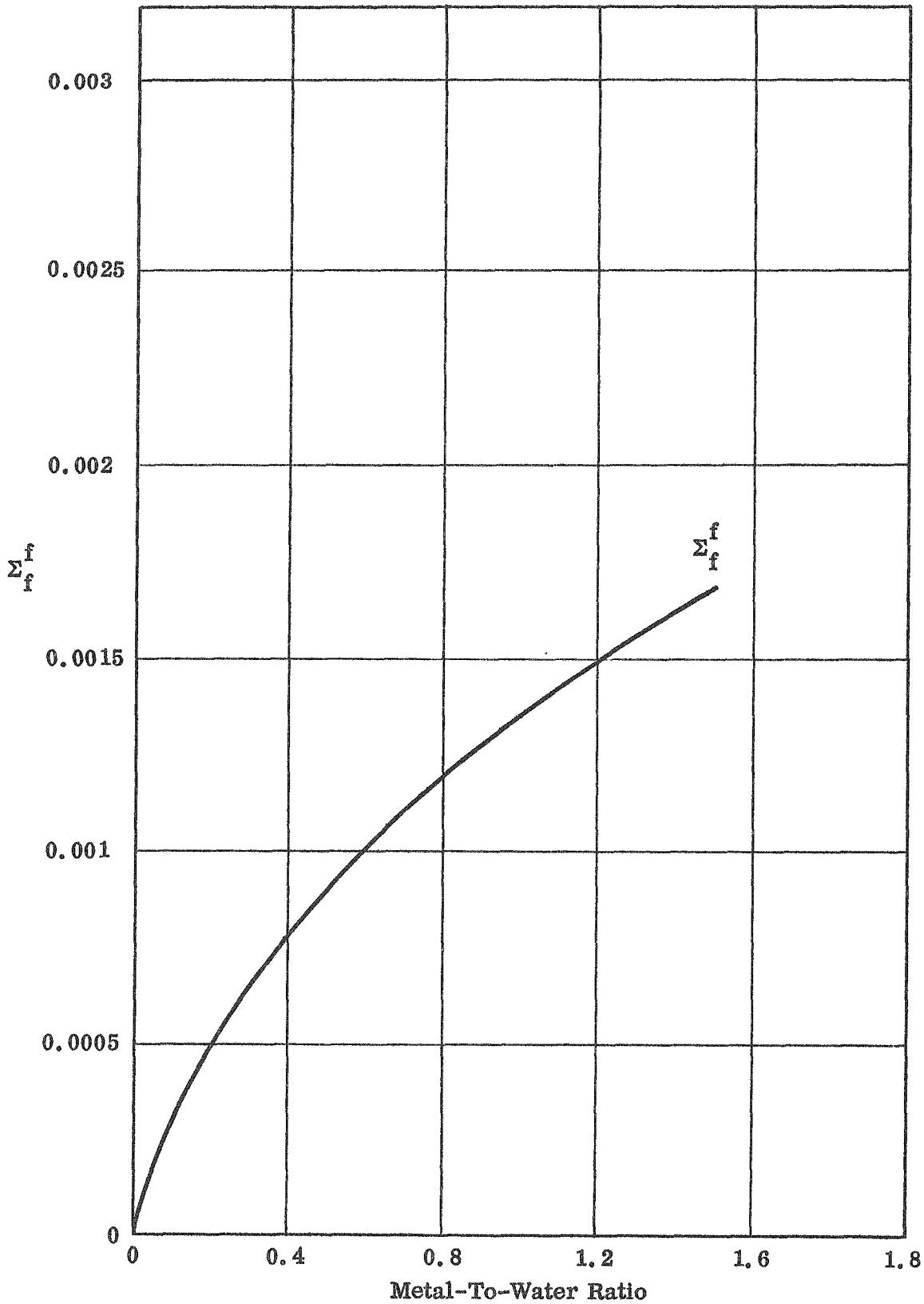


Figure 61b -- Fission Cross Section vs M/W Ratio (35% by Wt. of U, No Wedges)
A-48

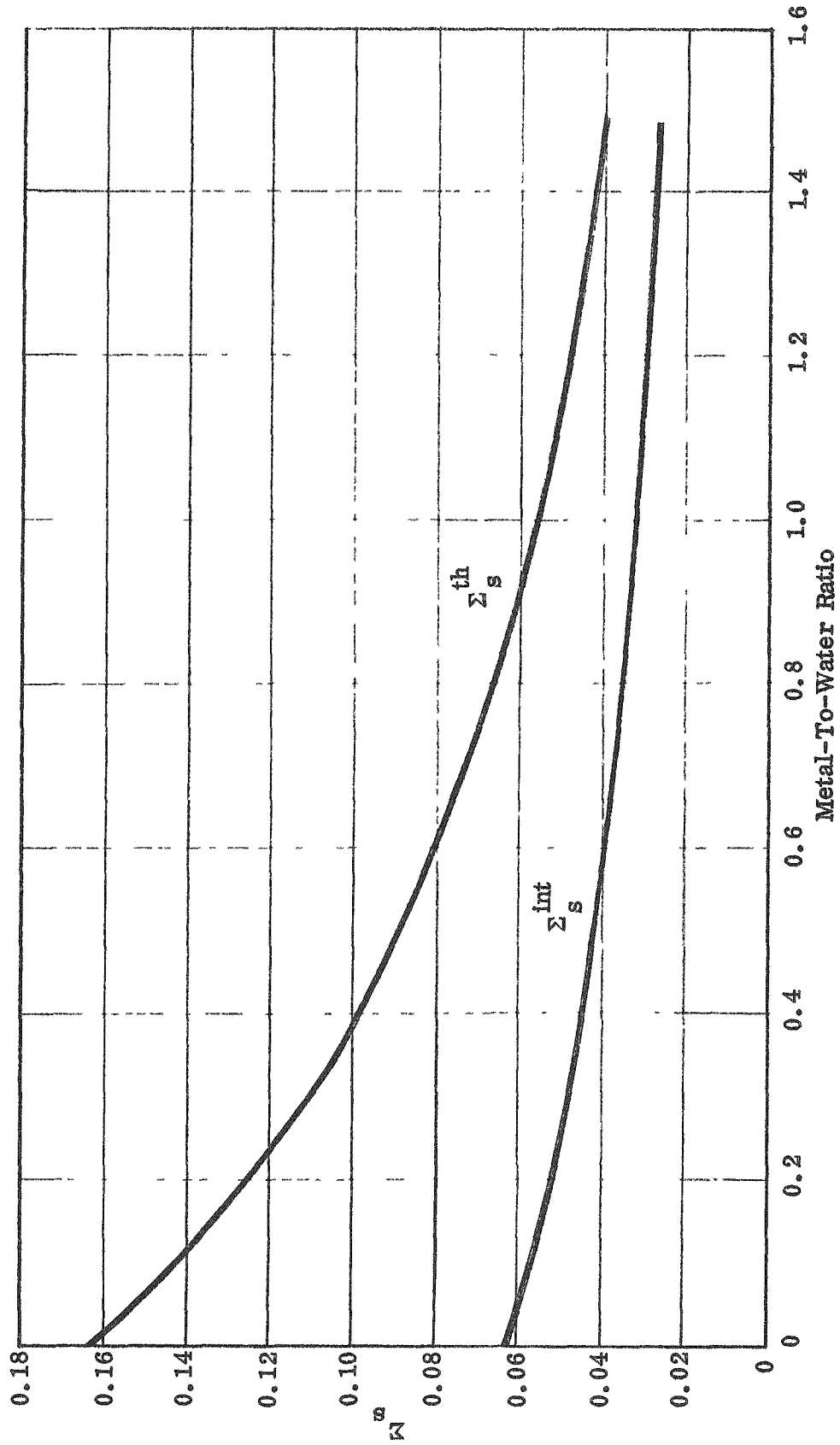


Figure 62 -- Source (From Moderator) Cross Section vs M/W Ratio (35% by Wt. of U, No Wedges)

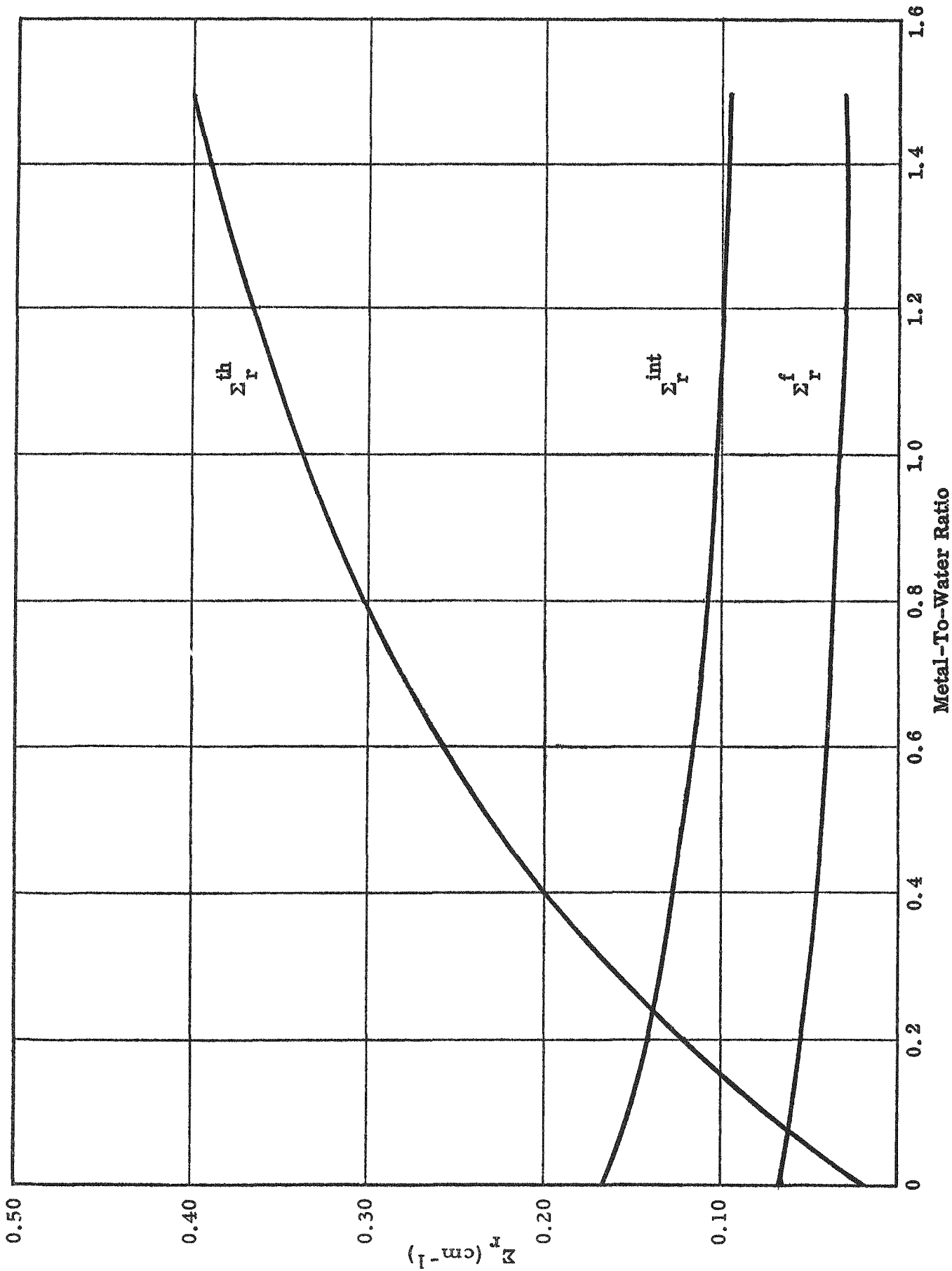


Figure 63 -- Removal Cross Section vs M/W Ratio (35% by Wt. of U, No Wedges)

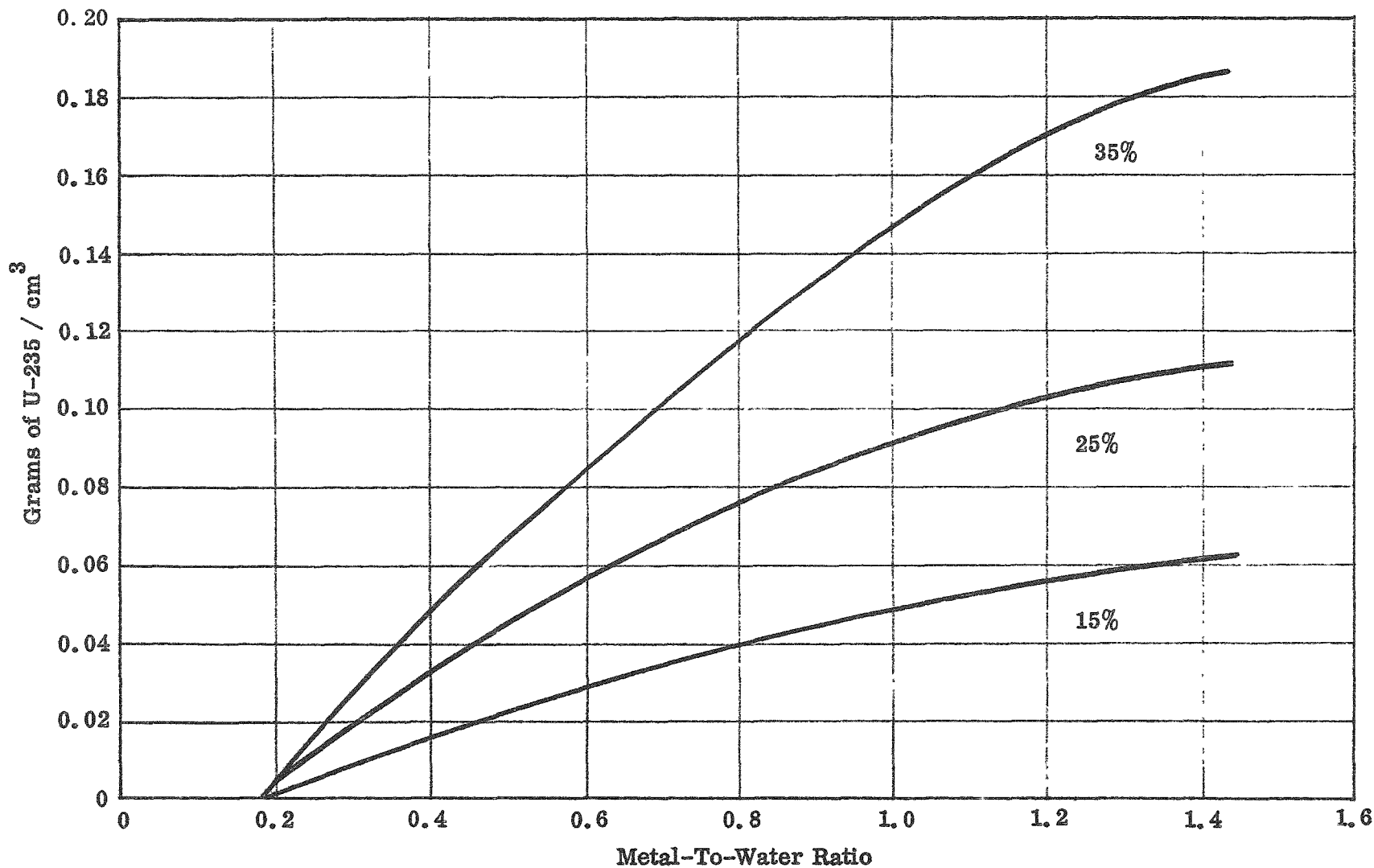


Figure 64 -- Weight Density in Core Region vs M/W Ratio (15, 25 and 35% by Wt. of U, With Wedges)

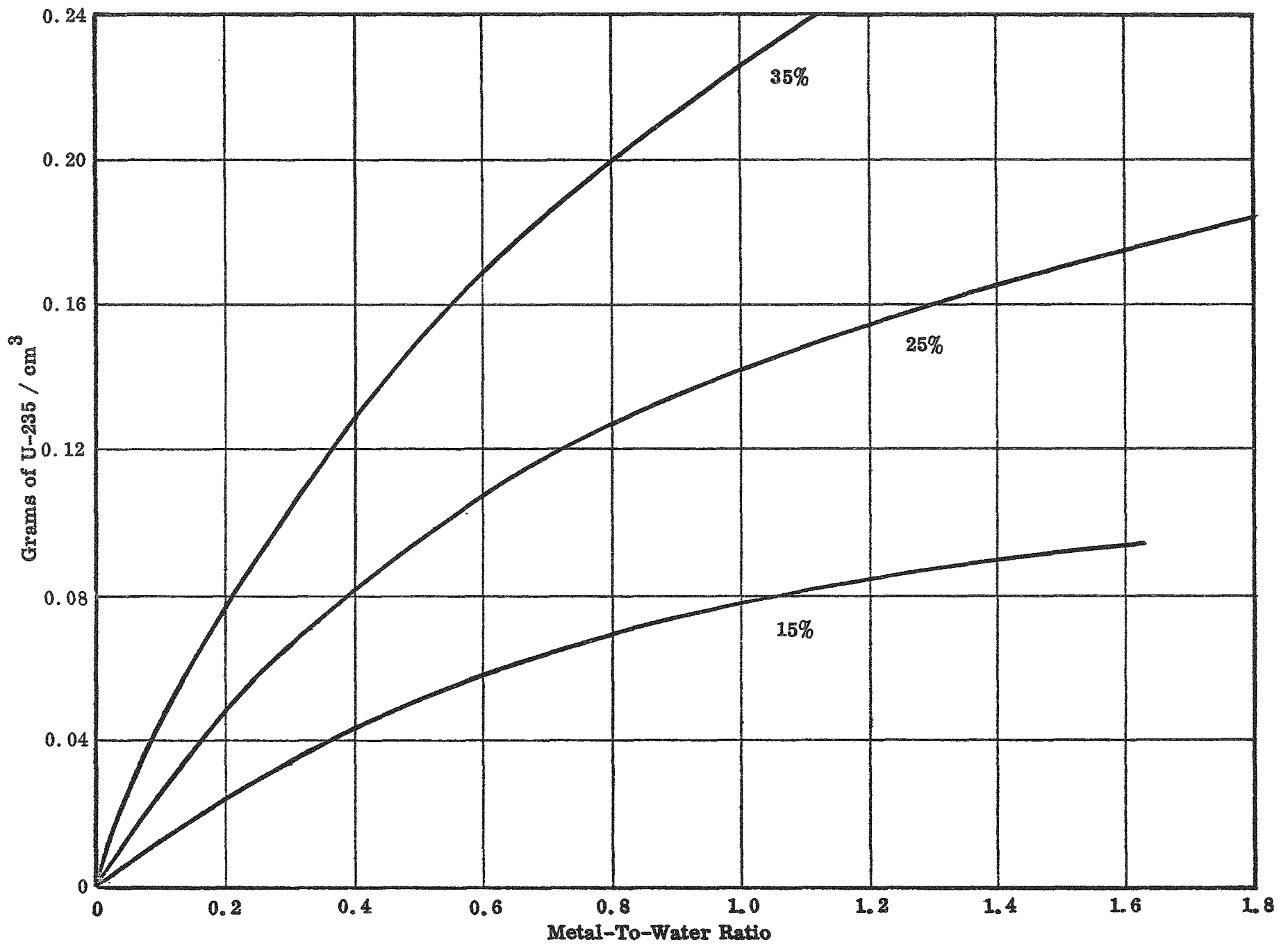


Figure 65 -- Weight Density in Core Region vs M/W Ratio (15, 25 and 35% by Wt. of U, No Wedges)

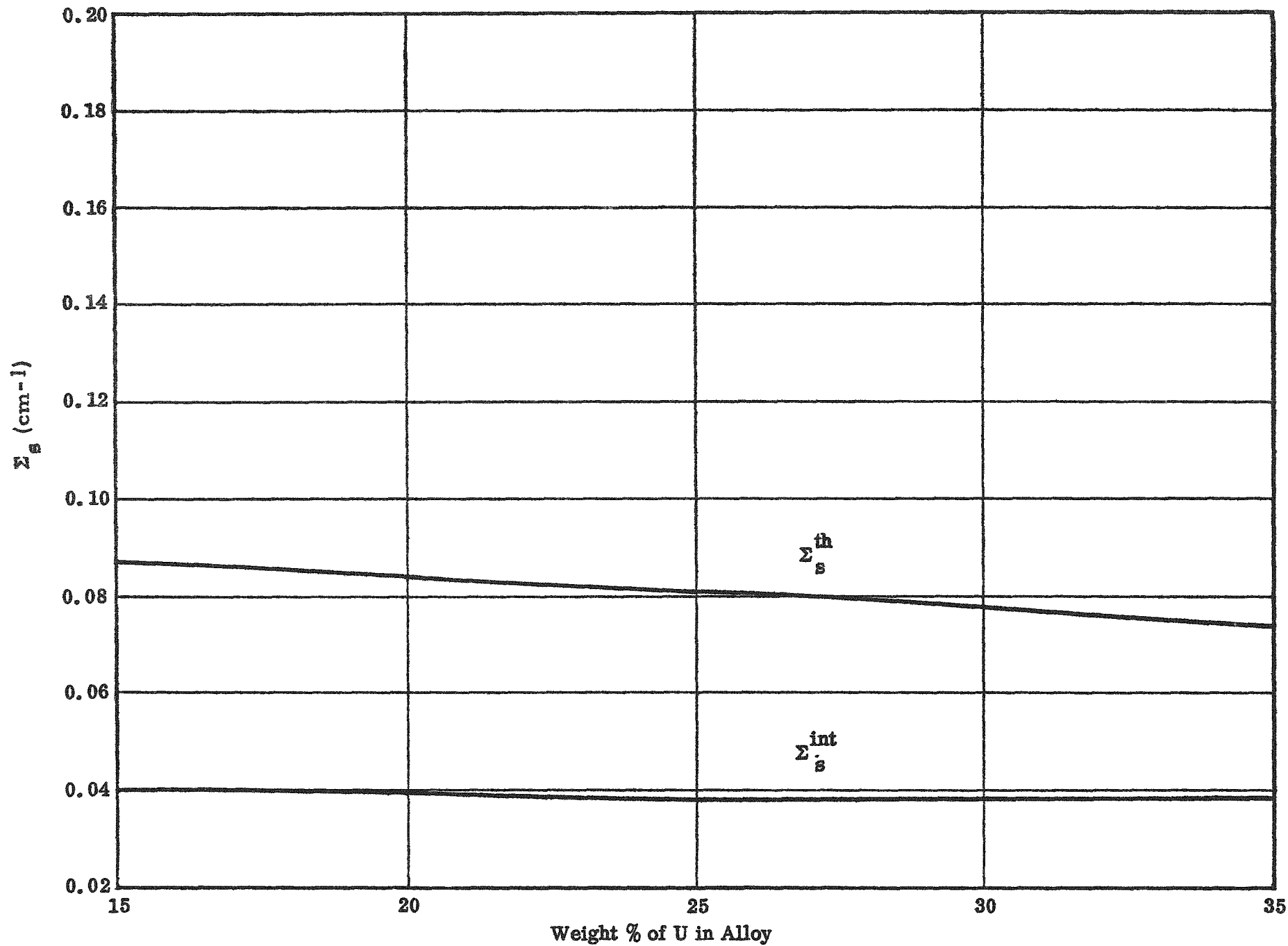


Figure 67 -- Source (From Moderator) Cross Section (No Wedges)

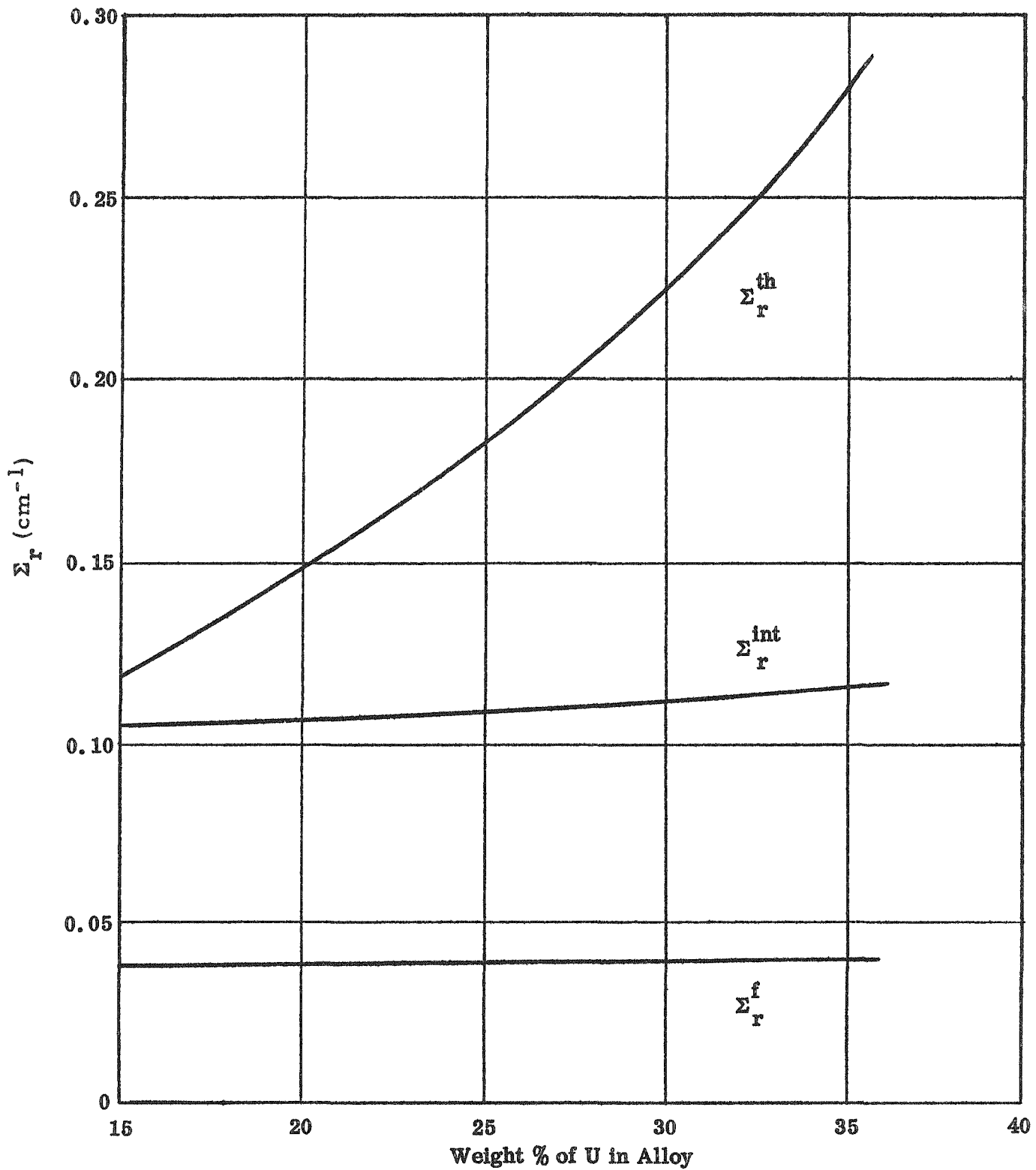


Figure 66 -- Removal Cross Section vs Weight Percent of U -- M/W=0.69 (No Wedges)
A-53

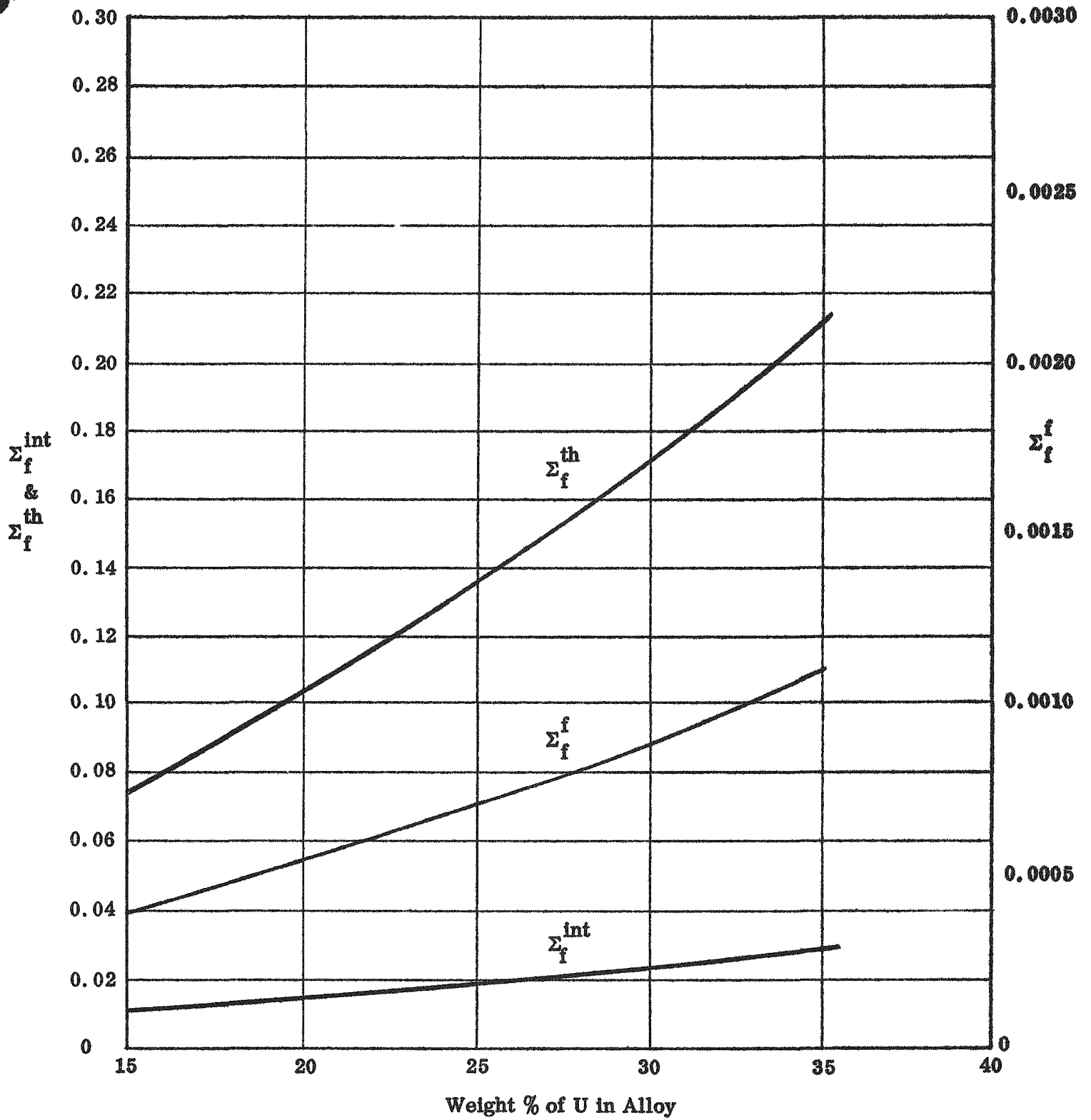


Figure 68a -- Fission Cross Section vs Weight Percent of U in Alloy (No Wedges)
A-55

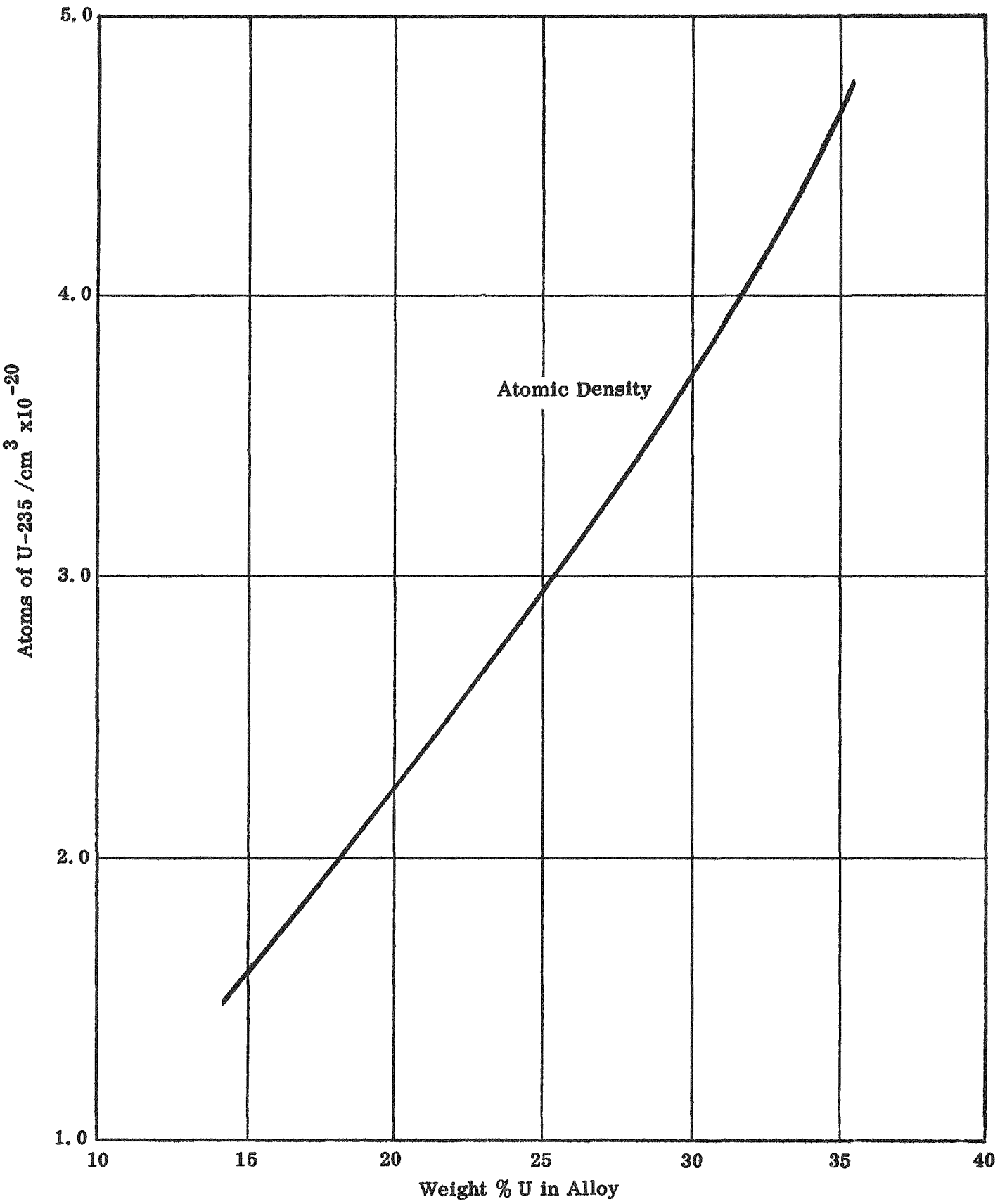


Figure 69a -- Atomic Density vs Weight Percent of U in Alloy -- M/W = 0.69 (No Wedges)
A-56

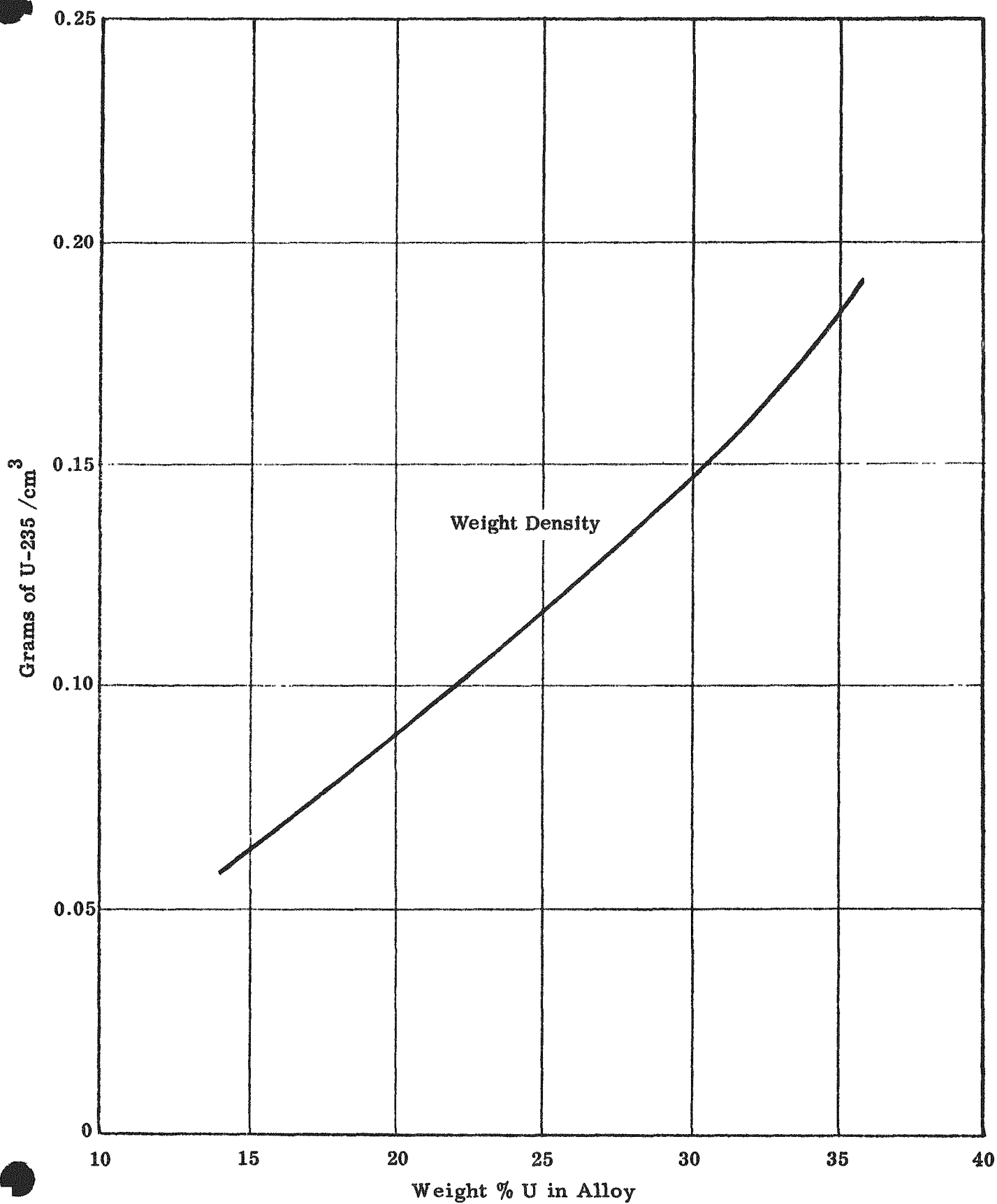


Figure 69b -- Weight Density vs Weight Percent of U in Alloy -- M/W = 0.69 (No Wedges)



APPENDIX B

DERIVATION OF THERMAL PERFORMANCE RELATIONSHIPS

The fuel plate surface temperature at any point along the coolant channel may be described in the conventional fashion by applying the following temperature difference relationship (see Table B-I for nomenclature).

$$T_s(x) - T_{in} = [T_s(x) - T_m(x)] + [T_m(x) - T_{in}] \quad (1)$$

The correlations available permit the evaluation of the bracketed quantities since

$$[T_s(x) - T_m(x)] = F_{film} \cdot \Delta T_{film} \quad (2)$$

and

$$[T_m(x) - T_{in}] = F_{bulk} \cdot \Delta T_{bulk} \quad (3)$$

In the customary fashion the "hot spot factors" are applied to ΔT_{film} and the hot channel factors are applied to ΔT_{bulk} . Substituting yields

$$T_s(x) - T_{in} = F_{film} \cdot \Delta T_{film} + F_{bulk} \cdot \Delta T_{bulk} \quad (4)$$

By the definition of h

$$q'' = h \Delta T_{film} \quad (5)$$

Longitudinal heat conduction within the fuel plates and coolant stream is less than .5% of maximum surface heat flux. Consequently, longitudinal conduction is neglected, and the surface heat flux at any point is proportional to the rate of heat generation of that point. The flux may be represented by the assumed cosine distribution

$$q''(x) = q''_{max} \cos \frac{\pi x}{2a} \quad (6)$$

h is assumed to be given by the modified Colburn equation⁽²⁾

$$\frac{hD_{eq}}{k_f} = .023 \left(\frac{D_{eq} V \rho}{\mu} \right)_f^{.8} \left(\frac{C_p \mu}{k} \right)_f^{.3} \quad (7)$$

where the subscript, f, refers to the so-called film temperature which is defined for this equation as

$$T_f(x) = \frac{T_s(x) + T_m(x)}{2} \quad (8)$$

Solving equation (7) for h yields

$$h = \frac{.023 \rho_f^{.8} C_{p_f}^{.3} k_f^{.7}}{\mu_f^{.5}} \cdot \frac{v^{.8}}{D_{eq}^{.2}} \quad (9)$$

where the coefficient on the right is a function of the film temperature only

$$\frac{.023 \rho_f^{.8} C_{p_f}^{.3} k_f^{.7}}{\mu_f^{.5}} = .023 \left(\frac{\rho^{.8} C_p^{.3} k^{.7}}{\mu^{.5}} \right)_f \equiv b \quad (10)$$

Substituting h and q'' in equation (5) and solving for ΔT_{film} yields

$$\Delta T_{film} = \frac{q''_{max} \cos \frac{\pi x}{2a}}{b \frac{v^{.8}}{D_{eq}^{.2}}} \quad (11)$$

The bulk temperature rise, ΔT_{bulk} , is found by relating the heat capacity of the flowing fluid and the integral of the heat flux over the fuel surface area from the coolant inlet to a point in question. Considering a heat balance over a differential length of the fuel plate surface

$$q''(x) W \Delta x = m C_p [T_m(x + \Delta x) - T_m(x)] \quad (12)$$

The mass flow rate of coolant

$$m = \rho V \cdot \frac{W t_w}{2} \quad (13)$$

and the metal volume to water volume ratio,

$$R = \frac{W t_p}{W t_w} = \frac{t_p}{t_w} \quad (14)$$

Substituting and rearranging

$$q''(x) \cdot W = \frac{\rho V W t_p C_p}{2R} \frac{[T_m(x + \Delta x) - T_m(x)]}{\Delta x} \quad (15)$$

In the limit equation (15) becomes

$$\frac{dT_m(x)}{dx} = \frac{2R q''(x)}{\rho C_p V t_p} = \frac{2R q''_{max}}{\rho C_p V t_p} \cos \frac{\pi x}{2a} \quad (16)$$

Integrating from $-\frac{L}{2}$ to x

$$T_m(x) - T_{in} = \frac{2Rq''_{max}}{\rho C_p V t_p} \cdot \frac{2a}{\pi} \left[\sin \frac{\pi x}{2a} - \sin \left(-\frac{\pi L}{4a} \right) \right] \quad (17)$$

$$\Delta T_{bulk} \equiv T_m(x) - T_{in} = \frac{2Rq''_{max}}{\rho C_p V t_p} \frac{2a}{\pi} \left[\sin \frac{\pi x}{2a} + \sin \frac{\pi L}{4a} \right] \quad (18)$$

Combining equations (4), (11) and (18)

$$T_s(x) - T_{in} = F_{film} \frac{q''_{max} \cos \frac{\pi x}{2a}}{b \frac{V \cdot 8}{D_{eq} \cdot 2}} + F_{bulk} \frac{2Rq''_{max}}{\rho C_p V t_p} \cdot \frac{2a}{\pi} \left[\sin \frac{\pi x}{2a} + \sin \frac{\pi L}{4a} \right] \quad (19)$$

It is convenient to express q''_{max} in terms of the longitudinal average power density, \bar{p} , and the metal-to-water ratio, R

$$\bar{p} = \frac{\int_{-\frac{L}{2}}^{\frac{L}{2}} q''(x) W dx}{\frac{t_w + t_p}{2} WL} = \frac{2q''_{max}}{\left(\frac{1}{R} + 1\right) t_p L} \int_{-\frac{L}{2}}^{\frac{L}{2}} \cos \frac{\pi x}{2a} dx \quad (20)$$

$$\bar{p} = \frac{2q''_{max}}{\left(\frac{1}{R} + 1\right) t_p L} \cdot \frac{2a}{\pi} \cdot 2 \sin \frac{\pi L}{4a} \quad (21)$$

Rearranging

$$q''_{max} = \frac{\pi t_p L \left(\frac{1}{R} + 1\right) \bar{p}}{8a \sin \frac{\pi L}{4a}} \quad (22)$$

and substituting in equation (19) yields, after simplification

$$T_s(x) - T_{in} = \frac{\pi L t_p \left(\frac{1}{R} + 1\right)}{8Va \sin \frac{\pi L}{4a}} \left[F_{film} \frac{D_{eq} \cdot 2 V \cdot 2 \cos \frac{\pi x}{2a}}{b} + F_{bulk} \frac{4aR}{\pi \rho C_p t_p} \left(\sin \frac{\pi x}{2a} + \sin \frac{\pi L}{4a} \right) \right] \quad (23)$$

Performance is limited by the maximum surface temperature; it is convenient to find the average power density, \bar{p} , associated with this maximum performance condition by finding the position (value of x) at which $T_s(x)$ is maximum. This may be done by setting

$$\frac{dT_s(x)}{dx} = 0$$

and solving for x . Note that since b represents a combination of the coolant physical properties, it is a function of x . It is convenient, however, to treat b as a constant in the differentiation and subsequently to adjust the position of maximum surface temperature by an iterative procedure.

Neglecting the hot channel and hot spot factors and differentiating equation (23) with respect to x , setting the derivative equal to zero and solving for $\tan \frac{\pi x}{2a}$

$$\tan \frac{\pi x}{2a} = \frac{4aRb}{\pi \rho C_p t_{p,eq} \cdot 2V \cdot 2} \quad (24)$$

The implied value of x corresponds to the position at which the surface temperature is maximum provided the appropriate value for b is used.

Substituting the sine and cosine terms implied by equation (24) in (23), x is eliminated and T_s becomes the singular allowable surface temperature parameter.

$$\bar{p} = \frac{8Va (T_s - T_{in}) \sin \frac{\pi L}{4a}}{\pi Lt_p \left(\frac{1}{R} + 1 \right) \left[\frac{F_{film} D_{eq} \cdot 4V \cdot 4 \pi \rho C_p t_p}{\sqrt{(4aRb)^2 + (\pi \rho C_p t_{p,eq} \cdot 2V \cdot 2)^2}} + \frac{F_{bulk} 16a^2 R^2 b^2}{\sqrt{(4aRb)^2 + (\pi \rho C_p t_{p,eq} \cdot 2V \cdot 2)^2}} + \frac{F_{bulk} 4aR}{\pi \rho C_p t_p} \sin \frac{\pi L}{4a} \right]} \quad (25)$$

Equation (25) was coded for the IBM 650 computer; the relationship between b and coolant temperature was made available to the computer so that the proper value of b could be found for each set of independent parameters used. The program was stopped when the value of \bar{p} changed less than .5% in two successive iterations.

TABLE B-I
HEAT TRANSFER NOMENCLATURE

Symbol	Definition	Units
T_{in}	Reactor inlet coolant temperature	$^{\circ}F$
T_{out}	Reactor outlet coolant temperature	$^{\circ}F$
T_m	Mixed mean coolant temperature	$^{\circ}F$
T_s	Heat transfer surface temperature	$^{\circ}F$
T_f	Local surface and mixed-mean temperature arithmetic average	$^{\circ}F$
ΔT_{film}	Surface to mixed-mean temperature difference	$^{\circ}F$
ΔT_{bulk}	Local coolant to inlet coolant temperature difference	$^{\circ}F$
x	Longitudinal distance from center of core	ft
L	Length (or height) of core	ft
δ	Reactor reflector savings	ft
a	Half height of mathematical core	ft
F_{film}	Hot spot factor	-
F_{bulk}	Hot channel factor	-
q''	Local heat flux	$\frac{BTU}{hr\ ft^2}$
q''_{max}	Maximum heat flux	$\frac{BTU}{hr\ ft^2}$
q'''	Volume heat source	$\frac{BTU}{hr\ ft^3}$
h	Heat transfer coefficient	$\frac{BTU}{hr\ ft^2\ ^{\circ}F}$
D_{eq}	Equivalent diameter of coolant channel	ft
t_w	Thickness of coolant channel (plate spacing)	ft
t_p	Thickness of fuel plate	ft

R	Ratio of metal volume to water volume	-
V	Average coolant velocity	$\frac{\text{ft}}{\text{hr}}$
m	Mass flow rate of coolant	$\frac{\text{lb}}{\text{hr}}$
\bar{p}	Longitudinal average power density	$\frac{\text{BTU}}{\text{hr ft}^3}$
W	Width of fuel plate and coolant channel	ft
b	Coolant physical property	$\frac{\text{BTU}}{\text{hr}^2 \text{ft}^{2.6} \text{ } ^\circ\text{F}}$
ρ	Density	$\frac{\text{lb}}{\text{ft}^3}$
c_p	Heat capacity	$\frac{\text{BTU}}{\text{lb } ^\circ\text{F}}$
k	Thermal conductivity	$\frac{\text{BTU}}{\text{hr ft } ^\circ\text{F}}$
μ	Viscosity	$\frac{\text{lbs}}{\text{ft hr}}$

APPENDIX C

MATERIALS CONSIDERATIONS

The high power density necessary for the operation of this reactor requires that high temperatures and large flow velocities be employed. However, as mentioned in the introduction, aluminum is the most desirable material for most applications. This necessitates a complete survey of the use of aluminum alloys in high temperature water to determine applicability in this system. Much of the corrosion data given here can be found in two summary reports.^{1,2*} The effect of radiation on materials of construction is considered also because of the high exposure level to which structural materials will be subjected in AETR service.

A. THE CORROSION OF NORMAL ALUMINUM ALLOYS IN HIGH TEMPERATURE WATER

Below 200°C aluminum has a low corrosion rate in neutral or slightly acidic high purity water. Type 1100 (commercially pure) aluminum has a corrosion rate of about 1.3 mils per year in distilled water at 200°C compared with 0.05 mils per year at 125°C. If the water is pure, this will be uniform corrosion, but impurities such as chloride ions tend to cause pitting. The water conditions, especially pH, have a great effect on corrosion rate. There is a minimum pH for optimum corrosion resistance decreasing from pH 6.5 to pH 2 as the temperature increases from 50°C to 315°C. Flow velocity has a large effect on corrosion at high pH and much less in acidic solution.³

Corrosion tests have been made on some commercial aluminum alloys. Groot and Peekema⁴ tested many alloys in Hanford 200 E area water (processed river water). Most alloys had approximately the same corrosion rate, only the 2024 being significantly poorer. Strom and Boyer⁵ tested 2024, 6061, 5052, Alclad 2024, and Alclad 7075 in distilled water at 350°F and 480°F. The Alclad 2024 had the best corrosion resistance, 5052 had the worst. The rate for the better alloys was less than 0.3 mils per year at 350°F. Huddle and Wilkens⁶ found that commercially pure aluminum (99.0% Al) has much better corrosion

*References are listed at the end of this Appendix.

resistance than high purity metal (99.8% Al), the high purity material failing by intergranular corrosion at 125°C in less than 100 hours.

Below 200°C the corrosion is regular, showing a parabolic rate.^{6,7} A protective film, mainly Boehmite ($\text{Al}_2\text{O}_3 \cdot \text{H}_2\text{O}$) is formed on the aluminum and regulates the corrosion rate. There is some disagreement as to the exact makeup and function of the oxide.

Above about 200°C a different corrosion mechanism is important. After a period of uniform corrosion many aluminum alloys fail catastrophically by intergranular attack. The time before this occurs decreases with increasing temperature, and also depends on the alloy. High purity material is very subject to attack. There is a difference of opinion as to the effect of cold work. Draley⁸ found that cold worked material corroded more readily than as cast samples, but LaVigne⁹ found that cold working to 60% improved the resistance to intergranular attack.

Draley, among others, postulates that atomic hydrogen formation at the metal-oxide interface causes blisters, which then break exposing fresh aluminum surface.^{8,10} Analysis of the surface of intergranularly corroded 1100 aluminum reveals a large amount of hydrogen which is not present in aluminum exposed to the same conditions but not subject to intergranular corrosion.¹¹

Dillon, Wilson, and Troutner¹² tested many alloys for resistance to intergranular corrosion at 250°C to 350°C. Most commercial alloys not containing significant amounts of nickel or copper failed in six weeks at 250°C. Of the common alloys, 2017, 2024, 6053, 6061, 7075, and 4043 lasted the full period. At 350°C only a few alloys resisted attack for six weeks: M-388, 2018, 4032, 112, A-132, 142, 333. These aluminum alloys all contained either nickel or copper together with minor amounts of other elements. No detailed corrosion measurements were made.

By coupling the aluminum to stainless steel or zirconium, the beginning of blister corrosion can be retarded. Since these other materials are cathodic to aluminum, this is an example of anodic protection. Intergranular corrosion was also prevented by making the sample anodic with an external voltage source.

Draley has suggested three methods of retarding intergranular corrosion:⁸

- (1) Prepare aluminum without voids or dislocations and the atomic hydrogen will, first, have a low diffusion rate and, second, will not be able to accumulate and form blisters
- (2) Provide cathodes, preferably of low hydrogen overvoltage, for the corrosion reaction, liberating hydrogen in a condition (molecular) or at a point where it is not possible for it to diffuse into the aluminum metal
- (3) Supply an additive to the aluminum metal which makes it impervious to the diffusion of atomic hydrogen.

Method one is not practical for general use. However, Draley found that as-cast material has greater resistance to intergranular attack than cold-worked. He postulated that LaVigne's different results were caused by surface grain orientation and compacting.¹¹ The third method, solid solution alloying, has so far been unsuccessful.

Method two does help to retard catastrophic attack. Samples were nickel plated to provide cathodic layer and the aluminum did resist intergranular corrosion. However, there are many practical objections to using a mechanical coating on the metal, especially under radiation. Alloying to provide a cathodic second phase has proven to be the best scheme. These results will be discussed in detail later in this section.

Huddle and Wilkens⁶ provided a more general explanation of aluminum corrosion. They explained it on the basis of failure of the oxide film. Five mechanisms of failure were given:

- (1) If the pH of the water is outside a relatively narrow range (e.g. 4-9 at 25°C) the film is soluble
- (2) If the temperature is such that continued film growth takes place, a stage will be reached where unless the film is relatively plastic and can accommodate the stress due to volume changes, failure will occur by cracking or flaking
- (3) Application of anodic or cathodic potentials may affect breakdown either by influencing the solution (e.g. change of pH adjacent to the surface) or by modifying the process of film growth
- (4) Hydrogen originating from the water may diffuse through the film to react with underlying metal in such a way as to cause failure

- (5) The metallurgical character of the grain boundary - lack of registry between crystal lattices, increase of solute concentration in the disarray metal, or actual precipitation - may lead to intergranular attack.

These investigators pointed out that the pH of the solution is not necessarily the pH next to the corroding surface. Therefore, method one is difficult to evaluate in detail. Their conclusions as to the best methods of protection were that alloying with nickel, iron, and silicon should help by providing cathodes throughout the material.

There is general agreement that alloying is the best solution and that the resistance to disintegration improves with the amount, the dispersion and the ability of the second phase to act as cathodes.^{11,12} Huddle and Wilkens¹⁴ summarized the properties of the most desirable alloying element:

- (1) Low solid solubility at working temperature
- (2) Formation of a phase from which H_2 is readily liberated, thereby preventing gas absorption
- (3) Uniform distribution of this cathodic phase as small particles

Many elements have been tested, but nickel is the only one that fulfills all the objectives. The results of many alloying studies have led to the development of a standard alloy for use in high temperature water. It is known as M-388 (or X-8001), and the commercial composition limits are: 0.45-0.70 iron, 0.9-1.3 nickel, 0.17 max. silicon, 0.15 max. copper, 0.008 max. lithium, 0.03 max. cadmium, 0.001 max. boron, 0.05 max. each and 0.15 max total of other elements, remainder aluminum.

A number of promising aluminum alloys are currently under development. For example, M-400 (1% Fe, 1% Ni) under some conditions exhibits better corrosion resistance than M-388. Other alloys under test offer greater strength at high temperatures and might be available for future use.

It should be pointed out that alloying retards intergranular corrosion, but it has little effect on the general corrosion rate of the aluminum. Therefore, the corrosion rate is expected to rise with increasing temperature, and to be approximately the same for different alloys in the absence of intergranular corrosion.

B. THE PROPERTIES OF X8001 (M-388)

1. Corrosion Resistance

Corrosion tests on aluminum are difficult to control, especially when they are made at high temperature and flow rates. Therefore, there are many discrepancies among measurements from different laboratories. This makes it necessary in most high temperature applications to test the aluminum under operating conditions before actual use.

Some of the most important variables that affect the corrosion rate are:

- a. Water purity
- b. pH
- c. Temperature
- d. Flow velocity
- e. Hydrogen concentration in water
- f. Rigidity of sample
- g. Duration of test
- h. Surface condition of sample
- i. Metallurgical condition of sample
- j. Irradiation conditions

(1) The water purity has a large effect on corrosion rate. In low purity water, such as at Hanford, corrosion will be fairly rapid, even at low temperatures. There is also apt to be pitting, especially when chloride ion is present. However, chromate ion tends to protect the metal from pitting, but increases the corrosion rate at elevated temperature² For reactor service it is advisable to have a conductivity of about 2 micromhos. Unless stated otherwise, the tests reported here were all performed in high purity water.

Many inhibitors have been tried with aluminum, but there is only one, phosphoric acid, that is effective. When the pH is reduced to about 4 with phosphoric acid, the corrosion rate decreases greatly. The reduction in pH is one reason, but much of the rate decrease is due to beneficial effects on the oxide film by the phosphate ion. Troutner⁷ analyzed the film formed at

195°C in water with 5 ppm of phosphate ions added. The corrosion product was augelite, a basic aluminum phosphate, $\text{Al}_2\text{PO}_4(\text{OH})_3$ or $2\text{Al}_2\text{O}_3 \cdot \text{P}_2\text{O}_5 \cdot 3\text{H}_2\text{O}$. Coher¹⁵ found a mixture of alumina, Boehmite, and augelite under similar conditions. The use of phosphate inhibitors in a reactor would be somewhat questionable since stainless steel in the system might be attacked. There is also evidence of some decomposition of the phosphate under irradiation, and the water decomposition rate also increases.

The amount of corrosion product in the water seems to have an effect. In general, the larger the metal area to water ratio and presumably the higher the aluminate ion concentration, the smaller the corrosion rate. Hanford results show that a nine-fold increase in the metal area to water ratio results in 1/3 the corrosion rate,¹⁶ but results of other investigations do not show this great a change. Hanford is carrying out some experiments with aluminum oxide solubility in order to formulate a relationship between aluminate ion concentration and corrosion rate.¹⁷

(2) As in low temperature aluminum corrosion, pH is an important variable. The pH of minimum corrosion decreases with temperature for X8001 as it does for 1100, being 4.9 at 205°C and lower than 3.1 at 300°C.¹⁸ In corrosion testing, there is the problem of measuring the pH at operating temperature, the value often changing as the temperature is raised. In reactor operation, the pH will generally be chosen as 5.5 to 6, or as low as possible without seriously affecting the corrosion rate of stainless steel in the system. In Figures 70 and 71, corrosion rates of X8001 vs. flow velocity are plotted for two different pH ranges at two temperatures.

(3) The corrosion rate increases rapidly with temperature. Lobsinger and Atwood¹⁹ found that the rate under given conditions followed an Arrhenius plot between 130°C and 240°C. When the logarithm of the corrosion rate was plotted against the reciprocal of the absolute temperature, a straight line resulted.

Dillon⁷ measured an activation energy of 12.2 Kcal/mole. However, the scatter in the measured points was appreciable. Huddle and Wilkens⁶ reported on activation energy of 10 to 15 Kcal/mole for 99.0% aluminum.

The corrosion rate of X8001 has been found to be slightly lower than the rate in water at the same temperature.^{11,12}

(4) As seen from Figures 70 and 71, corrosion rate is quite dependent on flow velocity. No information is available on the affect of velocities over 25 ft/sec at a pH of less than 7. Above 18 ft/sec there is much scatter in the results which leads to the belief that some other variables were not under control. One of these is probably the rigidity of the sample and its effect on oxide cracking. The data plotted in Figures 70 and 71 were compiled from results reported by many people. The points shown with dotted circles represent tests that were either not completely under control, or involved another variable.

Honeycutt²¹ found no erosion of aluminum at low temperatures up to at least 100 ft/sec. However, Krenz²² found that there was erosion of the oxide film at 20 ft/sec at 260°C. The adherence and stability of the oxide is definitely a major problem in high temperature aluminum corrosion. More investigation is necessary before using aluminum at velocities greater than about 25 ft/sec.

(5) Hydrogen seems to have a beneficial effect on aluminum corrosion rates, but the results are not always reproducible. Medin and Clark¹³ found that degassed samples have two to four times greater corrosion rates than samples with H₂ added or natural H₂ buildup. Similar results have been obtained at Argonne² but they are not always reproducible when H₂ is added.²³ More work must be done on the effect of hydrogen concentration on corrosion rate.

(6) The rigidity of the sample is very important at high flow velocities. Since aluminum is protected by an oxide layer, this layer must remain intact or corrosion will increase greatly. In higher velocity tests, Krenz²² obtained corrosion rates ranging from 0.020 to 0.360 in./yr at 20 ft/sec and 260°C depending on

the rigidity of the sample. Hanford experience also points up the importance of specimen rigidity.

When the sample bends or vibrates, the oxide tends to flake off and fresh aluminum surface is exposed to the water. Therefore, the mechanical design of an aluminum structure is quite important. Since the strength of X8001 is quite low at elevated temperatures, maximum temperature and flow velocity might be limited by the allowable stress levels rather than by corrosion rate.

(7) The duration of the test is important since there is initial rapid corrosion while the film is formed. After this stage corrosion may follow either a parabolic or linear curve. The data are often not accurate enough to distinguish between the two types. Krenz²² found a constant rate after initial corrosion, but Dillon⁷ found a parabolic relationship for a period of time. After about two months at 363°C, or three months at 300°C, the rate increased and became constant. Similar data have been obtained by Cohen²⁰. If parabolic dependence can be extended over a longer time, total corrosion should be reduced. This change in rate effect can be used as a check on the effectiveness of various alloy compositions.

(8) Surface condition effects have not been explored to a great extent. It appears, however, that the corrosion rate is not greatly sensitive to normal variations in surface quality.

(9) The corrosion rate of X8001 has been found to be relatively insensitive to the amount of cold work.⁷ Fine grained samples are more resistant to blistering than coarse grained samples.¹³ Distribution of the second phase is important, small evenly distributed particles being necessary for corrosion resistance.¹¹

(10) Radiation seems to have little effect on the corrosion rate, although a slight decrease in the rate has been observed.^{22,24} However, there have been very few valid in-pile tests, and operating experience will be required before definite conclusions are reached.

2. Mechanical Properties

Very little information has been published concerning the mechanical properties of X8001. Data obtained from Alcoa²⁵ giving properties of a typical lot of X8001 are given in Table XVI. No creep data could be found.

TABLE XVI

TENSILE PROPERTIES OF M-388 (X8001)
(AFTER 100 HOURS AT TEMPERATURE)

Temp (°F)	Tensile Strength (PSI)	Yield Strength (PSI)	Elongation in 4D (%)
Room	20,000	17,800	23.2
300	15,300	14,000	30.0
400	11,700	10,100	31.5
500	7,300	6,200	34.0
600	3,300	2,600	66.0

C. RADIATION DAMAGE TO STRUCTURAL MATERIALS

Little work has been done at the high fluxes generated in the AETR. In a year of full power operation, the inner pressure vessel will receive about 2.2×10^{22} n/cm² total irradiation, a dosage that has been reached in only a few long term tests to date.

Bartz²⁶ carried out tensile tests on 1100 aluminum and 347 stainless steel which had received dosages up to 2.5×10^{22} neutrons (> 100 ev) in the MTR. In both cases there was a rapid initial increase in yield strength, tensile strength, and hardness and a decrease in elongation up to about 10^{22} for aluminum and 2×10^{21} for stainless. Beyond that point there were only minor changes up to the maximum irradiations reported. For 1100 aluminum, the yield strength rose from 18,400 psi to 26,500 psi, while the hardness rose from 8.4 R_F to 42.3 R_F. However, there was only a small decrease in elongation. The yield strength of type 347 stainless steel rose from 61,200 psi to 100,000 psi, and the hardness increased from 14.4 R_C to 21.8 R_C, coupled with a reduction in elongation from 63 to 44%. The results are reproduced in Figures 72 and 73.

Steele and Wallace²⁷ tested various aluminum alloys that had received 1.26×10^{21} n/cm² at 150°F. The relative decrease in ductility was much less than the increase in yield or tensile strength. For the same amount of increase in yield strength, ductility is less affected by neutron exposure than by strain hardening.

Currently, a number of potential loop materials are being tested at the MTR. Robinson²⁸ found that for most of the materials tested, the yield strength was still increasing at fast neutron dosages of about 10^{20} n/cm². However, the strength of some materials went through a maximum. In general, the yield strength increased from 1 1/2 to 2 1/2 times its initial value, although there was still reasonable elongation. The materials covered in this study are: 16-1 Croloy, Hastelloy-X, Inconel 702, Inconel-X (single aged and double aged), K-monel, and 410 stainless steel. Additional materials now being tested include AM-350, 414 stainless steel and 17-4 pH stainless steel.

REFERENCES

1. N. N. Ida, F. G. Tate, Max Bolotsky, "A Literature Search Into Light Metal Alloys," MND 1105, June 10, 1957. (Confidential)
2. M. D. Ferrier, Minutes of a Conference on Corrosion of Aluminum in Water at High Temperature, Chalk River, Ontario, CR-Met 700, December 12-19, 1956.
3. J. E. Draley, W. E. Ruther, "Aqueous Corrosion of 25 Aluminum at Elevated Temperatures," ANL-5001, February 1, 1953.
4. C. Groot, R. M. Peekema, "The Corrosion of Aluminum and its Alloys," HW 36692, May 13, 1955.
5. P. O. Strom, M. H. Boyer, "Static Corrosion of Aluminum Alloys at 350°F and 480°F in Distilled Water," LRL-64, October, 1953.
6. R. A. U. Huddle, N. J. M. Wilkens, "The Corrosion of Commercially Available "Pure" Aluminum in Demineralized Water Between 125° and 300°C," AERE M/R 1669, May 15, 1955.
7. R. L. Dillon, V. H. Troutner, "Observations on the Mechanisms and Kinetics of Aqueous Aluminum Corrosion," HW-51849, September 30, 1957.
8. J. E. Draley, W. E. Ruther, "Aqueous Corrosion of Aluminum," Part 2, Corrosion 12, pp. 480t-490t (October, 1956).
9. M. J. Lavigne, "Effects of Cold Working On Corrosion of High Purity Aluminum in Water of High Temperature," Met. I-3, November 4, 1954.
10. J. E. Draley, W. E. Ruther, "Corrosion Resistant Aluminum Above 200°C," ANL-5430, July 15, 1955.
11. J. E. Draley, W. E. Ruther, "Experiments in Corrosion Mechanism: Aluminum at High Temperatures," ANL-5658, April, 1957.
12. R. L. Dillon, R. E. Wilson, V. H. Troutner, "High Temperatures Aqueous Corrosion of Commercial Aluminum Alloys," HW-37636, January 11, 1956.
13. A. L. Medin, R. J. Clark, Jr., "Corrosion of Fuel Element Materials for Low Enrichment Power Reactor," APAE-Memo-44, August 1, 1956.
14. R. A. U. Huddle, N. J. M. Wilkens, "The Resistance of Binary Aluminum Alloys to Corrosion by Water at High Temperatures and Pressures," AERE M/R 1669A, May 2, 1956.
15. J. Cohen, "Corrosion of Experimental Aluminum Alloys in High Temperature Water," Report No. 7, WAPD-PWR-PM-1025, July, 1955.
16. R. L. Dillon, R. J. Lobsinger, "Corrosion of Aluminum in Deionized Water," HW-49431, January, 1957 - April, 1957.

17. R. L. Dillon, R. J. Lobsinger, "Corrosion of Aluminum in Deionized Water," HW-53963, September, 1957 - December 6, 1957.
18. V. H. Troutner, "Uniform Aqueous Corrosion of Aluminum-Effects of Various Ions," HW-50133, June 10, 1957.
19. R. J. Lobsinger, J. M. Atwood, "Corrosion of Aluminum in High Purity Water," Corrosion 13, pp. 582t-584t (September, 1957).
20. J. Cohen, "Corrosion of Experimental Aluminum Alloys in High Temperature Water," Report No. 9, WAPD-PWR-PMM-1247, August 22, 1957.
21. E. H. Honeycutt, Jr., "Erosion of Aluminum," DP-214, May, 1957.
22. F. H. Krenz, "Corrosion of Al-Ni Type Alloys in High Temperature Aqueous Service," Corrosion 13, pp. 575t-581t (September, 1957).
23. Reactor Engineering Division, Quarterly Report, Section II, ANL-5601, pp. 42-49, April - June, 1956.
24. Emil Louis Martinec, "Corrosion of an Al-Ni Alloy in a Reactor Test Loop," ANL-5783, September, 1957.
25. Private Communication from Roger Horner, April 22, 1958.
26. M. H. Bartz, "Radiation Damage Observations at the MTR," TID 7515, Part 1, August, 1956.
27. R. V. Steele, W. P. Wallace, "The Effect of Neutron Flux on the Mechanical Properties of Aluminum Alloys," LRL-145, May, 1954.
28. M. S. Robinson, "Radiation Damage Studies Program - ETR Loop Materials Progress Report #2," IDO-16409, September 16, 1957.

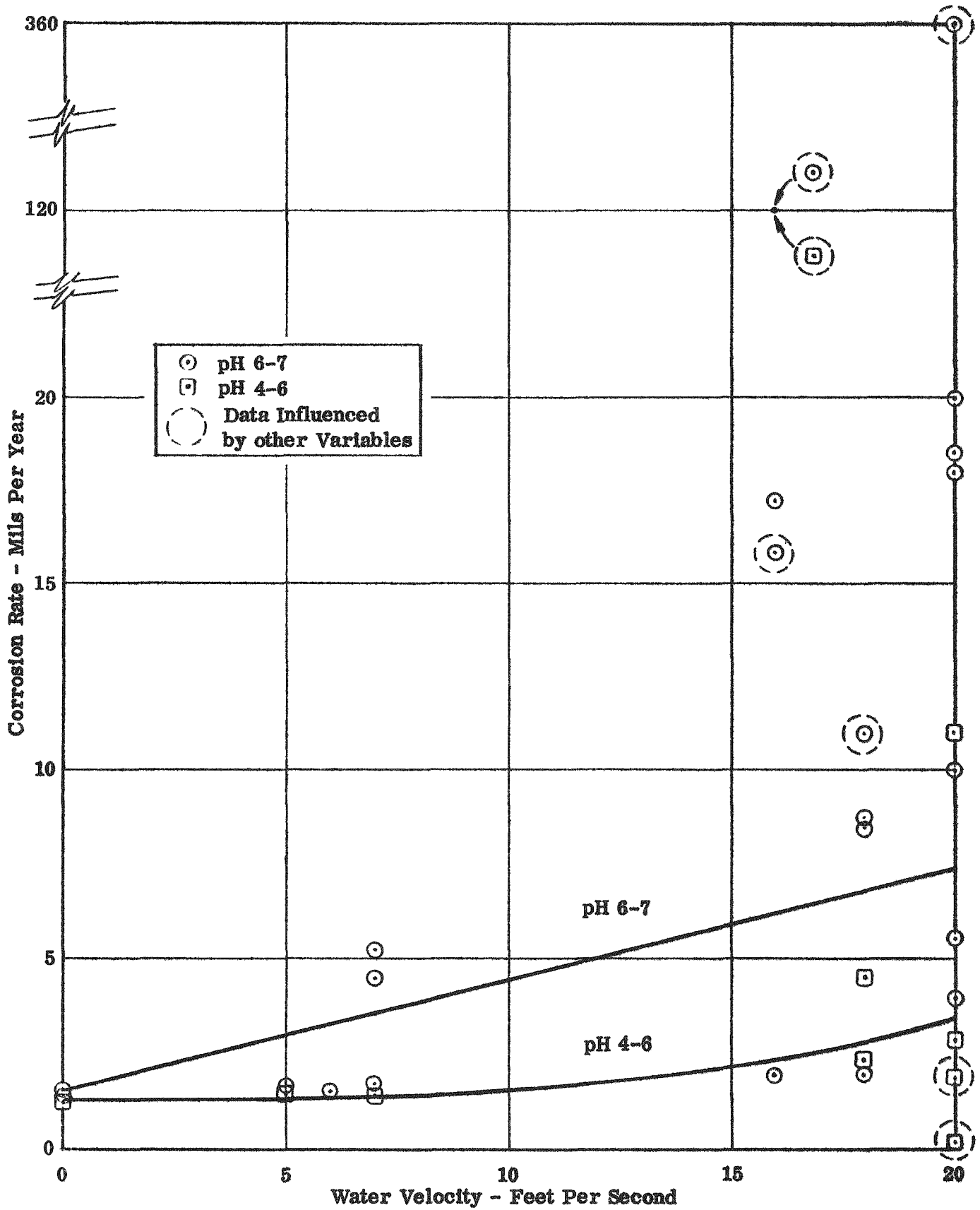


Figure 70 -- Corrosion of X8001 (M-388) Aluminum at 250°C

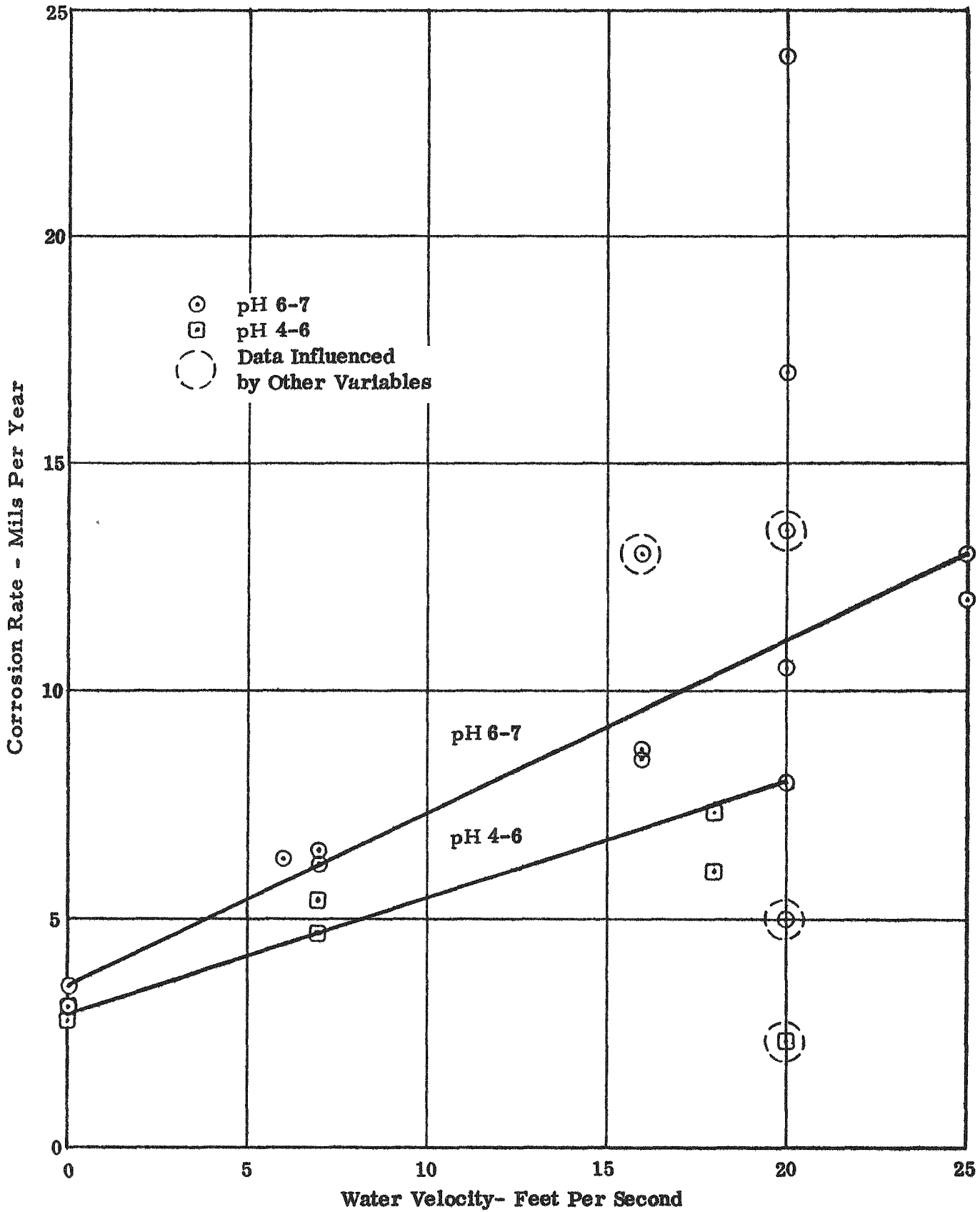


Figure 71 -- Corrosion of X8001 (M-388) Aluminum at 300°C

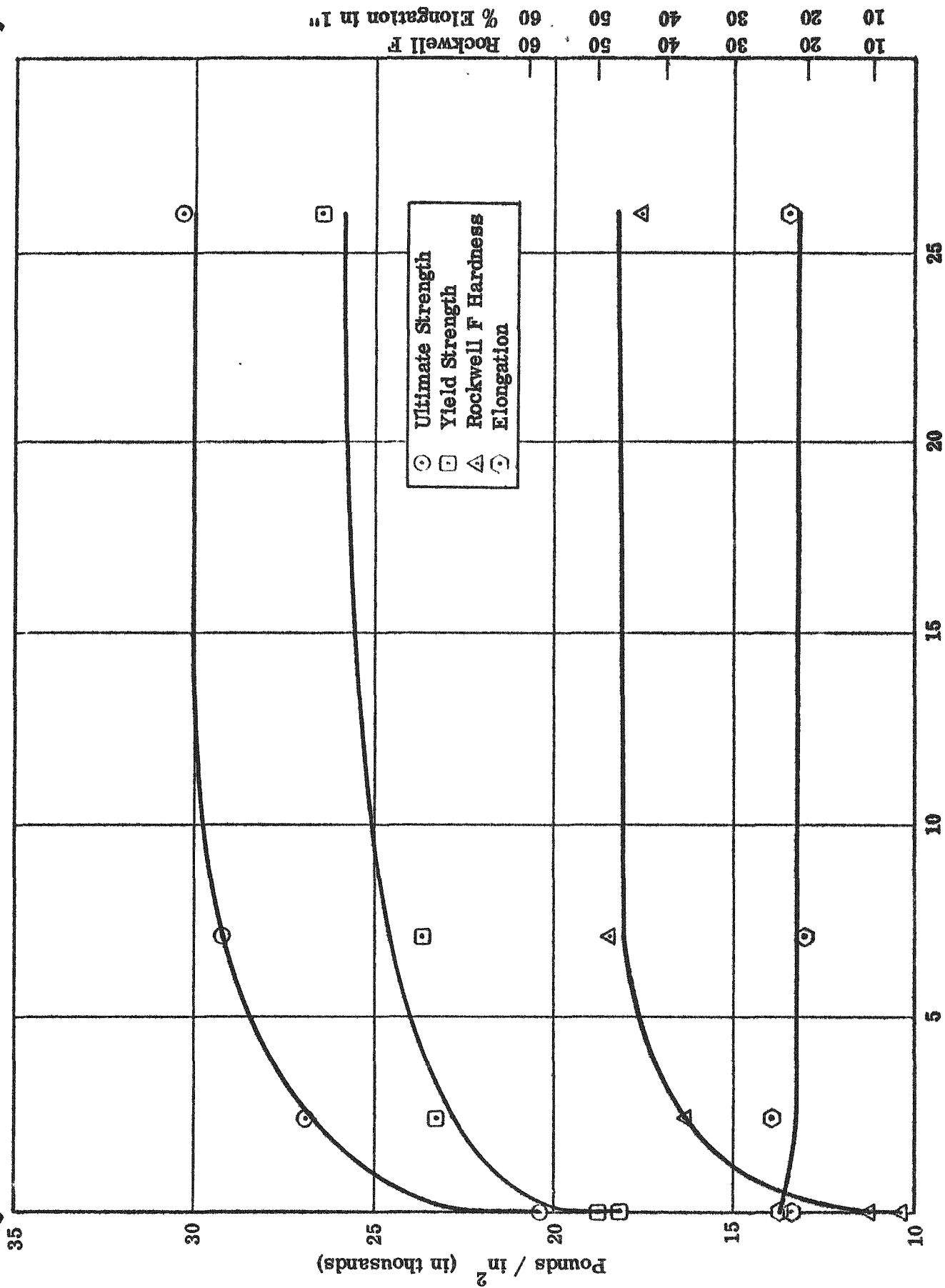


Figure 72 -- Radiation Damage to Aluminum Alloy 1100 (Ref. 26)

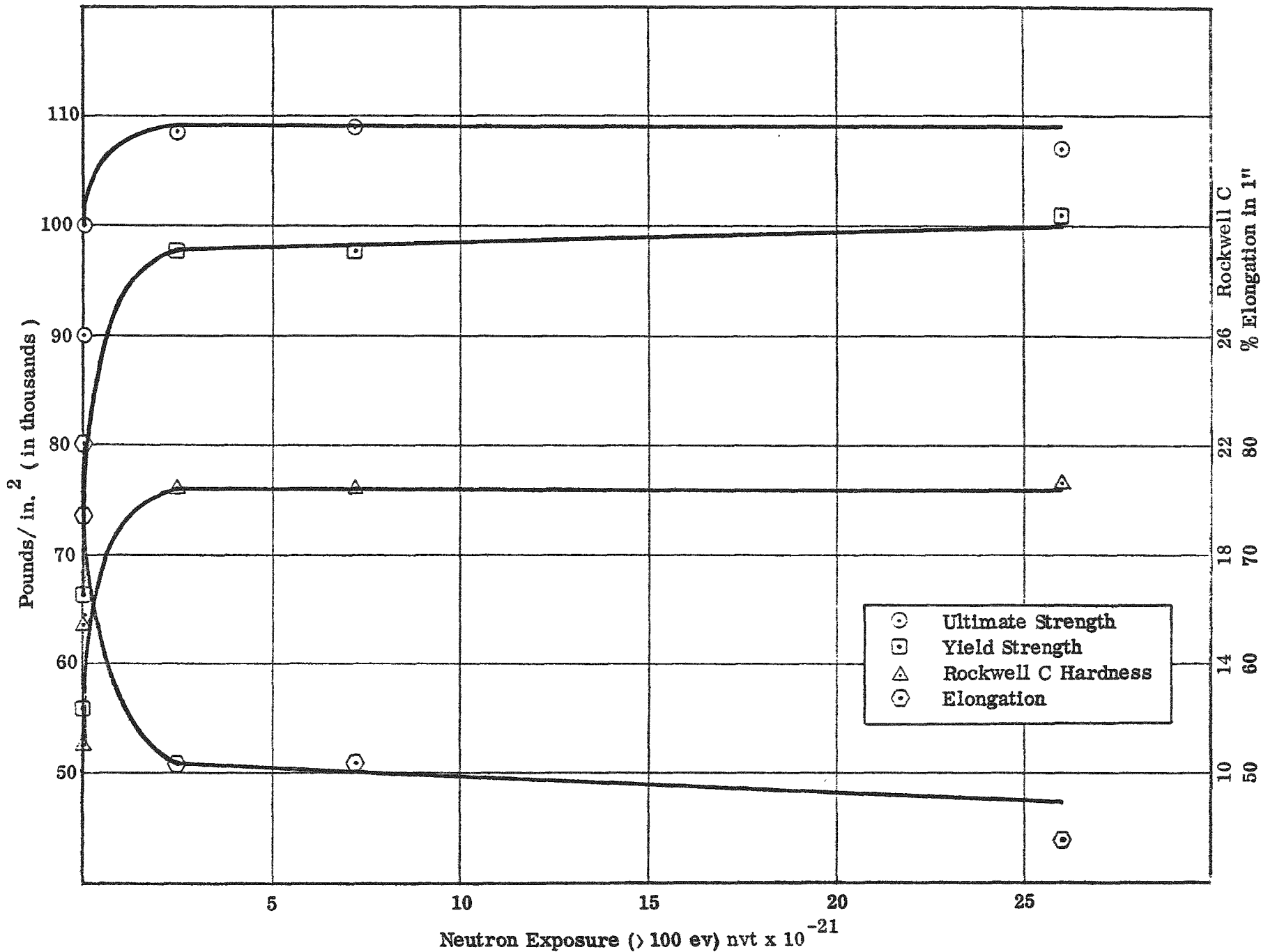


Figure 73 -- Radiation Damage to Stainless Steel (AISI Type 347) (Ref. 26)